January 2020

Contribution Of Intestinal Dysfunction To Alzheimer's Disease Progression

Mona Sohrabi Thompson

CONTRIBUTION OF INTESTINAL DYSFUNCTION TO ALZHEIMER'S DISEASE PROGRESSION

by

Mona Sohrabi Thompson

Master of Science, University of Tehran-Tehran, Iran, (2014)

A Dissertation

Submitted to the Graduate Faculty

of the

University of North Dakota

In partial fulfillment of the requirements

for the degree of Doctor of Philosophy in Biomedical Sciences

Grand Forks, North Dakota

May

2020

This dissertation , submitted by Mona Sohrabi Thompson in partial fulfillment of the requirements for the Degree of Doctor of Philosophy in Biomedical Sciences from the University of North Dakota, has been read by the Faculty Advisory Committee under whom the work has been done and is hereby approved.

DocuSigned by:
Dr. Colin K. Combs
6C43D661961F4C6...
Dr. Colin K. Combs

DocuSigned by:
Dr. Marc Basson
3F2662AB6643495...
Dr. Marc Basson

DocuSigned by:
Dr. John Watt
189C9CC8612F4E1...
Dr. John Watt

DocuSigned by:
Dr. James Porter
2759FC47C53F4E5...
Dr. James Porter

DocuSigned by:
donald sens
2D1BB76FF67A45D...
Dr. Donald Sens

Name of Committee Member 5

This dissertation is being submitted by the appointed advisory committee as having met all of the requirements of the School of Graduate Studies at the University of North Dakota and is hereby approved.

DocuSigned by:
Chris Nelson
13D0157109424B1...
Chris Nelson
Dean of the School of Graduate Studies

4/30/2020
Date

PERMISSION

Title: Contribution of Intestinal Dysfunction to Alzheimer's Disease Progression

Department: Biomedical Sciences

Degree: Doctor of Philosophy

In presenting this dissertation in partial fulfillment of the requirements for a graduate degree from the University of North Dakota, I agree that the library of this University shall make it freely available for inspection. I further agree that permission for extensive copying for scholarly purposes may be granted by the professor who supervised my dissertation work, or in his absence, by the Chairperson of the department or the dean of the School of Graduate Studies. It is understood that any copying or publication or other use of this dissertation or part thereof for financial gain shall not be allowed without my written permission. It is also understood that due recognition shall be given to me and to the University of North Dakota in any scholarly use which may be made of any material in my dissertation.

Mona Sohrabi Thompson
May, 2020

TABLE OF CONTENTS

LIST OF FIGURES

LIST OF TABLES

ACKNOWLEDGEMENTS

I would like to extend my sincerest appreciation to my advisor, Dr. Colin K. Combs, for the provided opportunity to work in his lab and funding this research. During my study, I was extensively supported by him. This dissertation would not have been possible without his guidance, continuous help, patience, wisdom, and encouragement. Not only have I had his explicit support in my professional life but also in my personal life - he was the surrogate father in my most special day, my marriage ceremony.

To my committee members: Dr. Marc Basson, Dr. John Watt, Dr. James Porter, and Dr. Donald Sens, I am extremely grateful for your assistance and suggestions throughout my research. I want to extend an additional thanks to Dr. Basson who gave me a chance for shadowing him during his colonoscopy operations. It was definitely one of the most precious experiences in my life. A special thanks to Dr. Watt for his support and guidance in my both personal and professional life. I would like to thank Dr. Porter for sending me valuable papers and his follow up on my research progress. I would also like to thank Dr. Sens for his collaboration and letting me utilize the Pathology equipment.

To the Biomedical Sciences faculty and staff at University of North Dakota (UND), thank you for supporting my education, accepting me as an international student in the department, overall support at seminars, and always listening and

giving me words of encouragement. I am most grateful to Dr. Kumi Nagamoto-Combs for her guidance during my research, accompanying me to choose my wedding dress, and being the surrogate mother in my wedding. I would like to thank Dr. Catherine Brissette for all her support and empathy during my time in UND. A special thanks to Dr. Bryon Grove for his assistance to analyze immunohistochemistry staining. I am greatly appreciative to Dr. Othman Ghribi for his absolute and invaluable support, empathy, and friendship in my professional and personal life. I want to extend a special thanks to Jennifer Hershey, Michael Ullrich, Joyce Rice, Julie Horn, Sarah Abrahamson, Beth Ann DeMontigny, Dr. Bony De Kumar, Dr. Suba Nookala, Dr. Santhosh Mukundan, Angela Floden, and all other lab mates for all their unconditional assistance, guidance, and kindness. I am extremely grateful to Bonnie Kee for her patience and help in formatting this dissertation.

I would like to thank Dr. Heidi Pecoraro, a pathologist from North Dakota State University Veterinary Diagnostic Laboratory, for her priceless assistance to evaluating intestinal histology in this dissertation.

A very special thanks to my dearest friends, Sema Oncel, Michelle Montgomery, Dr. Emily Biggane, Dr. Gaurav Datta, and Dr. Joshua A. Kulas, at UND for helping me survive all the stress and homesickness during these years and not letting me give up. I am grateful to Dr. Joshua Kulas for the most helpful discussions over scientific findings during my research.

Last but not least, I would like to express my sincere gratitude to my awesome parents, husband, and parents-in-law for their tremendous support and

love. Deepest thanks to my mom and dad who have always given me wings and made me fly to make my dreams come true. To my best friend and love of my life, my husband Derick, who has been my greatest supporter and believer throughout my graduate school career. I would not be where I am today without him.

I dedicate my dissertation to my family who have always been there for me and are truly my world.

ABSTRACT

Longer life expectancies, due to advanced medical care, social, and environmental conditions, helped increase the number and percentage of Americans aging to ≥85. The number of individuals with Alzheimer's disease (AD) age 65 or older is projected to be 7.1 and 13.8 million by 2025 and 2050, respectively. The total annual health care expense for AD patients is estimated to increase from $290 billion in 2019 to more than $1.1 trillion in 2050 (Association, 2019). Conclusively, AD is expected to become a more common cause of death and a major public health predicament due to aging of the baby boom generation in the United States.

Extracellular Aβ plaque deposition resulting from successive proteolytic cleavage of amyloid precursor protein (APP), intracellular neurofibrillary tangles, and neuroinflammation are pathophysiologic features of AD correlating with cognitive decline, language impairment, memory loss, and ultimately, death. Due to the behavioral manifestation and the neurodegenerative hallmarks, AD is typically considered a brain specific disease. However, peripheral inflammatory changes such as increased serum levels of TNF-α, worsen cognitive decline in AD patients. This suggests that systemic inflammatory changes may cross-talk to the brain to influence disease. In support of this idea, long-term use of non-steroidal anti-inflammatory drugs (NSAID) decreases the risk of AD. Interestingly,

colitis and colitis-associated colorectal cancer (CAC), which are characterized by accelerated levels of proinflammatory cytokines, induce anxiety, depression and cognitive/memory dysfunction in preclinical and clinical studies. Taken together, these studies suggest that peripheral immune changes influence AD progression in the brain.

This dissertation consists of three related but separate studies aimed at understanding the impact of peripheral manipulations on brain pathology using AD mouse models. In our first study, we asked whether the liver-derived hormone, insulin like growth factor-1 (IGF-1), has effects in the brain to potentiate or attenuate disease using the AβPP/PS1 mutant mouse model of AD. To test this idea, we used a brain penetrant IGF-1R inhibitor. The second study shifts to focus on peripheral inflammatory manipulations to examine possible influences on disease. This study utilized a common colitis-like model of oral dextran sulfate sodium (DSS) to quantify brain and intestinal changes in the $App^{NL\text{-}G\text{-}F}$ mutant knock-in mouse model of AD. The third study employed a more extensive intestinal inflammatory paradigm of colorectal tumorigenesis to also compare brain and intestinal changes using the $App^{NL\text{-}G\text{-}F}$ mice.

In the first study, the brain penetrant IGF-1R inhibitor (PPP, 1mg/kg/day) attenuated insoluble $A\beta_{1\text{-}40/42}$ and pro-inflammatory cytokine levels (eotaxin, TNF-α, IL-1α, and IL-1β) in the temporal cortices of AβPP/PS1 mice. Additionally, an attenuation in microgliosis and protein p-tyrosine levels was observed due to drug treatment. Our data suggests IGF-1R signaling is associated with disease progression in this mouse model. More importantly, modulation of the brain IGF-

1R signaling pathway was sufficient to attenuate aspects of disease phenotype. This suggested that small molecule therapy targeting liver-derived IGF-1 effects in the brain may be a viable intervention approach.

In the second study, chronic intestinal inflammation, induced by dissolving 2% dextran sulfate sodium (DSS) in the drinking water, resulted in bloody diarrhea, disrupted colonic epithelium, and weight loss in wild type and *App*$^{NL-G-F}$ male mice, changes similar to human inflammatory bowel disease (IBD). The inflammation correlated with increased levels of brain insoluble Aβ$_{1-40/42}$ and decreased microglial CD68 immunoreactivity in DSS treated compared to vehicle treated *App*$^{NL-G-F}$ mice. These data demonstrated that intestinal dysfunction is capable of altering plaque deposition and immune cell behavior in the brain. This study increased our understanding of the impact of peripheral inflammation on Aβ deposition and neuroinflammation in AD via an IBD-like model system.

In the third study, azoxymethane (AOM)/DSS administration produced genotype and sex dependent colitis-associated colorectal cancer (CAC) symptomatic parameters in spleens and colons of wild type, *App*$^{-/-}$, and *App*$^{NL-G-F}$ mice. As expected, AOM/DSS treatment exacerbated Aβ plaque load in male *App*$^{NL-G-F}$ mice. Interestingly, AOM/DSS treated male *App*$^{NL-G-F}$ mice also demonstrated worsened intestinal inflammation and increased colonic tumorigenesis compared to wild types. However, *App*$^{NL-G-F}$ female mice were protected against intestinal inflammation and tumorigenesis as well as any exacerbation of brain Aβ plaque load. These data demonstrated that the AD-associated autosomal dominant mutations of APP introduced into the *App*$^{NL-G-F}$

mouse line provide protection against intestinal disease as well as brain exacerbation in a sex-selective fashion.

Collectively, studies in this dissertation demonstrate that peripheral stimuli, whether hormonal or inflammatory, appear capable of altering disease phenotype in two commonly used mouse models of AD. In addition, there may be sex-selectivity of this peripheral to brain communication during disease. One conclusion from this work is that manipulations of peripheral events may be sufficient to alleviate brain changes in AD. This suggests the exciting possibility that therapeutic interventions need not penetrate into the brain to offer benefit.

CHAPTER I

INTRODUCTION

Dissertation Research Objectives and Organization

Chapter I introduces AD and its pathological characteristics in the brain, the importance of growth factor contribution to disease progression, the gut-brain axis and its relevance to AD, and a possible relationship between AD and gut dysfunction associated with colitis and CAC. Chapter II elaborates our initial effort to determine whether manipulating brain effects of a peripheral signal, IGF-1, could affect plaque deposition and neuroinflammation using an IGF-1R inhibitor and the AβPP/PS1 mouse model of AD. Based upon the success of this intervention, we elected to move away from growth factor interventions and focus instead on understanding whether peripheral inflammatory conditions contributed to brain changes during disease. Chapter III describes our effort to develop the necessary Swiss-roll protocol to study mouse colons histologically. Chapter IV summarizes results obtained using a mouse DSS model of colitis to verify that intestinal dysfunction and inflammation propagates to the brain using the *App*$^{NL\text{-}G\text{-}F}$ mouse model of AD. Chapter V continues assessing colonic inflammation through an AOM/DSS colonic tumorigenesis model to demonstrate that mutant APP expression exacerbates tumorigenesis and Aβ plaque deposition in male *App*$^{NL\text{-}G\text{-}F}$ mice but serves a protective function against both

tumor development and plaque exacerbation in female *App*$^{NL\text{-}G\text{-}F}$ mice. The results of all three studies are discussed in detail in Chapter VI.

Alzheimer's Disease (AD) Discovery and Overview

A 51-year-old woman, Auguste D., was hospitalized in the Frankfurt Community Psychiatric Hospital due to an untreatable paranoid symptomatology followed by a progressive, intensive, and deteriorative sleep disorder, memory disturbances, aggressiveness, crying, and confusion in November 1901. During his senior assistantship at the hospital, Dr. Alois Alzheimer, accurately recorded Auguste's course of disease development and progression until her death on April 8, 1906. The morphological and histological study of her postmortem brain revealed alterations which later would be called plaques and neurofibrillary tangles. This peculiar, severe disease process of the cerebral cortex was reported for the 1st time by Alois Alzheimer at the 37th meeting of South-West German Psychiatrists on November 3, 1906 in Tubingen. Later in 1910, Emil Kraepelin, Alzheimer's colleague, included Dr. Alzheimer's case study on Auguste D. in his 8th edition of *Psychiatrie* textbook and introduced this disorder as Alzheimer's disease (Alzheimer, Stelzmann, Schnitzlein, & Murtagh, 1995; Hippius & Neundörfer, 2003).

In 1984, amyloid protein was first sequenced from the meningeal blood vessels of AD patients by Glenner and Wong. In the same year, they reported the chemical relationship between Down's syndrome (DS) and AD due to the homology of the sequenced cerebrovascular amyloid protein isolated from an adult DS patient and the one from AD, suggesting localization of the genetic

abnormality to chromosome 21 (Glenner & Wong, 1984a, 1984b). A year later, the 40 residue amyloid protein (4 kDa) was isolated from the plaque core of both AD and aged DS brains (Masters et al., 1985). In 1987, Kang and colleagues discovered that the same highly aggregating amyloid protein (A4), purified from blood and cerebral plaque deposits of AD and DS patients, has a neuronal origin and is cleaved from a larger precursor protein containing 695 residues. The β-amyloid precursor protein A4 (APP) is located on chromosome 21 and resembles glycosylated cell surface receptors (Kang et al., 1987). Shortly afterwards, pathogenic mutations were identified in the *APP* gene which resulted in the upregulation of Aβ production in familial early-onset AD (X. D. Cai, Golde, & Younkin, 1993; Citron et al., 1992; Goate et al., 1991; Hendriks et al., 1992; Mullan et al., 1992; Suzuki et al., 1994; Wisniewski, Ghiso, & Frangione, 1991). Based upon these discoveries, the amyloid cascade hypothesis was formulated and described amyloid-beta (Aβ) aggregation as an initial phenomenon in AD pathogenesis. In this hypothesis, neurofibrillary tangles (NFTs), neuronal death, synaptic loss, vascular damage, and subsequent dementia all occur due to Aβ deposition (Hardy & Higgins, 1992).

APP Family

The human APP gene is a single-pass transmembrane protein containing 18 exons and contributes to neuronal development, signaling, intracellular transport, iron export, and homeostasis (G. F. Chen et al., 2017; Kang et al., 1987). It is located on chromosome 21 and belongs to the APP family of proteins. Besides APP, the APP family also includes APP-like protein 1 and 2 (APLP1 and

APLP2) in which the Aβ sequence is missing at the C-terminal end. APP family members consist of a long and diverse extracellular N-terminus and a short cytoplasmic C-terminus (Sprecher et al., 1993; Wasco et al., 1993). The APP gene undergoes alternative splicing to create isoforms with different amino acid lengths, including APP639, APP695, APP714, APP770, and APP751 (Golde, Estus, Usiak, Younkin, & Younkin, 1990; K. L. Puig & Combs, 2013; Tang et al., 2003). Structurally, the dimerization domains (E1 and E2), which bind heparin, zinc, and copper to form homo- or heterodimers, and acidic domain (Ac) are common in extracellular regions of APP family proteins, including APP695 and APLP1. APP751 contains a Kunitz protease inhibitor (KPI) domain in exon 7. Whereas, APP770 and APLP2, additional to the KPI domain, also carry an Ox-2 antigen (OX2) domain located in exon 8. Although APP695 and APLP1 are chiefly expressed in the brain, other APP isoforms and APLP2 are ubiquitously expressed in multiple organs throughout the body (Nalivaeva & Turner, 2013; van der Kant & Goldstein, 2015).

APP Processing

Missense mutations in the *APP* gene, which promote APP cleavage by β-site APP-cleaving enzyme 1 (BACE1) in secretory vesicles, as well as mutations in γ-secretase subunit (*presenilin*, *PSEN1* and *PSEN2*) genes lead to overproduction and secretion of Aβ in familial early-onset AD (EOAD). EOAD occurs before age 65 and accounts for about 5% of patients (Awada, 2015; Haass et al., 1995). Impaired Aβ clearance mediated by apolipoprotein E (APOEε4) is considered a primary pathologic event in sporadic late-onset AD

(LOAD), which accounts for almost 95% of all AD cases (Corder et al., 1993; Strittmatter et al., 1993; Yamazaki, Painter, Bu, & Kanekiyo, 2016).

Like other transmembrane proteins, APP translation occurs in the endoplasmic reticulum. The newly synthesized protein is transported to the trans Golgi network apparatus for posttranslational modifications and subsequently trafficked to the cell surface membrane via the secretory pathway (Greenfield et al., 1999; Walter & Haass, 2000). APP is processed by two distinct pathways, including the amyloidogenic APP processing pathway and non-amyloidogenic APP processing pathway. Different APP posttranslational modifications, i.e. N- and O-linked glycosylation, phosphorylation, ubiquitination, and tyrosine sulfations, may cause this transmembrane protein to favor one pathway over another. With a highly conserved YENPTY motif in the intracellular C-terminal end, APP binds to different intracellular adaptors, i.e. APP-binding family A (APBA or MINT) members and APP-binding family B member 1 (APBB1 or FE65), for various cytosolic trafficking and delivery to proteases (Agostinho, Pliassova, Oliveira, & Cunha, 2015; Jiang et al., 2014; King & Scott Turner, 2004).

In the amyloidogenic pathway, an intracellular adaptor protein, FE65, (APBB1) via its two distinct phosphotyrosine-binding (PTB) domains, binds to the NPXY (from a larger motif YENPTY) motifs presented in the C-terminus of both APP and Low-density lipoprotein receptor (LDLR)-related protein 1 (LRP1) (Fig. I-1A and C). This intracellular interaction results in rapid clathrin-mediated

Figure I- 1. APP amyloidogenic and non- amyloidogenic processing pathways.
A) In the amyloidogenic pathway, (1) binding of FE65 to the NPXY C-terminal motifs of APP and LRP1 (2) triggers a rapid clathrin-mediated internalization of APP. (3) In the acidic milieu of endosome (pH 4.5), APP is cleaved by β-secretase BACE1 to generate luminal sAPPβ and endosomal membrane-bound C99. (4) C99 is further processed by γ-secretase to release Aβ peptide and AICD fragments into the endosomal lumen and cytoplasm, respectively. (5) Mostly, sAPPβ and Aβ are recycled to the plasma membrane and exocytosed. Secreted Aβ monomers self-aggregate to form oligomers, protofibrils, insoluble fibrils, and subsequent Aβ plaques. (6) AICD is translocated into the nucleus to function as a transcription factor.
B) In the non-amyloidogenic pathway, (1) APP is retained at the cell surface where it is cleaved within the Aβ sequence by α-secretase to (2) release the extracellular sAPPα and produce a cell membrane-bound C83. (3) Following endocytosis, (4) C83 is cleaved by γ-secretase to generate luminal P3 and cytoplasmic AICD fragments. (5) P3 is secreted extracellularly and (6) AICD is translocated to nucleus, finally.
C) Summary of APP amyloidogenic and non-amyloidogenic processing pathways. APP, amyloid precursor protein; FE65 (APBB1), APP-binding family B member 1; LRP1, Low-density lipoprotein receptor (LDLR)-related protein 1; sAPPβ, soluble APPβ; C99 (CTFβ), membrane-bound C-terminal fragment-β; AICD, APP intracellular domain; sAPPα, soluble sAPPα; C83 (CTFα), membrane-bound C-terminal fragment-α. Created with Biorender.com.

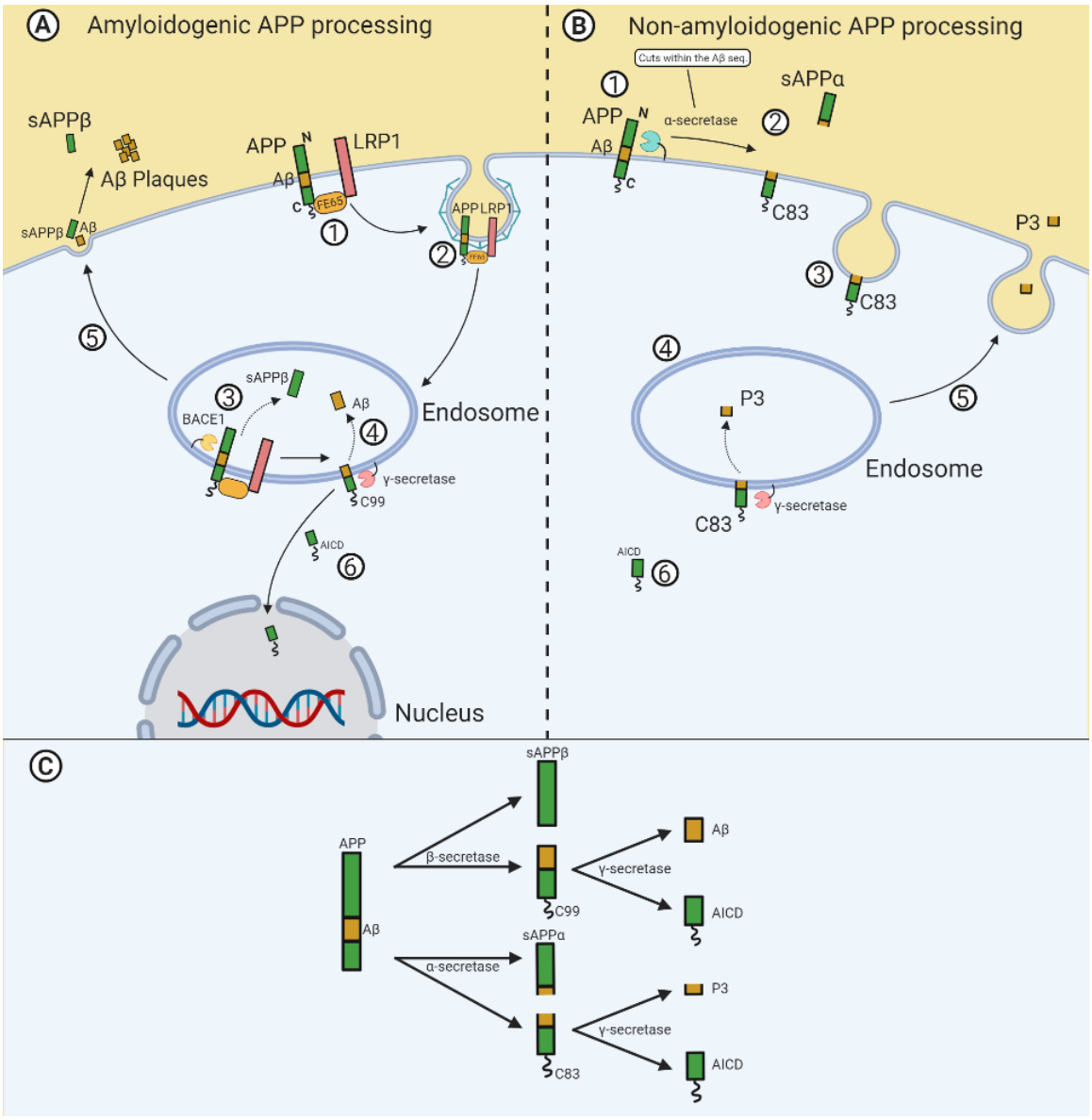
A
Amyloidogenic APP processing
sAPPβ
Aβ Plaques
APP
LRP1
Aβ
FE65
APP LRP1
sAPPβ
Aβ
BACE1
Endosome
γ-secretase
C99
AICD
Nucleus
B
Non-amyloidogenic APP processing
Cuts within the Aβ seq.
sAPPα
APP
α-secretase
Aβ
C83
P3
C83
P3
Endosome
C83
γ-secretase
AICD
C
sAPPβ
APP
β-secretase
Aβ
C99
Aβ
γ-secretase
AICD
sAPPα
α-secretase
P3
γ-secretase
C83
AICD

endocytic trafficking of APP (Cam, Zerbinatti, Li, & Bu, 2005; Nordstedt, Caporaso, Thyberg, Gandy, & Greengard, 1993; Pietrzik et al., 2004; Trommsdorff, Borg, Margolis, & Herz, 1998; F. Wu & Yao, 2009). Plasma membrane milieu (pH 7.5) is not optimal for β-secretase BACE1 activity. Subsequently, APP is cleaved by BACE1, which is activated in the acidic milieu of endosomes (pH 4.5), to release soluble APPβ (sAPPβ) in the endosomal lumen. Although it can be degraded by merging with lysosomes, sAPPβ is also recycled toward the cell surface membrane and exocytosed. The membrane-bound C-terminal fragment-β (CTFβ also known as C99) in the endosomal membrane is then processed by γ-secretase to generate a hydrophobic 37 to 49 amino acid Aβ peptide (4kDa) which can be secreted into the extracellular milieu via exosomes. Almost 90% of γ-secretase product is soluble $A\beta_{40}$ with the remaining portion as highly fibrillogenic $A\beta_{42}$ and $A\beta_{43}$ peptides which are often deposited in amyloid plaque cores. Upon γ-secretase cleavage, the APP intracellular domain (AICD) is released to the cytoplasm and translocated to the nucleus as a transcription factor (Cole & Vassar, 2007; De Strooper, 2003; Hussain et al., 1999; Konietzko, 2012; Lin et al., 2000; Nunan & Small, 2000; Rajendran et al., 2006; Sinha et al., 1999; Sisodia & St George-Hyslop, 2002; Thinakaran & Koo, 2008; Van Gool et al., 2019; Vassar et al., 1999; Yan et al., 1999). Secreted Aβ monomers, mostly $A\beta_{40}$ and $A\beta_{42}$, spontaneously self-aggregate to form soluble oligomers, protofibrils, insoluble larger fibrils, and amyloid plaques which are hypothesized to subsequently lead to disruption of

normal brain architecture, neuronal degeneration, and cognitive impairment in AD (Glenner & Wong, 1984b; Graham, Bonito-Oliva, & Sakmar, 2017).

Due to its slow rate of endocytosis, LRP1B association with APP is known to retain APP at the plasma membrane and promote the non-amyloidogenic pathway of metabolism (Cam et al., 2004). In this mechanism, APP is initially cleaved by α-secretase at the plasma membrane within the Aβ sequence (between amino acid 16 and 17) to extracellularly liberate a soluble APPα (sAPPα) ectodomain and to produce a membrane-bound C-terminal fragment-α (CTFα also known as C83). CTFα is endocytosed and further cleaved by γ-secretase to produce P3 (3 kDa) and ACID fragments (Golde, Estus, Younkin, Selkoe, & Younkin, 1992; Haass & Selkoe, 1993; Sisodia, 1992; Thinakaran & Koo, 2008) (Fig. I-1B and C).

Brain Changes in AD

Tens of billions of neurons transmit chemical and electrical signals between different brain regions and from the brain to other parts of the body in a healthy individual. Unlike most cells in human body, neurons continuously repair themselves and remodel their synaptic connections with other neurons. Neurogenesis, as well as remodeling, play a pivotal role in learning and memory. Brain shrinkage resulting from AD is due to neuronal loss, particularly, in brain regions involved in memory, language, and social behavior, including the entorhinal cortex and hippocampus as well as the cerebral cortex, respectively. Three important brain changes associated with AD include Aβ aggregation, NFTs, and brain chronic inflammation (Association, 2019; Health, 2018).

Cytotoxic deposition of Aβ plaques, which results from APP processing, is hypothesized to extracellularly interfere with neuronal communication leading to cell death (Association, 2019; Glenner & Wong, 1984b; Health, 2018). In healthy neurons, microtubules are stabilized by tau proteins and involved in transporting cargo along the cell. Hyperphosphorylation of tau in AD is hypothesized to cause disintegration of microtubule subunits due to decreased binding affinity of tau proteins to microtubules. Hyperphosphorylation of tau is mainly hypothesized to occur by the actions of glycogen synthase kinase 3β (GSK-3β), cyclin-dependent protein kinase 5 (cdk5), and cAMP-dependent protein kinase (PKA). Intracellular NFTs, resulting from accumulation of hyper and abnormal phosphorylation of microtubule-associated tau protein, presumably disrupts soma to dendrite and axons internal communication and the neuronal transport system (Association, 2019; Brunden, Trojanowski, & Lee, 2009; Health, 2018; Liu et al., 2006; Terry, 1963).

Microglia are brain resident macrophages which comprise the first line of cellular defense against brain injuries, pathogen invasions, and host-derived ligands, including pathogen-associated molecular patterns (PAMPs) and danger-associated-associated molecular patterns (DAMPs), recognized by pattern recognition receptors (PRRs). Removing the damaged cells by microglia restores the normal brain environment or cerebral homeostasis. Microglia undergo morphological changes from ramified cells to an activated amoeboid phenotype during phagocytosis. It has been well established that APP and Aβ activate microglia by triggering phagocytosis though PRRs and secretion of

proinflammatory mediators (i.e. IL-1β, IL-6, and TNF-α). Short-term secretion of proinflammatory cytokines promotes Aβ uptake by activated microglia. As the microglia age, they demonstrate phenotype changes and compromised activation toward stimulations, including Aβ, which may lead to neuronal damage and the increased risk of AD. In other words, the production of microglial inflammatory markers is chronically upregulated in AD due to long-term Aβ exposure and DAMPs accumulation. This leads to compromised microglial Aβ clearance activity (Fetler & Amigorena, 2005; Kigerl, de Rivero Vaccari, Dietrich, Popovich, & Keane, 2014; Kreutzberg, 1996; Nimmerjahn, Kirchhoff, & Helmchen, 2005; Ransohoff & Perry, 2009; Sarlus & Heneka, 2017; Streit, Miller, Lopes, & Njie, 2008) (Fig. I-2).

TREM2 is a cell surface receptor expressed on myeloid cells and is required for microglial phagocytosis of different substances, including Aβ. The combination of Aβ with TREAM2 ligands (LDL, APOE, and CLU lipoproteins) facilitates their uptake by microglia. The presence of mutations in TREM2 or the deleterious APOE4 isoform, primarily secreted by astrocytes, impairs the microglia phagocytic activity and advances the risk of AD. Among the *ε2*, *ε3*, and *ε4 APOE* alleles, which only differ in one amino acid, the APOEε4 isoform drastically increases the risk of LOAD (Castellano et al., 2011; D. V. Hansen, Hanson, & Sheng, 2018; Wolfe, Fitz, Nam, Lefterov, & Koldamova, 2018).

Figure I- 2. (1) Aβ is extracellularly secreted via the APP amyloidogenic processing pathway from neurons. (2) A can self-aggregate to form extracellular plaque deposition. (3) Aβ is intracellularly cleared via either the phagocytosis-associated combination of APOE (predominantly secreted by astrocytes) and TREM2 (microglial cell surface receptor) by microglia/macrophages or (4) APOE and LRP1-mediated endocytosis and lysosomal degradation through microglia, astrocytes, neurons, etc. (5) Clearance of Aβ also occurs through both extracellular proteolytic enzymes, including NEP, IDE, and MMP, and (6) LRP1-associated efflux across the BBB to the periphery. (7) Inversely, RAGE receptor influx of Aβ into the brain occurs across the BBB. (8) Extracellular Aβ along with intracellular neurofibrillary tangles, resulting from accumulation of hyperphosphorylated-tau, lead to neuronal death and synaptic loss. BBB, blood-brain barrier; NEP, neprilysin; IDE, insulin degrading enzyme; MMP, matrix metalloproteinase. Created with Biorender.com.

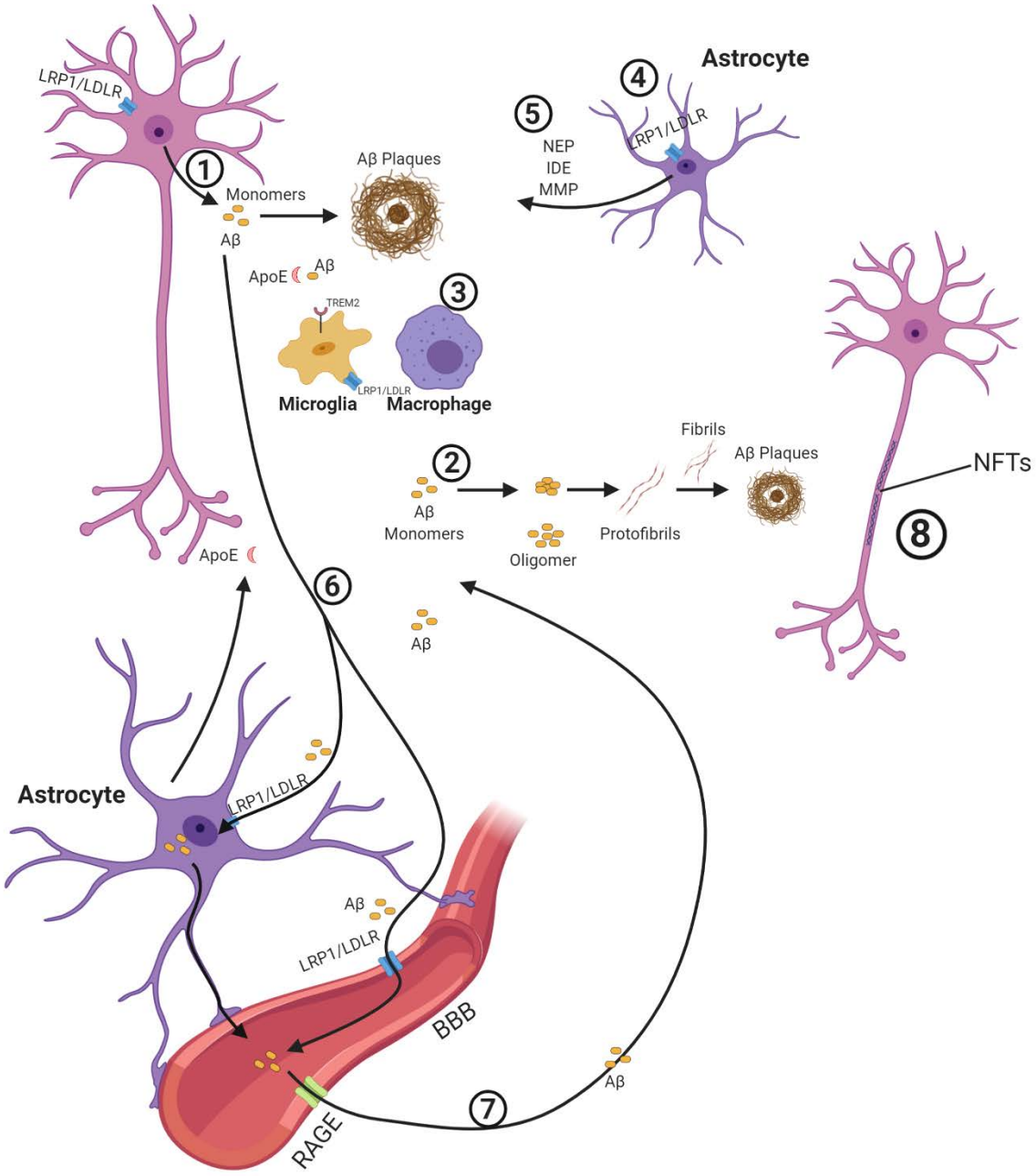
LRP1/LDLR
1
Monomers
Aβ
Aβ Plaques
ApoE
Aβ
TREM2
LRP1/LDLR
3
Microglia
Macrophage
Astrocyte
4
5
NEP
IDE
MMP
LRP1/LDLR
2
Aβ
Monomers
Oligomer
Protofibrils
Fibrils
Aβ Plaques
NFTs
8
ApoE
6
Aβ
Astrocyte
LRP1/LDLR
Aβ
LRP1/LDLR
BBB
RAGE
7
Aβ

The neurovascular unit in the central nervous system (CNS) consists of endothelial cells, pericytes, multiple layers of smooth muscle cells, basement membrane/basal lamina, astrocytes, neurons, and perivascular microglial cells. Vascular cells and astrocyte endfeet comprise the blood-brain barrier (BBB). Astrocytes control homeostasis of the CNS via modulating glutamatergic neurotransmission, oxidative stress regulation, growth factor secretion, regulating the extracellular neurotransmitters and ion concentrations, energy storage, and tissue repair following traumatic injuries. LDLR-related proteins (APOE and APP receptors), i.e. LRP1 and VLDLR, and advanced glycation end products (RAGE) receptors are two types of receptors which are involved in Aβ efflux into the blood circulation and Aβ influx into the brain across the BBB, respectively. A decrease in LRP1 and an increase in RAGE expression levels in AD can lead to BBB dysfunction and failure of Aβ clearance. Astrocytes secret APOE, apolipoprotein J (APOJ) or clusterin, α1-antichymotrypsin (ACT), and α2 macroglobulin (α2-M) extracellular chaperones which mediate Aβ clearance by facilitating its uptake via receptor-mediated endocytosis and transportation across the BBB. Compared to APOE4, APOE3 more effectively clears Aβ due to its higher affinity toward this protein. Beside astrocytes, other brain parenchyma cells including microglia, and neurons, endothelial cells, and smooth muscle cells are all involved in LRP1/LDLR receptor-mediated Aβ clearance. Reactive astrocytes also express endoproteases for cleavage and degradation of monomeric, oligomeric, and fibrillar forms of Aβ. These proteolytic enzymes include metalloendopeptidases neprilysin (NEP), insulin degrading enzyme (IDE), endothelin-converting

enzymes-1 and -2 (ECE1 and ECE2) as well as matrix metalloproteinase-2 and -9 (MMP-2 and MMP-9). Extensive proliferation of reactive astrocytes in AD results in an abnormal regulation of ionic concentrations, neurotransmitter transportations, energy metabolism and Aβ clearance (Beach, Walker, & McGeer, 1989; Bu, 2009; Z. Cai et al., 2018; Carter et al., 2019; Deane, Bell, Sagare, & Zlokovic, 2009; Itagaki, McGeer, Akiyama, Zhu, & Selkoe, 1989b; Ries & Sastre, 2016).

Topographical Distribution of Aβ and Neurofibrillary Tangles

The progressive Aβ deposition in different regions of the brain is classified into five phases. Phase 1 includes the deposition of Aβ plaques in the frontal, parietal, temporal, or occipital neocortex. Phase 2 is characterized by spreading plaque deposition into the allocortical regions, including the entorhinal region, CA1, and insular cortex. Diencephalic nuclei, caudate nucleus, putamen, substantia innominata, and the magnocellular cholinergic nuclei of the basal forebrain comprise the subcortical regions which are affected in phase 3. Additional β-amyloidosis occurs in specific brainstem nuclei, including inferior olivary nucleus, the reticular formation of the medulla oblongata, and the substantia nigra, in phase 4. Phase 5 is characterized by Aβ deposition in cerebellum and additional brainstem nuclei (Thal, Rub, Orantes, & Braak, 2002). In contrast, NFTs distribute into brain regions via six stages. Stage I is characterized by mild alterations in the transentorhinal region. Stage II is more aggressive and demonstrates tangles in the transentorhinal Pre-α and entorhinal Pre-α along with mild involvement of the hippocampus CA1 region. The

entorhinal and transentorhinal layer Pre-α are severely involved in stages III-IV. Stages III-IV are also called limbic III-IV stages due to aggregation of NFTs in limbic structures such as the subiculum of the hippocampal formation (stage III) and amygdala, thalamus as well as claustrum (stage IV). Finally, the neurofibrillary degeneration occurs in all isocortical areas in stages V-VI (Braak & Braak, 1991).

Trophic Factors and AD

Nerve growth factor (NGF), a neurotrophic factor, was discovered by Rita Levi-Montalcini in 1950 for its potential role to promote survival and development of sympathetic and sensory neurons in the peripheral nervous system. In the CNS, NGF regulates cholinergic neuronal survival, plasticity, and function (Hefti, Hartikka, & Knusel, 1989; Levi-Montalcini, 1987). NGF binds to two NGF-receptors (1) the high-affinity tropomyosin-related kinase receptor ($TrkA^{NGFR}$) with tyrosine kinase activity and (2) the low-affinity transmembrane glycoprotein pan-neurotrophin receptor ($p75^{NTR}$) to initiate signal transduction pathways (Huang & Reichardt, 2003). Due to the loss of cholinergic neurons in the basal forebrain associated with cognitive deficit and impairment of NGF signaling in AD, NGF is considered one potential therapeutic intervention (Bartus, Dean, Beer, & Lippa, 1982; K. S. Chen et al., 1997; Hampel et al., 2019; Latina et al., 2017; Mitra, Behbahani, & Eriksdotter, 2019).

Brain-derived neurotrophic factor (BDNF) is a member of the neurotrophin family that was discovered in 1982 (Barde, Edgar, & Thoenen, 1982). BDNF is synthesized in the cortex, hippocampus, and basal forebrain areas which are

involved in memory, learning, and cognitive functions. It promotes neurogenesis, neuronal survival, and function as well as synaptogenesis and synaptic plasticity via binding to TrkB and $p75^{NTR}$ receptors (Acheson et al., 1995; Huang & Reichardt, 2003; B. Lu, Nagappan, Guan, Nathan, & Wren, 2013). Reduced levels of BDNF were reported in patients with mild cognitive impairment, serum of AD patients, and AD postmortem brains (T. K. S. Ng, Ho, Tam, Kua, & Ho, 2019; Tanila, 2017).

The proangiogenic vascular endothelial growth factor (VEGF) was isolated and characterized by Napoleone Ferrara in 1989 (Ferrara, 2011). Besides enhancing angiogenesis and vasculogenesis via binding to tyrosine kinase receptors of endothelial cells, VEGF contributes to neuroprotection and neurogenesis (Jin et al., 2002; Millauer et al., 1993; Storkebaum, Lambrechts, & Carmeliet, 2004). VEGF binds to receptor tyrosine kinases, VEGFR1-R3, with high affinity (Simons, Gordon, & Claesson-Welsh, 2016). VEGF mediates angiogenesis, neurogenesis, neuroprotection, and astroglial proliferation in the neurovascular unit as well as memory improvement via neuronal plasticity and increasing long-term potentiation in the dentate gyrus (Argandona et al., 2012; Jin et al., 2002; Licht et al., 2011). VEGF is considered a potential marker to detect vascular alterations in AD (Mateo et al., 2007; Provias & Jeynes, 2014; J. B. Zhang et al., 2016).

Insulin growth factor-1 (IGF-1), or somatomedin, was characterized by Salmon and Daughaday in 1957 due to its ability to stimulate sulfate incorporation into cartilage (Salmon & Daughaday, 1957). IGF-1 exerts it effect

through binding to type I IGF-1 receptor (IGF-1R), a type 2 tyrosine kinase receptor. IGF-1 and IGF-1R have 40% and 60% amino acid sequence homology to proinsulin and insulin receptor (Samani, Yakar, LeRoith, & Brodt, 2007). Secretion of GH-releasing hormone (GHRH) from the hypothalamus stimulates expression of GH by the pituitary gland. This results in the subsequent secretion of IGF-1 by the liver. Although many tissues produce IGF-1, which functions through both autocrine/paracrine pathways, the liver is the main source of circulating IGF-1 (Baxter, 1986; V. S. Lim, 2010; Moller & Becker, 1992). A deficiency in GH-IGF-1 axis which leads to reduction of GH and IGF-1 signaling extends lifespan in animal models (Flurkey, Papaconstantinou, Miller, & Harrison, 2001; L. Kappeler et al., 2008; Sun et al., 2013).

Brain-Gut-Microbiota Axis in AD

In the 19th and early 20th century, association of the brain with the gut was critically investigated by William Beaumont, Ivan Petrovich Pavlov, Walter Bradford Cannon, Stewart Wolf (Aziz & Thompson, 1998). Later, the pivotal role of gut flora in modulating the gut-brain axis was recognized (Rhee, Pothoulakis, & Mayer, 2009). The central nervous system (CNS), including the brain and spinal cord, bi-directionally communicates with the gastrointestinal (GI) tract, its enteric nervous system (ENS), and the gut microbiota via the sympathetic and parasympathetic (vagus nerve) fibers, the hypothalamic-pituitary-adrenal (HPA) axis, endocrine (gut hormones) signaling, the immune system, metabolic (tryptophan) signaling, and microbial metabolites (short-chain fatty acids). This

well-established connection is called the brain-gut-microbiota axis (Dinan & Cryan, 2017; J. B. Furness, Callaghan, Rivera, & Cho, 2014) (Fig. I-3).

In 1899, the ENS was discovered by W.M. Bayliss and E.H. Starling via defining “the law of the intestine”, in which intestinal neural circuitry intrinsically generates gut motility. This is now known as the peristaltic reflex (Bayliss & Starling, 1899; M. B. Hansen, 2003). Later, it was reported that the ENS is developed by migration of cells from vagal neural crest to the mammalian bowel and colonization in the gut during embryogenesis (Gershon, Chalazonitis, & Rothman, 1993). The human ENS contains 200-600 million neurons which spread out along the GI tract via two major ganglionic and intervening nerve plexuses, including the myenteric and submucosal plexuses (J. B. Furness et al., 2014). The myenteric (Auerbach’s) plexus is located between the longitudinal and circular smooth muscle layers in the muscularis externa. It contains the majority of ENS neurons and extends along the digestive tract, inward towards the mucosa or outward towards the serosa, to regulate bowel relaxation and contraction. The submucosal (Meissner’s) plexus is situated within the connective tissue of the submucosa layer. It is adjacent to the intestinal lumen and distributed from the stomach through the rectum and controls epithelial secretion and local blood flow (John Barton Furness, 2006; Jabbur, el-Kak, & Nassar, 1988; Schneider, Wright, & Heuckeroth, 2019). Furthermore, the ENS, via releasing neurotransmitters, regulates the gut immune system. The epithelial cells, which line the mucosal surfaces, absorb nutrients and provide a barrier between the mucosal immune system and luminal contents, such as digestive

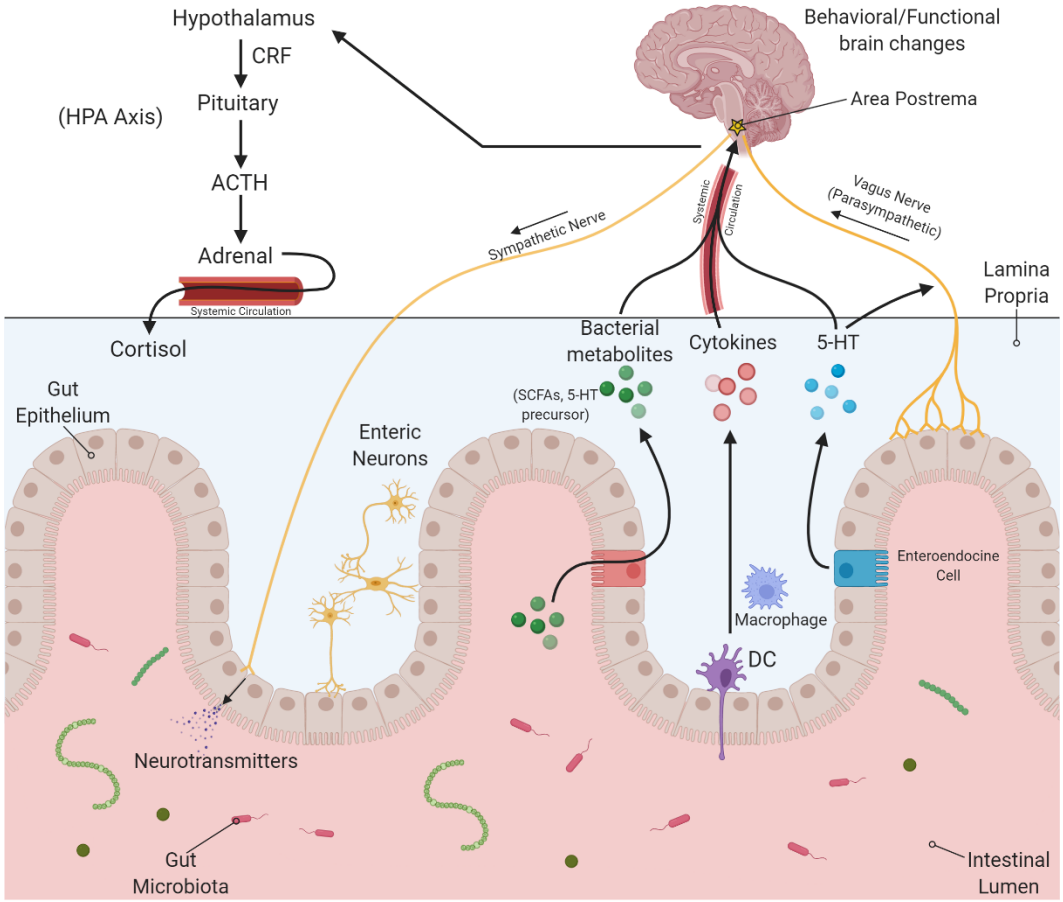

Figure I- 3. The bidirectional microbiota-gut-brain axis. Intestinal bacteria communicate with the brain via (1) endocrine (eg. cortisol) and metabolic, (2) immune (eg. cytokines), and (3) neural (vagus, sympathetic, and enteric nervous system) pathways. Cortisol secretion from the HPA axis via systemic circulation regulates the immune system, gut permeability and barrier function as well as gut microbial composition. The secreted neurotransmitters from the sympathetic nervous system modulate intestinal physiology as well as microbial composition. Conversely, gut microbiota send signals to the brain and influence behavior via releasing bacterial metabolites (eg. 5-HT precursors and SCFAs), induction of cytokine secretion from immune cells, neurotransmitter secretion from enteroendocrine cells (eg. 5-HT), and vagal (parasympathetic) afferent nerves. HPA, hypothalamus-pitutary-adrenal axis; CRF, corticotropin-releasing factor; ACTH, adrenocorticotropic hormone; 5-HT, 5-hydroxytryptamine; SCFAs, short-chain fatty acids; DC, dendritic cell; MQ, macrophage. Created with Biorender.com.

enzymes, toxins, and gut microbiota (Collins, Surette, & Bercik, 2012; Turner, 2009).

The ENS interacts with sympathetic and parasympathetic nervous systems, comprising the autonomic nervous system, which are a part of the peripheral nervous system. Unlike sympathetic and parasympathetic neurons, the ENS receives almost no afferent (sensory input) and efferent (motor output) fibers from the CNS and can independently control gastrointestinal behavior (Waxenbaum & Varacallo, 2019). Due to the fact that the number of enteric neurons outnumbers the total sympathetic and parasympathetic neurons and its phenotypic diversity, neurotransmitters, and signaling molecules are similar to the CNS, the ENS has been called a “second brain” or “the brain within the gut” (J. B. Furness et al., 2014; Gershon, 1999; Goldstein, Hofstra, & Burns, 2013). The sympathetic nervous system, via releasing the neurotransmitters from adrenergic neurons, such as norepinephrine, decreases intestinal motor function and secretion as well as changes the gut microbial composition. The vagus nerve, the major element of the parasympathetic nervous system and consisting of 80-90% afferent and 10-20% efferent fibers, is responsible for transferring information between the gut, the largest surface area exposed to the outside world, and the brain. (Breit, Kupferberg, Rogler, & Hasler, 2018; Collins et al., 2012; Tubbs et al., 2015).

The hypothalamic-pituitary-adrenal (HPA) axis, enteroendocrine system, and mucosal immune system comprise the humoral aspect of the brain-gut-microbiota axis. Enteroendocrine cells secrete cholecystokinin, ghrelin, and 5-

hydroxytryptamine (5-HT) to mediate this bi-directional communication. In response to stress, corticotropin-releasinng factor (CRF) is secreted from the paraventricular nucleus (PVN) located in hypothalamus and causes the secretion of adrenocorticotropic hormone (ACTH) from the pituitary gland into the systemic circulation. This leads to the release of glucocorticoids (cortisol), epinephrine, and norepinephrine from the adrenal gland cortex. The HPA axis, the major neuroendocrine system, interacts with the gut microbiota, which includes 100 trillion cells and encodes more than 3.3 million non-redundant genes, over 100-fold more genes than the human host genome (Collins et al., 2012; Farzi, Fröhlich, & Holzer, 2018; Qin et al., 2010).

The Gram-positive *Firmicutes* (~51%) and Gram-negative *Bacteroidetes* (~48%) along with *Cyanobacteria*, *Fusobacteria*, *Proteobacteria*, *Spirochetes*, *Verrucomicrobia* as well as different species of fungi, protozoa, and viruses (~1%) comprise the GI tract microbiota (Hill et al., 2014). Bacterial metabolites as well as secreted cytokines and hormones from mucosal immune cells and enteroendocrine cells in response to gut microbiota, respectively, can reach the brain via the bloodstream and area postrema or vagus nerve (Collins et al., 2012).

Considering the fact that the brain bi-directionally communicates with the gut, CNS disorders may be affected by a dysfunctional GI tract and pathophysiologically, one may precede the other (Kujawska & Jodynis-Liebert, 2018). For instance, autism spectrum disorder (ASD) is a neurodevelopmental disease which manifests early in life via deficits in social interaction and

communication as well as repetitive behaviors. Meta-analysis studies report dramatic prevalence of GI dysfunction in ASD children compared to healthy controls (McElhanon, McCracken, Karpen, & Sharp, 2014).

Parkinson's disease (PD), a neurodegenerative disorder, is diagnosed by non-motor (olfactory disturbances, sleep disorders, depression, and constipation) symptoms and motor (bradykinesia, rigidity, tremor, and postural instability) manifestations correlating with intracellular α-synuclein aggregation and loss of dopaminergic neurons. Precedence of constipation before development of motor symptoms and also accumulation of α-synuclein in the ENS as well as dorsal motor nucleus of the vagus nerve, support the idea that PD pathological hallmarks may originate in the ENS by mucosal invasion of a neurotropic pathogen that is later transmitted to the CNS (Braak, Rub, Gai, & Del Tredici, 2003; Klingelhoefer & Reichmann, 2015; Kujawska & Jodynis-Liebert, 2018).

APP is expressed in human neuronal (ENS) and non-neuronal tissues (endothelial cells) of the GI tract (Cabal et al., 1995). In addition, Aβ has been detected in non-neural tissues of some aged healthy individuals and in non-neural tissues, including intestine and blood vessels, of AD patients as well as in the ENS of APP overexpressing transgenic mice, suggesting that AD may be a systemic disorder (Joachim, Mori, & Selkoe, 1989; Semar et al., 2013). Elevated levels of APP and Aβ in the ENS and intestinal epithelial cells correlates with increased levels of luminal IgA, phenotype changes of immune cells, and proinflammatory markers in the AβPP/PS1 mouse model of AD. These results

are consistent with findings in the intestines of AD patients (K. L. Puig et al., 2015).

Inflammatory Bowel Disease (IBD)- Colitis

Inflammatory bowel disease (IBD), including Crohn's disease and ulcerative colitis, is a chronic relapsing inflammatory disease with increasing incidence and prevalence. IBD develops in young adulthood and continues throughout life. Aged individuals with IBD consist of patients with elderly-onset occurring at age ≥ 60 years and older patients who were diagnosed at younger ages (Cosnes, Gower-Rousseau, Seksik, & Cortot, 2011; Taleban, Colombel, Mohler, & Fain, 2015). It is clinically characterized by diarrhea+/- blood, abdominal pain, weight loss, and fatigue (Neurath, 2014). Anxiety, depression, and cognitive and memory dysfunctions are also characterized in IBD patients (Attree, Dancey, Keeling, & Wilson, 2003; Kurina, Goldacre, Yeates, & Gill, 2001; Petruo, Zeißig, Schmelz, Hampe, & Beste, 2017). Epithelial monolayer lining in the GI tract is a dynamic barrier which is maintained intact by the balance between epithelial apoptosis and proliferation (Chassaing, Aitken, Malleshappa, & Vijay-Kumar, 2014a). Genetic, environmental factors, and irregular immune response to gut microbiota may cause epithelial barrier dysfunction in the intestinal mucosa, although the genetic contribution to elderly-onset IBD is less than young-onset disease (Ananthakrishnan et al., 2016; Taleban et al., 2015). Subsequent to bowel epithelial damage, commensal bacteria and microbial metabolites are translocated into the bowel wall, where intestinal immune cells, such as dendritic cells and macrophages, are activated via toll-like receptor

(TLR) signaling and secrete large amount of pro-inflammatory cytokines, including IL-1β, IL-6, IL-18, and TNF-α. The imbalance between extreme and deficient apoptosis and/or anti-inflammatory and pro-inflammatory immune responses develops into GI tract diseases including chronic intestinal inflammation (Chassaing et al., 2014a; Neurath, 2014; S. C. Ng et al., 2011). Initiation of inflammation in the gut may induce CNS changes which lead to altered brain functions. For example, TNF-α is the main pro-inflammatory cytokine in IBD pathology and is targeted for treatment of the disease (Ślebioda & Kmieć, 2014). Increased serum levels of TNF-α due to systemic inflammation exacerbates cognitive impairment and neurodegeneration through activation of primed microglia in AD subjects (Holmes et al., 2009). Additionally, the brain may contribute to IBD severity and pathogenesis. Chronic stress, stressful life events, and depression exacerbate IBD, likely, via the autonomic nervous system and the HPA axis, the two stress pathways (Bernstein et al., 2010; Mawdsley & Rampton, 2005; Sgambato, Miranda, Ranaldo, Federico, & Romano, 2017).

Colitis-Associated Colorectal Cancer (CAC)

Colorectal cancer (CRC) is the third most common cancer-associated cause of death in the United States, according to the CDC. In most cases, a somatic mutation in Wnt signaling pathway genes results in sporadic CRC. It is occasionally caused by hereditary mutations, such as familial adenomatous polyposis (FAP) and hereditary non-polyposis CRC (HNPCC) caused by Lynch syndrome (Groden et al., 1991; Mármol, Sánchez-de-Diego, Pradilla Dieste, Cerrada, & Rodriguez Yoldi, 2017; Rowan et al., 2000). Prolonged non-resolving

ulcerative colitis, which was first reported in the 1920s, also contributes to CRC development but to a lesser extent (BARGEN, 1928; Breynaert, Vermeire, Rutgeerts, & Van Assche, 2008; Jess, Frisch, & Simonsen, 2013). Pro-inflammatory cytokines, including IFN-γ and TNF-α, exacerbate colonic barrier loss and ulcers via tight junction dysregulation and promoting intestinal epithelial cell apoptosis (Nava et al., 2010; Su et al., 2013). Whereas, intestinal activation of IL-22-STAT3 leads to mucosal wound healing. Additionally, IL-6 through the NF-κB-IL-6-STAT3 cascade prevents apoptosis of normal and pre-malignant intestinal epithelial cells (IECs) and promotes tumorigenesis of tumor initiating IECs (Greten et al., 2004; Grivennikov et al., 2009; Pickert et al., 2009). These results suggest that cytokine imbalance plays a pivotal role in dysregulation of IEC proliferation contributing to colitis-associated colorectal cancer (CAC).

In CAC, early mutations in the tumor suppressor *p53* gene in IECs and the presence of TNF-α and PAMPs lead to NF-κB upregulation. Subsequently, NF-κB activation can induce IL-6 secretion involved in tumorigenesis as well as ROS activation which causes DNA damage followed by loss of the *APC* gene as a late event in this type of CRC (Bollrath & Greten, 2009; Cooks et al., 2013; Grivennikov et al., 2009; Kameyama et al., 2018; Tilstra et al., 2012). Barrier disruption as a result of colonic dysplasia causes bacterial invasion into the lamina propria and exacerbates the tumor pro-inflammatory milieu (Brennan & Garrett, 2016).

An inverse relationship between AD and cancer risk is reported in different human and animal studies (Ham et al., 2018; Ibáñez, Boullosa, Tabarés-

Seisdedos, Baudot, & Valencia, 2014; J. E. Lee, Kim, & Lee, 2018; Musicco et al., 2013; Sherzai, Parasram, Haider, & Sherzai, 2020). However, an epidemiological investigation revealed that high constipation prevalence is common in both AD and CRC (T. Zhang et al., 2018).

CHAPTER II

IGF-1R INHIBITOR AMELIORATED NEUROINFLAMMATION IN AN ALZHEIMER'S DISEASE TRANSGENIC MOUSE MODEL

Introduction

Alzheimer's disease (AD), as the most common form of dementia, comprises 60%-80% of all cases ("2016 Alzheimer's disease facts and figures," 2016). Extracellular amyloid β (Aβ) plaques and intracellular neurofibrillary tangles are AD pathological features hypothesized to lead to neuronal death and cognitive dysfunction (Glenner & Wong, 1984b; Terry, 1963). Since aging is the main risk factor for AD, slowing down this process may delay disease onset or progression (Guerreiro & Bras, 2015). The growth hormone (GH)/insulin-like growth factor (IGF-1) signaling pathway is hypothesized to be one of the primary pathways regulating lifespan in general. Partial inactivation of the IGF-1 receptor (IGF-1R) gene or insulin-like signaling extends longevity and postpones age-related dysfunction in nematodes, flies, and rodents (Holzenberger et al., 2003; Laurent Kappeler et al., 2008; Kenyon, 2010; Taguchi, Wartschow, & White, 2007; Tatar, Bartke, & Antebi, 2003; Xu et al., 2014). Also, genetic mutations in the human IGF-1R, GH-R or low levels of IGF-1 correlate with lifespan extension (Guevara-Aguirre et al., 2011; Milman et al., 2014; Suh et al., 2008; van der Spoel et al., 2015). Therefore, pharmacologic inhibition of the GH/IGF-1 pathway

is a promising strategy for impeding or slowing down age-related diseases (Longo et al., 2015).

However, the role of IGF-1 in regulating age-associated AD remains unclear. For instance, lower serum IGF-1 levels correlate with increased cognitive decline and risk of AD (Okereke et al., 2007; Westwood et al., 2014). In addition, patients with familial AD demonstrate lower levels of circulating IGF-1 compared to controls (Mustafa et al., 1999). An *ex vivo* study revealed IGF-1 resistance along with insulin resistance through the PI3K pathway in AD patient brains (Talbot et al., 2012). Finally, IGF-1 treatment diminished Aβ accumulation by improving its transportation out of the brains of AD mouse models while IGF-1R inhibition aggravated both behavioral and pathological AD symptoms in mice (E. Carro, Trejo, Gomez-Isla, LeRoith, & Torres-Aleman, 2002; Eva Carro et al., 2006).

On the other hand, administration of a potent inducer of circulating IGF-1 levels (MK-677) failed to delay AD progression in a randomized trial (Sevigny et al., 2008). Also, acute or chronic delivery of IGF-1 exerted no beneficial effect on AD pathological hallmarks in rodent models *in vivo* (Lanz et al., 2008). Moreover, high levels of serum IGF-1 were detected in individuals diagnosed with AD or other forms of dementias in one cross-sectional study (Johansson et al., 2013). Decreased insulin/IGF-1 signaling (IIS) in aged women carrying polymorphisms which lead to reduced IIS activity correlated with better cognitive behavior in another study (Euser, van Heemst, van Vliet, Breteler, & Westendorp, 2008). In a familial study, higher serum IGF-1 at midlife increased the risk of late-onset AD

(van Exel et al., 2014). Middle-aged and older males with high circulating IGF-1 levels at baseline were diagnosed with cognitive impairment after approximately 8 years in a longitudinal study (Tumati, Burger, Martens, van der Schouw, & Aleman, 2016). A higher prevalence and incidence of dementia and AD were associated with higher levels of IGF-1R stimulating activity in an elderly, population-based cohort study (de Bruijn et al., 2014). Consistent with these findings, a body of studies have demonstrated that genetically ablating IGF-1R signaling improves neuroprotection and protects against AD progression by alleviating AD hallmarks including Aβ deposition, neuroinflammation, neuronal and synaptic loss, and behavioral dysfunction in AD mouse models (Cohen et al., 2009; Freude et al., 2009; George et al., 2017; Gontier, George, Chaker, Holzenberger, & Aïd, 2015).

Presumably, this dichotomy of effects is, in part, mediated through effects of IGF-1 on its receptor. The IGF-1R and the insulin receptor (IR) are homologous tyrosine kinase proteins with remarkably different functions (Arcaro, 2013; Larsson, Girnita, & Girnita, 2005; Rothenberg, White, & Kahn, 1990). Upon binding of IGF-1R ligands (IGF-1, IGF-2, and supraphysiological concentration of insulin), the receptor becomes auto-phosphorylated on three key tyrosine residues (Y1131, Y1135, and Y1136) in the activation loop (Baserga, 1999; Favelyukis, Till, Hubbard, & Miller, 2001; LeRoith, Werner, Beitner-Johnson, & Roberts, 1995). Phosphorylation of this receptor leads to activation of two major signaling pathways including RAS/RAF/MEK/ERK and PI3K/Akt which results in proliferation and protein synthesis/anti-apoptosis/autophagy, respectively

(Gallagher & LeRoith, 2010; Gontier et al., 2015). Inhibition of IGF-1R-mediated signaling is considered a viable therapeutic strategy against cancer, including glioblastoma, to confront tumor growth (Girnita et al., 2004; Yin et al., 2010). PPP, a cyclolignan compound, is a potent, selective, competitive, and reversible inhibitor which targets IGF-1R autophosphorylation at the substrate level (Girnita et al., 2004). Thus, it has no described effect on the function of IR or other tyrosine kinase receptors (Girnita et al., 2004; R. Vasilcanu et al., 2008). Inhibition of IGF-1R by PPP preferentially downregulates the PI3K/Akt signaling pathway through blocking activation loop phosphorylation (D. Vasilcanu et al., 2004).

Based on the potential role of IGF-1R suppression against AD development and according to our previous data which reported diminished gliosis and Aβ burden in the df/df/AβPP/PS1 transgenic mice which express low levels of brain IGF-1 (Kendra L. Puig et al., 2016), we hypothesized that applying a short-term pharmaceutical intervention might attenuate disease presentation. To test this idea, we intraperitoneally injected PPP into the AβPP/PS1 mouse line and wild type littermate controls for a week to investigate changes in gliosis and plaque deposition.

Methods

Animals

In this study, the wild-type (WT) C57BL/6J mouse line and the C57BL6 AβPP/PS1 (strain 005864 B6.Cg-Tg (AβPPswe,PSEN1dE9)85Dbo) transgenic

mice were originally purchased from the Jackson Laboratory (Bar Harbor, Maine) and maintained, as a colony, under standard housing conditions including a 12 h light:12 h dark cycle and 22 ± 1 °C temperature with *ad libitum* access to food and water at the University of North Dakota Center for Biomedical Research. This transgenic mouse model of AD expresses the human amyloid beta (A4) precursor protein (hAβPP) and the human presenilin 1 (hPSEN1), respectively, carrying the Swedish and deltaE9 mutations under the control of the mouse prion promoter. AβPP/PS1 mice develop significant amyloid plaque deposition and gliosis in their brains by 6-7 months of age. Due to limited animal availability, only male littermate control WT and AβPP/PS1 mice at 9-10 months of age (n = 7-9 per genotype) were used. They were randomly divided into vehicle and drug treated groups for 7-day treatments. 24 h (day 8) after ending the treatments, mice were euthanized followed by cardiac perfusion and the blood, brains, spleens, and livers were collected to quantify histologic and biochemical changes. All procedures involving animals were reviewed and approved by the UND Institutional Animal Care and Use Committee (UND IACUC). The investigation conforms to the National Research Council of the National Academies Guide for the Care and Use of Laboratory Animals (8^{th} edition).

Microglia Cultures

Microglia were obtained from cortices of postnatal 0-3-day-old C57BL/6J pups. Cortices were briefly trypsinized, triturated, and cultured for 10-14 days on top of an adherent astrocyte layer from the same cortices in a T-75 flask. Complete media consisting of DMEM/F12 with 10% FBS, 5% horse serum

penicillin and streptomycin was partially replaced at 7 days *in vitro*. Because the microglia are loosely adhered and floating, to isolate microglia from the astrocytes, flasks were shaken to remove any loosely adhered microglia but not astrocytes. Media was collected and centrifuged briefly to pellet microglia. Microglia were resuspended into complete media, counted and plated onto poly-L-lysine coated 96 well plates at a density of 40,000 cells/well. Cells were pretreated with or without 100ng/mL IGF-1 (R&D Systems, Minneapolis, MN) for 7 days prior to Aβ stimulation. Fresh complete media with or without IGF-1 was replaced every two days.

Antibodies and Reagents

The Y188 antibody targeting AβPP was purchased from Abcam (Cambridge, MA, USA). The 4G10 antibody to target p-tyrosine (05-321) was purchased from Millipore (Darmstadt, Germany). The anti-oligomer antibody, A11, and anti-fibrillar protein antibody, OC, were gifts from Rakez Kayed. Anti-Aβ 6E10 antibody was purchased from Covance (Emeryville, CA, USA). Iba-1 and CD68 (MCA1957) antibodies against microglia markers were purchased from Wako Chemicals USA, Inc (Richmond, VA, USA) and BIO-RAD (CA, USA), respectively. Antibodies targeting α-tubulin (TU-02: sc-8035), actin (I-19: sc-1616), and GAPDH (6C5: sc-32233) were purchased from Santa Cruz Biotechnology (Santa Cruz, CA, USA). Antibodies against GFAP (D1F4Q) to target astrocytes, p-AKT (Ser473) (193H12), AKT (pan) (C67E7), p-p44/42 MAPK (p-ERK1/2) (Thr202/Tyr204), p44/42 MAPK (ERK1/2), IGF-1R β, p-SAPK/JNK (Thr183/Tyr185), and SAPK/JNK were purchased from Cell Signaling

Technology, Inc (Danvers, MA, USA). To detect p-IGF-1R (pY1161) for brain immunohistochemistry and p-IR/IGF1-R (pYpY1162/1163) for western blotting, antibodies were purchased from Abcam (Cambridge, MA, USA) and Life Technologies (Grand Island, NY, USA), respectively. The 4G8 antibody against the Aβ peptide was purchased from Biolegend (San Diego, CA, USA). The mouse on mouse (M.O.M) kit, Vector VIP kit, biotinylated anti-rat, anti-rabbit, and anti-mouse antibodies were purchased from Vector Laboratories Inc (Burlingame, CA, USA). The horseradish peroxidase conjugated secondary antibodies were purchased from Santa Cruz Biotechnology (Santa Cruz, CA, USA). Picropodophyllin (PPP), IGF-1R inhibitor, was purchased from EMD Millipore (Billerica, MA, USA). The cytokine ELISA kits were purchased from R&D Systems (Minneapolis, MN, USA). The human $A\beta_{1\text{-}40/42}$ ELISA kits were purchased from EMD Millipore (Billerica, MA, USA).

Intraperitoneal Injection of PPP

The male AβPP/PS1 and age-matched WT mice were randomly divided into two treatment (drug and vehicle) groups per genotype. PPP dissolved in DMSO was given to drug treated groups with a dosage of 1mg/kg/day while the vehicle groups received DMSO via ip. injection, totaling 7 days. Efficacy of this PPP concentration (1mg/kg) was confirmed in our preliminary studies.

Tissue Enzyme-Linked Immunosorbent Assays (ELISA)

On the collection day, spleen and right temporal cortices of brain hemispheres were isolated and flash frozen. Temporal cortices and spleens were lysed in Raybiotech lysis buffer and centrifuged (17968 g, 4°C, 10 min) and

cytokine and soluble $A\beta_{1\text{-}40/42}$ ELISAs were performed from the supernatants according to the manufacturer's protocol. The temporal cortices pellets were resuspended in 5M guanidine HCL/50mM Tris HCL, pH 8.0, centrifuged (17968 g, 4°C, 10 min), and the supernatants were removed to quantify insoluble $A\beta_{1\text{-}40/42}$ levels by ELISA according to the manufacturer's protocol. The Bradford method or BCA kit (Thermo Scientific, IL, USA) were used to quantify protein concentrations (Bradford, 1976).

Immunohistochemistry (IHC)

The left-brain hemisphere was immersion fixed in 4% paraformaldehyde, replaced with 30% w/v sucrose in PBS three times. Briefly, the brains were then embedded in 15% gelatin followed by immersion fixing in 4% paraformaldehyde, 15%, then 30% sucrose. The gelation blocks were serially sectioned (40μm) via freezing microtome (Kumi Nagamoto-Combs, Gunjan D. Manocha, Kendra Puig, & Colin K. Combs, 2016). The serial sectioned brains were immunostained using anti-Aβ (4G8; 1:1000 dilution), Iba-1 (1:1000 dilution), GFAP (1:1000 dilution), and CD68 (1:1000 dilution) antibodies following citrate antigen retrieval, and p-IGF-1R (1:1000 dilution), and p-tyrosine (4G10; 1:1000 dilution) antibodies followed by their respective secondary antibodies. Vector VIP was used to visualize the immunoreactivity and images were taken using an upright Leica DM1000 microscope and Leica DF320 digital camera system. Immunohistochemistry quantitation of hippocampi was performed via calculating the mean optical density (n=6). Adobe Photoshop software (Adobe Systems, San Jose, CA) was used to make figures.

Western Blotting

Flash frozen hippocampi and livers were lysed in RIPA buffer (20 mM Tris, pH 7.4, 150 mM NaCl, 1 mM $Na3VO_4$, 10 mM NaF, 1 mM EDTA, 1 mM EGTA, 0.2 mM phenylmethylsulfonyl fluoride, 1% Triton X-100, 0.1% SDS, and 0.5% deoxycholate) with protease inhibitors (AEBSF 1mM, Aprotinin 0.8 M, Leupeptin 21 M, Bestatin 36 M, Pepstatin A 15 M, E-64 14 M), centrifuged (14,000 rpm, 4°C, 10 min), and the supernatants were collected. Hippocampal proteins were resolved by 10% sodium dodecyl sulfate polyacrylamide gel electrophoresis (SDS-PAGE) and transferred to polyvinylidene difluoride membranes (PVDF) for western blotting using anti- p-IR/IGF1-R, IGF-1Rβ, p-AKT, AKT, p-JNK, JNK, p-ERK, ERK, p-tyrosine, AβPP (Y188), CD68, GFAP, and α-tubulin (loading control) antibodies. For the liver western blotting, anti- p-IR/IGF1-R, IGF-1Rβ, and actin (loading control) antibodies were used. The BCA kit (Thermo Scientific, IL, USA) was used to quantify protein concentrations. Enhanced chemiluminescence was used to detect antibody binding using an Aplegen Omega Lum G imaging system. Optical density values were normalized to their respective loading controls (p-IGF-1R, p-AKT, p-JNK, and p-ERK blots against their respective IGF-1R, AKT, JNK, and ERK total proteins and p-tyrosine, AβPP, CD68, and GFAP blots against α-tublin) from the same membrane, and then averaged (± SEM).

Dot Blot

Total, oligomeric, and fibrillar protein from the hippocampal lysates in RIPA buffer were dot blotted onto PVDF membranes and detected using 6E10,

A11, and OC antibodies, respectively. Enhanced chemiluminescence was used to detect antibody binding using an Aplegen Omega Lum G imaging system. Optical density values were normalized to α-tubulin, loading control.

MTT Assay

Microglia were pretreated with or without 100ng/mL IGF-1 for 7 days in complete medium on a clear 96 well plate prior to Aβ stimulation. Media was replaced with serum free DMEM/F12 with or without 100ng/mL IGF-1 or 100nM $A\beta_{42}$ (A-1165, rPeptide, Athens, GA) for 24 h. Aβ oligomers were resuspended with water at a 250μM concentration for 5 min and slowly inverted to mix. Aβ conformation was confirmed via western blots for each experiment. MTT reagent (3-(4,5-dimethylthiazol-2-yl)-2,5-diphenyl tetrazolium bromide) was added to the media at a concentration of 100μg/mL for 1 h. Media was removed and replaced with isopropanol. Optical density was read at 560nm with a 650nm correction wavelength on a Bio-Tek ELx800 plate reader (Winooski, VT).

Phagocytosis Assay

Microglia were pretreated with or without IGF-1 for 7 days, on a black 96 well plate prior to Aβ stimulation. Media was replaced with DMEM/F12 only with or without 100ng/mL IGF-1, 1μM FITC-human Aβ, or FITC-*Escherichia coli* bioparticle as a positive control, 0.125mg/mL. Phagocytosis was measured by the uptake of fluorescein isothiocyanate (FITC)-conjugated $A\beta_{42}$. The $A\beta_{42}$ peptide was fibrillized as recommended by the manufacturer (rPeptide, Athens GA) and previously described (Floden, 2006). Cells were treated for 6 h, media was removed, and wells were rinsed with 0.25mg/mL trypan blue in PBS to

quench any extracellular peptide or bioparticles that were not internalized. The intracellular fluorescence was read at 480nm excitation and 520nm emission via Bio-Tek FLx800 fluorescent plate reader (Winooski, VT).

Culture Media Enzyme-Linked Immunosorbent Assays (ELISA)

Microglia were pretreated with or without IGF-1 for 7 days in complete media. Media was replaced with serum free DMEM/F12 with or without 100ng/mL IGF-1, or 100nM $A\beta_{42}$ for 24 h. Aβ oligomers were resuspended with water at a 250μM concentration for 5 min and slowly inverted to mix. Aβ conformation was confirmed via western blots for each experiment. Media was removed and TNF-α levels quantified using a mouse TNF-α DuoSet ELISA kit according to the manufacturer's protocol (R&D Systems, Minneapolis, MN). The optical density was read on a Bio-Tek ELx800 plate reader (Winooski, VT) at 450nm and 550nm corrected wavelength and pg/mL TNF-α was calculated via standard curve.

Statistical Analysis

The *in vivo* data were analyzed by two-way ANOVA multiple comparisons followed by Uncorrected Fisher's LSD test using GraphPad Prism 8 software. One-way ANOVA followed by Uncorrected Fisher's LSD test was used to analyze the *in vitro* data including the MTT assays, phagocytosis assays, and TNF-α ELISAs. Data are represented as the mean ± SEM. Significance is indicated by P value measurements with a $P < 0.05$ considered significant; *$P < 0.05$; **$P < 0.01$; ***$P < 0.001$; ****$P < 0.0001$.

Results

Aβ Levels Were Attenuated by IGF-1R Inhibitor Treatment of AβPP/PS1 Mice

The inhibitory effect of drug on IGF-1R phosphorylation was confirmed via i.p. injection of 1mg/kg PPP. The wild type and AβPP/PS1 controls as well as the drug treated AD mouse model were euthanized and the hippocampal tissues were collected 15 minutes after the injection. Western blot results showed downregulation of p-IGF-1R and p-tyrosine levels indicative of attenuation of IGF-1R signaling (Fig. II-1).

Both WT and AβPP/PS1 lines (9-10-month-old) were treated with 1mg/kg/day PPP in order to determine the impact of IGF-1R inhibition on Aβ deposition. ELISA analysis indicated a significant decrease of insoluble $A\beta_{1\text{-}40/42}$

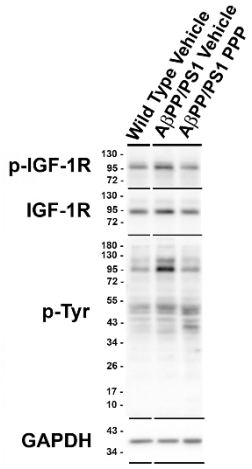

Figure II- 1. i.p. administration of 1mg/kg PPP decreased p-IGF-1R and p-tyrosine levels in AβPP/PS1 mouse brains. Hippocampi from vehicle wild type and AβPP/PS1 as well as PPP treated AβPP/PS1 mice were collected 15 min following ip. injection of 1mg/kg PPP. Western blots were performed to investigate the protein changes in including IGF-1R, p-IGF-1R, and p-tyrosine. GAPDH was used as the loading control.

but not soluble $A\beta_{1\text{-}40/42}$ levels in temporal cortices of AβPP/PS1 mice treated with PPP compared to vehicle controls (Fig. II-2A). Anti-Aβ immunohistochemistry quantitation of hippocampi regions revealed no dramatic Aβ level changes. However, plaque density reduced in the drug treated AD mice versus the vehicle treated group, represented via higher magnification (Fig. II-2B). As an additional means of addressing changes in Aβ, we performed dot blot analysis from hippocampal lysates using anti-oligomer antibody, A11, anti-fibril antibody, OC, and total Aβ antibody, 6E10. Dot blots showed no change in A11 detectable protein due to IGF-1R inhibition (Fig. II-2C). Contrary to our expectations, the dot blot results did not show a decrease in OC immunodetection as was predicted from the ELISA, perhaps due to a lack of specificity of OC for $A\beta_{1-40/42}$ only (Fig. II-2C). These findings suggest that insoluble Aβ plaque deposition, in particular, was affected by IGF-1R function.

Microgliosis Was Attenuated in PPP Treated AβPP/PS1 Mice

Brain inflammatory changes are hypothesized to be a critical component of AD pathophysiology mediated, in part, by Aβ-stimulated microglial activation and expression of inflammatory cytokines in AD brains (S.-H. Choi et al., 2013; Itagaki, McGeer, Akiyama, Zhu, & Selkoe, 1989a; Marco Prinz, Josef Priller, Sangram S. Sisodia, & Richard M. Ransohoff, 2011; W.-Y. Wang, M.-S. Tan, JT. Yu, & L. Tan, 2015). Based on the attenuated plaque deposition and insoluble Aβ levels in the PPP treated AβPP/PS1 mice, we expected that inactivation of IGF-1R signaling via PPP would also alter reactive gliosis. To assess the impact of PPP treatment on glial activation, immunohistochemistry was performed.

Microglial activation was visualized using two different antibodies, anti-Iba-1 and anti-CD68. PPP treatment attenuated the Aβ-associated hippocampi immunoreactivity for CD68 but not Iba-1 antibody supporting the idea that IGF-1R signaling may be contributing to a reactive microglia phenotype (Fig. II-3).

Interestingly, astrocyte activation, assessed using anti-GFAP immunoreactivity, did not demonstrate any robust changes following PPP treatment suggesting an uncoupling of astrogliosis following inhibition of IGF-1R signaling (Fig. II-3). To begin assessing what cell types might be affected by IGF-1R inhibition in the brain, antibodies for the phosphorylated, active form of the IGF-1R (p-IGF-1R) and p-tyrosine were used for immunostaining. AβPP/PS1 mice demonstrated a robust plaque-associated, microglia-like pattern of p-IGF-1R and p-tyrosine immunoreactivity suggesting that microglia are the cell types with the highest levels of active IGF-1R signaling in these mice (Fig. II-4).

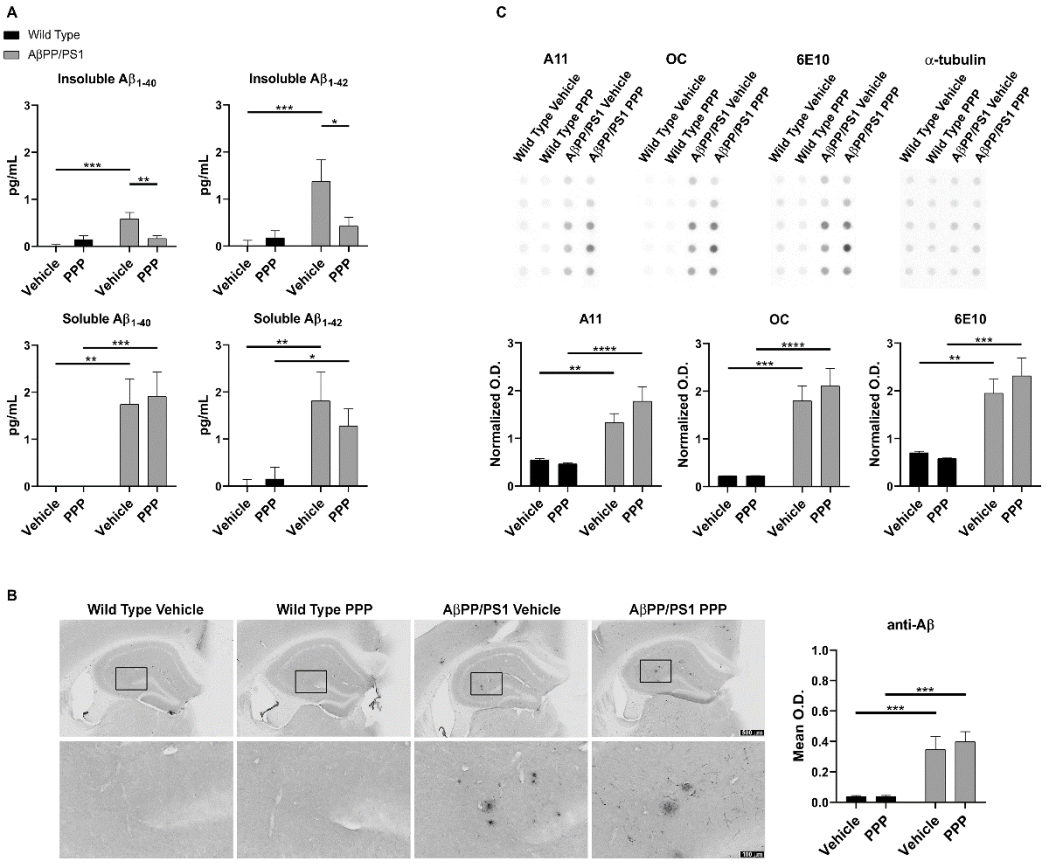

Figure II- 2. IGF-1R inhibitor treatment attenuated Aβ levels in AβPP/PS1 mice. A) Temporal cortex lysates collected from male wild type (WT) and AβPP/PS1 mice, treated with vehicle (DMSO) or picropodophyllin (PPP, 1mg/kg) for 7 days, were used to perform ELISAs for insoluble and soluble $A\beta_{1\text{-}40/42}$, Data are mean ± SEM, *p<0.05, **p<0.01, ***p<0.001, and ****p<0.0001 (n=7-9 animals). B) Immunohistochemistry was performed on both WT and AβPP/PS1 mouse brains using anti-Aβ (4G8) antibody and mean optical density was measured (n=6 animals/condition). Representative hippocampal images are shown. C) Hippocampal lysates from vehicle and PPP treated WT and AβPP/PS1 mice were dot blotted to quantify total Aβ (6E10), oligomeric peptide (A11), and fibrillar peptide (OC) changes. Data are mean O.D. ± SEM, **p<0.01, ***p<0.001, and ****p<0.0001 (n=5 animals), (Fisher's LSD test).

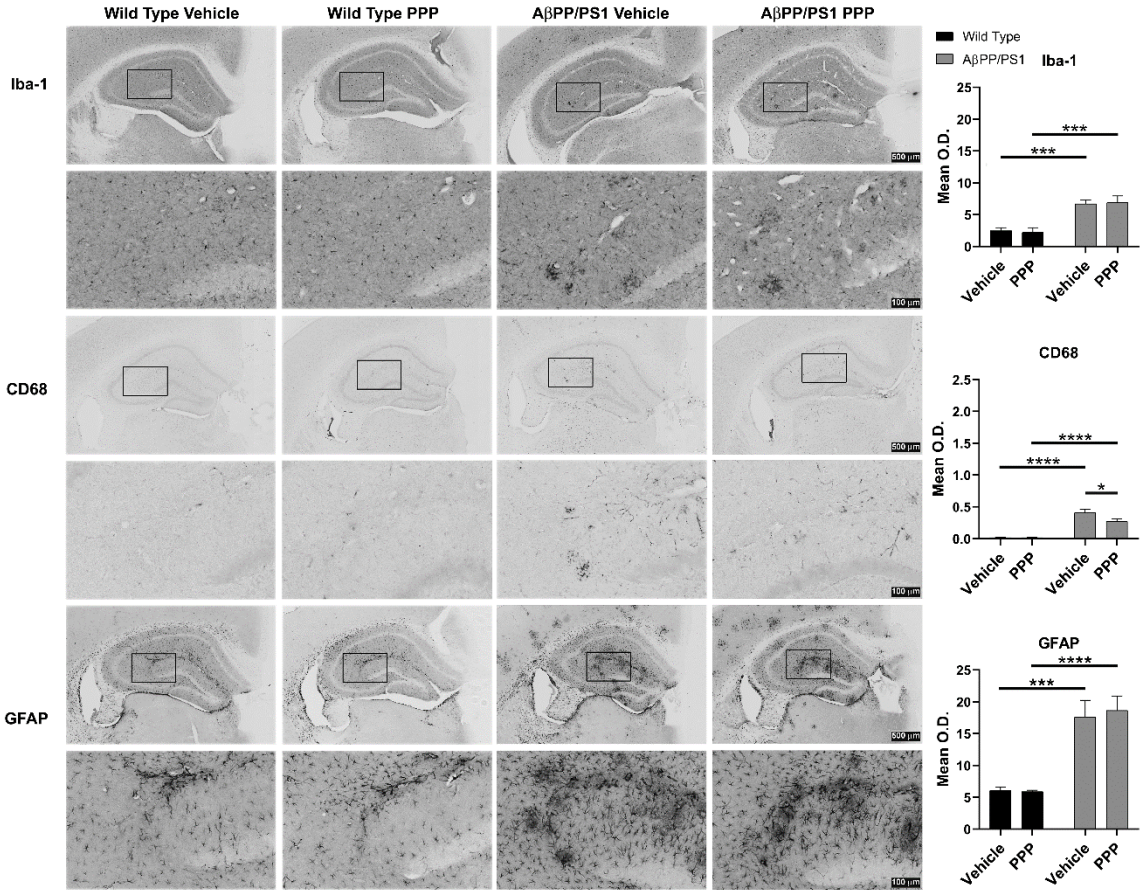

Figure II- 3. IGF-1R inhibitor treatment attenuated microgliosis but not astrocytosis immunoreactivity in AβPP/PS1 mice. Immunohistochemistry was performed from vehicle (DMSO) and PPP (1mg/kg, 7 days) treated WT and AβPP/PS1 mouse brains using anti-Iba1, anti-CD68 (markers of microglia), and anti-GFAP (astrocyte marker) antibodies and mean optical density was measured. Antibody binding was visualized using Vector VIP as the chromogen. Representative hippocampal images are shown (n=6 animals/condition).

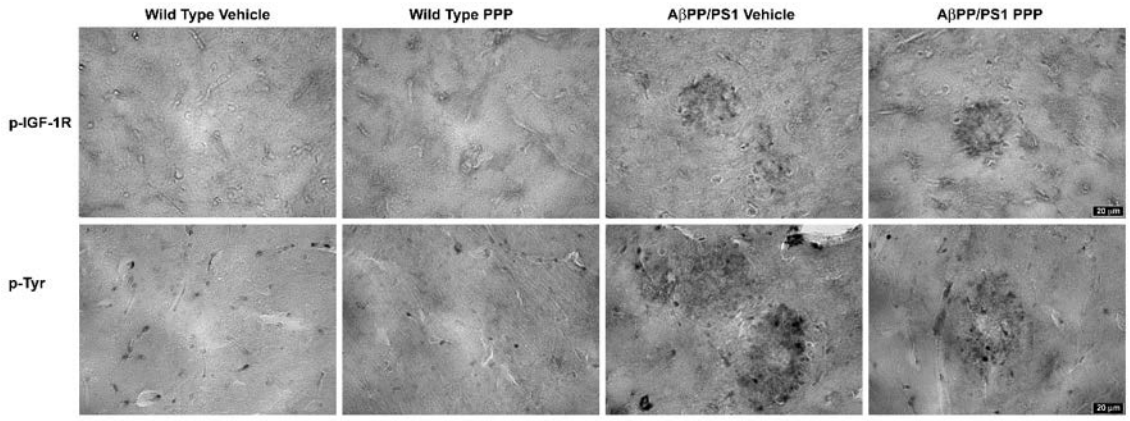

Figure II- 4. p-IGF-1R and p-tyrosine immunoreactivity demonstrated a microglial-like pattern. Immunohistochemisty was performed from vehicle and PPP treated wild type and AβPP/PS1 mouse brains using p-IGF-1R and p-tyrosine (4G10) antibodies. Representative hippocampal images are shown via 20x magnification.

PPP Decreased Protein Markers of Microglial Activation

To provide a more quantitative assessment of changes in microgliosis and IGF-1 receptor inhibition following PPP treatment, western blot analysis of hippocampi was performed. In order to quantify PPP-dependent changes in IGF-1R signaling, protein levels of active IGF-1R and p-IGF-1R were quantified. p-IGF-1R protein levels were increased in AβPP/PS1 mice compared to wild type controls and were unaffected by PPP treatment (Fig. II-5). Kinases associated with the IGF-1R response were also compared in treated versus untreated mice. Similar to the IGF-1R findings, active p-Akt and p-JNK levels were not altered by PPP treatment of AβPP/PS1 mice compared to wild type controls (Fig. II-5). Levels of active, p-ERK did not differ between strain and treatment (Fig. II-5). To better support the microglial qualitative immunostaining results, protein levels of CD68 and p-tyrosine were also quantified. Total protein p-tyrosine levels were

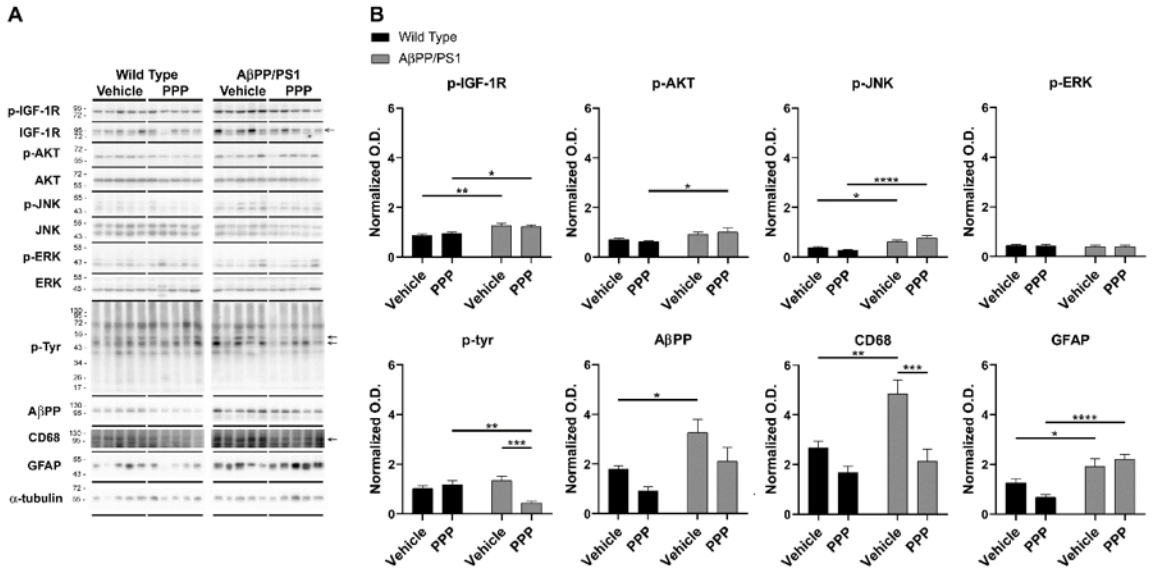

Figure II- 5. p-tyrosine and CD68 levels were attenuated by inhibitor treatment in AβPP/PS1 mice. Hippocampal lysates from vehicle and PPP (1mg/kg, 7 days) treated WT and AβPP/PS1 mice were A) western blotted to B) quantify protein changes related to IGF-1R signaling, microgliosis, and AβPP levels. p-IGF-1R, p-AKT, p-JNK, and p-ERK blots were normalized to their respective IGF-1R, AKT, JNK, and ERK loading controls. The p-tyrosine, AβPP, CD68, and GFAP blots were normalized to their respective α-tublin loading controls. Data are mean O.D. ± SEM, *p<0.05, **p<0.01, ***p<0.001, and ****p<0.0001 (n=5 animals), (Fisher's LSD test).

assessed based upon our previous studies which indicated a tyrosine kinase-dependent activation of microglia in response to Aβ oligomer stimulation (Dhawan, Floden, & Combs, 2012). PPP treated AβPP/PS1 mice demonstrated a significant decrease in both CD68 and p-tyrosine protein levels validating a drug-dependent decrease in microgliosis (Fig. II-5). In agreement with our ELISA, dot blot, and immunostaining results, protein levels of AβPP were not significantly altered by PPP treatment in either wild type or AβPP/PS1 mice (Fig. II-5). As

expected, based upon the immunostaining results, the AβPP/PS1-associated increase in GFAP protein levels was not attenuated by PPP treatment (Fig. II-5).

PPP Treatment Did Not Affect Phosphorylation Levels of Liver IGF-1R

Although the PPP-mediated inhibitory effect on microgliosis did not correlate with a long-term reduction in brain levels of p-IGF-1R, we investigated whether the drug was exerting any maintained effect on peripheral p-IGF-1R levels. Based upon the high expression of IGF-1 and its receptor in the liver, we quantified liver phosphorylation levels of the receptor (Mauras, 1997). Unlike the brain, livers of AβPP/PS1 mice demonstrated no elevation in levels of p-IGF-1R compared to wild type mice demonstrating that the elevated activity associated with disease differs across organs and is unique to the brain (Fig. II-6). However, like the brain, PPP treated wild type and AβPP/PS1 mice demonstrated no significant decrease in p-IGF-1R protein levels compared to the vehicle treated groups demonstrating that the drug regimen had no lasting adverse effects on IGF-1R signaling (Fig. II-6).

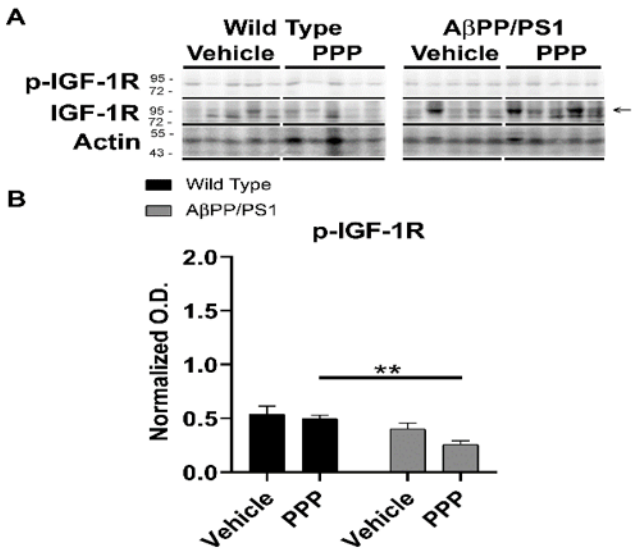

Figure II- 6. Liver p-IGF-1R levels were not altered by inhibitor treatment in AβPP/PS1 mice. Liver lysates from vehicle and PPP (1mg/kg, 7 days) treated WT and AβPP/PS1 mice were A) western blotted to B) quantify p-IGF-1R protein changes. p-IGF-1R blots were normalized to their respective IGF-1R loading controls. Actin was used as a loading control. Data are mean O.D. ± SEM, **p<0.01 (n=5 animals), (Fisher's LSD test).

PPP Treated AβPP/PS1 Mice Had Reduced Levels of Multiple Cytokines in the Temporal Cortex

Cytokine levels were quantified from the temporal cortices of vehicle and PPP treated mice to correlate with the observed changes in microglial activation. Vehicle treated AβPP/PS1 mice had significantly higher levels of GM-CSF, IL-1β, and IL-6 compared to vehicle treated wild type mice validating an immune phenotype in the brains of AD mice (Fig. II-7).

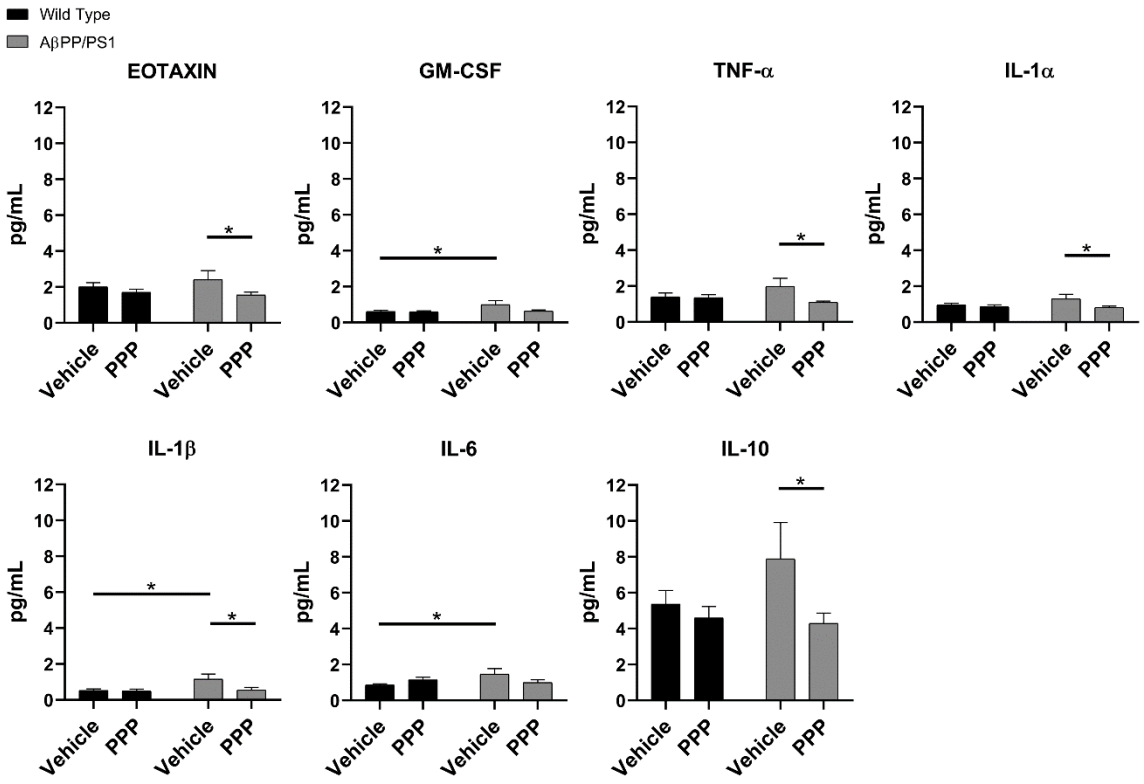

Figure II- 7. IGF-1R inhibitor treatment attenuated the levels of select cytokines in the brains of AβPP/PS1 mice. ELISAs were performed to quantify levels of cytokines in temporal cortex lysates from WT and AβPP/PS1 mice that were vehicle or PPP (1mg/kg, 7 days) treated. Data are mean values normalized to tissue wet weight ± SEM, *p<0.05 (n=6-8 animals), (Fisher's LSD test).

More importantly, PPP treatment significantly decreased eotaxin, TNF-α, IL-1α, IL-1β, and IL-10 levels in the drug treated AβPP/PS1 mice compared to their vehicle controls (Fig. II-7). The levels of other protein markers did not change due to different strains or drug treatment (Fig. II-8). These data corresponded well with the observed reduction in microglial reactive phenotype and suggested that inhibition of IGF-1 signaling is sufficient to attenuate select proinflammatory cytokines levels in brains of AD mice.

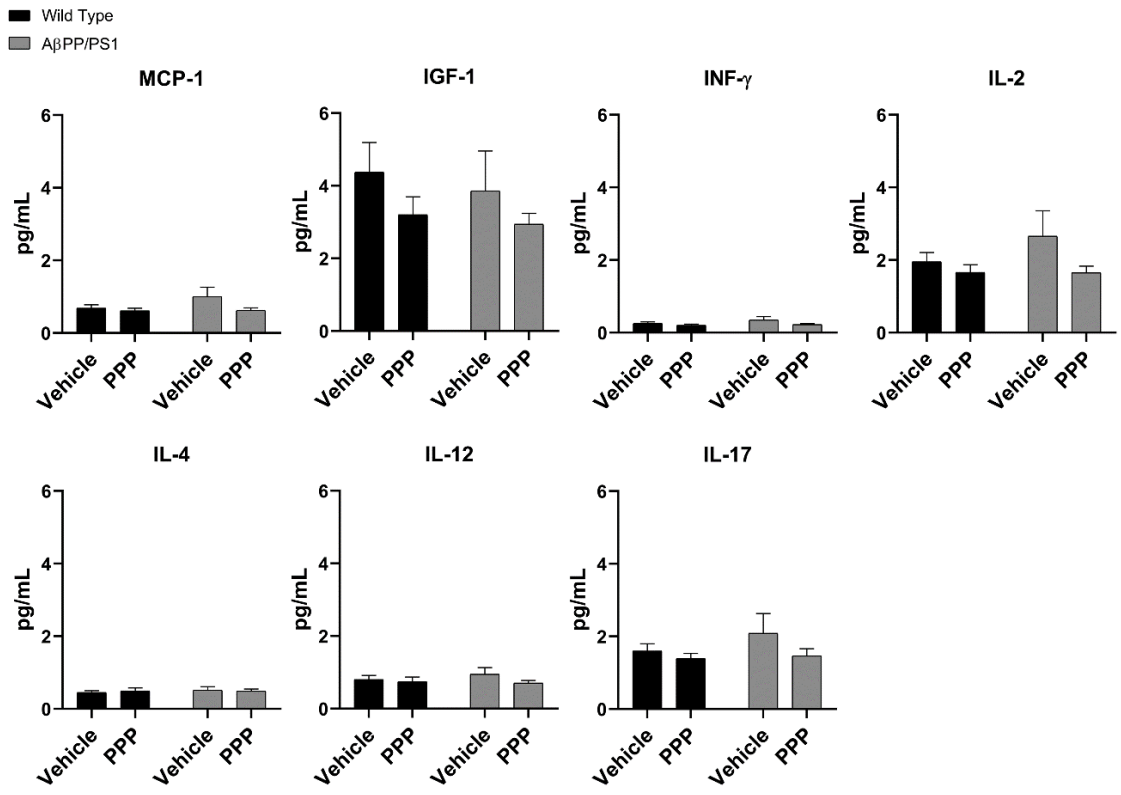

Figure II- 8. PPP did not affect the levels of some cytokines in mouse temporal cortices. ELISAs were performed to quantify levels of temporal cortex cytokines in vehicle and PPP (1mg/kg, 7 days) treated wild type and AβPP/PS1 mice. Data are mean values normalized to tissue wet weight ± SEM, *p<0.05 (n=6-8 animals), (Fisher's LSD test).

Spleen Cytokine Levels Were Not Changed in PPP Treated AβPP/PS1 Mice

In order to assess the effect of PPP treatment on peripheral inflammatory markers, spleen cytokine ELISAs were also performed. Contrary to our expectations, vehicle treated AβPP/PS1 mice had no elevation of spleen cytokine levels compared to vehicle wild type mice suggesting that the proinflammatory changes are selective for the brain in the AD mice (Fig. II-9). In addition, PPP treatment had no effect on the concentrations of any cytokines in either strain suggesting that the immunomodulatory effect of IGF-1R inhibition was unique to the brain in these mice (Fig. II-9).

IGF-1R Stimulation via IGF-1 and Aβ Combination Altered Microglial TNF-α Secretion *in vitro*

Based upon our data, the IGF-1R inhibitor dramatically modified microglial phenotype and cytokine levels in the AβPP/PS1 brains. To test the idea that the effects of IGF-1R inhibition we observed were mediated by primarily altering microglial activation behavior, we examined the effect of prolonged IGF-1 stimulation on microglial phenotype. Microglia derived from postnatal day 0-3 cultures were stimulated for 7 days with IGF-1 to model prolonged IGF-1R stimulation *in vivo*. IGF-1 pre-conditioned microglia did not differ in their ability to phagocytose Aβ fibrils or bacterial bioparticles when compared to untreated microglia (Fig. II-10A).

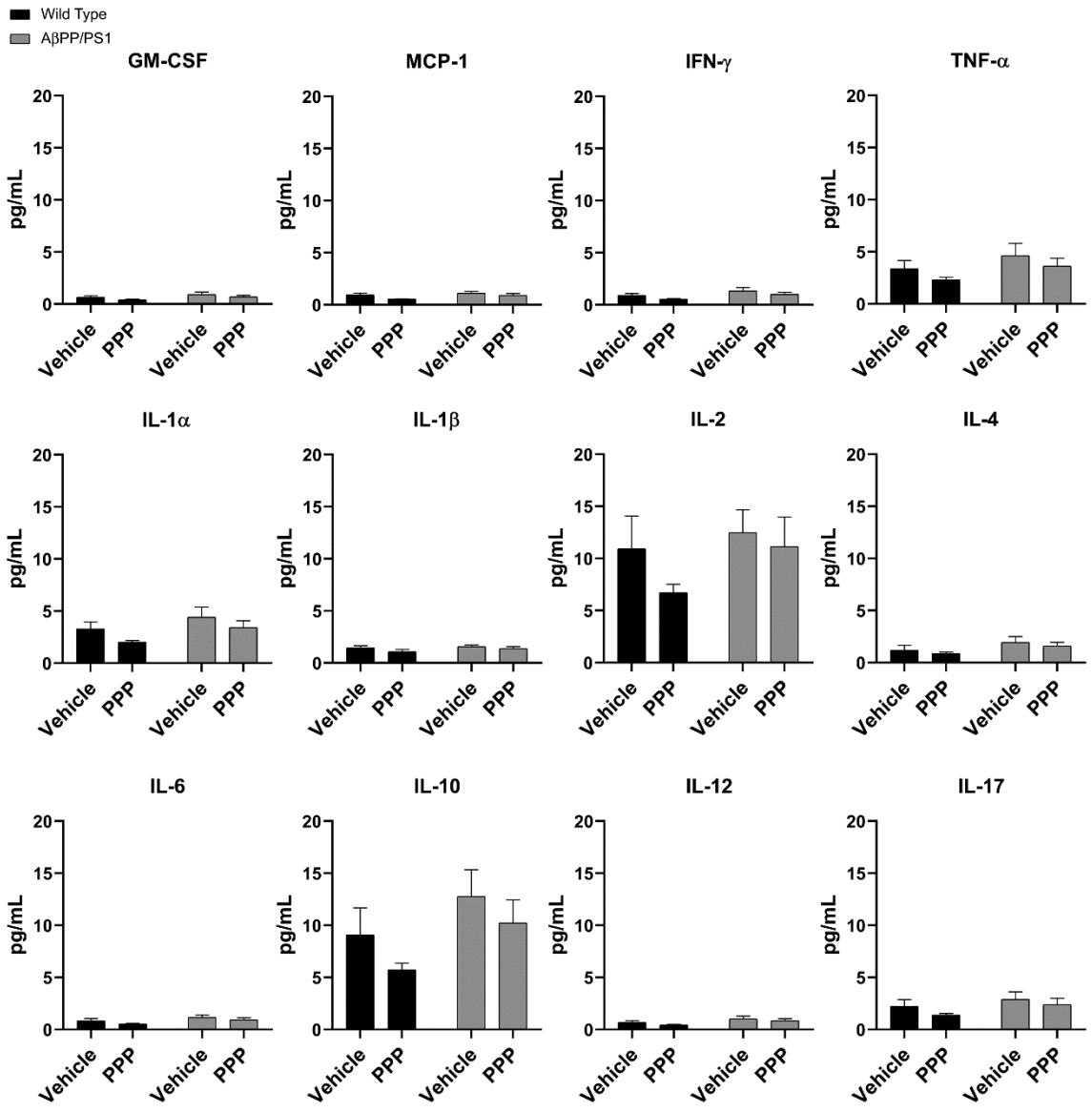

Figure II- 9. IGF-1R inhibitor treatment exerted no effect on cytokine levels in the spleens of AβPP/PS1 mice. ELISAs were performed to quantify levels of cytokines in spleen lysates from the vehicle or PPP (1mg/kg, 7 days) treated WT and AβPP/PS1 mice. Data are mean values normalized to tissue wet weight ± SEM, *$p<0.05$, (n=5-7 animals), (Fisher's LSD test).

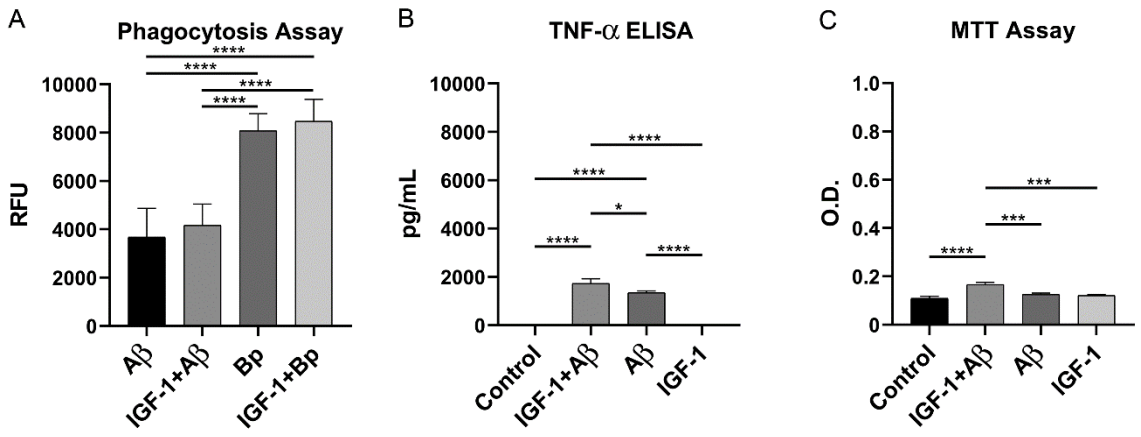

Figure II- 10. Microglia exposed to prolonged IGF-1 stimulation did not have altered phagocytosis but increased cytokine secretory ability when exposed to $A\beta_{42}$. Microglia were stimulated in serum containing media with 100ng/mL IGF-1 for 7 days replacing the media every 2 days. The microglia were then stimulated an additional 24 h with or without 100nM $A\beta_{42}$ or 100ng/mL IGF-1 in serum free media. A) 1μM FITC-$A\beta_{42}$ or 0.25mg/mL FITC *E. coli* bioparticle positive control were added to the cells for 6 h to assess phagocytic uptake. B) TNF-α secretion was quantified via ELISA from the media. C) Alternatively, cell viability was assessed via an MTT assay. Graphs are means values ± SEM, *p<0.05, **p<0.01, ***p<0.001, and ****p<0.0001, (n=3), (Fisher's LSD test).

In addition, IGF-1 pre-treatment had no effect on basal TNF-α secretion but did significantly increase Aβ-stimulated TNF-α secretion compared to IGF-1 pretreatment alone or Aβ stimulation alone (Fig. II-10B). Similarly, IGF-1 pretreated microglia had significantly increased mitochondrial dehydrogenase activity as assessed by an MTT assay when co-stimulated with Aβ peptide compared to IGF-1 pretreatment alone or Aβ stimulation alone (Fig. II-10C). This data demonstrated that prolonged IGF-1R stimulation altered microglia behavior only in the presence of a concomitant Aβ stimulation.

CHAPTER III

A PROTOCOL FOR MAKING AND SECTIONING MULTIPLE EMBEDDED SWISS-ROLLS IN A GELATIN MATRIX

Introduction

Chapter II summarized proof-of-concept findings demonstrating that modulating effects of a peripheral stimulus, IGF-1, could affect the brain in AD mice. Based upon this, the overall project goals shifted to focus on peripheral inflammatory conditions as potential stimuli to the brain during AD. In particular, contributions of intestinal dysfunction on brain presentation of disease are the remaining focus of the dissertation. In order to begin studying inflammatory changes in the colon we elected to develop a medium throughput method for visualizing staining throughout the entire mouse colon.

This Swiss-roll protocol was developed in order to examine histologic changes following colonic disruption via utilizing either DSS or AOM/DSS administration. The appropriate methodological approach for intestinal preparation enables researchers to create representative histological and immunostaining images which validate their biochemical data. The Swiss-roll technique was first introduced by Reilly and Kirsner in 1965. Later, Moolenbeek and Ruitenberg described a detailed procedure to longitudinally study the rodent intestine in 1981 (Moolenbeek & Ruitenberg, 1981).

In this protocol, our slightly different approach for co-embedding four different Swiss-rolls in a gelatin block provides a full-length overview of cross-sectional colons on a single slide. A single gelatin block is prepared by simultaneously embedding at least four different intestinal Swiss-rolls. In addition, the tissue orientation can be adjusted for each sample as desired which facilitates the comparison of different colon samples on a single gelatin section. Finally, the gelatin sections containing tissue samples are stable at least overnight at room temperature for staining. The protocol allows for longitudinal histologic examination of multiple tissue samples on a single slide simultaneously. In this method, antigenicity is retained for immunohistology. In addition, the accessibility of samples during the prolonged hardening time required of the gelatin matrix allows the tissue samples to be adjusted/re-adjusted to provide the desired orientation and spatial arrangement for ideal cross sections with similar planes of section and optimum space utilization for slide mounting. In addition, the room temperature stability of the gelatin matrix and the ability to contain numerous tissue samples in a block allows the flexibility of performing thicker sections for free-floating tissue staining and ease of mounting a single gelatin sheet rather than individual tissue sections. This is a convenient approach for allowing precise preparation of multi-tissue blocks and simultaneous sectioning, staining, and slide mounting of tissue for subsequent comparisons (III-Graphical abstract).

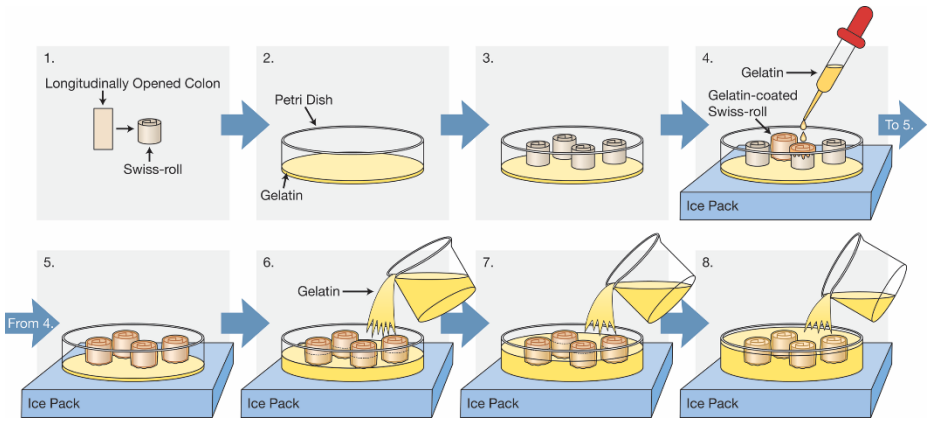

Methods

Materials

- 15% gelatin (Sigma, G2500-1KG) in PBS+ 0.02% Na Azide or 1:500 (from 10% stock)
- 4% paraformaldehyde (PFA)
- 15% and 30% sucrose in PBS + 0.02% Na Azide or 1:500 (from 10% stock)
- Swiss-roll intestines
- Immunohistochemistry (IHC) solution containing 0.5% bovine serum albumin (BSA, Equitech-Bio, Inc.), 0.1% Triton X-100 (Sigma-Aldrich), 5% normal goat serum (NGS, Equitech-Bio, Inc.), and 0.02% Na Azide in PBS.

Mice

Mice were euthanized followed by cardiac perfusion. Animal protocol was reviewed and approved by the UND Institutional Animal Care and Use Committee (UND IACUC). The investigation conforms to the National Research

Council of the National Academies Guide for the Care and Use of Laboratory Animals (8th edition).

Swiss Roll Preparation

1. After euthanizing a mouse, forceps were used to pull up the abdomen at the midline and make a V-shaped incision using surgical scissors.
2. The incision was extended by cutting the skin along with peritoneum from the pelvis toward the anus.
3. The colon was located and surgical scissors were used to carefully cut it out from the cecum toward the distal colon.
4. The colon was removed from the peritoneal cavity and surgical scissors used to remove the cecum.
5. Surrounding fat tissue was removed from the remaining colon using forceps.
6. Feces were gently washed from the colon in a proximal to distal direction using a gavage needle and syringe filled with cold PBS.
7. The colon was held using fine-tipped forceps and cut longitudinally from the distal to the proximal end using fine-tipped scissors.
8. With the luminal side upward the colon was picked up by the distal end via fine-tipped forceps and wrapped around one end of a toothpick.
9. The colon was wrapped around the toothpick from the distal to the proximal end by holding both ends of the toothpick with fingers and gently rolling.

10. Once the roll was finished, a few drops of PBS were added onto the fine end of the toothpick and the role was gently slid toward the fine end of the toothpick to release the Swiss-roll.

11. Holding both sides of the roll with blunt end forceps a 27G1/2 needle was pushed through the roll.

12. The roll was fixed in place by bending the sharp end of the needle using blunt end forceps. This method was obtained from Whittem et al with some modifications (Whittem, Williams, & Williams, 2010).

13. The Swiss-roll was transferred to a 5 mL microcentrifuge tube filled with 4% PFA and store at 4°C for 5 days.

14. The PFA was replaced with 30% sucrose on the 5th day. This step was repeated one more time after four more days. The tubes were stored at 4°C in 30% sucrose until ready to make the gelatin block.

15. Once the rolls were ready, they were embedding into a gelatin block (K. Nagamoto-Combs, G. D. Manocha, K. Puig, & C. K. Combs, 2016).

16. To make the blocks, 15% gelatin in PBS with 0.02% Na Azide was pre-warmed (30-40°C) then dissolved at 40-42°C in a shaking incubator set on high speed until the gelatin went into solution completely.

17. The bottom of a petri dish was labeled using a permanent Sharpie marker. 1/3 of the petri dish was filled with the gelatin solution and allowed to cool down to room temperature for 10 minutes. The dish was transferred to 4°C for 10-20 minutes to completely solidify. This thin layer of gelatin in the

petri dish provided a level stage to stick multiple (4 to 6) different samples upright in order to have roughly identical sections/regions of all tissues on a single slide for future comparison.

18. After completing cryoprotection, the Swiss-rolls were removed from the sucrose and the needle removed using blunt end forceps to straighten the tip to allow the needle to be removed.

19. The Swiss-rolls were dabbed on a Kimwipe to remove any extra sucrose.

20. The rolls were then soaked in a well (e.g. use a 6 or 12 well plate) containing a 15% fresh gelatin solution and allowed to equilibrate in the oven at 40°C for 20-30 minutes.

21. The petri dish was brought to room temperature and Swiss-rolls were transferred from the gelatin solution to the petri dish using blunt end forceps. The flat side of the rolls were placed onto the gelatin in the petri dish. 4 or more Swiss-rolls were used per gelatin block.

22. The rolls were allowed to stick onto the gelatin surface for 2-3 minutes at room temperature, adjusting tissue orientation as needed.

23. The petri dish was set atop a flat rack, which previously was pre-cooled at -20°C, containing an ice pack. The gelatin block making procedure was done on a laboratory bench at room temperature. The cold surface cooled down the gelatin-soaked samples, keeps them upright and attached to the gelatin bottom layer, and prevents the bottom gelatin layer from melting and releasing the Swiss-rolls as they are covered with warm gelatin

solution in the following step. The gelatin solution was next removed from the oven to cool down a bit for about 5 minutes prior to adding to the rolls. Gelatin solution was added dropwise onto each roll to just cover them (Fig. III-1) and allowed to solidify for ~ 2 minutes, again adjusting tissue orientation as needed.

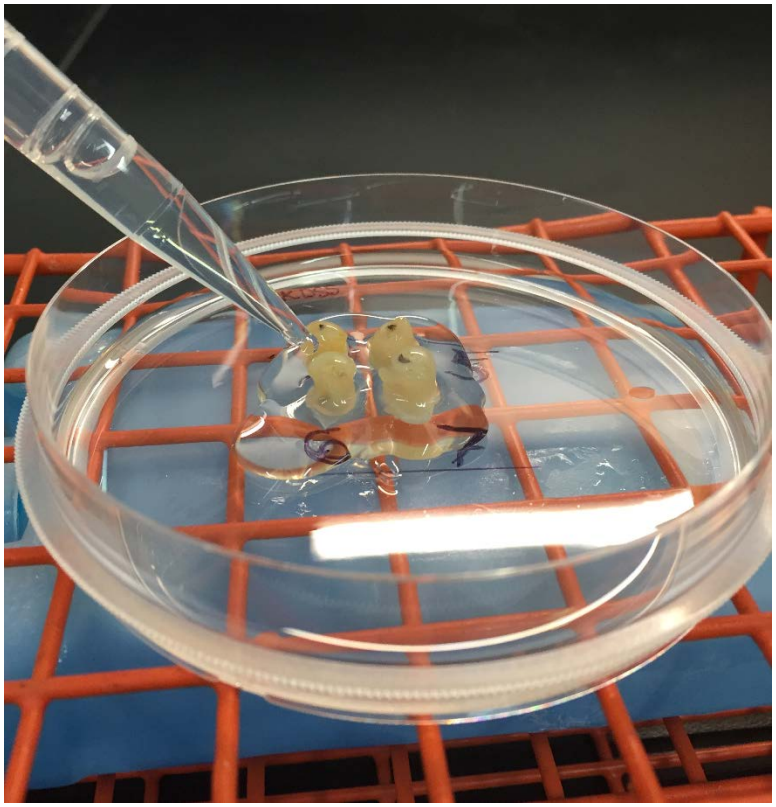

Figure III- 1. Four colon Swiss-rolls were placed into a petri dish containing a thin layer of 15% gelatin solution sitting atop an ice pack chilled surface. After 2-3 minutes, additional gelatin solution was added dropwise to gradually cover each roll.

24. Warm gelatin solution was gently poured on top of the rolls until they were covered to almost half of their height without making bubbles (Fig. III-2).

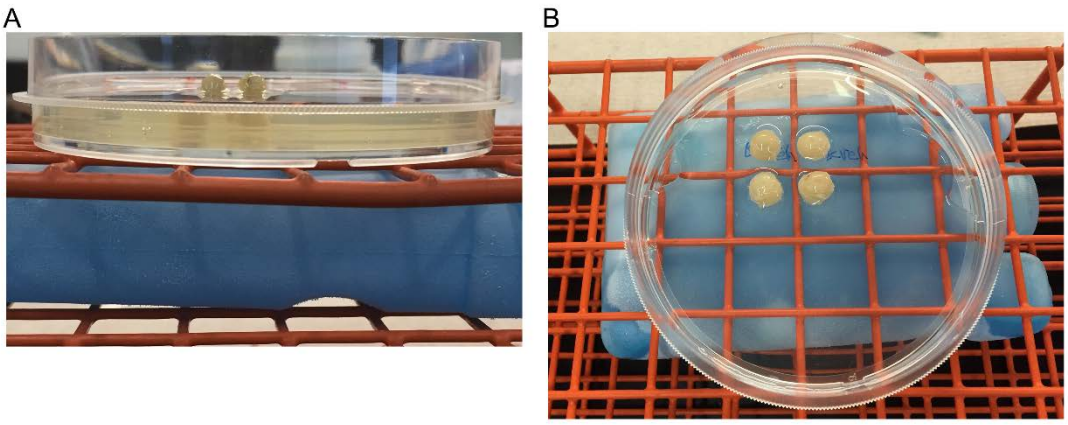

Figure III- 2. Gelatin solution was added gently to the petri dish atop the ice pack chilled surface until the rolls were covered halfway. A) Side and B) overhead images are shown.

25. After approximately 2 minutes, the rolls were carefully covered with additional gelatin solution and ice packs were placed on both sides of the petri dish and it was allowed to cool for about 20 minutes (Fig. III-3). The cold surface cooled down the bottom of the petri dish. The ice packs on both sides of the petri dish helped cool down the newly added gelatin layer. An optimal cold environment around the petri dish accelerated the solidification of the block and prevented the fixed Swiss-rolls from becoming detached during the addition of warm gelatin. However, if the area around the petri dish was too cold, subsequent gelatin layers could not appropriately merge into a single layer.

26. The petri dish was transferred to 4°C for 30 minutes to fully solidify.

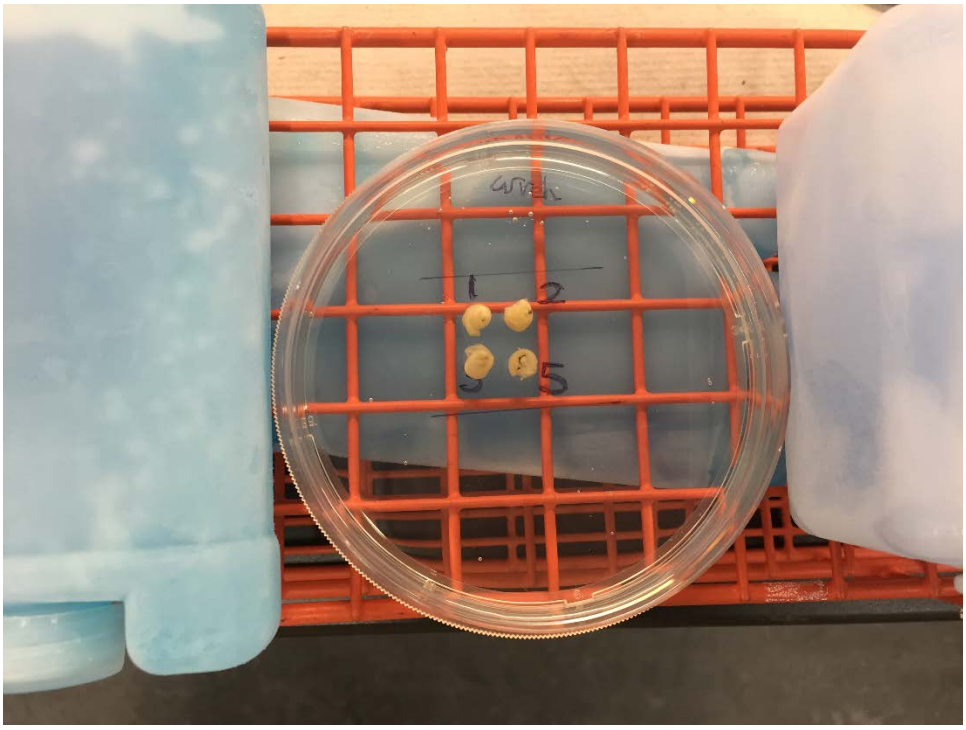

Figure III- 3. Additional gelatin solution was added until all four Swiss-rolls were completely covered and allowed to partially solidify for 20 minutes. atop the ice pack chilled surface. The petri dish was transferred to 4°C for 30 minutes to allow the gelatin solution to fully solidify.

27. The cooled gelatin block was trimmed when solidified. A spatula was used to pry out the solidified gelatin from the petri dish. The block was placed onto a smooth surface and extra gelatin was carefully trimmed away using a long blade and a slide (25x75x1mm) to make the required block size (Fig. III-4).

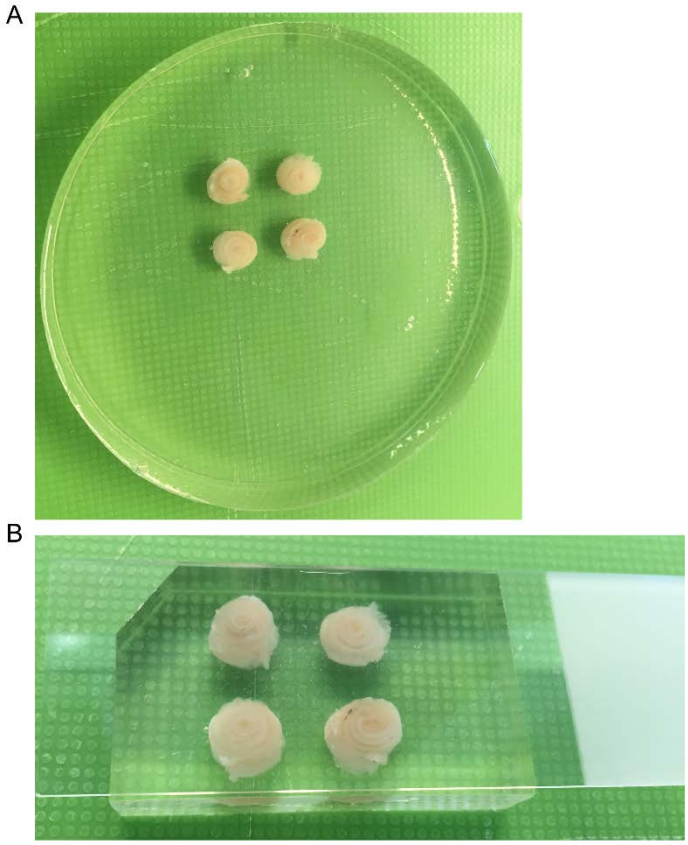

Figure III- 4. The solidified gelatin was A) removed from the petri dish and B) trimmed to the same size as a double-subbed 25x75x1mm slide.

28. The trimmed gelatin block was fixed in 4% PFA for 24 hours. The fixative solution covered the gelatin block completely. The PFA was replaced with 15% sucrose for another 24 hours. The block was stored at 4°C in a plastic specimen container or a collection cup which was slightly larger (approximately 5X as large as the block) than the gelatin block.

29. The gelatin block remained in sucrose at 4°C until it sank to the bottom of the 15% sucrose container.

30. The 15% sucrose was replaced with 30% sucrose for another 48 hours. The 30% sucrose was replaced with one more 30% sucrose incubation for an additional 48 hours until the block sank. The fully cryoprotected block was then ready to be sectioned.

Swiss Roll Sectioning

1. In order to section the block using a chambered cryostat (e.g. LEICA CM1850), the gelatin block was first dried off with a Kimwipe to remove any excess sucrose solution then transferred to a styrofoam container containing crushed dry ice and 2-Methylbutane (Fisher Chemical, 95% minimum) to freeze the block. To avoid cracks from forming in the block it was preferable to not keep it in the dry ice-2-Methylbutane mixture for greater than 10-20 seconds depending on the size of the gelatin block.
2. Once the block was frozen evenly, optimal cutting temperature (OCT) compound was used to adhere the block onto the cutting stage at -20°C inside a cryostat.
3. The frozen block was sectioned using a microtome knife (e.g. flat back permanent knife 16 cm- profile c- steel, Leica Biosystems Nussloch GmbH, Order No. 14 0216 07100, made in Germany) at -27°C to -35°C for 10 micron thick sections and they were mounted onto double-subbed slides (25x75x1mm) right away. To prevent the thin gelatin section from rolling on the knife, a small paint brush was placed at the edge of the newly sectioned tissue to hold on to it while sectioning was being completed. This step helped keep the thin gelatin section containing the

tissue to stay stretched out and facilitated mounting the section onto the slide.

A traditional chambered cryostat was used for sectioning 10 microns due to its adjustable temperature which keeps the section frozen during the sectioning and mounting steps. A sliding microtome (e.g. LEICA SM2000R) can be used for thicker sectioning (40 microns) which is appropriate for free-floating tissue staining as in our prior work using brains (K. Nagamoto-Combs et al., 2016). We have also used the Swiss-roll gelatin matrix approach to make mouse heart and lung blocks for mounted staining.

4. The hardened gelatin blocks are stable at 4°C. Although we typically store the mounted slides at -20°C, they are stable overnight at room temperature before starting the staining.

Histologic and Immunostaining

1. For H&E and Alcian blue staining, the slides were first removed from -20°C and allowed to dry at room temperature or in front of a fan for at least 1 hour or 30 min, respectively. The tissues were then hydrated by successive incubations in 95%, 75% alcohol, and distilled water, 5-7 dips each.

2. To demonstrate utility of the gelatin embedded section for histologic stains we performed H&E staining. The slides were stained with Hematoxylin (HARRIS HEMATOXYLIN, American MasterTech Scientific) for 5 minutes, rinsed in tap water, followed by 2 dips in hydrochloric acid 1N solution

(Fisher Chemical) for differentiation of the color, and a final rinse in tap water. The sections were then blued in the 28-30% ammonium hydroxide (NEWCOMERSUPPLY) for 5-10 seconds and rinsed thoroughly with tap water. The slides were then rinsed in 75% alcohol for a minute followed by 30-50 seconds in Eosin (AQUEOUS EOSIN Y, American MasterTech Scientific) as a counterstain. The slides were dehydrated with incubations in 95% alcohol, 100% alcohol (x2) for 3-5 dips each, and xylene (x3) for 1 minute each followed by coverslipping using Permount (Fisher Chemical) (Fig. III-5).

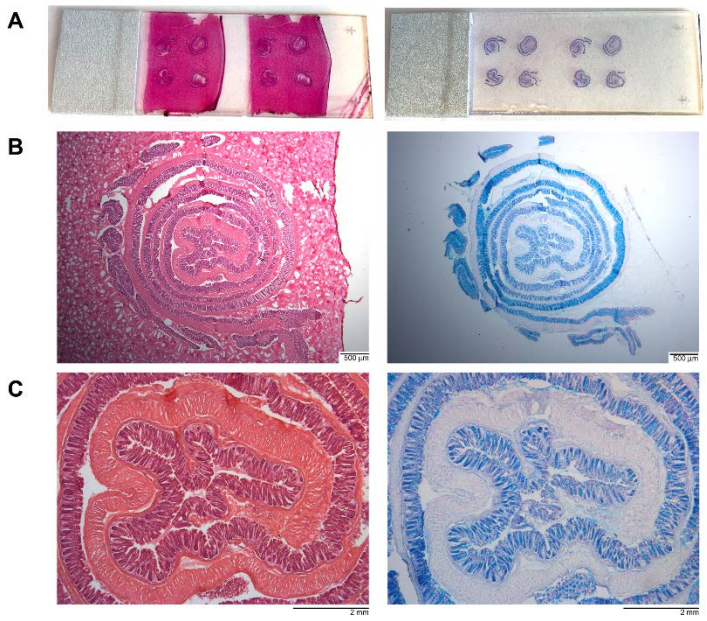

Figure III- 5. Representative H&E and Alcian blue staining of gelatin embedded tissue sections are shown with digital images of the A) entire slides, B) 1.25X magnification, and C) 4X magnification to demonstrate the whole length of cross-sectioned colon obtained by cutting the prepared blocks

3. Alcian blue staining was performed by placing the slides in 3% aqueous acetic acid for 3 minutes followed by 1% aqueous Alcian blue (NEWCOMERSUPPLY kit) pH 2.5 for 20-30 minutes. The excess stain was removed by rinsing the slides in tap water then distilled water. Then, the slides were counterstained in Nuclear Fast Red stain (Kernechtrot) for 2-3 minutes and rinsed in distilled water thoroughly. The slides were dehydrated in 95% alcohol and 100% alcohol 15-30 seconds (2 dips) each and three times in xylene for 1 minute each before being coverslipped using Permount (Fisher Chemical) (Fig. III-5).

4. In order to validate that antigenicity was maintained in gelatin embedded tissue sections, immunohistochemistry (IHC) was performed. The dried slides were placed in a Pro*Histo* antibody amplifier plate (PHI-AA1-1), a plate which is divided into 12 boxes (1 slid per well), and rinsed twice with PBS, 5 minutes each. Any type of plastic or glass microscope slide staining jars would suffice and no rocking is needed for this staining. In order to block endogenous peroxidase activity, tissue slides were incubated in PBS containing 0.3% H_2O_2 (30% Hydrogen Peroxide in water, Fisher BioReagents) for 5 minutes at room temperature. After incubation in IHC solution for 30 minutes to 1 hour at room temperature to block non-specific antibody binding, the primary antibody was added. The tissue slides were immunostained using an anti-CD68 (rat anti-mouse antibody, 1:1000 dilution in IHC solution, MCA1957, BIO-RAD) antibody overnight at 4°C. This macrophage marker antibody demonstrates robust

intestinal immunoreactivity in our hands (K. L. Puig et al., 2015). On the following day, the primary antibody was removed and the slides were rinsed in IHC solution 4-5 times, 5-10 minutes each. The biotinylated secondary antibody (rabbit anti-rat IgG antibody mouse adsorbed, 1:2000 dilution in IHC solution, BA-4001, Vector Laboratories, Inc.) was added for 2 hours at room temperature. VECTASTAIN Avidin-Biotin Complex (ABC, Vector Laboratories, Inc.) kit was used to increase the detection sensitivity of the biotinylated secondary antibody. The AB solution (1:500 dilutions each) was prepared in PBS and incubated for 30 minutes at room temperature before use. After removing the secondary antibody, the slides were rinsed 2 times in IHC solution and 2 times in PBS, 5 minutes each. The AB solution was added for 2.5 hours at room temperature followed by 4 rinses in PBS, 5 minutes each. To visualize the immunoreactivity, the Vector VIP Peroxidase (HRP) Substrate kit (SK-4600, Vector laboratories, Inc., Burlingame, CA) was used according to manufacture protocol. Vector VIP Substrate develops a purple color after reacting with peroxidase (HRP) enzyme. The images were taken using an upright Leica DM1000 microscope and Leica DF320 digital camera system (Fig. III-6).

As can be seen, it is feasible to simultaneously stain and mount a minimum of 4-6 different tissues in a single block as well as mount 2 different blocks containing the same or different treatments on a single standard microscope slide (25x75x1mm). This simultaneous IHC processing allows us to decrease reagent use, reduce variability in staining intensity across samples, and

improve tissue comparisons across samples during subsequent analysis. Most importantly, developing this method allowed us to proceed with studying intestinal inflammatory conditions such as colitis and CAC in mice.

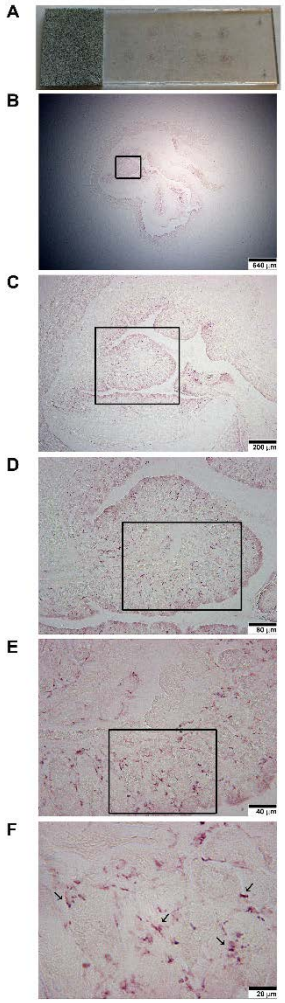

Figure III- 6. Representative CD68 immunoreactivity of gelatin embedded tissue sections are shown with digital images of A) a whole slide containing two gelatin sections, 4 samples each, B) 1.25X magnification, C) 4X magnification, D) 10X magnification, E) 20X magnification, E) 20X magnification, and F) 40X magnification images to confirm that our protocol does not attenuate CD68 antigenicity. Boxes demarcate image areas displayed in higher magnification images.

CHAPTER IV

GUT INFLAMMATION INDUCED BY DEXTRAN SULFATE SODIUM EXACERBATED Aβ PLAQUE DEPOSITION IN THE *APP^{NL-G-F}* MOUSE MODEL OF ALZHEIMER'S DISEASE

Introduction

Alzheimer's disease (AD) is a progressive age-related neurodegenerative disorder. Besides extracellular Aβ plaque deposition and intracellular neurofibrillary tangles, neuroinflammation plays a pivotal role in the susceptibility, onset, and progression of AD ("2016 Alzheimer's disease facts and figures," 2016; Anand, Gill, & Mahdi, 2014; Beach et al., 1989; Glenner & Wong, 1984b; Itagaki et al., 1989b; H. R. Kim et al., 2019; Kinney et al., 2018; Kohler et al., 2016; Masters et al., 2015; Mosher & Wyss-Coray, 2014; Nichols et al., 2019; Querfurth & LaFerla, 2010; Terry, 1963). Numerous retrospective studies demonstrate a significant reduction in the risk of AD in correlation with prolonged use of non-steroidal anti-inflammatory drugs (NSAID) early in life (Etminan, Gill, & Samii, 2003; in t' Veld et al., 2001; J. Wang et al., 2015; C. Zhang, Wang, Wang, Zhang, & Zhang, 2018). A midlife elevation of inflammatory markers due to systemic inflammation was also associated with increased cognitive decline over the course of 20 years in older adulthood in a longitudinal human study (Walker, Gottesman, et al., 2019). Observational studies demonstrated that individuals with one or more major infections, including *pneumonia*, during midlife

or later adulthood were exposed to higher risk of diminished brain volumes, dementia, and AD pathology hallmarks (Walker, Ficek, & Westbrook, 2019).

In addition to the central nervous system being affected by aging, elderly frequently suffer from gastrointestinal inflammation and dysfunction, including fecal incontinence, constipation, microscopic colitis, and diarrhea (Camilleri, Cowen, & Koch, 2008; Holt, 2001; Leung & Rao, 2009; Roach & Christie, 2008; Schuster, Kosar, & Kamrul, 2015; van Hemert, Skonieczna-Żydecka, Loniewski, Szredzki, & Marlicz, 2018). Indeed, inflammatory bowel disease (IBD), including colitis and Crohn's disease, is associated with the risk of developing cognitive impairment, anxiety, and depression in patients (Attree et al., 2003; Castaneda, Tuulio-Henriksson, Aronen, Marttunen, & Kolho, 2013; Dancey, Attree, Stuart, Wilson, & Sonnet, 2009; Kurina et al., 2001; Navabi et al., 2018; van Langenberg, Yelland, Robinson, & Gibson, 2017). This relationship may be due to the fact that the gastrointestinal (GI) tract bi-directionally communicates with the brain via the well-established gut-brain axis, including direct neuronal communication, endocrine signaling markers, and the immune system (Westfall et al., 2017). In our prior work we have shown intestinal changes in both human AD and mouse models that correlate with changes in the brains supporting the notion that brain and intestinal changes may be linked during disease (G. D. Manocha et al., 2019; K. L. Puig et al., 2015). The human GI tract harbors 100 trillion microbes, 10 times more than total cells in the human body, which mostly reside in the colon and play a critical role in regulating intestinal function (Khanna & Tosh, 2014). Dysbiosis, changes in intestinal microbial diversity, have been

reported in both human and animal models of IBD (Casén et al., 2015; Emge et al., 2016; Frank et al., 2007; Halfvarson et al., 2017; Jang et al., 2018; Putignani et al., 2016; S. L. Wang et al., 2019; Zuo & Ng, 2018) and Alzheimer's disease alike (Shen, Liu, & Ji, 2017; Vogt et al., 2017; L. Zhang et al., 2017) again suggesting a gut-brain connection during disease. Most importantly, intestinal inflammation in IBD mouse models results in microglial activation, altered neurogenesis, and increased cortical inflammation (Han et al., 2018; Riazi et al., 2008; Zonis et al., 2015).

In this study, we tested the hypothesis that induction of moderate colonic inflammation potentiates the progression of AD through inflammatory changes propagated from the intestine to the brain. Wild type and *App*$^{NL\text{-}G\text{-}F}$ mice were orally treated with 2 cycles of 2% dextran sulfate sodium (DSS) for 3 days followed by a 14 day interval. Mice were assessed for changes in memory and anxiety-like behavior during the second recovery phase and sacrificed 20 days after the last DSS exposure to investigate the long-lasting impact of gut inflammation on AD mouse brains. Our data demonstrated that chronic DSS administration decreased locomotion activity but not memory function and increased Aβ plaque load correlating with decreased microglial phagocytosis phenotype in the AD mouse model.

Methods

Animals

App$^{NL\text{-}G\text{-}F}$ mice (KI:RBRC06344) were obtained from Dr. Takashi Saito and Dr. Takaomi C. Saido, RIKEN BioResource Center, Japan. These mice carry the

humanized Aβ region, including Swedish (NL), Arctic (G), and Beyreuther/Iberian (F) mutations which promotes Aβ production, enhances Aβ aggregation through facilitating oligomerization and reducing proteolytic degradation, and increases $A\beta_{42/40}$ ratio, respectively (Saito et al., 2014). This transgenic mouse model of AD develops cortical Aβ amyloidosis as early as 2 months. To perform this study, wild-type (WT) C57BL/6 mice originally purchased from the Jackson Laboratory (Bar Harbor, Maine) and the App^{NL-G-F} transgenic mice were maintained, as a colony, under standard housing conditions including a 12 h light:12 h dark cycle and 22 ± 1°C temperature with *ad libitum* access to food and water at the University of North Dakota Center for Biomedical Research. Only male C57BL/6 control WT and App^{NL-G-F} mice at 6-10 months of age (n = 9-11 per treatment group) were used due to limited animal availability (Table IV-1). Mice were randomly divided into vehicle and DSS treated groups for 9 weeks of investigation. Mice were euthanized followed by cardiac perfusion and the brain, spleen, and colon were collected to quantify histologic and biochemical changes on week 9. All procedures involving animals were reviewed and approved by the UND Institutional Animal Care and Use Committee (UND IACUC). The investigation conforms to the National Research Council of the National Academies Guide for the Care and Use of Laboratory Animals (8^{th} edition).

Table IV- 1. Animal numbers and age at the beginning of the experiment

Gender	Genotype	Age at the beginning of the Experiment	Genotype	Age at the beginning of the Experiment
Male	**Wild Type Vehicle (n=9)**	7-8 month-old	**Wild Type DSS (n=11)**	6-7 month-old
Male	***App*$^{NL-G-F}$ Vehicle (n=10)**	9-10 month-old	***App*$^{NL-G-F}$ DSS (n=10)**	10 month-old

Dextran Sulfate Sodium (DSS) Exposure and Assessment of the Severity of Colitis-Like Symptoms

In order to mimic the effect of gut inflammation on the progression of AD in adulthood, 6-10 months-old male *App*$^{NL-G-F}$ mice and matched age and sex wild type mice were randomly divided into 4 experimental groups (Table IV-1). Each genotype was treated with vehicle (autoclaved drinking water) or 2% dextran sulfate sodium (DSS) for 2 cycles, 3 days each, with a 14 day interval for recovery before initiation of the second DSS exposure as described in Fig. IV-1 (Wirtz et al., 2017).

Colitis-like disease was induced in two groups by dissolving DSS (2%, w/v, MW=36-50 kDa, MP Biomedicals, LLC, Santa Ana, CA, USA) in autoclaved drinking water. During the second cycle of the DSS treatment to the end of the study, mice were weighed individually. Drinking water as well as food intake were monitored during the second DSS bout. The disease activity index (DAI) is associated with the presence of gut lesions and inflammation and represents the percentage of body weight loss, stool consistency, and the presence of gross bleeding in feces. A Hemoccult test kit (Beckman Coulter Inc., CA, USA) was used to determine occult blood in the stool samples. DAI was

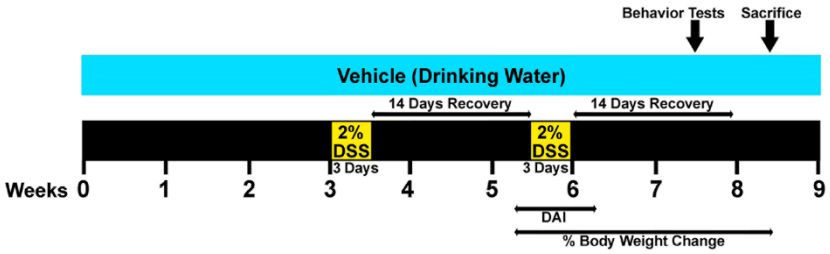

Figure IV- 1. Schematic of the experimental design and timeline of DSS treatment and different assessments. 2% DSS was dissolved in the drinking water and fed ad libitum to male C57BL/6 wild type and *App*$^{NL\text{-}G\text{-}F}$ mice (AD mouse model) at 6-10 months of age for two cycles of three days each. DAI was scored from 1 day pre exposure to 2 days post exposure during the second bout of DSS treatment. The percentage of body weight loss was calculated starting from the second DSS treatment untill the week of euthanasia. On week 7, 12 days after exposure of DSS, mice were tested for behavioral functions. On the following week, brain, colon, and spleen tissues were collected in order to examine the effect of gut integrity disruption during the inflammation resolving phase.

evaluated and scored in a blinded fashion at 1 day prior to DSS treatment (day 0), during the second cycle of 2% DSS administration, and 2 days post exposure, totaling 5 days, as previously described with slight modifications (Table IV-2) (Chassaing, Aitken, Malleshappa, & Vijay-Kumar, 2014b; Cooper, Murthy, Shah, & Sedergran, 1993; Eichele & Kharbanda, 2017; Ghia, Blennerhassett, Kumar-Ondiveeran, Verdu, & Collins, 2006; Snider et al., 2016).

Each parameter was scored on a scale of 0-4 and summed to get a score out of 12 for the maximum DAI per mouse for each condition. The daily DAI per mouse was subtracted from its respective day 0 to get the normalized score. Body weight loss was calculated as the percentage ratio by dividing the body weight on each specific day to the body weight on day 0 during the second cycle

Table IV- 2. Disease activity index (DAI) scoring performed to assess the colitis induced by DSS

Score	Weight loss (%)	Stool Consistency	Occult/gross bleeding
0	WI <1 %	Normal	Normal
1	1% ≤ WI < 5%		+
2	5% ≤ WI < 10%	Loose stools	++
3	10% ≤ WI < 20%		+++
4	WI ≤ 20%	Diarrhea	Gross bleedings

of 2% DSS administration until the week of mice collection (Fig. IV-1). The method of scoring is quite analogous to clinical symptoms observed in human IBD. Mice were approximately 8-12 months of age at the time of collection. On the 8th week, animals were euthanized via CO_2 asphyxiation followed by cardiac perfusion with PBS. The colon weights and lengths between the cecum and rectum as well as spleen weights were measured. The brain, colon, and spleen were collected for further histochemical and biochemical analysis.

Behavioral Analysis: Open Field and Cross-Maze Tests

On the 7th week, open field (OF) and cross maze (CM) tests were performed to assess the effect of DSS treatment on behavior during the second recovery phase. Locomotor activity and working memory were evaluated by OF and CM tests, respectively. To evaluate general locomotion associated with treatment, animals were placed individually in the same quadrant of a 19cm × 45cm × 25cm open field apparatus to freely explore and move for 10 min. The distance traveled, time spent in the center of the field as well as time mobile were scored by blind raters from video captured by Anymaze software (Stoelting Co. Wood Dale, IL, USA). Following the test, the animals were placed back into their home cages for at least 30 min prior to the next behavior assessment.

CM testing allows mice to explore a cross-shaped maze at their own discretion without any added stress or motivation such as lights, sound, food deprivation, etc. Mice were placed in the same arm of the CM and allowed to move and choose other arms for 10 min. A choice was considered when all 4 feet were within an arm. The total entries were recorded and the number of alternations was counted (defined as 4 consecutive entries into 4 different arms), and % alternation for each mouse was calculated as follows, # alternations/(total entries-3)x100, by personnel blinded to the study paradigm. Immediate re-entry into the same arm, after exiting it, was not considered as an arm choice. The chance alternation rate for this task is 22.2%. The test was performed using Anymaze software (Stoelting Co. Wood Dale, IL, USA). After completion of the test, mice were returned to their home cages until tissue collection.

Histological Staining of Colonic Tissue

On the day of collection, distal colons were made into Swiss-rolls, fixed in 4% paraformaldehyde (PFA) for 5 days, and cryoprotected via two successive changes of 30% sucrose. The Swiss-rolls were embedded into gelatin blocks and were serially sectioned using a chambered cryostat for 10μm thick sections. Colon sections were stained for histology H&E (Hematoxylin and eosin) and Alcian blue stains as described in detail previously (Sohrabi & Combs, 2019). An upright Leica DM1000 microscope and Leica DF320 digital camera system were used to capture images and figures were made using Adobe Photoshop software.

Immunohistochemistry (IHC)

Left brain hemispheres were fixed in 4% PFA for 5 days followed by cryoprotection via two successive changes of 30% sucrose. Brains were embedded in 15% gelatin and serially sectioned into 40μm sections using a sliding microtome (K. Nagamoto-Combs et al., 2016). Sections were immunostained using antibodies against Iba-1 (1:1000 dilution, rabbit, 019-19741, Wako Chemicals USA, Inc., Richmond, VA, USA), CD68 (1:1000 dilution, rat anti-mouse, MCA1957, Bio-Rad Laboratories, Inc., CA, USA), GFAP (1:1000 dilution, D1F4Q, rabbit mAb, Cell Signaling Technology, Inc., Danvers, MA, USA), and β-Amyloid (1:500 dilution, D54D2, rabbit mAb, Cell Signaling Technology, Inc., Danvers, MA, USA) to detect microglia, astrocytes, and Aβ plaques, respectively. For Aβ immunostaining, antigen retrieval was required and performed using 25% formic acid (Sigma-Aldrich) for 25 min at room temperature prior to blocking (Burlingame, CA, USA). Immunostaining was performed for the Swiss-rolls via using rat anti-mouse CD68 (1:1000 dilution, MCA1957, Bio-Rad Laboratories, Inc., CA, USA) and anti-claudin-4 (1:500 dilution, ZMD.306, rabbit pAb, Invitrogen/ThermoFisher scientific, Waltham, MA, USA) antibodies to target the intestinal macrophages and tight junction proteins, respectively (Sohrabi & Combs, 2019). Antigen retrieval was performed for claudin-4 immunostaining using citrate antigen unmasking solution (1:100 dilution, H-3300, Vector laboratories, Inc., Burlingame, CA, USA) for 40 min at 80°C prior to blocking. Tissues were rinsed in PBS and blocked in PBS solution containing 0.5% bovine serum albumin (BSA, Equitech-Bio, Inc.), 0.1% Triton X-100 (Sigma-Aldrich), 5%

normal goat serum (NGS, Equitech-Bio, Inc.), and 0.02% Na Azide for at least 30 min. After 24 hr of incubating tissues with primary antibodies at 4°C, respective biotinylated secondary antibodies were used, including rabbit anti-rat IgG antibody mouse adsorbed and goat anti-rabbit IgG (Vector Laboratories, Inc., Burlingame, CA, USA). A VECTASTAIN Avidin-Biotin Complex (ABC) kit was used followed by the Vector VIP Peroxidase (HRP) Substrate kit (SK-4600) to visualize the antibody binding (Vector laboratories, Inc., Burlingame, CA, USA). Images were taken using an upright Leica DM1000 microscope and Leica DF320 digital camera. Immunohistochemistry quantitation of temporal cortices and hippocampi was performed from 3 serial sections per brain (n=8) via converting the images to greyscale and calculating the mean optical density for each image using Adobe Photoshop CS3 software.

Enzyme-Linked Immunosorbent Assay (ELISA)

On the collection day, right hippocampi and parietal cortices of brain hemispheres and middle regions of the colons were isolated and flash frozen. Hippocampi, parietal cortices, and middle colons were lysed in RIPA buffer (20 mM Tris, pH 7.4, 150 mM NaCl, 1 mM $Na3VO_4$, 10 mM NaF, 1 mM EDTA, 1 mM EGTA, 0.2 mM phenylmethylsulfonyl fluoride, 1% Triton X-100, 0.1% SDS, and 0.5% deoxycholate), lysis buffer 17 (R&D Systems, a Bio-techne brand, Minneapolis, MN, USA), and 1% Triton X-100 in PBS, respectively, with protease inhibitor cocktail (P8340, Sigma-aldrich, MO, USA). Tissues were centrifuged (12,000 rpm, 4°C, 10 min) and the supernatants were collected. Hippocampi supernatants were used to perform soluble $A\beta_{1\text{-}40/42}$ ELISAs (human Amyloid

$\beta_{40/42}$ Brain EZBRAIN40/42 ELISA, EMD Millipore, Billerica, MA, USA). The hippocampi pellets were re-suspended in 5M guanidine HCL/50mM Tris HCL, pH 8.0, centrifuged (12,000 rpm, 4°C, 10 min), and the supernatants were removed to quantify insoluble $A\beta_{1\text{-}40/42}$ levels by using the same ELISA kit according to the manufacturer's protocol. TNF-α, IL-1β, and IL-6 cytokine ELISAs were performed from the parietal cortices supernatants according to the manufacturer's protocol (Quantikine ELISAs, R&D Systems, a bio-techne brand, Minneapolis, MN, USA). The collected colon supernatants were used to perform lipocalin-2 ELISA (Mouse Lipocalin-2/NGAL DuoSet ELISA, R&D Systems, a bio-techne brand, Minneapolis, MN, USA) according to the manufacturer's protocol. The BCA kit (Thermo Scientific, IL, USA) was used to quantify protein concentrations and Aβ, lipocalin-2, and cytokine levels were normalized to the protein content of each homogenized sample.

Western Blotting

Protein contents were assessed for the collected hippocampi supernatants, previously lysed in RIPA buffer containing protease inhibitor cocktail, via a BCA kit. 5 μg of protein per sample was resolved by 10% sodium dodecyl sulfate polyacrylamide gel electrophoresis (SDS-PAGE) and transferred to polyvinylidene difluoride membranes (PVDF) for western blotting. Membranes were blocked for 1h in 5% bovine serum albumin (BSA) in tris-buffered saline solution (TBST) followed by applying anti-amyloid precursor protein (1:1000 dilution, Y188, ab32136, rabbit mAb, Abcam, Cambridge, MA, USA), BACE (1:1000 dilution, D10E5, rabbit mAb, Cell Signaling Technology, Inc., Danvers,

MA, USA), Cox-2 (1:500 dilution, Cyclooxygenase 2, rabbit pAb, ab15191, Abcam, Cambridge, MA, USA), and VCAM-1 (1:1000 dilution, H-276: sc-8304, rabbit pAb, Santa Cruz Biotechnology, Inc., CA, USA) primary antibodies overnight at 4°C. Chemiluminescent visualization was used to detect antibody binding using donkey anti-rabbit IgG and goat-anti mouse IgM horseradish peroxidase (HRP)-conjugated secondary antibodies (Santa Cruz Biotechnology, Inc., CA, USA). Exposures were captured using an Aplegen Omega Lum G imaging system. Optical density values were normalized to the loading control α-tubulin (1:10000 dilution, TU-02: sc-8035, mouse mAb, Santa Cruz Biotechnology, Inc., CA, USA) optical density values from the same membrane.

Statistical Analysis

All *in vivo* data were analyzed by two-way ANOVA multiple comparisons followed by Uncorrected Fisher's LSD test using GraphPad Prism 8 software. Data are represented as the mean ± SEM. Significance is indicated by P value measurements with a $P < 0.05$ considered significant; *$P < 0.05$; **$P < 0.01$; ***$P < 0.001$; ****$P < 0.0001$.

Results

DSS Induced Colitis-Like Symptoms in Wild Type and *App^{NL-G-F}* Mice

6-10 months-old male *App^{NL-G-F}* mice and matched age and sex wild type mice were treated with 2% DSS for 2 bouts (Fig. IV-1) to induce colonic inflammation. Symptomatic parameters of colitis, including DAI, % body weight loss, colon length, and spleen and colon weights were monitored and recorded. During the second administration of DSS, both wild type and AD mouse models

displayed significantly greater disease activity scores and % body weight losses compared to their respective untreated groups starting on days 1 and 4, respectively (Fig. IV-2A and B).

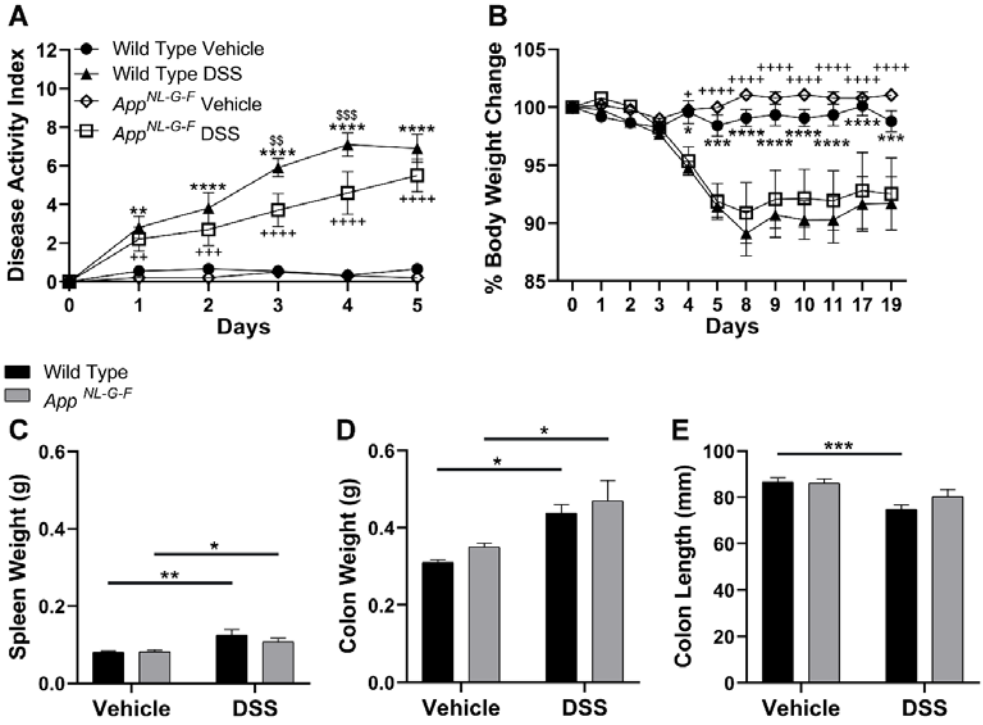

Figure IV- 2. DSS treatment induced symptomatic parameters of colitis-like disease in both genotypes compared to controls. A) DAI was monitored on day 0, during the second cycle of 2%DSS (3 days), and 2 days post DSS exposure in both DSS and vehicle treated groups per genotype. (**p<0.01, ****p<0.0001 wild type vehicle vs. wild type DSS; $^{++}$p<0.01, $^{+++}$p<0.001, $^{++++}$p<0.0001 *App*$^{NL-G-F}$ vehicle vs. *App*$^{NL-G-F}$ DSS; $^{\$\$}$p<0.01, $^{\$\$\$}$p<0.001 wild type DSS vs. *App*$^{NL-G-F}$ DSS comparing on the same day, mean ± SEM, n=9-11 animals). B) the percentage of body weight changes was calculated during the second DSS epxposure untill week of tissue collection. (*p<0.05, ***p<0.001, ****p<0.0001 wild type vehicle vs. wild type DSS; $^{+}$p<0.05, $^{++++}$p<0.0001 *App*$^{NL-G-F}$ vehicle vs. *App*$^{NL-G-F}$ DSS comparing on the same day, mean ± SEM, n=9-11 animals). (C-D) Spleen and colon weights as well as colon length were measured from wild type and *App*$^{NL-G-F}$ mice to indicate colonic inflammation. (*p<0.05, **p<0.01, ***p<0.001, mean ± SEM, n=9-10 animals).

Wild type mice developed greater DAI compared to *App*$^{NL-G-F}$ mice on days 3-4 due to DSS treatment (Fig. IV-2A). Mice were expected to recover to their initial weight during the course of recovery (Snider et al., 2016). However, both wild type and *App*$^{NL-G-F}$ DSS treated mice showed a consistent reduction in body weight without complete recovery after ending the second cycle of DSS exposure until euthanasia in comparison with their controls (Fig. IV-2B). Body weight loss and rectal bleeding are associated with shortening and thickening of the colon as well as splenomegaly, as other biological markers for assessment of colonic inflammation (Chassaing et al., 2014b; Chassaing et al., 2012). The 2% chronic DSS treated group in both genotypes demonstrated a significant increase in spleen and colon weights typically related to anemia as a result of rectal bleeding (Chassaing et al., 2012) and the granulomatous nature of inflammation (Chassaing et al., 2014b), respectively (Fig. IV-2C and D). Colonic length significantly decreased in wild type but not *App*$^{NL-G-F}$ mice after inflammation induction (Fig. IV-2E). Overall, these results demonstrated that 2 cycles of chronic DSS treatment produced a time-dependent DAI in both wild type and *App*$^{NL-G-F}$ genotypes.

DSS Treatment Decreased Mobility of *App*$^{NL-G-F}$ Mice

To determine whether induction of moderate colonic inflammation negatively affects locomotor activity and working memory, wild type and *App*$^{NL-G-F}$ mice were examined in the open field (OF) and cross maze (CM) paradigms 12 days after completing the second cycle of DSS, during the resolving inflammation phase, respectively. The OF test examines general locomotion and

anxiety-like behavior via primarily exploratory behavior (Crawley, 1985). Interestingly, *App*$^{NL-G-F}$ mice showed a greater distance traveled at baseline compared to wild type mice in vehicle treated groups in the OF test. The genotype-dependent increase in mobility as well as time mobile were attenuated due to DSS administration in the *App*$^{NL-G-F}$ mice. However, DSS exposure exerted no effect on time spent in the center of the OF in both genotypes (Fig. IV-3A). This suggests a basal increase in locomotion activity in *App*$^{NL-G-F}$ mice that had long-lasting attenuation following DSS treatment in *App*$^{NL-G-F}$ mice.

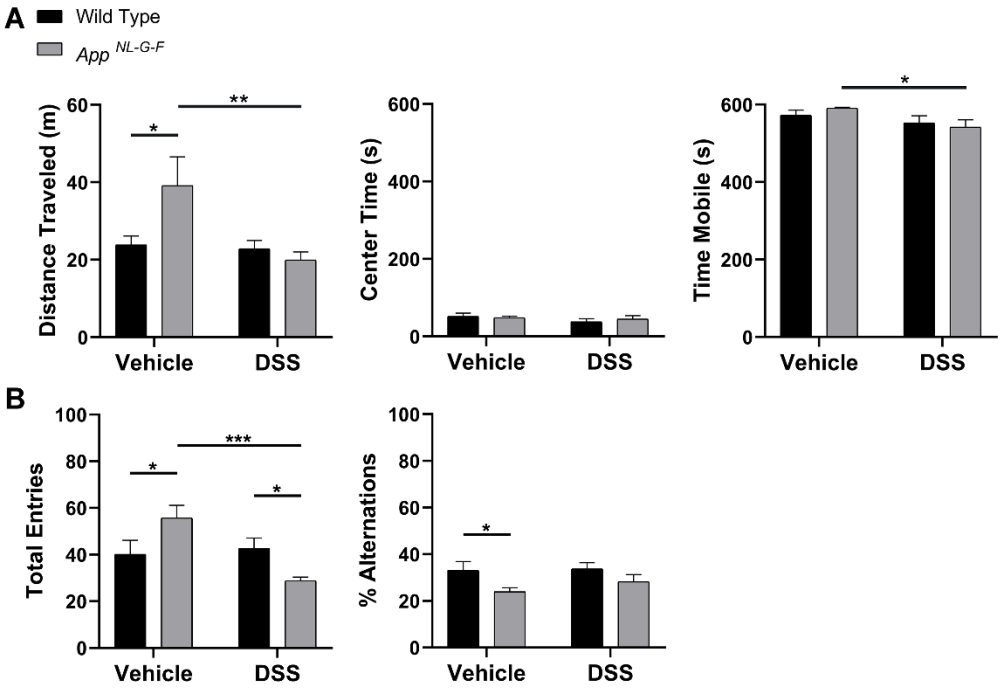

Figure IV- 3. DSS treatment decreased mobility of *App*$^{NL-G-F}$ mice in both OF and CM tests. A) General locomotor activity or anxiety-like behavior was assessed by quantifying the distance traveled, time spent in the center as well as time mobile using OF test. B) Total entries (locomotion) and percentage of alternations in different arms of the CM test were quantified to evaluate working memory in both genotype vehicle and DSS treated groups. ($^{*}p<0.05$, $^{**}p<0.01$, $^{***}p<0.001$, mean ± SEM, n=8-10 animals tested at 8-12 months of age).

To assess the working memory changes induced by 2 bouts of 2% DSS treatment, performance in the CM paradigm, which is a “+” shaped apparatus with four white arms, was examined for both genotypes (B. Wang et al., 2017). Consistent with the OF results, the total number of arm choices, indicating locomotor activity, was greater in vehicle treated *App*$^{NL\text{-}G\text{-}F}$ mice compared to the wild type control group. The total entries were reduced in *App*$^{NL\text{-}G\text{-}F}$ mice after DSS administration (Fig. IV-3B). As we expected, a significant reduction was observed in the % alternations made by the *App*$^{NL\text{-}G\text{-}F}$ vehicle treated group in comparison with the wild type controls suggesting the presence of baseline memory deficit in this mouse model of AD. However, there was no significant decrease in % alternations due to DSS treatment (Fig. IV-3B). This is likely due to the fact that the alternation rate (%) representing working memory was calculated as the number of alternations divided by (total entries-3)x100 for each mouse, while total entries (locomotion) significantly decreased in *App*$^{NL\text{-}G\text{-}F}$ DSS treated mice. These findings indicated that DSS exposure negatively affected *App*$^{NL\text{-}G\text{-}F}$ mice locomotion in a persistent fashion during the second recovery phase.

DSS Administration Disrupted Colonic Epithelial Integrity and Increased Inflammation

In order to perform histological examination of colonic inflammation induced by DSS, H&E and Alcian blue staining were performed on the distal colon Swiss-rolls (Fig. IV-4A). Hematoxylin and eosin staining showed minimal hyperplasia or crypt elongation (an increase in epithelial numbers in longitudinal crypts relative to baseline epithelial cell numbers per crypt), mixed leukocytes

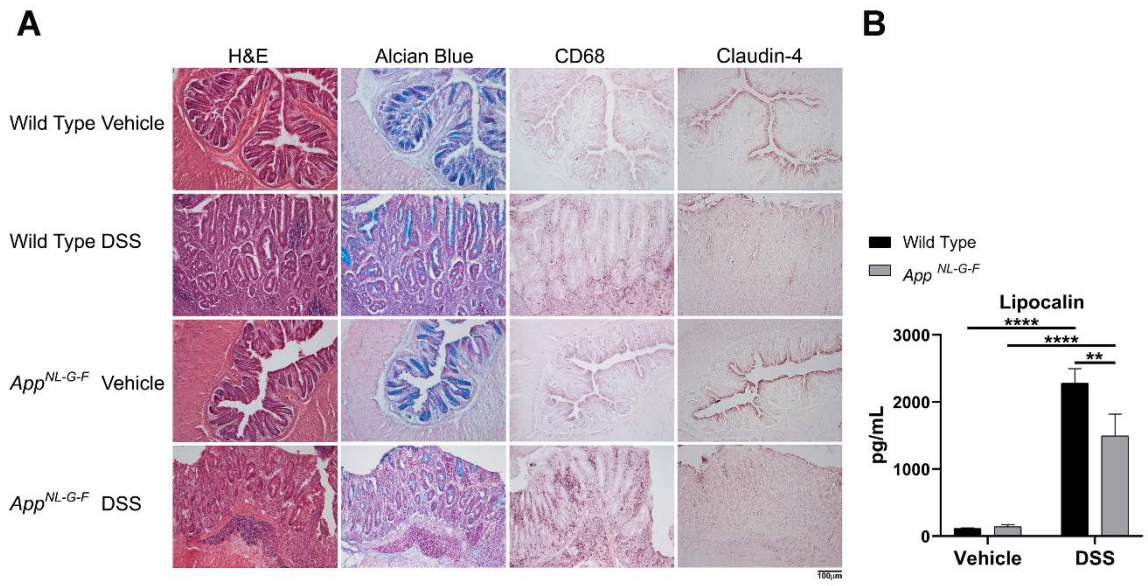

Figure IV- 4. DSS treatment resulted in colonic inflammation in both wild type and *App*$^{NL-G-F}$ mice. A) H&E and Alcian blue staining along with anti-CD68 and claudin-4 immunostaining of cross sectional Swiss-roll sections of the distal colon were performed to examine the severity of epithelial erosion, loss of goblet cells, infiltration of macrophages, and changes of the tight junction levels in colon sections of DSS treated vs. vehicle groups in both genotypes (n= 4 Swiss-rolls/condition/genotype). B) The changes in lipocalin2 levels, as an anti-microbial siderophore-binding peptide involved in IBD, were assessed to determine the extent of intestinal inflammation in both wild type and *App*$^{NL-G-F}$ mice following DSS exposure. ($^{**}p<0.01$, $^{****}p<0.0001$, mean ± SEM, n=8 animals).

infiltration, goblet cell loss, and to some extent erosion (i.e. loss of surface epithelium), ulceration (epithelial defect reaching beyond muscularis mucosae), and crypt loss (musoca devoid of crypts) in both DSS treated groups compared to their controls (Fig. IV-4A) (Erben et al., 2014). To better assess goblet cell loss caused by chronic DSS exposure, mucin-producing goblet cells were visualized by performing Alcian blue staining. Alcian blue stains acidic mucus secreted by goblet cells (G. G. Adams & Dilly, 1989). Wild type and *App*$^{NL-G-F}$ DSS treated mice demonstrated reduced staining of goblet cells compared to their controls

(Fig. IV-4A). It has been reported that the number of CD68 positive macrophages increases in colon specimens of IBD patients compared to normal individuals (Rugtveit, Brandtzaeg, Halstensen, Fausa, & Scott, 1994). Therefore, CD68 immunostaining was performed to visualize infiltrating, activated macrophages, into the lamina propria and colonic submucosa. As expected, a robust increase in macrophage infiltration to the site of inflammation was observed in both DSS treated genotypes in comparison with controls (Fig. IV-4A). Claudin proteins, tight junction proteins that regulate paracellular permeability, undergo changes in expression levels and distribution in IBD (Perše & Cerar, 2012). Claudin-4 staining decreases or redistributes in surface epithelial areas of IBD biopsies compared to its strong expression in normal colonic epithelium (Prasad et al., 2005). Immunohistochemistry staining showed a dramatic reduction in claudin-4 immunoreactivity of tight junction areas in the surface epithelium in wild type and *App*$^{NL\text{-}G\text{-}F}$ mice due to colonic inflammation compared to their controls (Fig. IV-4A). Lipocalin-2 (Lcn2), a 25 kDa neutrophil gelatinase-associated lipocalin (NGAL) glycoprotein, was first isolated from human neutrophil granules (Kjeldsen, Cowland, & Borregaard, 2000). Fecal Lcn2 is a stable, highly sensitive, and non-invasive marker which determines the extent of intestinal inflammation (Chassaing et al., 2012). Colonic lipocalin ELISA demonstrated over 13 and 20-fold increases in response to DSS treatment in *App*$^{NL\text{-}G\text{-}F}$ and wild type mice compared to their controls, respectively (Fig. IV-4B). These findings suggest that 2% chronic DSS administration induced mild to moderate intestinal inflammation in both genotypes.

Gut Inflammation Induced by DSS Exacerbated Aβ Accumulation in *App*$^{NL-G-F}$ Mice Brains

Wild type and *App*$^{NL-G-F}$ mice were treated with 2 cycles of 2% DSS and sacrificed 20 days (on week 8th) after the last exposure (Fig. IV-1) to assess long-lasting brain changes. The impact of moderate disruption of gut epithelial barrier and gut inflammation on Aβ deposition in different brain regions was assessed. Aβ immunohistochemistry demonstrated that plaque load significantly increased in both hippocampi and temporal cortices of *App*$^{NL-G-F}$ mice in response to DSS treatment compared to their controls (Fig. IV-5A and B).

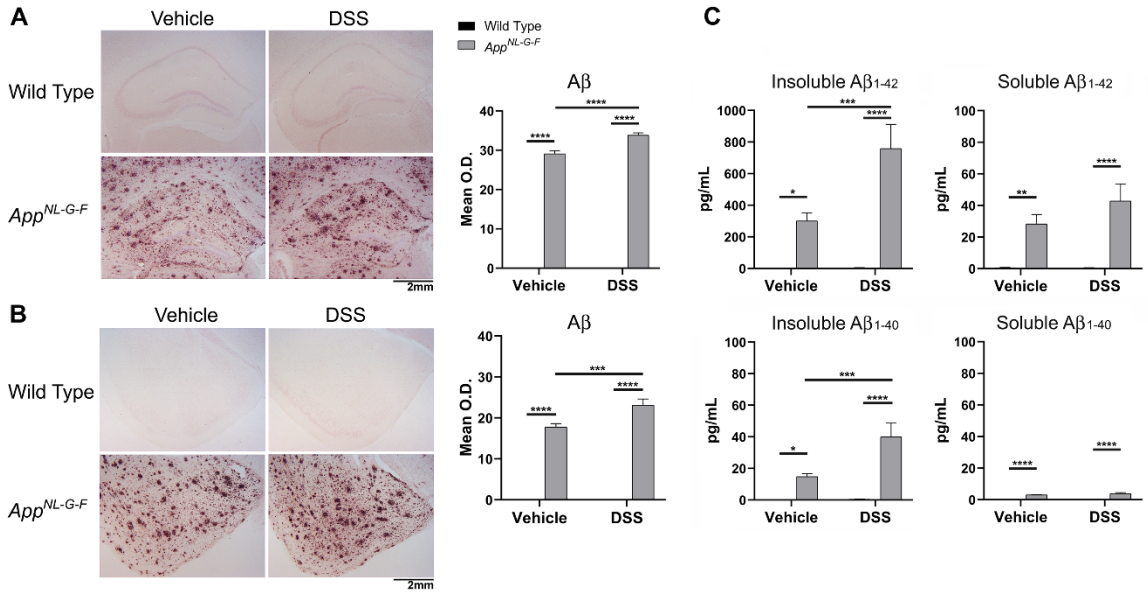

Figure IV- 5. DSS treatment elevated hippocampal and temporal cortex Aβ levels in *App*$^{NL-G-F}$ mice. A-B) Immunohistochemistry was performed on both wild type and *App*$^{NL-G-F}$ brains using anti-Aβ antibody. Mean optical density was measured using 3 different hippocampus sections/mouse. Representative hippocampi and temporal cortices are shown. C) Hippocampi, collected from vehicle and DSS treated wild type and *App*$^{NL-G-F}$ mice, were lysed to perform ELISAs for human insoluble Aβ$_{1-40/42}$ and soluble Aβ$_{1-40/42}$. (*p<0.05, **p<0.01, ***p<0.001, ****p<0.0001, mean ± SEM, n=8 animals).

Similarly, Aβ ELISA of hippocampi demonstrated more than 2-fold increase in both insoluble $A\beta_{1-40}$ and $A\beta_{1-42}$ in DSS treated *App*$^{NL-G-F}$ mice in comparison with the vehicle treated group. Soluble $A\beta_{1-40/42}$ showed no statistically significant changes due to DSS administration, although there was an increase trend in the DSS treated *App*$^{NL-G-F}$ mice (Fig. IV-5C). These data indicate that inducing moderate intestinal inflammation leads to exacerbation of AD pathology via elevating Aβ plaque deposition as a maintained brain change even during the resolution phase of gut inflammation.

Microglial Phagocytic Phenotype Decreased Due to the Moderate Colitis-Like Symptoms Induced by DSS Treatment

It is well established that brain specialized inflammatory cells, microglia and astrocytes, become activated and express inflammatory cytokines in various brain diseases, including AD. Impaired microglial phagocytosis activity in response to Aβ plaque deposition plays a hypothesized role in pathogenesis and progression of AD (D. V. Hansen et al., 2018; Itagaki et al., 1989b; Nichols et al., 2019; M. Prinz, J. Priller, S. S. Sisodia, & R. M. Ransohoff, 2011; W. Y. Wang, M. S. Tan, J. T. Yu, & L. Tan, 2015). We expected that propagation of gut inflammation induced by DSS to the brain would also affect brain gliosis correlating with the elevated Aβ levels. Immunohistochemistry was performed to investigate the impact of colonic barrier disruption and gut inflammation on glial activation. Notably, astrocytosis, visualized using anti-GFAP immunoreactivity, did not reveal any dramatic alterations following DSS administration in wild type or *App*$^{NL-G-F}$ hippocampi compared to their controls (Fig. IV-6). Microgliosis was

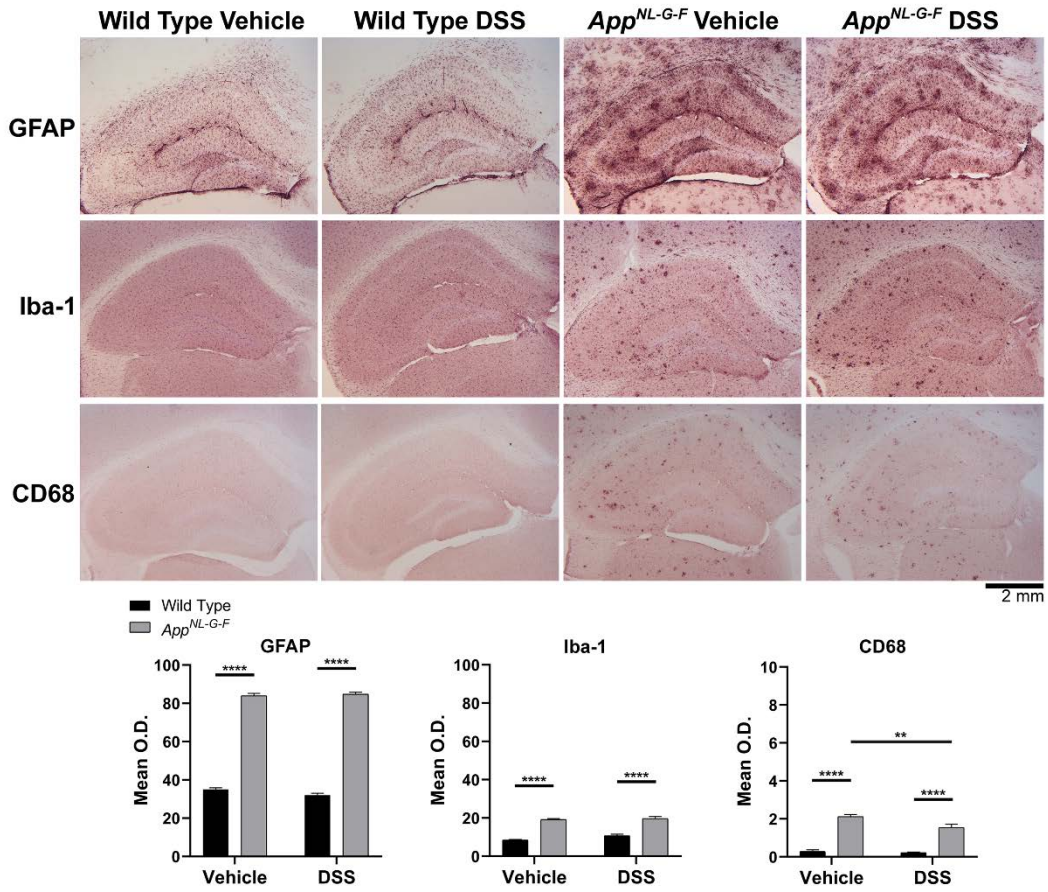

Figure IV- 6. DSS treatment reduced microglia CD68 immunoreactivity in *App*$^{NL-G-F}$ mice. Immunohistochemistry was performed on both wild type and *App*$^{NL-G-F}$ brains using anti-GFAP, Iba-1, and CD68 antibodies. Mean optical density was measured using 3 different hippocampus sections/mouse. Representative hippocampi are shown. ($^{**}p<0.01$, $^{****}p<0.0001$, mean ± SEM, n=8 animals/condition).

assessed using two different antibodies, anti-Iba-1 and CD68. Interestingly, moderate colonic inflammation diminished Aβ-associated microglial phagocytic phenotype, demonstrated by CD68 immunoreactivity, in *App*$^{NL-G-F}$ mice versus their vehicle controls. Similar to GFAP, the motility-related microglial protein, Iba-1, (Franco-Bocanegra, McAuley, Nicoll, & Boche, 2019) was not altered in response to gut inflammation induced by DSS in both genotype hippocampi

(Fig. IV-6). This suggested that moderate gut inflammation resulted in a selective phenotype change in gliosis with no change in astrocytes but reduced microglial phagocytic phenotype that correlated with increased Aβ plaque accumulation in the brain.

DSS Treatment Did Not Change Brain Cytokine Levels

Parietal cortices were lysed and cytokines levels quantified by ELISA to assess inflammatory cytokine profile changes, including TNF-α, IL-1β, and IL-6, as a result of 2 cycles of 2% DSS treatment in both wild type and *App*$^{NL-G-F}$ mice. The brain levels of TNF-α were below detection level and IL-1β levels were not changed across experimental groups and genotypes (data not shown). As expected, vehicle treated AD mice demonstrated significantly higher IL-6 levels compared to their wild type control. The cytokine levels were not significantly elevated by DSS treatment in wild type and *App*$^{NL-G-F}$ mice compared to controls, however (Fig. IV-7). This finding suggests that moderate gut inflammation does not lead to long-term effects on brain IL-6 levels.

DSS Treated *App*$^{NL-G-F}$ Mice Brains Demonstrated Changes in Neurodegeneration and Neuroinflammatory Markers

Based upon the changes in Aβ plaque load and microglial phenotype, we next investigated the changes in levels of proteins involved in Aβ processing, inflammation, and vascular phenotype in the mouse brains 20 days following the DSS treatments via western blots. Hippocampi lysates were used to quantify APP and BACE (β-secretase) protein levels, two proteins required for Aβ production in AD. No increases were observed in APP protein levels due

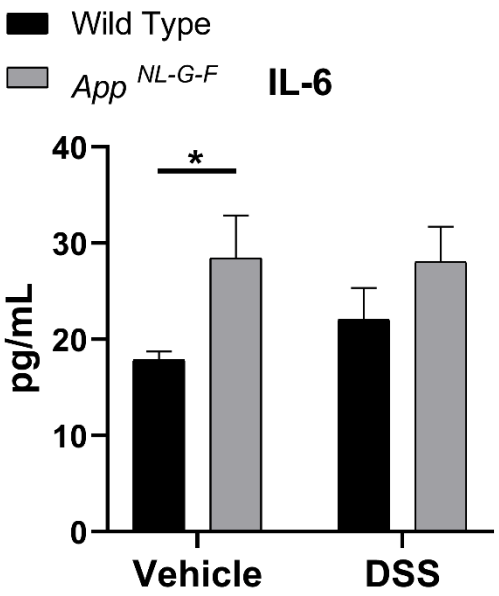

Figure IV- 7. Brain IL-6 levels did not change due to DSS treatment. Parietal cortices collected from vehicle and DSS treated wild type and *App*$^{NL-G-F}$ mice and were lysed to quantify protein levels of IL-6 by ELISA. (*p<0.05, mean ± SEM, n=8 animals).

to gut inflammation in either genotypes. However, DSS exposure increased β-secretase protein levels in *App*$^{NL-G-F}$ mice compared to the wild type group consistent with our Aβ ELISA and immunohistochemistry results showing elevated Aβ levels and plaque deposition after DSS treatment (Fig. IV-8). Protein levels of cyclooxygenase-2 (cox-2), an inflammatory marker, and vascular cell adhesion molecule-1 (VCAM-1), a mediator of leukocyte binding and transmigration through endothelial cells during inflammation, (Chung et al., 2010; Cook-Mills, Marchese, & Abdala-Valencia, 2011) were also elevated in *App*$^{NL-G-F}$ mice compared to the wild type group due to DSS exposure (Fig. IV-8). These results suggest that DSS treatment increased Aβ processing and vascular reactivity in *App*$^{NL-G-F}$ mice verifying that peripheral intestinal inflammation

preferentially affects the brains of diseased mice and is maintained even during the gut healing phase.

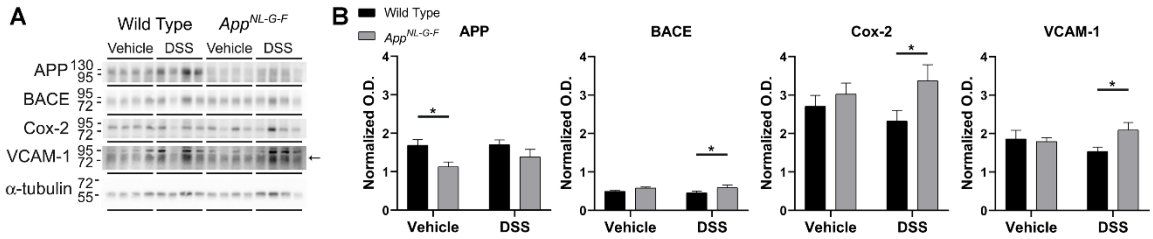

Figure IV- 8. DSS treatment increased BACE, Cox-2, and VCAM-1 levels in *App*$^{NL-G-F}$ compared to wild type mice. A) Hippocampal lysates from vehicle and DSS treated wild type and *App*$^{NL-G-F}$ mice were western blotted to B) quantify protein changes related to APP, BACE, Cox-2, and VCAM-1 levels using α-tubulin as the loading control. (*$p<0.05$, mean ± SEM, n=8 animals).

CHAPTER V

EFFECT OF ALZHEIMER'S DISEASE ASSOCIATED *APP* MUTATIONS ON THE PROGRESSION OF COLORECTAL CANCER INDUCED BY AOM/DSS IN MICE

Introduction

Amyloid precursor protein (APP) along with APP-like protein 1 and 2 (APLP1 and APLP2) are members of the highly conserved APP family (Sprecher et al., 1993; Wasco et al., 1993). Although APP is known for its critical contribution in Alzheimer's disease (AD) development and progression in the central nervous system, it is expressed in many other cell types (Arai et al., 1991; Golde et al., 1990; Nalivaeva & Turner, 2013; K. L. Puig & Combs, 2013; Schlossmacher et al., 1992; Tang et al., 2003). APP and β-site APP cleaving enzyme 1 (BACE1) are robustly expressed in brain tissue (Haass, Kaether, Thinakaran, & Sisodia, 2012). In AD brains, APP is processed into soluble APPβ (sAPPβ), the primary Aβ element of the neuritic plaques, and APP intracellular domain (AICD) fragments via the subsequent cleavage of BACE1 and γ-secretase in the amyloidogenic pathway. In the non-amyloidogenic pathway, APP is cleaved by α-secretase (ADAM10) and γ-secretase to produce sAPPα, P3, and AICD sequences (Cole & Vassar, 2007; Gandy, Caporaso, Buxbaum, Frangione, & Greengard, 1994; Y. Li, Zhou, Tong, He, & Song, 2006).

Notably, APP/sAPP is upregulated in multiple cancers, including breast, prostate, pancreatic, thyroid, colon, oral squamous cell carcinoma, and melanoma (Botelho, Wang, Arndt-Jovin, Becker, & Jovin, 2010; Hansel et al., 2003; Ko et al., 2004; Krause et al., 2008; S. Lim et al., 2014; Meng, Kataoka, Itoh, & Koono, 2001; Pietrzik et al., 1998; Seguchi, Kataoka, Uchino, Nabeshima, & Koono, 1999; Takagi et al., 2013; Takayama et al., 2009; Venkataramani et al., 2010; Woods & Padmanabhan, 2013). The full-length APP and its soluble proteolytic product, sAPPα, which is processed by the non-amyloidogenic pathway promotes migration and proliferation of breast cancer cells *in vitro* and in a xenograft *in vivo* model as well as in pancreatic cancer cells (Tsang et al., 2018; Woods & Padmanabhan, 2013). Human colorectal adenocarcinoma cell lines secrete sAPPα containing a Kunitz protease inhibitor domain as their primary trypsin inhibitor (Seguchi et al., 1999). Inhibition of APP expression using antisense RNA leads to suppression of human colon carcinoma cell growth *in vitro* and in xenograft nude mice (Meng et al., 2001). Additionally, AICD, can serve as a transcription factor to regulate protein synthesis both in primary and cancerous human dividing cells (Sobol et al., 2015). A body of investigations reveal an inverse link between AD and cancer in both human and mice (Ham et al., 2018; Ibáñez et al., 2014; J. E. Lee et al., 2018; Musicco et al., 2013; Roe et al., 2010; Sherzai et al., 2020).

To determine whether expression of APP or preferentially increased metabolism of APP into Aβ and sAPPβ fragments might influence the progression of cancer, we utilized a common colitis-associated colorectal cancer

(CAC) model which is slightly different than the dextran sulfate sodium (DSS)-induced colitis-like model in our previous study. In addition, effects of this additional model of intestinal inflammation on brain Aβ deposition were assessed. Both male and female C57BL/6 wild type control, *App*$^{-/-}$, and *App*$^{NL-G-F}$ mice at 5-8 months of age were treated with azoxymethane (AOM) and DSS to model human colorectal cancer. We observed sex- and genotype-dependent tumorigenesis and differentiation in our animal models. Notably, CAC also increased the Aβ plaque load in the brains of only *App*$^{NL-G-F}$ male mice.

Methods

Animals

Both male and female APP knockout mice (*App*$^{-/-}$) strain B6.129S7-App^{tm1Dbo}/J (https://www.jax.org/strain/004133), wild-type (*App*$^{+/+}$) C57BL/6 mice, and APP transgenic (*App*$^{NL-G-F}$) mice (KI:RBRC06344) were utilized in the present investigation. *App*$^{-/-}$ and wild-type mice were originally purchased from the Jackson Laboratory (Bar Harbor, Maine). *App*$^{NL-G-F}$ mice were obtained from Dr. Takashi Saito and Dr. Takaomi C. Saido, RIKEN BioResource Center, Japan (Saito et al., 2014). The mouse *App* gene was inactivated via deletion of its promoter, first exon, and the signal peptide of APP in *App*$^{-/-}$ mice (Zheng et al., 1995). The inserted humanized Aβ region in *App*$^{NL-G-F}$ mice carries Swedish (NL), Arctic (G), and Beyreuther/Iberian (F) mutations which enhances Aβ production, promotes Aβ aggregation through facilitating oligomerization and reducing proteolytic degradation, and increases the $A\beta_{42/40}$ ratio, respectively (Saito et al., 2014). Animals were maintained as a colony, provided food and water *ad libitum,*

and housed under standard conditions including a 12 h light:12 h dark cycle and 22 ± 1°C temperature at the University of North Dakota Center for Biomedical Research. Due to limited animal availability, 6-11 male and female mice per treatment group at 5-8 months-old were used to perform the experiment (Table V-1).

Table V- 1. Animal numbers and age at the beginning of the experiment

Gender	Genotype	Age at the Time of Saline Injections	Genotypes	Age at the Time of AOM Injections
Male	**Wild Type (n=11)**	5–6 month old	**Wild Type (n=11)**	5–6 month old
Male	***App*$^{-/-}$ (n=8)**	5–8 month-old	***App*$^{-/-}$ (n=10)**	5–8 month-old
Male	***App*$^{NL-G-F}$ (n=6)**	5 month-old	***App*$^{NL-G-F}$ (n=6)**	5 month-old
Female	**Wild Type (n=9)**	5–6 month-old	**Wild Type (n=11)**	5–6 month-old
Female	***App*$^{-/-}$ (n=9)**	5–7 month-old	***App*$^{-/-}$ (n=11)**	5–7 month-old
Female	***App*$^{NL-G-F}$ (n=10)**	5 month-old	***App*$^{NL-G-F}$ (n=10)**	5 month-old

Each genotype per gender was randomly divided into vehicle (saline i.p. injection and drinking water) and drug (AOM i.p. injection and dissolved DSS in drinking water) treated groups for 17 weeks of investigation (Fig. V-1).

The brain, spleen, and colon were collected to quantify histologic and biochemical changes after euthanizing animals by CO_2 asphyxiation and subsequent cardiac perfusion with PBS. All procedures involving animals were reviewed and approved by the UND Institutional Animal Care and Use Committee (UND IACUC). The investigation conforms to the National Research Council of the National Academies Guide for the Care and Use of Laboratory Animals (8^{th} edition).

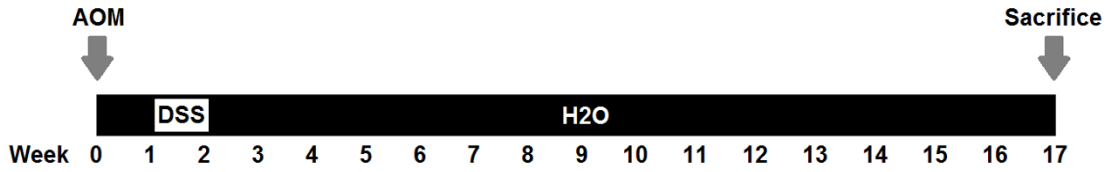

Figure V- 1. Schematic of the experimental design and timeline of AOM/DSS treatment. Wild type, *App*$^{-/-}$, and *App*$^{NL-G-F}$ male and female mice received 10mg/kg of AOM via i.p. injection on week 0. On week 1, the drug treated groups were exposed to 1.5% dissolved DSS in autoclaved drinking water for 7 days. Vehicle groups received saline intraperitoneally on week 0 and consumed the autoclaved drinking water throughout the experiment. Mice were sacrificed on week 17 and brains, normal and cancerous colon tissues as well as spleens were collected for further histological and biochemical assessments.

Induction of CAC via AOM/DSS Treatment

In order to induce CAC similar to humans, drug treated mice per genotype per gender were intraperitoneally injected with AOM (10mg/kg, Sigma-Aldrich, St. Louis, MO, USA) on day 0 (week 0) followed by exposure to dissolved DSS (1.5%, w/v, MW=36-50 kDa, MP Biomedicals, LLC, Santa Ana, CA, USA) in autoclaved drinking water starting on week 1 for 7 days. Vehicle control groups only received saline i.p. injections on day 0 and consumed autoclaved water throughout the study (Fig. V-1) (De Robertis et al., 2011; S. M. Lee et al., 2016; Tanaka, Oyama, Sugie, & Shimizu, 2016). The average DSS consumption was measured per mouse per day during the 7 days of exposure (Table V-2). During the 17 weeks, mice were weighed once a week to monitor the weight changes, except week 1 in which mice were maintained in isolated chambers due to the carcinogenic nature of AOM. The %body weight changes was calculated by dividing the mouse body weight per each week to its initial weight on week 0, as

Table V- 2. DSS consumption dissolved in drinking water during 7 days of exposures

Gender	Genotypes	Average DSS Consumption/Mouse/Day For 7 Days (mL)
Male	**Wild Type (n=11)**	6.6
Male	***App*$^{-/-}$ (n=10)**	5
Male	***App*$^{NL-G-F}$ (n=6)**	6.7
Female	**Wild Type (n=11)**	4.6
Female	***App*$^{-/-}$ (n=11)**	4.5
Female	***App*$^{NL-G-F}$ (n=10)**	6

the percentage ratio. At the end of week 17 post-treatment, mice were collected and the colon weights and lengths from the cecum to rectum as well as spleen weights were measured. Tumor numbers were recorded following mouse sacrifice from the proximal to distal colon. Tumor areas (mm^2) were calculated, as an average for each mouse, using Adobe Photoshop CS3 software (Adobe Systems, San Jose, CA) from colon images that were taken on the day of collection. For further biochemical and histological investigations, the brain, normal and cancerous colon tissues, and spleens were collected.

Histological Staining and Scoring of Colonic Swiss-Rolls

After collecting tumors and normal adjacent tissues, the full-length colon from proximal to distal were made into Swiss-rolls. Briefly, following 5 days of fixation in 4% paraformaldehyde (PFA) and cryoprotection via two successive changes of 30% sucrose, the Swiss-rolls were embedded into 15% gelatin blocks. The blocks, after 4% PFA fixation and subsequent sucrose cryoprotection, were serially sectioned into 10μm thick sections via a chambered

cryostat. Hematoxylin and eosin (H&E) staining was performed to assess the extent of inflammation in AOM/DSS treated animals (Sohrabi & Combs, 2019). The stained sections were then examined by a pathologist blinded to the experimental groups. CAC scores were assigned based on the extent and severity of inflammation, mucosal hyperplasia, and dysplasia. Scoring methods were as follow: A) inflammation score: 0= normal (within normal limits); 1= mild (small, focal, or widely separated, limited to lamina propria); 2= moderate (multifocal or locally extensive, extending to submucosa); 3= severe (transmural inflammation), B) mucosal hyperplasia score: 0= normal (within normal limits); 1= mild (crypts 2-3 times normal thickness, normal epithelium); 2= moderate (crypts 2-3 times normal thickness, hyperchromatic epithelium, reduced goblet cells, scattered arborization); 3= severe (crypts ≥ 4 times normal thickness, marked hyperchromasia, few to no goblet cells, high mitotic index, frequent arborization), C) neoplastic transformation score: 0= normal; 1= low grade dysplasia; 2= high grade dysplasia/adenomatous polyp; 3= Adenocarcinoma. Both individual and sum of 3 histology scores were graphed for accurate analysis of mice colonic Swiss-rolls.

Human colon normal and tumor frozen tissue array slides were purchased from BioChain (Newark, CA, USA). H&E histological staining as well as anti-AβPP Y188 (1:1000 dilution, Abcam, Cambridge, MA, USA) immunostaining were performed to assess APP expression.

All stained slides were scanned using a Hamamatsu 2.0HT digital slide scanner and figures were made using Adobe Photoshop CS3 software (Adobe Systems, San Jose, CA).

Brain Immunohistochemistry (IHC)

Left brain hemispheres were collected and fixed in 4% PFA for 5 days. Following two successive changes of 30% sucrose and embedding the brains in 15% gelatin blocks, the tissues were serially sectioned into 40μm sections using a sliding microtome (K. Nagamoto-Combs et al., 2016). To perform immunostaining against Aβ, antigen retrieval was required using 25% formic acid (Sigma-Aldrich) for 25 min at room temperature. After at least 30 min blocking with IHC solution [0.5% bovine serum albumin (BSA, Equitech-Bio, Inc.), 0.1% Triton X-100 (Sigma-Aldrich), 5% normal goat serum (NGS, Equitech-Bio, Inc.), and 0.02% Na Azide], brain sections were incubated with primary antibody β-Amyloid (1:500 dilution, D54D2, rabbit mAb, Cell Signaling Technology, Inc., Danvers, MA, USA) at 4°C overnight. On the following day, tissues were incubated using biotinylated secondary antibody goat anti-rabbit IgG (Vector Laboratories, Inc., Burlingame, CA, USA) for 2 h. To visualize the antibody binding, a VECTASTAIN Avidin-Biotin Complex (ABC) kit was used followed by the Vector VIP Peroxidase (HRP) Substrate kit (SK-4600) (Vector laboratories, Inc., Burlingame, CA, USA). The brain sections were then imaged using a Hamamatsu 2.0HT digital slide scanner. To determine the area of the Aβ positive regions within the hippocampus, hippocampal images (3 sections per mouse; 5 animals per condition; total of 15 hippocampal sections/condition) were

extracted from the images of the brain sections using image processing tools in Fiji and Aβ positive regions were outlined using a trainable segmentation algorithm available as a plugin in Fiji and the total areas of the outlined regions were measured and expressed as percentages of the area of the hippocampus sections (Arganda-Carreras et al., 2017). Figures were made using Adobe Photoshop CS3 software (Adobe Systems, San Jose, CA).

Statistical Analysis

Two-way ANOVA multiple comparisons followed by Uncorrected Fisher's LSD tests were performed using GraphPad Prism 8 software to analyze our data, which are represented as the mean ± SEM. Significance is indicated by P value measurements with a $P < 0.05$ considered significant; *$P < 0.05$; **$P < 0.01$; ***$P < 0.001$; ****$P < 0.0001$.

Results

Human Colonic Epithelial Cells Expressed APP

H&E staining demonstrated human normal tissue along with well, moderately, and poorly differentiated colon tumors in colorectal cancer (Fig V-2A and B). Immunostaining of the same human normal colon and range of differentiated tumors demonstrated expression of APP by intestinal epithelial cells (FigV-2C and D). Our human colon array findings are in line with a report from Venkataramani et. al which shows robust APP staining in human colon cancer tissue (Venkataramani et al., 2010). Although this data did not provide any information regarding processing of APP, it did confirm that APP is

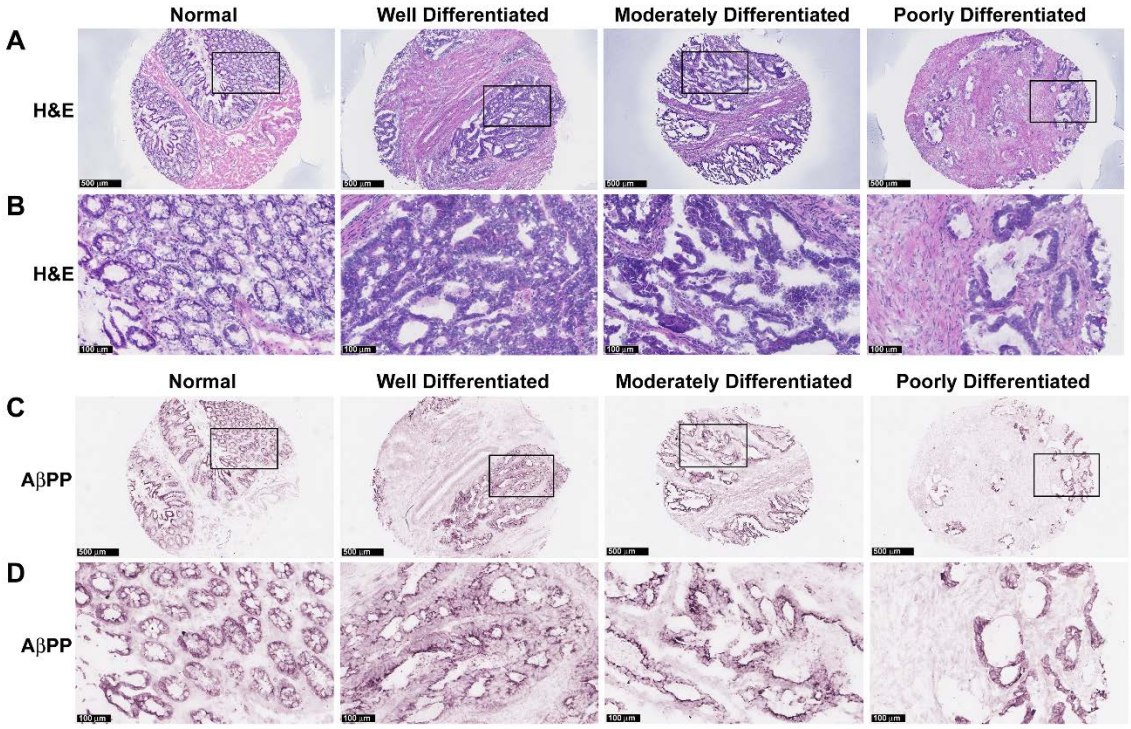

Figure V- 2. Histology and APP immunohistochemistry of human normal colon and colorectal cancer tissue arrays. Representative H&E staining of human normal colon and colorectal cancer ranging from well to poorly differentiated tumors are shown with A) 5X magnification and B) 20X magnification. Representative APP immunoreactivity demonstrated APP expression in epithelial cells in human normal colon tissue and colorectal cancer tumors shown with C) 5X magnification and D) 20X magnification. Boxes demarcate areas displayed in higher magnification images.

expressed by colonic epithelial cells in a fashion independent of healthy or tumorigenic condition.

AOM/DSS Exposure Reduced Overall Survival Rates and Body Weights Except for Female *App*$^{NL-G-F}$ Mice

Survival rates of AOM/DSS treated mice were demonstrated based on Kaplan-Meier survival curves. On week 2, the survival rate of male AOM/DSS treated groups decreased to 91%, 40%, and 83% for wild type, *App*$^{-/-}$, and *App*$^{NL-G-F}$ mice, respectively. The survival rate of female wild type went from 91% on week 1 to 73% on week 2.

At the same week, the survival proportion of female *App*$^{-/-}$ animals reduced to 82%. However, 100% of the female *App*$^{NL-G-F}$ drug treated group survived throughout the study (Fig. V-3A and B).

The % weight loss were only graphed for mice that survived the whole procedure. AOM/DSS treatment robustly increased the % weight loss of both males and females on week 2 compared to their respective vehicle controls (Table V-3) (Fig V-3C and D). Wild type and *App*$^{NL-G-F}$ males, and to a lesser extent wild type females, did not return to a final body weight similar to their respective vehicle controls even by week 17. However, there were no significant differences between the final body weight of *App*$^{-/-}$ male and female, and *App*$^{NL-G-F}$ females starting from weeks 5, 4, and 3 to the end of the study, respectively. Both genders across genotypes were provided 1.5% DSS dissolved in their drinking water. However, Table V-2 demonstrates a slightly higher average DSS consumption in males compared to females. This is likely due to greater body weight in males versus females resulting in greater consumption. Overall, these results suggest both sex and genotype differences in response to the AOM/DSS treatment.

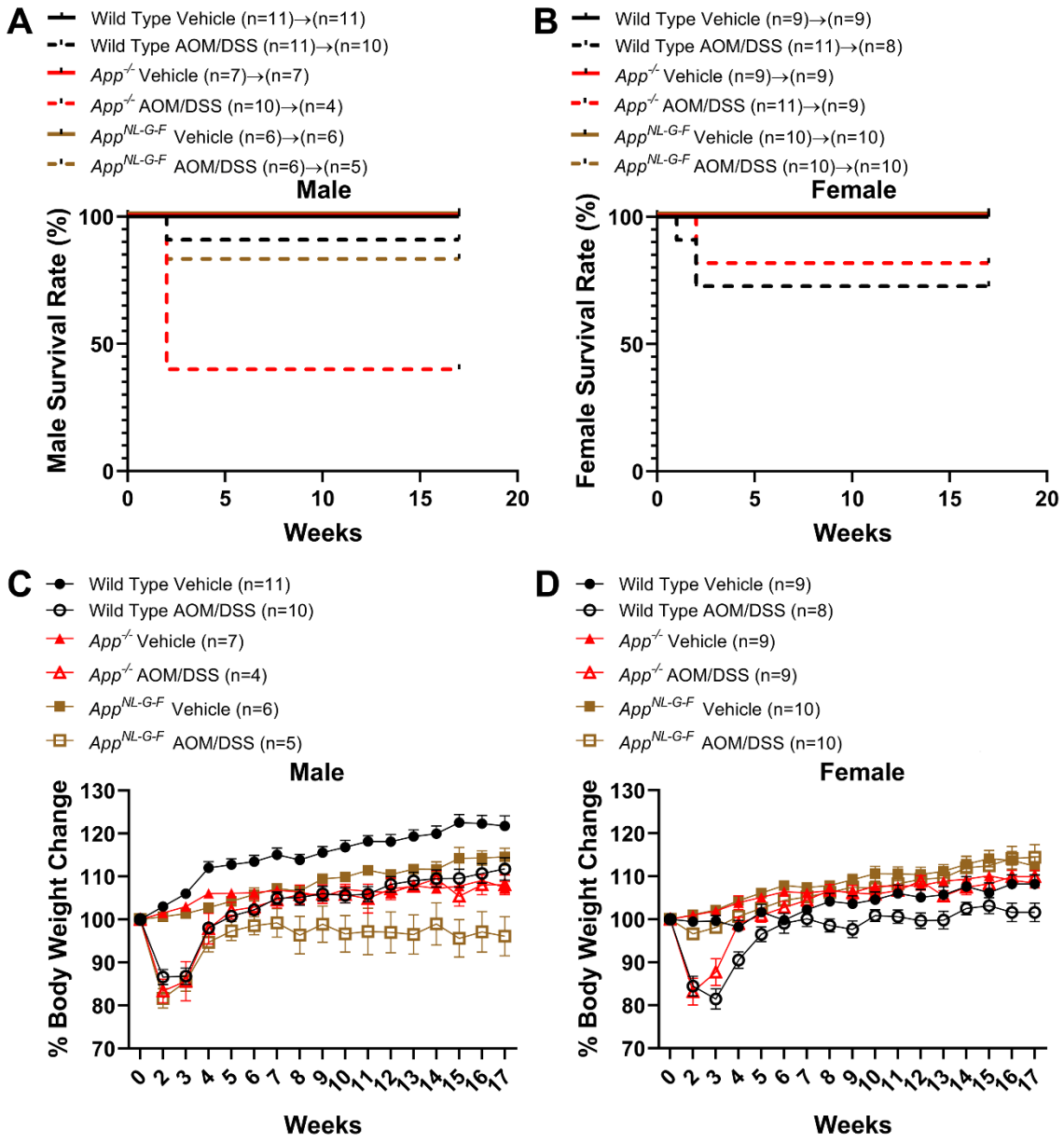

Figure V- 3. The survival rate and %body weights were reduced following AOM/DSS treatment except for *App*$^{NL-G-F}$ female mice. Kaplan-Meier survival curves were generated for A) male and B) female vehicle or AOM/DSS treated wild type, *App*$^{-/-}$, and *App*$^{NL-G-F}$ mice. The percentage of body weight changes was calculated for 17 weeks for C) male and D) female vehicle or survivors of the AOM/DSS treatment.

Table V- 3 . The % weight loss changes per week per genotype and gender for 17 weeks.

Male	P Value	Significant
Week 0: Wild Type Vehicle vs. Wild Type AOM/DSS	>0.05	ns
Week 2: Wild Type Vehicle vs. Wild Type AOM/DSS	<0.0001	****
Week 3: Wild Type Vehicle vs. Wild Type AOM/DSS	<0.0001	****
Week 4: Wild Type Vehicle vs. Wild Type AOM/DSS	<0.0001	****
Week 5: Wild Type Vehicle vs. Wild Type AOM/DSS	<0.0001	****
Week 6: Wild Type Vehicle vs. Wild Type AOM/DSS	<0.0001	****
Week 7: Wild Type Vehicle vs. Wild Type AOM/DSS	<0.0001	****
Week 8: Wild Type Vehicle vs. Wild Type AOM/DSS	<0.001	***
Week 9: Wild Type Vehicle vs. Wild Type AOM/DSS	<0.0001	****
Week 10: Wild Type Vehicle vs. Wild Type AOM/DSS	<0.0001	****
Week 11: Wild Type Vehicle vs. Wild Type AOM/DSS	<0.0001	****
Week 12: Wild Type Vehicle vs. Wild Type AOM/DSS	<0.0001	****
Week 13: Wild Type Vehicle vs. Wild Type AOM/DSS	<0.0001	****
Week 14: Wild Type Vehicle vs. Wild Type AOM/DSS	<0.0001	****
Week 15: Wild Type Vehicle vs. Wild Type AOM/DSS	<0.0001	****
Week 16: Wild Type Vehicle vs. Wild Type AOM/DSS	<0.0001	****
Week 17: Wild Type Vehicle vs. Wild Type AOM/DSS	<0.0001	****
Week 0: *App*$^{-/-}$ Vehicle vs. *App*$^{-/-}$ AOM/DSS	>0.05	ns
Week 2: *App*$^{-/-}$ Vehicle vs. *App*$^{-/-}$ AOM/DSS	<0.0001	****
Week 3: *App*$^{-/-}$ Vehicle vs. *App*$^{-/-}$ AOM/DSS	<0.0001	****
Week 4: *App*$^{-/-}$ Vehicle vs. *App*$^{-/-}$ AOM/DSS	<0.05	*
Week 5: *App*$^{-/-}$ Vehicle vs. *App*$^{-/-}$ AOM/DSS	>0.05	ns
Week 6: *App*$^{-/-}$ Vehicle vs. *App*$^{-/-}$ AOM/DSS	>0.05	ns
Week 7: *App*$^{-/-}$ Vehicle vs. *App*$^{-/-}$ AOM/DSS	>0.05	ns
Week 8: *App*$^{-/-}$ Vehicle vs. *App*$^{-/-}$ AOM/DSS	>0.05	ns
Week 9: *App*$^{-/-}$ Vehicle vs. *App*$^{-/-}$ AOM/DSS	>0.05	ns
Week 10: *App*$^{-/-}$ Vehicle vs. *App*$^{-/-}$ AOM/DSS	>0.05	ns
Week 11: *App*$^{-/-}$ Vehicle vs. *App*$^{-/-}$ AOM/DSS	>0.05	ns
Week 12: *App*$^{-/-}$ Vehicle vs. *App*$^{-/-}$ AOM/DSS	>0.05	ns
Week 13: *App*$^{-/-}$ Vehicle vs. *App*$^{-/-}$ AOM/DSS	>0.05	ns
Week 14: *App*$^{-/-}$ Vehicle vs. *App*$^{-/-}$ AOM/DSS	>0.05	ns
Week 15: *App*$^{-/-}$ Vehicle vs. *App*$^{-/-}$ AOM/DSS	>0.05	ns
Week 16: *App*$^{-/-}$ Vehicle vs. *App*$^{-/-}$ AOM/DSS	>0.05	ns
Week 17: *App*$^{-/-}$ Vehicle vs. *App*$^{-/-}$ AOM/DSS	>0.05	ns
Week 0: *App*$^{NL-G-F}$ Vehicle vs. *App*$^{NL-G-F}$ AOM/DSS	>0.05	ns
Week 2: *App*$^{NL-G-F}$ Vehicle vs. *App*$^{NL-G-F}$ AOM/DSS	<0.0001	****
Week 3: *App*$^{NL-G-F}$ Vehicle vs. *App*$^{NL-G-F}$ AOM/DSS	<0.0001	****
Week 4: *App*$^{NL-G-F}$ Vehicle vs. *App*$^{NL-G-F}$ AOM/DSS	<0.01	**
Week 5: *App*$^{NL-G-F}$ Vehicle vs. *App*$^{NL-G-F}$ AOM/DSS	<0.05	*
Week 6: *App*$^{NL-G-F}$ Vehicle vs. *App*$^{NL-G-F}$ AOM/DSS	<0.05	*
Week 7: *App*$^{NL-G-F}$ Vehicle vs. *App*$^{NL-G-F}$ AOM/DSS	<0.05	*
Week 8: *App*$^{NL-G-F}$ Vehicle vs. *App*$^{NL-G-F}$ AOM/DSS	<0.01	**
Week 9: *App*$^{NL-G-F}$ Vehicle vs. *App*$^{NL-G-F}$ AOM/DSS	<0.001	***
Week 10: *App*$^{NL-G-F}$ Vehicle vs. *App*$^{NL-G-F}$ AOM/DSS	<0.0001	****
Week 11: *App*$^{NL-G-F}$ Vehicle vs. *App*$^{NL-G-F}$ AOM/DSS	<0.0001	****
Week 12: *App*$^{NL-G-F}$ Vehicle vs. *App*$^{NL-G-F}$ AOM/DSS	<0.0001	****
Week 13: *App*$^{NL-G-F}$ Vehicle vs. *App*$^{NL-G-F}$ AOM/DSS	<0.0001	****
Week 14: *App*$^{NL-G-F}$ Vehicle vs. *App*$^{NL-G-F}$ AOM/DSS	<0.0001	****
Week 15: *App*$^{NL-G-F}$ Vehicle vs. *App*$^{NL-G-F}$ AOM/DSS	<0.0001	****
Week 16: *App*$^{NL-G-F}$ Vehicle vs. *App*$^{NL-G-F}$ AOM/DSS	<0.0001	****
Week 17: *App*$^{NL-G-F}$ Vehicle vs. *App*$^{NL-G-F}$ AOM/DSS	<0.0001	****

Female	P Value	Significant
Week 0: Wild Type Vehicle vs. Wild Type AOM/DSS	>0.05	ns
Week 2: Wild Type Vehicle vs. Wild Type AOM/DSS	<0.0001	****
Week 3: Wild Type Vehicle vs. Wild Type AOM/DSS	<0.0001	****
Week 4: Wild Type Vehicle vs. Wild Type AOM/DSS	<0.01	**
Week 5: Wild Type Vehicle vs. Wild Type AOM/DSS	<0.05	*
Week 6: Wild Type Vehicle vs. Wild Type AOM/DSS	>0.05	ns
Week 7: Wild Type Vehicle vs. Wild Type AOM/DSS	>0.05	ns
Week 8: Wild Type Vehicle vs. Wild Type AOM/DSS	<0.05	*
Week 9: Wild Type Vehicle vs. Wild Type AOM/DSS	<0.05	*
Week 10: Wild Type Vehicle vs. Wild Type AOM/DSS	>0.05	ns
Week 11: Wild Type Vehicle vs. Wild Type AOM/DSS	<0.05	*
Week 12: Wild Type Vehicle vs. Wild Type AOM/DSS	<0.05	*
Week 13: Wild Type Vehicle vs. Wild Type AOM/DSS	<0.05	*
Week 14: Wild Type Vehicle vs. Wild Type AOM/DSS	<0.05	*
Week 15: Wild Type Vehicle vs. Wild Type AOM/DSS	>0.05	ns
Week 16: Wild Type Vehicle vs. Wild Type AOM/DSS	<0.01	**
Week 17: Wild Type Vehicle vs. Wild Type AOM/DSS	<0.01	**
Week 0: *App*$^{-/-}$ Vehicle vs. *App*$^{-/-}$ AOM/DSS	>0.05	ns
Week 2: *App*$^{-/-}$ Vehicle vs. *App*$^{-/-}$ AOM/DSS	<0.0001	****
Week 3: *App*$^{-/-}$ Vehicle vs. *App*$^{-/-}$ AOM/DSS	<0.0001	****
Week 4: *App*$^{-/-}$ Vehicle vs. *App*$^{-/-}$ AOM/DSS	>0.05	ns
Week 5: *App*$^{-/-}$ Vehicle vs. *App*$^{-/-}$ AOM/DSS	>0.05	ns
Week 6: *App*$^{-/-}$ Vehicle vs. *App*$^{-/-}$ AOM/DSS	>0.05	ns
Week 7: *App*$^{-/-}$ Vehicle vs. *App*$^{-/-}$ AOM/DSS	>0.05	ns
Week 8: *App*$^{-/-}$ Vehicle vs. *App*$^{-/-}$ AOM/DSS	>0.05	ns
Week 9: *App*$^{-/-}$ Vehicle vs. *App*$^{-/-}$ AOM/DSS	>0.05	ns
Week 10: *App*$^{-/-}$ Vehicle vs. *App*$^{-/-}$ AOM/DSS	>0.05	ns
Week 11: *App*$^{-/-}$ Vehicle vs. *App*$^{-/-}$ AOM/DSS	>0.05	ns
Week 12: *App*$^{-/-}$ Vehicle vs. *App*$^{-/-}$ AOM/DSS	>0.05	ns
Week 13: *App*$^{-/-}$ Vehicle vs. *App*$^{-/-}$ AOM/DSS	>0.05	ns
Week 14: *App*$^{-/-}$ Vehicle vs. *App*$^{-/-}$ AOM/DSS	>0.05	ns
Week 15: *App*$^{-/-}$ Vehicle vs. *App*$^{-/-}$ AOM/DSS	>0.05	ns
Week 16: *App*$^{-/-}$ Vehicle vs. *App*$^{-/-}$ AOM/DSS	>0.05	ns
Week 17: *App*$^{-/-}$ Vehicle vs. *App*$^{-/-}$ AOM/DSS	>0.05	ns
Week 0: *App*$^{NL-G-F}$ Vehicle vs. *App*$^{NL-G-F}$ AOM/DSS	>0.05	ns
Week 2: *App*$^{NL-G-F}$ Vehicle vs. *App*$^{NL-G-F}$ AOM/DSS	<0.05	*
Week 3: *App*$^{NL-G-F}$ Vehicle vs. *App*$^{NL-G-F}$ AOM/DSS	>0.05	ns
Week 4: *App*$^{NL-G-F}$ Vehicle vs. *App*$^{NL-G-F}$ AOM/DSS	>0.05	ns
Week 5: *App*$^{NL-G-F}$ Vehicle vs. *App*$^{NL-G-F}$ AOM/DSS	>0.05	ns
Week 6: *App*$^{NL-G-F}$ Vehicle vs. *App*$^{NL-G-F}$ AOM/DSS	>0.05	ns
Week 7: *App*$^{NL-G-F}$ Vehicle vs. *App*$^{NL-G-F}$ AOM/DSS	>0.05	ns
Week 8: *App*$^{NL-G-F}$ Vehicle vs. *App*$^{NL-G-F}$ AOM/DSS	>0.05	ns
Week 9: *App*$^{NL-G-F}$ Vehicle vs. *App*$^{NL-G-F}$ AOM/DSS	>0.05	ns
Week 10: *App*$^{NL-G-F}$ Vehicle vs. *App*$^{NL-G-F}$ AOM/DSS	>0.05	ns
Week 11: *App*$^{NL-G-F}$ Vehicle vs. *App*$^{NL-G-F}$ AOM/DSS	>0.05	ns
Week 12: *App*$^{NL-G-F}$ Vehicle vs. *App*$^{NL-G-F}$ AOM/DSS	>0.05	ns
Week 13: *App*$^{NL-G-F}$ Vehicle vs. *App*$^{NL-G-F}$ AOM/DSS	>0.05	ns
Week 14: *App*$^{NL-G-F}$ Vehicle vs. *App*$^{NL-G-F}$ AOM/DSS	>0.05	ns
Week 15: *App*$^{NL-G-F}$ Vehicle vs. *App*$^{NL-G-F}$ AOM/DSS	>0.05	ns
Week 16: *App*$^{NL-G-F}$ Vehicle vs. *App*$^{NL-G-F}$ AOM/DSS	>0.05	ns
Week 17: *App*$^{NL-G-F}$ Vehicle vs. *App*$^{NL-G-F}$ AOM/DSS	>0.05	ns

AOM/DSS Treatment Did Not Induce Colorectal-associated Symptoms in Female *App*$^{NL-G-F}$ Mice

The granulomatous nature of inflammation and extent of anemia induced by DSS exposure is associated with an increase of colon and spleen weights as well as shortening of colon length (Chassaing et al., 2014a). On week 17, the AOM/DSS treated male groups demonstrated a significant decrease in colon length of wild type mice, an increase in colon weight of *App*$^{-/-}$ mice, and an increase in colon and spleen weights of *App*$^{NL-G-F}$ mice compared to their respective controls (Fig. V-4A-C). Colon length and weight were significantly less in *App*$^{-/-}$ compared to *App*$^{NL-G-F}$ male mice in the AOM/DSS treatment groups. Colon and spleen weights were significantly higher in *App*$^{NL-G-F}$ vs. wild type males in drug treated groups.

In females, AOM/DSS administration dramatically shortened wild type colon length and increased wild type and *App*$^{-/-}$ colon and spleen weights compared to their vehicle controls (Fig. V-4D-F). Interestingly, colon weight and length as well as spleen weight of *App*$^{NL-G-F}$ mice did not differ due to AOM/DSS treatment vs. their vehicle group. Female *App*$^{NL-G-F}$ colon length was significantly higher than wild type and *App*$^{-/-}$ mice in AOM/DSS treated groups. Colon and spleen weights of wild type females were greater than *App*$^{-/-}$ and *App*$^{NL-G-F}$ AOM/DSS treated groups. These data suggest increased sex-related CAC inflammation in *App*$^{NL-G-F}$ males compared to females.

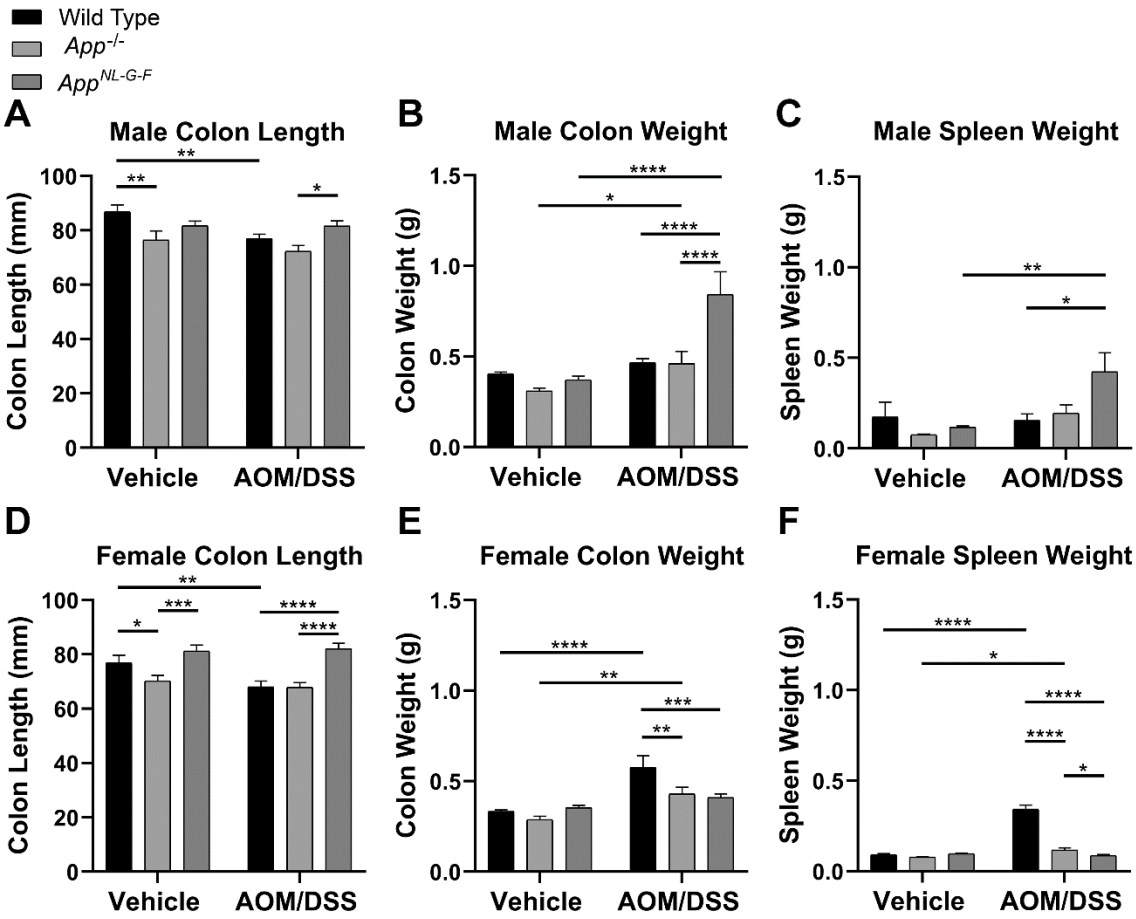

Figure V- 4. AOM/DSS treatment affected colon and spleen weights and colon lengths in a sex and genotype-dependent manner. Colon and spleen weights and colon length were measured from wild type, *App*$^{-/-}$, and *App*$^{NL-G-F}$ A-C) male and D-F) female vehicle and AOM/DSS treated mice to quantify inflammation, *p<0.05, ** p<0.01, ***p<0.001, and ****p<0.0001 (mean ± SEM, n=4-11 animals).

AOM/DSS Administration Produced Various Sex- and Genotype-Dependent Tumor Numbers and Areas

In males, *App*$^{NL-G-F}$ mice (n=5) demonstrated significantly greater tumor number and area compared to wild types (n=10) and developed more tumors than the *App*$^{-/-}$ group (n=4) following AOM/DSS treatment (Fig. V-5A and B). In contrast, female wild type (n=8) and *App*$^{-/-}$ (n=9) AOM/DSS treated animals

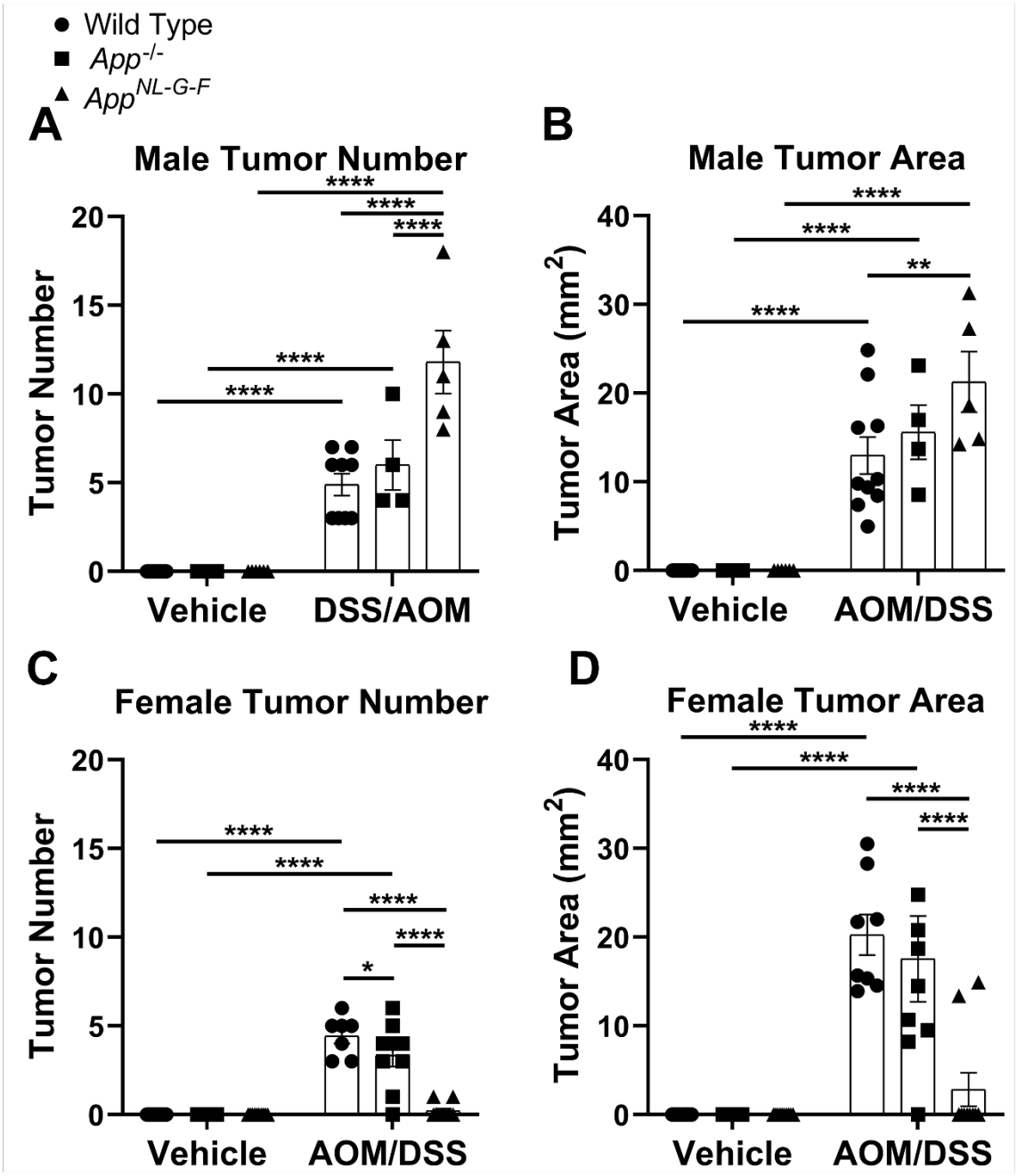

Figure V- 5. AOM/DSS treatment induced tumors in a sex and genotype-dependent manner. Tumor number and area were counted and measured, respectively, from wild type, *App*$^{-/-}$, and *App*$^{NL-G-F}$ male and female mice to indicate the extent of disease induced by AOM/DSS exposure across strain and sex, *p<0.05, ** p<0.01, ***p<0.001, and ****p<0.0001 (mean ± SEM, n=4-11 animals).

displayed significantly more tumors with greater tumor areas compared to *App*$^{NL-G-F}$ mice (n=10) with only 20% tumor development (Fig. V-5C and D). The number of tumors in female wild types was significantly more than *App*$^{-/-}$ group tumors. Tumorigenesis was not observed in male and female vehicle treated groups. These data indicate an association of sex and APP expression/processing with progression of tumors in the AOM/DSS murine model.

Histologic Severity of Tumorigenesis and Inflammation Induced by AOM/DSS Treatment Were Sex- and APP-Associated

AOM/DSS exposure induced moderate to severe inflammation in wild type, *App*$^{-/-}$, and *App*$^{NL-G-F}$ males (Fig. V-6A-E). Both *App*$^{-/-}$, and *App*$^{NL-G-F}$ AOM/DSS treated groups demonstrated significantly greater mucosal hyperplasia, neoplastic transformation, and subsequent total histology score compared to wild type mice. Except minimal incidental inflammation observed in the male wild type vehicle group, none of controls revealed colonic pathology (Fig. V-6A-E).

Inversely, the majority of *App*$^{NL-G-F}$ females, except one, did not develop robust inflammation following AOM/DSS administration compared to the wild type and *App*$^{-/-}$ groups (Fig. V-7A-E). However, wild type and *App*$^{-/-}$ females showed drastically greater inflammation, mucosal hyperplasia, neoplastic transformation, and total histology scoring compared to the *App*$^{NL-G-F}$ female drug treated group (Fig. V-7A-E). Taken together, these observations suggest different genotype and sex susceptibility toward CAC in which males resulted in worse colonic pathology in *App*$^{-/-}$ survivors and *App*$^{NL-G-F}$ compared to wild type mice and in

females led to poor tumorigenesis in *App*$^{NL-G-F}$ compared to *App*$^{-/-}$ and wild type groups. Surprisingly, *App*$^{NL-G-F}$ males developed adenocarcinoma whereas females demonstrated normal to mild colonic histology.

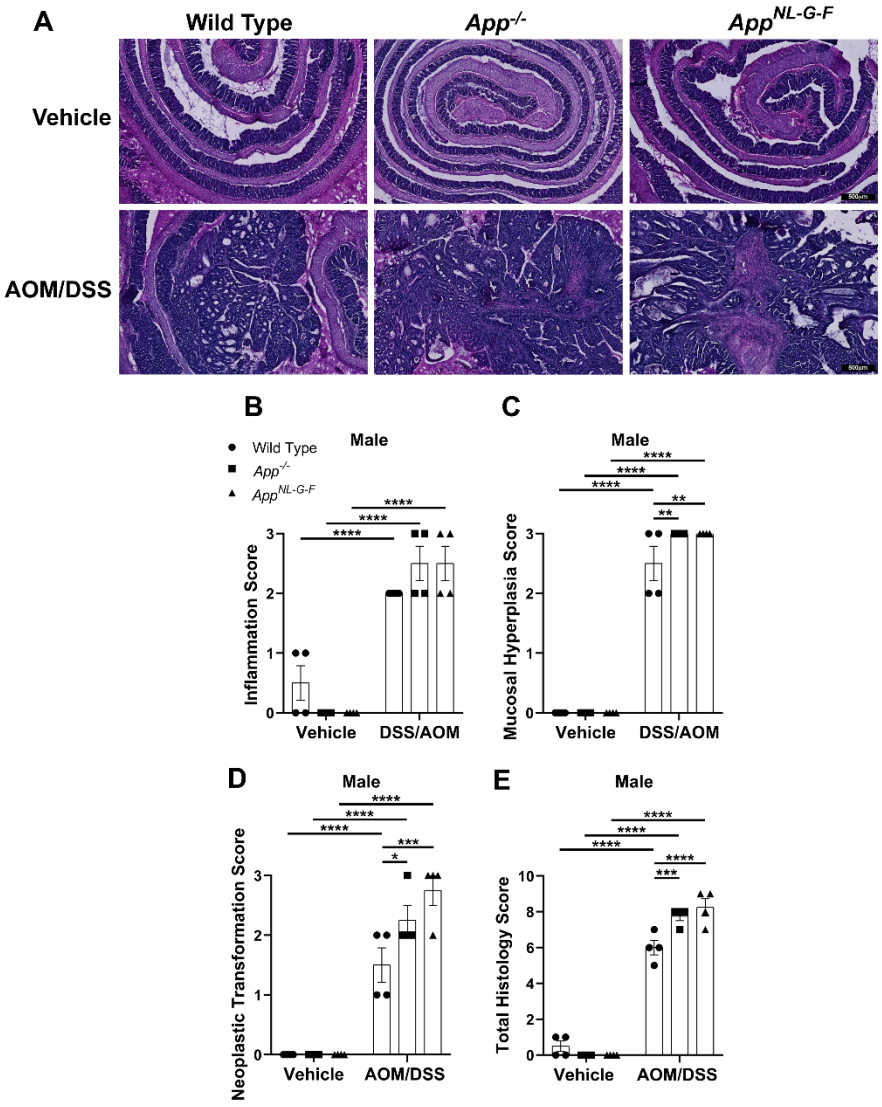

Figure V- 6. The extent of tumorigenesis following AOM/DSS treatment in male mice was genotype dependent. A) Representative H&E staining of Swiss-rolls of normal colon and AOM/DSS-induced CAC are shown with 4X magnification. Histological lesions of wild type, *App*$^{-/-}$, and *App*$^{NL-G-F}$ animal colons are shown by scoring B) inflammation, C) mucosal hyperplasia, D) neoplastic transformation, and E) total histology, *p<0.05, ** p<0.01, ***p<0.001, and ****p<0.0001 (mean ± SEM, n=4 animals).

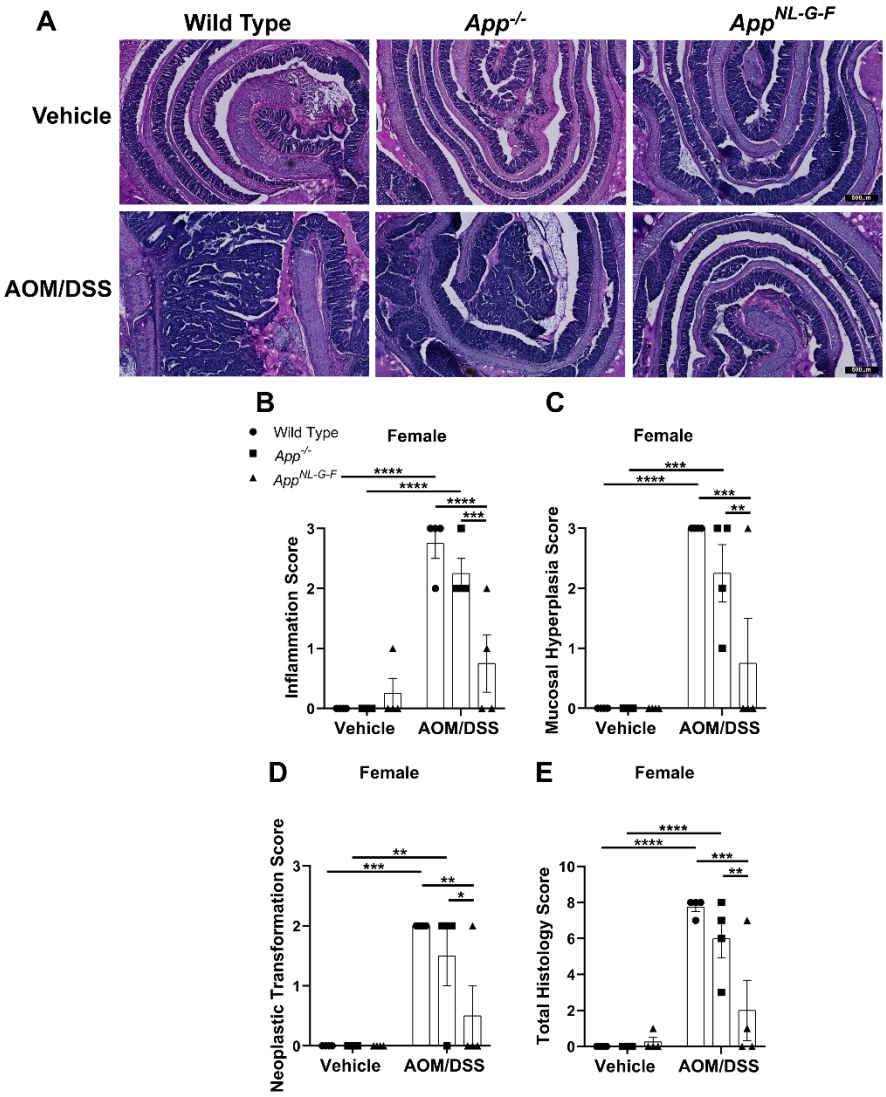

Figure V- 7. *App*$^{NL-G-F}$ females were resistant to CAC induced by AOM/DSS administration compared to wild type and *App*$^{-/-}$ counterparts. A) Representative H&E staining of normal and cancerous colons are shown with 4X magnification. Colon B) inflammation, C) mucosal hyperplasia, and D) neoplastic transformation were scored individually, and E) total histology was calculated, *p<0.05, ** p<0.01, ***p<0.001, and ****p<0.0001 (mean ± SEM, n=4 animals).

CAC Induced by AOM/DSS Administration Exacerbated Aβ Accumulation in *App*$^{NL-G-F}$ Males with No Effect on Females

The primary goal of the study was to determine whether wild type or mutant AβPP expression altered the colonic tumorigenic response following AOM/DSS treatment. However, based upon our prior findings that DSS-induced colitis-like conditions exacerbated brain Aβ pathology, we asked whether the AOM/DSS induced tumorigenesis might have a similar effect on the brain. The impact of CAC induced by AOM/DSS on Aβ accumulation in the brain was assessed by immunohistochemistry. Aβ plaque quantitation in the hippocampus showed a significant increase of amyloid plaque load in *App*$^{NL-G-F}$ AOM/DSS treated males compared to their respective vehicle group (Fig. V-8A-B).

However, hippocampal Aβ deposition did not change due to drug treatment in female *App*$^{NL-G-F}$ mice compared to their vehicle group (Fig. V-8C-D). As expected, both male and female wild type and *App*$^{-/-}$ mice brains were devoid of detectable Aβ aggregation. These data confirmed a direct impact of gut inflammation and tumorigenesis on exacerbation of Aβ pathology in an AD mouse model. More importantly, it paralleled our intestinal findings in that male *App*$^{NL-G-F}$ mice responded more robustly to AOM/DSS treatment overall with regard to gut inflammation, tumorigenesis, and brain plaque deposition.

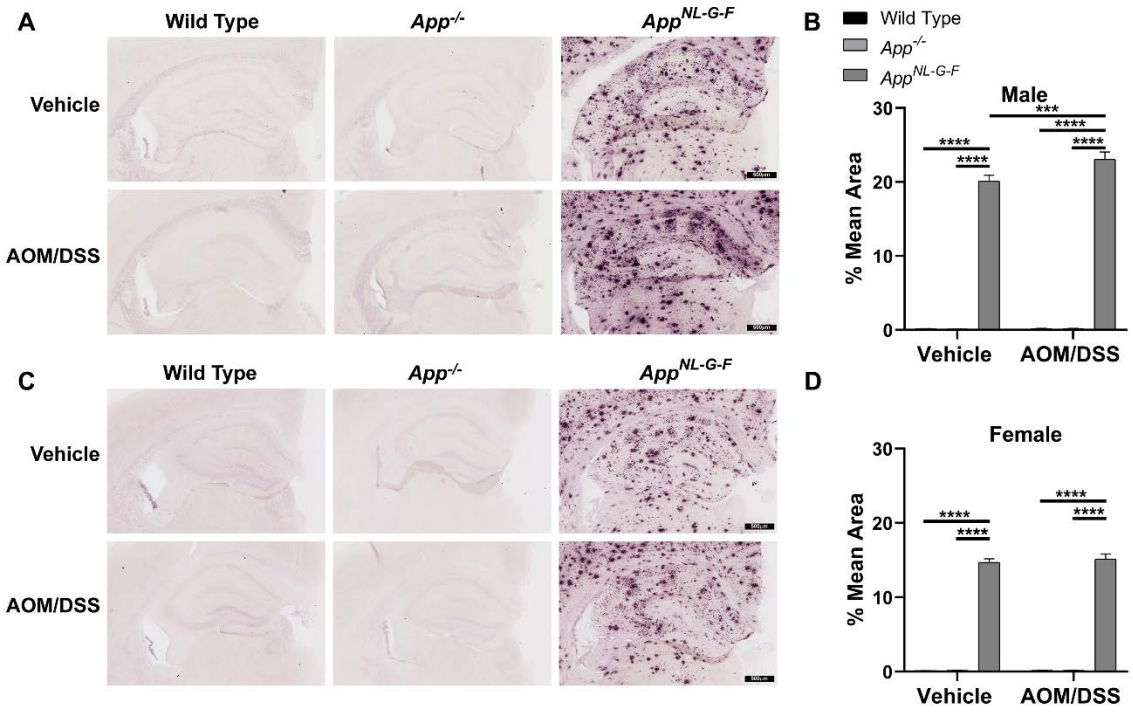

Figure V- 8. Aβ deposition was exacerbated in *App*$^{NL-G-F}$ male but not female hippocampi following CAC induced by AOM/DSS exposure. A, C) Immunohistochemistry was performed on serial brain sections (40µm) from male and female AOM/DSS treated wild type, *App*$^{-/-}$, and *App*$^{NL-G-F}$ mice as well as vehicles using anti-Aβ antibody. Representative images are shown with 4X magnification. B, D) %mean area was measured using 3 different sizes of hippocampus sections/mouse/condition, ***p<0.001 and ****p<0.0001 (mean ± SEM, n=5 animals).

CHAPTER VI

DISCUSSION

Study I

IGF-1R Inhibitor Ameliorated Neuroinflammation in an Alzheimer's Disease Transgenic Mouse Model

We observed that reversible pharmacologic inhibition of IGF-1R via PPP reduced insoluble $A\beta_{1\text{-}40/42}$ levels, eotaxin, TNF-α, IL-1α, IL-1β, and IL-10 levels in temporal cortices of 9-10 month-old AβPP/PS1 mice. This correlated with decreased protein levels of p-tyrosine, CD68, and microglia phagocytic activity in the AβPP/PS1 hippocampi as a result of the IGF-1R inhibitor treatment.

Previously, we demonstrated higher levels of IGF-1 in parietal cortex but not hippocampus of AβPP/PS1 mice at 6 months of age compared to WT mice (Kendra L. Puig et al., 2016). The present data also revealed no significant differences in IGF-1 levels between these two genotypes in the temporal cortices of 9-10-month-old mice before or after the drug exposure (Fig. II-8). Consistent with our prior work, this suggests that there is heterogeneity of IGF-1 levels in brain regions. Besides local expression of IGF-1, roughly 95% of this protein is transported from the liver to the brain crossing the blood-brain barrier suggesting there may be some regional selectivity of import (E. Carro, Nuñez, Busiguina, & Torres-Aleman, 2000; Yamamoto & Murphy, 1995). Also, higher levels of serum IGF-1 have been demonstrated both in 3xTg-AD mice and AD patients compared

to controls (Parrella et al., 2013; Vardy et al., 2007). Thus, in order to investigate the levels of local brain IGF-1, the circulating IGF-1 and its transport into the brain must be considered in future work (M. M. Adams et al., 2009). Nevertheless, our data demonstrate that transient pharmacologic inhibition of the brain IGF-1R is a feasible strategy, in addition to genetic elimination of IGF-1 or its receptor, to study the effect of this growth factor in the CNS.

Much of the mechanistic effects of IGF-1R signaling inhibition related to AD using inhibitors or genetic deletion of the receptor rely on *in vitro* studies. For example, like IGF-1, $A\beta_{1-42}$ monomers reportedly activate the IGF-1R/PI3K/Akt/CREB pathway in mature cultures of pure cortical neurons after a 30 min exposure. CREB (cyclic adenosine monophosphate response element binding protein) activation induces expression of BDNF (brain-derived neurotropic factor) involved in memory formation. PPP and LY294002, the PI3K inhibitor, reverse this effect (Zimbone et al., 2018). Similarly, activated IGF-1R, due $A\beta_{1-42}$ monomer stimulation, promotes glucose uptake in cultured neurons at physiological concentrations. This is also inhibited by PPP treatment (Giuffrida et al., 2015). In contrast, $A\beta_{1-42}$ monomers, under pathological conditions, accumulate into oligomers leading to neuronal and synaptic loss (Giuffrida et al., 2015). Even though $A\beta$ oligomers show attenuating effects on active p-CREB levels, no changes were observed on p-Akt levels *in vitro* (Zimbone et al., 2018) indicating direct activation of the IGF-1R pathway via monomeric $A\beta_{1-42}$. This suggests that $A\beta$ oligomers may not downregulate p-CREB via inhibiting the IGF-1R/Akt signaling pathway since CREB is also activated by other signaling

pathways (Ortega-Martínez, 2015). In another study, astrocyte-specific IGF-1R knockout cultures demonstrated increased mitochondrial ROS production, and diminished $A\beta_{1\text{-}42}$ uptake (Logan et al., 2018). These studies suggest distinct roles of IGF-1R in different cell types that support both potentiating and attenuating functions during disease.

Human and AD mouse model studies also demonstrate dichotomous effects of IGF-1R in AD. Similar to our data, several human and animal AD studies support an exacerbating role for IGF-1R signaling in AD. For instance, hyperactivation of the PI3K/Akt/mTOR pathway has been reported in post-mortem tissue from the inferior parietal lobe of amnestic mild cognitive impairment and AD patients compared to controls. Activation of this pathway leads to protein synthesis/protein homeostasis and downregulation of autophagy/protein clearance (Tramutola et al., 2015). A decrease in autophagy function, as a result of PI3K/Akt/mTOR pathway activation, is associated with the aggregation of $A\beta_{1\text{-}42}$ proteins in the brain (Tramutola et al., 2015). Similarly, $A\beta$ accumulation upregulates mTOR signaling and pharmacological inhibition of mTOR with rapamycin decreases $A\beta_{1\text{-}42}$ and tau levels and alleviates cognitive deficits by promoting autophagy in an AD mouse model (Caccamo, Majumder, Richardson, Strong, & Oddo, 2010). In another study, a natural plant extract, curcumin, led to induction of autophagy, inhibition of $A\beta$ production, and cognitive improvement via attenuating the PI3K/Akt/mTOR pathway in AβPP/PS1 mice (C. Wang, Zhang, Teng, Zhang, & Li, 2014). Additionally, a beneficial effect of inhibiting the insulin/IGF-1 signaling cascade via NT219 has been reported in

nematodes. The inhibitor induced a reduction of p-IGF-1R and degradation of the insulin receptor substrates 1 and 2 (IRS1/2) leading to the enhanced stress resistance and protection against Aβ and polyQ$_{40}$ proteotoxicity, AD and Huntington's disease associated proteins, respectively (El-Ami et al., 2014). However, others have reported beneficial effects of IGF-1R signaling in AD. A sporadic AD rat model which was developed by intracerebral administration of streptozotocin (STZ) revealed increased AD characteristics including, p-tau, Aβ$_{42}$, and neuroinflammation, and impaired IGF-1R/Akt signaling. However, T3D-959 treatment, an orally active brain-penetrating PPARδ/γ dual nuclear receptor agonist and a potent insulin sensitizer, ameliorated cognitive deficits and AD pathological hallmarks via promoted expression of insulin/IGF-1/Akt signaling proteins in the temporal lobes (de la Monte, Tong, Schiano, & Didsbury, 2017). Except for the latter study, many investigations of IGF-1R signaling, including our own, were performed using AβPP/PS1 mice which is a familial AD model that overexpresses mutant AβPP/PS1. The AβPP/PS1 model demonstrates robust plaque deposits but no p-tau containing neurofibrillary tangles as a limitation that may ultimately alter our ability to extrapolate findings to human disease.

It was notable that IGF-1R inhibition demonstrated clear insoluble Aβ$_{1\text{-}40/42}$ attenuating effects but not soluble Aβ changes in our study (Fig. II-2). This is consistent with results from Gontier and colleagues who generated the ADINKO model via knocking out the IGF-1R gene in adult neurons of AβPP/PS1 mice by injecting tamoxifen at 2 months of age. They reported decreased Aβ monomer, oligomer, insoluble Aβ, and amyloid plaque density correlating with reduction of

both proteotoxicity and neuronal loss in the forebrain (Gontier et al., 2015). Interestingly, similar results, including decreased Aβ pathology, were not observed by ablating the neuronal IGF-1R in 17 month-old AβPP/PS1 (ADINKO) mice when they had already developed advanced disease symptoms (George et al., 2017). According to Paranjape and colleagues, soluble $A\beta_{1-42}$ protofibrils more rigorously stimulate TNF-α production in primary microglia compared to $A\beta_{1-40}$ protofibrils (Paranjape, Gouwens, Osborn, & Nichols, 2012). More importantly, $A\beta_{1-42}$ is the more dominant form in plaques due to its higher rate of fibrillization and insolubility compared to $A\beta_{1-40}$ (Serrano-Pozo, Frosch, Masliah, & Hyman, 2011). This suggests that IGF-1R inhibition resulted in the production of a less immunostimulatory form of Aβ. It is curious that our drug treatment with the IGF-1R inhibitor decreased insoluble but not soluble levels of $A\beta_{1-40/42}$. One possible explanation for this difference in Aβ conformation changes is that fibril clearance or aggregation are altered by inhibiting IGF-1R. Collectively, these data illustrate the complexity of IGF-1 and its associated receptor in mediating changes in the transgenic mice and suggest that anti-amyloid therapeutic strategies that interfere with IGF-1R signaling may be dependent upon age, particular cell type, disease state, and even the conformation of Aβ.

Our data also demonstrated an immunomodulatory effect of PPP treatment via reducing cytokine levels including eotaxin, TNF-α, IL-1α, IL-1β, IL-10 in the AβPP/PS1 temporal cortex (Fig. II-7). Elevated levels of eotaxin in the serum and IL-6, IL-1β, and TNF-α in the cerebrospinal fluid of AD patients have been reported previously (Blum-Degen et al., 1995; C. Choi et al., 2008;

Tarkowski et al., 2003). TNF-α, IL-6, and IL-1β levels were also elevated in plasma of AD patients compared to control subjects in a meta-analysis study (Swardfager et al., 2010). Moreover, an IL-1α allele 2 polymorphism is associated with AD development (Du et al., 2000). These reports indicate that rodent cytokine changes are relevant to the human disease. These immune regulatory consequences of IGF-1R inhibition parallel findings from others demonstrating that 16 months of rapamycin administration decreases hippocampal IL-1β levels correlating with improved learning and memory (Majumder et al., 2012). In addition, intracerebroventricular injection of Aβ oligomers, which induces synaptic and cognitive deficits, failed to induce neuroinflammation and behavioral dysfunction in neuronal IGF-1R knockout mice (Clarke et al., 2015; Ferreira, Lourenco, Oliveira, & De Felice, 2015; George et al., 2017; Lesné et al., 2013).

Our strategy for assessing beneficial effects of attenuated IGF-1R signaling relied on use of PPP, a reversible, selective inhibitor of the IGF-1R which preferentially targets the PI3K/Akt pathway (D. Vasilcanu et al., 2004). In addition, this drug is reported to be brain penetrant although our current study did not quantify this (Yin et al., 2010). PPP treatment is expected to inhibit phosphorylation of IGF-1R, but not other tyrosine kinase receptors (Girnita et al., 2004; R. Vasilcanu et al., 2008). PI3K/Akt/mTOR is considered a primary signaling response of the IGF-1R (Gontier et al., 2015) and therefore a likely target for modulating and assessing IGF-1R effects in the brain. Indeed, elevated mTOR signaling has been reported in the 3xTg AD mice at 6 and 12 months of

age as well as in AD brains (Caccamo et al., 2010; Oddo, 2012; Pei & Hugon, 2008; Tramutola et al., 2015). Consistent with this, higher levels of phosphorylated Akt in 6-month-old AβPP/PS1 mice compared to controls have also been reported. However, 17 month-old AβPP/PS1 mice demonstrate lower levels of Akt phosphorylation compared to their respective controls (George et al., 2017). Similarly, we also observed increased levels of phosphorylated IGF-1R, but not Akt, in 9-10-month-old AβPP/PS1 mice compared to the WT controls (Fig. II-5). Collectively, these results suggest that IGF-1R signaling responses may vary depending upon the age of the mice or the transgenic mouse line. In addition, the level of signaling response changes may be downstream of receptor phosphorylation itself.

Despite the clear brain effects of PPP administration, this was not reflected in any changes in levels of either IGF-1R or Akt phosphorylation in the drug treated hippocampi via western blot analysis (Fig. II-5). This is expected based upon the short half-life of PPP (2-4 hours) and is the most likely explanation for this lack of effect since we collected mouse brains one day after the last injection of the inhibitor and acute drug effects on phosphorylation events were no longer present (Economou et al., 2008). Indeed, this encouraging transient effect provided some assurance that IGF-1R inhibition can be targeted in the brain without long-term consequences of impairing receptor signaling. However, our global assessment of tyrosine kinase-based signaling responses via anti-p-tyrosine western blotting demonstrated a significant decrease in protein levels in the drug treated mouse brains suggesting that some persistent signaling

responses were still decreased even one day after drug treatment that will need to be identified (Fig. II-5). Also, in support of the rapid, transient nature of IGF-1R signaling, Ito and colleagues detected a rapid increase of IGF-1R phosphorylation 30 min after $A\beta_{1-42}$ oligomer microinjection into the hippocampus of an AD mouse model. Although long-term effects of IGF-1R phosphorylation were not monitored in this study, co-microinjection of PPP resulted in an attenuated increase of p75 neurotrophin receptor levels 24 h after injection in a prior work consistent with our findings of drug-dependent attenuation of protein changes (Ito et al., 2012). In accordance with the idea that drug treatment-dependent effects on acute IGF-1R-related signaling responses are transiently detectable, rapamycin treatment did not change the levels of total or phosphorylated mTOR although it did decrease levels of $A\beta_{42}$ and deposition, tau pathology, and early learning and memory impairments in 3xTg AD mice (Caccamo et al., 2010). By contrast, neuronal knock-out IGF-1R AD (ADINKO) mice demonstrated decreased cortical phosphorylated Akt/Akt (Gontier et al., 2015). This difference might be due to the long-term and irreversible inactivation of the IGF-1R response in that mouse model. Collectively, these findings support the idea that although pharmacologic manipulation of the IGF-1R signaling response results in significant changes in the brain, assessment of receptor signaling responses likely depends upon treatment times and the analysis method. We employed a short-term treatment of 7 days with a minimal dosage of 1mg/kg to exert reversible effects on IGF-1R signaling responsible for beneficial effects on Aβ levels and inflammatory state in these AD mice. This concentration

is far less than prior work which used 10-20mg/kg in mice to exert brain effects on central control of body temperature or glioma growth and produced no lasting effects on brain p-IGF-1R levels (Cintron-Colon et al., 2017; Yin et al., 2010). However, our preliminary data supported the efficacy of acute PPP injection at 1mg/kg dosage 15 min after drug administration (Fig. II-1).

We observed a somewhat cell selective effect of attenuated microgliosis while astrogliosis remained unchanged in the hippocampus of the male AβPP/PS1 drug treated group compared to vehicle controls (Fig. II-3,5). Interestingly, others have found similar results of attenuated microglial accumulation in the cortex and hippocampus of both genders of ADINKO mice (Gontier et al., 2015). Moreover, higher astrogliosis was reported in the hippocampus of female ADINKO mice without any changes in female cortex or male ADINKO hippocampus and cortex versus controls (Gontier et al., 2015). These results suggest that genetic as well as pharmacological inactivation of IGF-1R correlates with attenuated microgliosis without a clear linkage to associated changes in astrogliosis in different AD mouse models.

Perhaps this is not surprising given the fact that microglial function from altered phagocytosis to cytokine secretion is associated with the progression of AD (McQuade & Blurton-Jones, 2019). According to our data, PPP administration attenuated microgliosis and total p-tyrosine levels which was in correlation with our previous report (Dhawan et al., 2012). This suggests that immunomodulatory effects of IGF-1R inhibition in the brain may be mediated through altered microglial phenotype (Fig. II-5). Surprisingly, however, we did not observe any

effects of IGF-1R stimulation on microglial phagocytic ability for either Aβ or bacterial bioparticles (Fig. II-10A). However, IGF-1 stimulation did alter Aβ-stimulated TNF-α secretion from microglia *in vitro* suggesting that IGF-1 does alter Aβ-mediated microglial secretion phenotype (Fig. II-10B). Interestingly, we also observed that co-stimulation with Aβ and IGF-1 increased mitochondrial dehydrogenase activity assessed via MTT reduction assay (Fig. II-10C). Our data indicate that IGF-1 stimulation of Aβ plaque-associated microglia *in vivo* may indeed be contributing to microglial reactivity.

Our *in vivo* study suggests that short-term pharmacologic inhibition of the IGF-1R can decrease AD-related pathological features including Aβ deposition, microgliosis, and select cytokine changes. Importantly, this effect appears to be partially selective for microglia compared to astrocytes and insoluble Aβ compared to soluble. However, since the IGF-1R is key to biological pathways involved in the aging process and age-related diseases, additional work is needed to investigate the effect of chronic administration of PPP or other pharmacologic IGF-1R inhibitors on the progression of AD. Furthermore, more comprehensive assessment of disease phenotype including behavioral outcomes corresponding with complete evaluation of pharmacological suppression of IGF-1R signaling will be needed to better validate the IGF-1R as a valid long-term target for disease attenuation.

Study II

Gut Inflammation Induced by Dextran Sulfate Sodium Exacerbated Aβ Plaque Deposition in the *App^{NL-G-F}* Mouse Model of Alzheimer's Disease

To the best of our knowledge, this is the first study investigating a direct contribution of intestinal inflammation to Aβ plaque levels and reactive gliosis using the *App^{NL-G-F}* transgenic mouse model. We have previously reported that colonic inflammation correlates with brain Aβ plaque deposition starting at 3 months of age in *App^{NL-G-F}* mice and increased pro-inflammatory markers and macrophages in the ileums of *App^{NL-G-F}* and APP/PS1 mice compared to controls (G. D. Manocha et al., 2019; K. L. Puig et al., 2015). In this study, we report that chronic intestinal disruption induced by two cycles of DSS exposure resulted in moderate colitis-like symptoms in wild type and AD animals with significant motor dysfunction in *App^{NL-G-F}* mice. Damage to colonic integrity led to an increase in Aβ plaque load in hippocampi and temporal cortices along with a decrease in microglial phagocytic phenotype in *App^{NL-G-F}* mice maintained during the healing or recovery phase after injury. Taken together, these findings suggest that basal intestinal inflammation, which has been reported in our previous studies, exacerbated by DSS administration in AD animals can propagate to the brain and promote Aβ plaque formation likely via a reduction in Aβ clearance and to some extent increased APP processing.

It is important to point out that we used the DSS-induced colitis model as a general means of driving intestinal inflammation and not to indicate that IBD, per se, influences the risk of AD. DSS, is a negatively charged sulfated

polysaccharide that induces intestinal inflammation by disrupting intestinal epithelial integrity to increase colonic permeability leading to translocation of gut microbiota and their metabolites from the lumen into underlying tissue and infiltration of leukocytes into the lamina propria and submucosa followed by the production of pro-inflammatory cytokines (Chassaing et al., 2014b). Colonic disruption induced by DSS results in diarrhea, weight loss, and gross rectal bleeding, pathology similar to individuals with ulcerative colitis (Okayasu et al., 1990; Perše & Cerar, 2012). This is a controllable, reproducible, simple, and rapid method to induce inflammation and provides the opportunity to study the resolution of inflammation compared to the bacterial induction or transgenic models, in which colonic inflammation continues without amelioration. Although DSS studies are often performed in younger mice from 6-18 weeks of age (Bercik et al., 2011; Di Martino et al., 2016; Emge et al., 2016; Han et al., 2018; Hassan et al., 2014; Jirkof et al., 2013; M. Kumar, Kissoon-Singh, Coria, Moreau, & Chadee, 2017; Loren et al., 2017; F. Lu, Fernandes, & Davis, 2010; Mar et al., 2014; Mitrovic, Shahbazian, Bock, Pabst, & Holzer, 2010; Villaran et al., 2010; Zonis et al., 2015) we elected to use older mice at 24-40 weeks of age to allow us to examine AD-related brain changes. In spite of this older age paradigm, symptomatic parameters, colon histology (erosions and goblet cell loss) and changes in immunohistochemistry staining (tight junction protein levels and CD68) as well as lipocalin-2 ELISA assessments demonstrated successful colitis-like pathology induction in both genotypes in line with other reports (Chassaing et al., 2012; Emge et al., 2016; Perše & Cerar, 2012; Reichmann et

al., 2015; S. L. Wang et al., 2019). According to Snider and colleagues, mice are expected to recover to their initial weight during the course of recovery (Snider et al., 2016). However, neither wild type nor *App*$^{NL\text{-}G\text{-}F}$ animals completely recovered after ending the second cycle of DSS treatment in our paradigm. This could be due to treating mice with DSS at an older age in our study. However, similar to our data, Chassaing and colleagues reported that weight loss and loose stool continued for 5 weeks after DSS removal in mice with a C57BL/6 background (Chassaing et al., 2014b).

It has been reported that wild type animals with DSS-induced colitis show prolonged immobility, abnormal behavioral stress responses, memory impairment, and alterations in expression levels of genes involved in the limbic system (Emge et al., 2016; Reichmann et al., 2015; Reichmann, Painsipp, & Holzer, 2013). Indeed, we expected to observe exacerbation of memory deficits, at least, in our DSS treated mice. Our OF and CM data revealed that DSS administration did persistently decrease mobility of *App*$^{NL\text{-}G\text{-}F}$ mice compared to their controls assessed during the second resolution phase, 12 days post exposure. However, our OF and CM tests did not demonstrate any anxiety-like or memory deficits due to DSS treatment. It could be that only transient behavioral deficits were induced by DSS-induced inflammation which normalized during the interval phase. Consistent with our data, previous studies reported exacerbation of anxiety-like behavior or memory dysfunction when assessed during active colonic inflammation, 0-3 days after DSS cessation. These behavioral changes resolved during the recovery phase even though the colitis-like symptoms,

including shortened colon length, colonic histological damages, and the increased myeloperoxidase (MPO) activity, were still present (Emge et al., 2016; Jang et al., 2018; Reichmann et al., 2015). For example, wild type mice treated with 3% DSS for 5 days demonstrated recognition memory deficits and anxiety-like behavior 3 days post exposure, during active disease, tested by novel object recognition task and light/dark box test, respectively. However, behavior was no longer different 9 days post DSS treatment compared to controls (Emge et al., 2016). Similarly, impaired learning and memory in the Y-maze and passive avoidance tasks were resolved, during recovery of inflammation, 15 days after colitis induced by 2.5% 2,4,6-trinitrobenzenesulfonic acid (TNBS) for 5 days (Jang et al., 2018). Taken together, these data indicate that disruption of gut barrier integrity induced by chemicals results in a transient anxiety-like condition and memory dysfunction which returns to basal levels during resolving of inflammation. Nevertheless, the prolonged immobility observed in our study may represent gut inflammation-associated major depression which can be measured by the tail suspension and forced swimming tests (Cryan, Mombereau, & Vassout, 2005; Petit-Demouliere, Chenu, & Bourin, 2005). More importantly, the long-lasting attenuation in locomotor activity could be attributed to brain responses due to intestinal dysbiosis in *App*$^{NL-G-F}$ versus wild type mice basally or resulting from DSS treatment (Håkansson et al., 2015; Shen et al., 2017; Vogt et al., 2017; S. L. Wang et al., 2019; L. Zhang et al., 2017). Additional behavioral assessments and microbiome studies may help to further understand the differences observed.

In correlation with the intestinal inflammation induced by the DSS treatment, we observed a modest increase in select brain proinflammatory markers, Cox-2 and VCAM-1, in *App*$^{NL-G-F}$ mice compared to wild type mice. However, we observed no DSS-induced increase in brain cytokines levels in either line. Similarly, there were no increases in markers of gliosis but instead a significant decrease in a microglial phagocytic marker, CD68. It was surprising that we did not observe an increase in either GFAP or Iba-1 immunoreactivity but instead a decrease in CD68 immunoreactivity in the DSS treated *App*$^{NL-G-F}$ mice in spite of a slight but significant increase in Aβ levels and Aβ plaque deposition in the treated mice. It is unknown why the increase in plaque load is disconnected from these common markers of gliosis. Nevertheless, the decreased CD68 immunoreactivity indicates a potential change in Aβ phagocytic ability which correlates with the increased plaque deposition observed. A more extensive profiling of microglial phenotype, in particular, is clearly required following DSS treatments.

Although our hypothesis was supported that intestinal dysfunction can alter brain inflammatory changes, it is not clear why the *App*$^{NL-G-F}$ mice were selectively vulnerable. One possibility for this bias in effect could be that the *App*$^{NL-G-F}$ mice have elevated basal inflammation that exacerbates select consequences of DSS exposure in some fashion. Our prior work did observe increased age-associated intestinal inflammation in *App*$^{NL-G-F}$ mice compared to controls (G. D. Manocha et al., 2019). Consistent with this idea, a recent study showed that systemic inflammation attenuated microglial clearance capacity

leading to a permanent increase in Aβ deposition starting on day 2 post LPS challenge in aged APP/PS1 mice (Tejera et al., 2019). These results are in concordance with a human postmortem brain study which reported decreased CD68 and increased protein levels of IL-6 in AD patients with terminal systemic infection at the time of death compared to AD individuals without systemic infection (Rakic et al., 2018).

Alternatively, it could be that both lines experienced transient brain changes that resolved to varying degrees during the recovery phase. This idea is consistent with prior work demonstrating that systemic inflammation induced by injection of the bacterial cell wall component, LPS, transiently increased CD68 immunoreactivity 2 days after challenge followed by resolution 10 days post exposure in mice 15 month of age, with no effect on 5 month-old, wild type mice. Likewise, a transient increase in GFAP immunoreactivity as well as brain and peripheral pro-inflammatory cytokine levels (IL-1β and TNF-α), which peaked 2 days after induction of peripheral inflammation, returned back to basal levels 10 days post treatment in wild type mice with both ages. (Tejera et al., 2019). Elevated levels of hippocampal TNF-α also resolved 15 days after colitis induced by TNBS in another study (Jang et al., 2018). This suggests that the moderate inflammatory challenge model we employed may lead to transient brain inflammatory changes that could be exacerbated by prolonged or multiple challenges as might be experienced during a lifetime of intestinal disease.

One possibility for the elevated Aβ levels and plaque deposition observed following DSS treatment is due to exposure to bacteria or bacterial products

through the disrupted colonic epithelium. It is feasible that Aβ production is upregulated in response to the bacterial extravasation since numerous studies have reported the anti-microbial property of Aβ (D. K. Kumar et al., 2016; Moir, Lathe, & Tanzi, 2018; Soscia et al., 2010). For example, Aβ overexpression protects female 5XFAD transgenic mice from meningitis induced by an intra-cerebral injection of *Salmonella Typhimurium* (D. K. Kumar et al., 2016). Similarly, a transgenic *C. elegans* model of AD (GMC101) was also protected against *Candida albicans* infection due to Aβ expression *in vitro* and *in vivo* in the same study (D. K. Kumar et al., 2016). Although viral related, Aβ accumulation has been detected in herpes simplex virus type 1 (HSV1)-infected cells as well as mouse brains. This data correlated with localization of HSV1 DNA in amyloid plaques of AD brains (Wozniak, Mee, & Itzhaki, 2009). The virus also upregulates BACE1 expression suggesting that HSV1 induces Aβ processing and plaque formation (Ill-Raga et al., 2011; Itzhaki, 2018). Similar observations have been made following intranasal infection with a respiratory pathogen, *Chlamydia pneumoniae*, which induced amyloid deposition in non-transgenic BALB/c mouse brains with increasing density, size, and number of deposits as infection progressed (Little, Hammond, MacIntyre, Balin, & Appelt, 2004). Likewise, systemic lipopolysaccharide (LPS) administration induces Aβ formation, neuroinflammation, and cognitive deficit in animal models (J. W. Lee et al., 2008; Zhao et al., 2019).

In addition to the possibility that elevated brain Aβ levels in DSS treated mice is a general anti-microbial response, there is a particular relationship

between intestinal bacterial changes and AD. For instance, Polysaccharide A (PSA) produced by Bacteroidetes species *Bacteroides fragilis*, a gram-negative anaerobic commensal bacteria in the human GI tract, protects against central nervous system demyelination and inflammation. However, in its enterotoxigenic capacity, *Bacteroides fragilis* might be associated with inflammatory bowel disease and neuro-inflammatory signaling in AD due to secretion of toxins, including LPSs and toxic proteolytic peptides (Fathi & Wu, 2016; Lukiw, 2016; K. J. Rhee et al., 2009; Y. Wang et al., 2014). In addition, higher levels of the gut microbiota-derived metabolite, trimethylamine *N*-oxide (TMAO), have been detected in cerebrospinal fluid of individuals with mild cognitive impairment (MCI) and AD compared to healthy controls (D. Li et al., 2018; Vogt et al., 2018). AD patients demonstrate decreased microbial diversity and altered gut microbiota composition compared to controls, including decreased Firmicutes and Actinobacteria, particularly the *Bifidobacterium* genus, as well as increased Bacteroidetes (Vogt et al., 2017). Also, *Odoribacter* and *Helicobacter* abundance at the genus level, which belong to the Bacteroidetes and Proteobacteria phylum, respectively, are elevated in APP/PS1 transgenic mice compared to wild type controls (Shen et al., 2017). Increased Proteobacteria and decreased short-chain fatty acid (SCFA) levels in APP/PS1 mice compared to wild type control have also been reported (L. Zhang et al., 2017). Interestingly, similar to AD animal models and humans, it has been reported that TNBS and DSS-induced colonic inflammation also cause dysbiosis via increasing gram-negative bacteria, such as Proteobacteria and Bacteroidetes, and decreasing gram-positive bacteria,

including Firmicutes (Emge et al., 2016; Jang et al., 2018; S. L. Wang et al., 2019). In addition, long-term combinational antibiotic cocktail treatments reduce Aβ plaque deposition, decrease numbers of plaque-localized astrocytes (GFAP) and microglia (Iba-1), and change microglial morphology to a ramified state in male APP/PS1 mice (Minter et al., 2016). Germ-free APP transgenic mice show decreased brain Aβ deposition compared to their counterparts with intact gut microbiota, while this effect is reversed after colonization of the germ free mice with microbiota from intact AD mice (Harach et al., 2017). More importantly, gut microbiota and their metabolites, such as SCFAs, modulate microglia maturation, differentiation, and function (Erny et al., 2015). These data collectively suggest the involvement of specific intestinal bacteria or their metabolites in the progression of AD. Future efforts to determine intestinal microbiome changes and subsequent communication mechanisms to the brain may elucidate how the DSS-induced inflammation potentiated plaque deposition.

Taken together, our study suggests that short-term peripheral inflammation induced by DSS treatment was sufficient to induce long-lasting changes in brain Aβ levels, plaque deposition, and microglial phenotype. Extensive immune, neuronal, and glial characterization of temporal brain changes during repeated intestinal inflammatory bouts early and later in life to model different onsets and time courses of human intestinal disease will provide information regarding whether intestinal inflammation can alter the rate or severity of AD in mice. In addition, identifying the cross-talk mechanisms of communicating intestinal dysfunction to the brain whether it is microbiome,

endocrine, immune, or nervous related may identify means of attenuating the peripheral contribution to AD.

Study III

Effect of Alzheimer's Disease Associated *APP* Mutations on the Progression of Colorectal Cancer Induced by AOM/DSS in Mice

In our previous investigations, we reported a contribution of colitis-like inflammation induced by DSS on exacerbation of Aβ plaque load in $App^{NL\text{-}G\text{-}F}$ males suggesting that peripheral inflammatory changes communicate to the brain to exacerbate AD. In this study, we report that prolonged colonic inflammation induced by AOM/DSS administration developed genotype dependent CAC symptomatic parameters, including decreased colon length, increased spleen and colon weights, increased tumor number and area as well as colonic histology in a fashion significantly greater in $App^{NL\text{-}G\text{-}F}$ males vs. respective females and wild type males. Autosomal dominant AD mutations in *APP* resulted in exacerbated brain plaque load, worsened intestinal inflammation, and increased colonic tumorigenesis in male mice compared to wild types due to AOM/DSS treatment while these same mutations provided protection against intestinal inflammation and tumor development with no change in brain plaques in female $App^{NL\text{-}G\text{-}F}$ mice. The survival rate in male wild type mice was greater than wild type females, whereas AOM/DSS treated $App^{-/-}$ and $App^{NL\text{-}G\text{-}F}$ males showed lower survival rate than their respective females.

In order to recapitulate human-like colorectal cancer in mice and investigate its correlation with expression of wild type or mutant AβPP in both

sexes, an AOM/DSS combined treatment was utilized to induce the CAC due to its high reproducibility, simplicity, potency, and affordability. This model provides a shorter latency period compared to only AOM or DSS treated models. In this paradigm, the procarcinogen AOM, a metabolite of 1,2 dimethylhydrazine (DMH), reaches the liver via the bloodstream following i.p. injection. Hydroxylation of AOM by cytochromes P450 in the liver leads to formation of methylazoxymethanol (MAM), a macromolecule alkylating agent. MAM is transported to the colon via bile and targets the colonic mucosa to induce an O^6-methyl-deoxyguanosine (O^6mG) $\rightarrow$ A transition mutation in DNA with a ~12 h half-life. In concert with this, DSS damages the colonic epithelial monolayer lining to induce intestinal inflammation (Chassaing et al., 2014a; De Robertis et al., 2011; Neufert, Becker, & Neurath, 2007; Parang, Barrett, & Williams, 2016; Rosenberg, Giardina, & Tanaka, 2009).

Interestingly, the incidence rate of dementia, including AD, is greater in women than men (Beam et al., 2018; Mielke, 2018; Vina & Lloret, 2010). In contrast, colorectal cancer incidence and mortality is higher in men compared to women (Douaiher et al., 2017; White et al., 2018). Similarly, a meta-analysis of population-based cohort studies reports a greater risk of ulcerative colitis-associate colorectal cancer in males (Jess, Rungoe, & Peyrin-Biroulet, 2012). It is important to note that there is also a sex difference in colonic tumor location. For instance, women are at higher risk of developing right-sided (proximal) colon cancer. While, left-sided (distal) colon cancer is common in men (S. E. Kim et al., 2015). AOM/DSS treatment predominantly develops tumor in the distal part of

colon and mimics colorectal cancer in men (De Robertis et al., 2011; Parang et al., 2016). This may partially explain the sex differences we observed although not the increased severity observed in male *App*$^{NL\text{-}G\text{-}F}$ mice compared to wild types males or the reduced severity of female *App*$^{NL\text{-}G\text{-}F}$ mice compared to wild type females.

Different sex and genotype susceptibility to AOM/DSS treatment has been observed in other reports. Similar to our *App*$^{NL\text{-}G\text{-}F}$ data, microscopic and histological examinations demonstrate more severe CAC in AOM/DSS male ICR mice, including earlier tumor incidence and significantly higher total tumor number, compared to females (S. M. Lee et al., 2016). Specific STAT1 deletion in intestinal epithelial cells (STAT1$^{\Delta IEC}$) is associated with increased intestinal tumor load in males but not females with colitis-associated colorectal cancer following AOM/DSS exposure demonstrating a male-specific tumor suppressive function of epithelial STAT1 in mice and human colorectal cancer (Crnčec et al., 2018). Comparing *App*$^{NL\text{-}G\text{-}F}$ males with females and *App*$^{NL\text{-}G\text{-}F}$ females versus wild type females may indicate a female-selective tumor suppressor function of AD mutant APP. Further work is needed to characterize and manipulate processing of APP into Aβ, N-terminal, and AICD fragments in both sexes of *App*$^{NL\text{-}G\text{-}F}$ mice to determine whether mutant expression alone or proteolytic fragments of APP are involved in the increased susceptibility (males) or protection (females) against CAC compared to wild type mice.

One possibility for explaining the sex differences in susceptibility to AOM/DSS treatment is simply differences in sex hormone function. For example,

early administration of estradiol to male ICR AOM/DSS treated mice alleviates inflammation and prevents from colorectal cancer (Son et al., 2019). AOM/DSS treatment in ovariectomized female ICR mice leads to the increased proximal colon tumor number and incidence rate compared to the control AOM/DSS female group. 17β-estradiol (E2) administration following ovariectomy significantly suppresses the increased colonic tumorigenesis. However, mice ovariectomy exerts no effect on tumorigenesis in the distal colon in comparison with the AOM/DSS control female group (Song et al., 2019). The androgen receptor (AR) is a fundamental transcription factor involved in the pathophysiology of prostate and breast cancers, in which sex hormones play pivotal roles. Interestingly, it controls target genes which promote tumor growth or proliferation activity, including APP, via androgen-dependent AR-binding sites (ARBS) (Takagi et al., 2013; Takayama et al., 2009). This suggests that APP may be an androgen-dependent growth factor. It will be of interest to determine whether sex hormone receptor signaling is responsible for the differences we observed when comparing male and female *App*$^{NL-G-F}$ mice and well as wild type versus *App*$^{NL-G-F}$ male and female mice.

App$^{-/-}$ males and females followed a different pattern compared to *App*$^{NL-G-F}$ and wild type mice regarding % weight loss. Despite developing tumors, both genders regained weight back to their vehicle control levels. Also, *App*$^{-/-}$ males demonstrated higher susceptibility and death rate following drug treatment compared to their female counterparts. 6 out 10 *App*$^{-/-}$ male mice died during treatment with the 4 remaining animals demonstrating colonic tumors. *App*$^{-/-}$ mice

are viable and fertile and demonstrate reactive gliosis as well as a 15-20% decrease in weight compared to their age-matched wild-type controls (Zheng et al., 1995). This basal difference perhaps reflects a growth factor property of APP *in vivo* (Rossjohn et al., 1999). Indeed, APP knockdown via lentiviral shRNA expression results in cell motility and growth prevention by inducing apoptosis in breast cancer cells *in vitro* and in a xenograft mouse model (S. Lim et al., 2014). Similarly, inhibition of APP expression and subsequent sAPP generation using antisense techniques robustly reduces thyrotropin-induced thyroid epithelial cell proliferation (Pietrzik et al., 1998). However, our *App*$^{-/-}$ mouse data suggests that genetic ablation of the *APP* gene did not protect against colonic tumorigenesis in males or females but instead conferred some selective mortality risk to male mice.

This apparent discrepancy with a mitogenic role for APP and sAPPα could be due to developmental compensation in the *App*$^{-/-}$ mice. It is important to note that both APP and APP-like protein 2 (APLP2) are ubiquitously expressed throughout the body, including colon tissue (K. L. Puig & Combs, 2013; van der Kant & Goldstein, 2015; W. Wu et al., 2012). Double knockouts for *App*$^{-/-}$/*APLP2*$^{-/-}$ or *APLP1*$^{-/-}$/*APLP2*$^{-/-}$, and knockouts for *App*$^{-/-}$/*APLP1*$^{-/-}$/*APLP2*$^{+/-}$ mice demonstrate early postnatal lethality. However, *App*$^{-/-}$/*APLP1*$^{-/-}$ mice are viable (Heber et al., 2000; von Koch et al., 1997). These results indicate that either APP or APLP2 is required for mouse viability and APLP2 could take over the function of APP (Zheng & Koo, 2006) in the intestines of *App*$^{-/-}$ mice which might explain the lack of protection against cancer development. APLP2 lacks the Aβ region

but undergoes proteolysis similar to APP. Cleavage of APLP2 via α-, β-, and γ-secretases leads to production of sAPLP2, a membrane-bound C-terminal fragment, p3/ Aβ-like fragments, and an APP-like intracellular domain (ALID similar to AICD) allowing this protein to possibly compensate for genetic deletion of *App*. (Eggert et al., 2004; Endres, Postina, Schroeder, Mueller, & Fahrenholz, 2005; Pastorino et al., 2004; Scheinfeld, Ghersi, Laky, Fowlkes, & D'Adamio, 2002; Walsh et al., 2003).

Although the focus of this study was to assess the effects of mutant APP expression on tumorigenesis, our prior work demonstrated that prolonged colonic inflammation in a DSS-induced colitis-like paradigm was sufficient to exacerbate brain amyloidosis in male mice. We observed as similar effect in this study in which robust tumorigenesis and neoplasm in $App^{NL\text{-}G\text{-}F}$ male mice resulted in a significant increase in Aβ plaque load. This potentiation of plaque load was not observed in female $App^{NL\text{-}G\text{-}F}$ mice consistent with their overall minimal change in intestinal inflammation and tumor count. Therefore, besides the primary conclusion of mutant APP expression altering tumorigenic susceptibility in a sex-dependent manner, we also confirmed that robust intestinal inflammatory conditions are sufficient to communicate to the brain to worsen brain pathology associated with AD. Future work with an inflammatory stimulus equivalent in both male and female intestines will better determine whether there is a sex-bias in gut-brain communication. In addition, the mechanisms by which intestinal dysfunction communicates to the brain will need to be determined. For example,

the well-described brain-gut-microbiota axis is a likely component of this communication mechanism (Martin, Osadchiy, Kalani, & Mayer, 2018).

Taken together, we report that prolonged colonic inflammation resulting from AOM/DSS-induced CAC in *App*$^{NL-G-F}$ males, but not females, increased Aβ deposition and tumorigenic potential. However, mutant *APP* expression in *App*$^{NL-G-F}$ females provided a sex-dependent colonic tumor suppressor function which exerted no impact on Aβ aggregation compared to *App*$^{NL-G-F}$ vehicle females.

Limitations and Future Directions of Work Presented in This Dissertation

The research presented in this dissertation indicates a significant role of peripheral manipulation, more specifically intestinal inflammation, on the development and progression of AD. The reciprocal role of mutant *APP* in colonic tumorigenesis is also addressed in a sex-dependent manner in an AD mouse model. There are a few limitations of the studies presented in this dissertation as well as some logical next steps for future work.

The AD transgenic models containing familial mutations (AβPP/PS1 and *App*$^{NL-G-F}$) enabled us to study the role of an IGF-1R inhibitor as well as colitis-like and CAC pathologies on an early onset familial AD paradigm. These familial cases of AD represent a minority of human cases and are characterized by robust Aβ production atypical of the more common late onset sporadic form of AD. In order to assess the role of peripheral manipulation and gut inflammation on late onset AD, we could in the future use a B6.129S2-Tg(APP)8.9Btla/J mouse provided from the Jackson laboratory. This transgenic mouse model

carries a humanized *APP* gene without mutations which would provide an opportunity to study induction of APP amyloidogenic processing and Aβ aggregation in the brain as a direct consequence of disrupting the intestinal barrier. Mice carrying a humanized APOE4 (heterozygous or homozygous) could be employed for a similar purpose of trying to better model human late onset disease, since APOE4 represents a significant risk for late onset disease. These transgenic mice cannot develop an AD phenotype by themselves (Onos, Sukoff Rizzo, Howell, & Sasner, 2016) and require crossing to the B6.129S2-Tg(APP)8.9Btla/J mouse in order for the combined cross to develop AD-like pathology.

To further study the effect of PPP on AD pathology improvement, chronic administration and a higher dosage of PPP (20mg/kg, twice a day, intraperitoneally) at least for 3 weeks could be performed in future investigations (Menu et al., 2006). In addition, behavioral changes correlating with the brain pathological alterations should be assessed. As with any pharmacologic intervention, the appropriate ADMET and PK/PD studies are also needed for PPP to optimize a long-term treatment strategy that would better assess its efficacy for treating AD in the mice.

To better assess the impact of DSS-induced colitis-like pathology on the progression of AD, a younger AD mouse model (1-2 month old) with less or no Aβ deposition could be utilized in future work. Sensitive, movement-limited more appropriate behavioral tests, including the step-down and fear conditioning assessments, could also be performed right after ending the last DSS exposure

to minimize any confounds from lack of mobility and to capture impairment prior to recovery (Bercik et al., 2011; Bravo et al., 2011). In addition, we could consider an intervention to attenuate the colitis-induced exacerbation of disease. For example, Natalizumab or Adalimumab are attractive therapeutic possibilities which might be able to attenuate the peripheral immune dysfunction and exert benefits in the brain without a necessity to penetrate blood-brain barrier (BBB). Natalizumab (Tysabri), a humanized monoclonal antibody against α_4 integrin subunit, prevents cell migration across the BBB and gastrointestinal tracts via blocking the interaction of $\alpha_4\beta_1$ and VCAM-1 as well as $\alpha_4\beta_7$ and MAdCAM-1, respectively. Adalimumab is a human monoclonal anti-TNF-α antibody that currently is used for inflammatory bowel disease (Paramsothy, Rosenstein, Mehandru, & Colombel, 2018). Indeed, prior work from our group has already demonstrated a therapeutic benefit in APP/PS1 mice using tail vein delivery of anti-$\alpha_4\beta_7$ antibody (G. Manocha, Ghatak, Puig, & Combs, 2018).

Although the sex differences in tumorigenic susceptibility in male versus female *App*$^{NL\text{-}G\text{-}F}$ mice implies a sex hormone difference, the fact that both sexes differed significantly from sex matched wild type mice suggests that the APP mutations also had a role in tumor growth. In order to better understand this complexity, future work to begin dissecting apart mutant *APP*-associated colonic tumorigenesis could employ RNAseq or microarray regional analysis from colons and even brains to better understand the sex and genotype susceptibilities. The impact of APP or its processed fragments on tumorigenesis could also be evaluated using other human cancer models, including breast and prostate

cancers to determine whether the changes we observed are colon cancer specific. In addition, β-, α-, and γ-secretase inhibitors, including verubescestat, batimastat, GI254023X, and semagascestat, could be administered as intervention therapeutics to assess whether preventing or promoting amyloidogenic processing in a sex-selective fashion alters colon tumor development. This could offer the exciting possibility of repositioning drugs developed for treating APP processing in AD to find new use in cancer biology. In addition, to assess whether mutant APP expression modulates cell proliferative activity and apoptosis in the colon, 5-bromo-2′-deoxyuridine (BrdU) and terminal deoxynucleotidyl transferase dUTP nick end labeling (TUNEL) staining can be performed, respectively, in a future work to compare to histologic, biochemical, and molecular biology changes.

Summary Conclusions

The work presented in this study suggests a significant contribution of peripheral intestinal dysfunction, more specifically colitis-like and CAC pathophysiology, on exacerbation of AD characterized by increased Aβ deposition.

Interestingly, mutant *APP* expression in the *App*$^{NL-G-F}$ AD mouse model modulates colonic inflammation and tumorigenesis and subsequent brain effects in a genotype and sex-dependent manner. Mutant *APP* appears to provide a specific tumor suppressor function in the colons of the female *App*$^{NL-G-F}$ mice compared to both wild type females and *App*$^{NL-G-F}$ males. However, mutant *APP* expression exacerbates both colonic inflammation and neoplasm in *App*$^{NL-G-F}$

male mice compared to wild type males which communicates to the brain to significantly increase Aβ plaque load.

REFERENCES

2016 Alzheimer's disease facts and figures. (2016). *Alzheimers Dement, 12*(4), 459-509. doi:10.1016/j.jalz.2016.03.001

Acheson, A., Conover, J. C., Fandl, J. P., DeChiara, T. M., Russell, M., Thadani, A., & .Lindsay, R. M. (1995). A BDNF autocrine loop in adult sensory neurons prevents cell death. *Nature, 374*(6521), 450-453. doi:10.1038/374450a0

Adams, G. G., & Dilly, P. N. (1989). Differential staining of ocular goblet cells. *Eye (Lond), 3 (Pt 6)*, 840-844. doi:10.1038/eye.1989.128

Adams, M. M., Forbes, M. E., Linville, M. C., Riddle, D. R., Sonntag, W. E., & Brunso-Bechtold, J. K. (2009). Stability of local brain levels of insulin-like growth factor-I in two well-characterized models of decreased plasma IGF-I. *Growth factors (Chur, Switzerland), 27*(3), 181-188. doi:10.1080/08977190902863639

Agostinho, P., Pliassova, A., Oliveira, C. R., & Cunha, R. A. (2015). Localization and Trafficking of Amyloid-beta Protein Precursor and Secretases: Impact on Alzheimer's Disease. *J Alzheimers Dis, 45*(2), 329-347. doi:10.3233/jad-142730

Alzheimer, A., Stelzmann, R. A., Schnitzlein, H. N., & Murtagh, F. R. (1995). An English translation of Alzheimer's 1907 paper, "Uber eine eigenartige Erkankung der Hirnrinde". *Clin Anat, 8*(6), 429-431. doi:10.1002/ca.980080612

Anand, R., Gill, K. D., & Mahdi, A. A. (2014). Therapeutics of Alzheimer's disease: Past, present and future. *Neuropharmacology, 76 Pt A*, 27-50. doi:10.1016/j.neuropharm.2013.07.004

Ananthakrishnan, A. N., Shi, H. Y., Tang, W., Law, C. C., Sung, J. J., Chan, F. K., & Ng, S. C. (2016). Systematic Review and Meta-analysis: Phenotype and Clinical Outcomes of Older-onset Inflammatory Bowel Disease. *J Crohns Colitis, 10*(10), 1224-1236. doi:10.1093/ecco-jcc/jjw054

Arai, H., Lee, V. M., Messinger, M. L., Greenberg, B. D., Lowery, D. E., & Trojanowski, J. Q. (1991). Expression patterns of beta-amyloid precursor protein (beta-APP) in neural and nonneural human tissues from Alzheimer's disease and control subjects. *Ann Neurol, 30*(5), 686-693. doi:10.1002/ana.410300509

Arcaro, A. (2013). Targeting the insulin-like growth factor-1 receptor in human cancer. *Frontiers in Pharmacology, 4*. doi:10.3389/fphar.2013.00030

Arganda-Carreras, I., Kaynig, V., Rueden, C., Eliceiri, K. W., Schindelin, J., Cardona, A., & Sebastian Seung, H. (2017). Trainable Weka Segmentation: a machine learning tool for microscopy pixel classification. *Bioinformatics, 33*(15), 2424-2426. doi:10.1093/bioinformatics/btx180

Argandona, E. G., Bengoetxea, H., Ortuzar, N., Bulnes, S., Rico-Barrio, I., & Lafuente, J. V. (2012). Vascular endothelial growth factor: adaptive changes in the neuroglialvascular unit. *Curr Neurovasc Res, 9*(1), 72-81. doi:10.2174/156720212799297119

Association, A. s. (2019). 2019 Alzheimer's disease facts and figures. *Alzheimer's & Dementia, 15*(3), 321-387.

Attree, E. A., Dancey, C. P., Keeling, D., & Wilson, C. (2003). Cognitive function in people with chronic illness: inflammatory bowel disease and irritable bowel syndrome. *Appl Neuropsychol, 10*(2), 96-104. doi:10.1207/s15324826an1002_05

Awada, A. A. (2015). Early and late-onset Alzheimer's disease: What are the differences? *J Neurosci Rural Pract, 6*(3), 455-456. doi:10.4103/0976-3147.154581

Aziz, Q., & Thompson, D. G. (1998). Brain-gut axis in health and disease. *Gastroenterology, 114*(3), 559-578. doi:10.1016/s0016-5085(98)70540-2

Barde, Y. A., Edgar, D., & Thoenen, H. (1982). Purification of a new neurotrophic factor from mammalian brain. *Embo j, 1*(5), 549-553.

BARGEN, J. A. (1928). Chronic ulcerative colitis associated with malignant disease. *Archives of Surgery, 17*(4), 561-576.

Bartus, R. T., Dean, R. L., 3rd, Beer, B., & Lippa, A. S. (1982). The cholinergic hypothesis of geriatric memory dysfunction. *Science, 217*(4558), 408-414. doi:10.1126/science.7046051

Baserga, R. (1999). The IGF-I Receptor in Cancer Research. *Experimental Cell Research, 253*(1), 1-6. doi:10.1006/excr.1999.4667

Baxter, R. C. (1986). The somatomedins: insulin-like growth factors. *Adv Clin Chem, 25*, 49-115. doi:10.1016/s0065-2423(08)60124-9

Bayliss, W. M., & Starling, E. H. (1899). The movements and innervation of the small intestine. *J Physiol, 24*(2), 99-143. doi:10.1113/jphysiol.1899.sp000752

Beach, T. G., Walker, R., & McGeer, E. G. (1989). Patterns of gliosis in Alzheimer's disease and aging cerebrum. *Glia, 2*(6), 420-436. doi:10.1002/glia.440020605

Beam, C. R., Kaneshiro, C., Jang, J. Y., Reynolds, C. A., Pedersen, N. L., & Gatz, M. (2018). Differences Between Women and Men in Incidence Rates of Dementia and Alzheimer's Disease. *J Alzheimers Dis, 64*(4), 1077-1083. doi:10.3233/jad-180141

Bercik, P., Park, A. J., Sinclair, D., Khoshdel, A., Lu, J., Huang, X., & Verdu, E. F. (2011). The anxiolytic effect of Bifidobacterium longum NCC3001 involves vagal pathways for gut-brain communication. *Neurogastroenterol Motil, 23*(12), 1132-1139. doi:10.1111/j.1365-2982.2011.01796.x

Bernstein, C. N., Singh, S., Graff, L. A., Walker, J. R., Miller, N., & Cheang, M. (2010). A prospective population-based study of triggers of symptomatic flares in IBD. *Am J Gastroenterol, 105*(9), 1994-2002. doi:10.1038/ajg.2010.140

Blum-Degen, D., Müller, T., Kuhn, W., Gerlach, M., Przuntek, H., & Riederer, P. (1995). Interleukin-1 beta and interleukin-6 are elevated in the cerebrospinal fluid of Alzheimer's and de novo Parkinson's disease patients. *Neuroscience Letters, 202*(1-2), 17-20. Retrieved from http://www.ncbi.nlm.nih.gov/pubmed/8787820

Bollrath, J., & Greten, F. R. (2009). IKK/NF-kappaB and STAT3 pathways: central signalling hubs in inflammation-mediated tumour promotion and metastasis. *EMBO Rep, 10*(12), 1314-1319. doi:10.1038/embor.2009.243

Botelho, M. G., Wang, X., Arndt-Jovin, D. J., Becker, D., & Jovin, T. M. (2010). Induction of terminal differentiation in melanoma cells on downregulation of beta-amyloid precursor protein. *J Invest Dermatol, 130*(5), 1400-1410. doi:10.1038/jid.2009.296

Braak, H., & Braak, E. (1991). Neuropathological stageing of Alzheimer-related changes. *Acta Neuropathol, 82*(4), 239-259. doi:10.1007/bf00308809

Braak, H., Rub, U., Gai, W. P., & Del Tredici, K. (2003). Idiopathic Parkinson's disease: possible routes by which vulnerable neuronal types may be subject to neuroinvasion by an unknown pathogen. *J Neural Transm (Vienna), 110*(5), 517-536. doi:10.1007/s00702-002-0808-2

Bradford, M. M. (1976). A rapid and sensitive method for the quantitation of microgram quantities of protein utilizing the principle of protein-dye binding. *Analytical Biochemistry, 72*, 248-254. Retrieved from http://www.ncbi.nlm.nih.gov/pubmed/942051

Bravo, J. A., Forsythe, P., & Chew, M. V., Escaravage, E., Savignac, H. M., Dinan, T. G., Cryan, J. F. (2011). Ingestion of Lactobacillus strain regulates emotional behavior and central GABA receptor expression in a mouse via the vagus nerve. *Proc Natl Acad Sci U S A, 108*(38), 16050-16055. doi:10.1073/pnas.1102999108

Breit, S., Kupferberg, A., Rogler, G., & Hasler, G. (2018). Vagus Nerve as Modulator of the Brain-Gut Axis in Psychiatric and Inflammatory Disorders. *Front Psychiatry, 9*, 44. doi:10.3389/fpsyt.2018.00044

Brennan, C. A., & Garrett, W. S. (2016). Gut Microbiota, Inflammation, and Colorectal Cancer. *Annu Rev Microbiol, 70*, 395-411. doi:10.1146/annurev-micro-102215-095513

Breynaert, C., Vermeire, S., Rutgeerts, P., & Van Assche, G. (2008). Dysplasia and colorectal cancer in inflammatory bowel disease: a result of inflammation or an intrinsic risk? *Acta Gastroenterol Belg, 71*(4), 367-372.

Brunden, K. R., Trojanowski, J. Q., & Lee, V. M. (2009). Advances in tau-focused drug discovery for Alzheimer's disease and related tauopathies. *Nat Rev Drug Discov, 8*(10), 783-793. doi:10.1038/nrd2959

Bu, G. (2009). Apolipoprotein E and its receptors in Alzheimer's disease: pathways, pathogenesis and therapy. *Nat Rev Neurosci, 10*(5), 333-344. doi:10.1038/nrn2620

Cabal, A., Alonso-Cortina, V., Gonzalez-Vazquez, L. O., Naves, F. J., Del Valle, M. E., & Vega, J. A. (1995). beta-Amyloid precursor protein (beta APP) in human gut with special reference to the enteric nervous system. *Brain Res Bull, 38*(5), 417-423. doi:10.1016/0361-9230(95)02006-d

Caccamo, A., Majumder, S., Richardson, A., Strong, R., & Oddo, S. (2010). Molecular Interplay between Mammalian Target of Rapamycin (mTOR), Amyloid-β, and Tau EFFECTS ON COGNITIVE IMPAIRMENTS. *Journal of Biological Chemistry, 285*(17), 13107-13120. doi:10.1074/jbc.M110.100420

Cai, X. D., Golde, T. E., & Younkin, S. G. (1993). Release of excess amyloid beta protein from a mutant amyloid beta protein precursor. *Science, 259*(5094), 514-516. doi:10.1126/science.8424174

Cai, Z., Qiao, P. F., Wan, C. Q., Cai, M., Zhou, N. K., & Li, Q. (2018). Role of Blood-Brain Barrier in Alzheimer's Disease. *J Alzheimers Dis, 63*(4), 1223-1234. doi:10.3233/jad-180098

Cam, J. A., Zerbinatti, C. V., Knisely, J. M., Hecimovic, S., Li, Y., & Bu, G. (2004). The low density lipoprotein receptor-related protein 1B retains beta-amyloid precursor protein at the cell surface and reduces amyloid-beta peptide production. *J Biol Chem, 279*(28), 29639-29646. doi:10.1074/jbc.M313893200

Cam, J. A., Zerbinatti, C. V., Li, Y., & Bu, G. (2005). Rapid endocytosis of the low density lipoprotein receptor-related protein modulates cell surface distribution and processing of the beta-amyloid precursor protein. *J Biol Chem, 280*(15), 15464-15470. doi:10.1074/jbc.M500613200

Camilleri, M., Cowen, T., & Koch, T. R. (2008). Enteric neurodegeneration in ageing. *Neurogastroenterol Motil, 20*(4), 418-429. doi:10.1111/j.1365-2982.2008.01134.x

Carro, E., Nuñez, A., Busiguina, S., & Torres-Aleman, I. (2000). Circulating insulin-like growth factor I mediates effects of exercise on the brain. *The Journal of Neuroscience: The Official Journal of the Society for Neuroscience, 20*(8), 2926-2933. Retrieved from http://www.ncbi.nlm.nih.gov/pubmed/10751445

Carro, E., Trejo, J. L., Gomez-Isla, T., LeRoith, D., & Torres-Aleman, I. (2002). Serum insulin-like growth factor I regulates brain amyloid-beta levels. *Nature Medicine, 8*(12), 1390-1397. doi:10.1038/nm793

Carro, E., Trejo, J. L., Spuch, C., Bohl, D., Heard, J. M., & Torres-Aleman, I. (2006). Blockade of the insulin-like growth factor I receptor in the choroid plexus originates Alzheimer's-like neuropathology in rodents: new cues into the human disease? *Neurobiology of Aging, 27*(11), 1618-1631. doi:10.1016/j.neurobiolaging.2005.09.039

Carter, S. F., Herholz, K., Rosa-Neto, P., Pellerin, L., Nordberg, A., & Zimmer, E. R. (2019). Astrocyte Biomarkers in Alzheimer's Disease. *Trends Mol Med, 25*(2), 77-95. doi:10.1016/j.molmed.2018.11.006

Casén, C., Vebø, H. C., Sekelja, M., Hegge, F. T., Karlsson, M. K., Ciemniejewska, E., & Rudi, K. (2015). Deviations in human gut microbiota: a novel diagnostic test for determining dysbiosis in patients with IBS or IBD. *Aliment Pharmacol Ther, 42*(1), 71-83. doi:10.1111/apt.13236

Castaneda, A. E., Tuulio-Henriksson, A., Aronen, E. T., Marttunen, M., & Kolho, K. L. (2013). Cognitive functioning and depressive symptoms in adolescents with inflammatory bowel disease. *World J Gastroenterol, 19*(10), 1611-1617. doi:10.3748/wjg.v19.i10.1611

Castellano, J. M., Kim, J., Stewart, F. R., Jiang, H., DeMattos, R. B., Patterson, B. W., & Holtzman, D. M. (2011). Human apoE isoforms differentially regulate brain amyloid-β peptide clearance. *Sci Transl Med, 3*(89), 89ra57. doi:10.1126/scitranslmed.3002156

Chassaing, B., Aitken, J. D., Malleshappa, M., & Vijay-Kumar, M. (2014a). Dextran sulfate sodium (DSS)-induced colitis in mice. *Curr Protoc Immunol, 104*, 15.25.11-15.25.14. doi:10.1002/0471142735.im1525s104

Chassaing, B., Aitken, J. D., Malleshappa, M., & Vijay-Kumar, M. (2014b). Dextran sulfate sodium (DSS)-induced colitis in mice. *Curr Protoc Immunol, 104*, Unit 15.25. doi:10.1002/0471142735.im1525s104

Chassaing, B., Srinivasan, G., Delgado, M. A., Young, A. N., Gewirtz, A. T., & Vijay-Kumar, M. (2012). Fecal lipocalin 2, a sensitive and broadly dynamic non-invasive biomarker for intestinal inflammation. *PLoS One, 7*(9), e44328. doi:10.1371/journal.pone.0044328

Chen, G. F., Xu, T. H., Yan, Y., Zhou, Y. R., Jiang, Y., Melcher, K., & Xu, H. E. (2017). Amyloid beta: structure, biology and structure-based therapeutic development. *Acta Pharmacol Sin, 38*(9), 1205-1235. doi:10.1038/aps.2017.28

Chen, K. S., Nishimura, M. C., Armanini, M. P., Crowley, C., Spencer, S. D., & Phillips, H. S. (1997). Disruption of a single allele of the nerve growth factor gene results in atrophy of basal forebrain cholinergic neurons and memory deficits. *J Neurosci, 17*(19), 7288-7296. doi:10.1523/jneurosci.17-19-07288.1997

Choi, C., Jeong, J.-H., Jang, J. S., Choi, K., Lee, J., Kwon, J., &. Kang, S. W. (2008). Multiplex analysis of cytokines in the serum and cerebrospinal fluid of patients with Alzheimer's disease by color-coded bead technology. *Journal of Clinical Neurology (Seoul, Korea), 4*(2), 84-88. doi:10.3988/jcn.2008.4.2.84

Choi, S.-H., Aid, S., Caracciolo, L., Minami, S. S., Niikura, T., Matsuoka, Y., & Bosetti, F. (2013). Cyclooxygenase-1 inhibition reduces amyloid pathology and improves memory deficits in a mouse model of Alzheimer's disease. *Journal of Neurochemistry, 124*(1), 59-68. doi:10.1111/jnc.12059

Chung, D. W., Yoo, K. Y., Hwang, I. K., Kim, D. W., Chung, J. Y., Lee, C. H., & Won, M. H. (2010). Systemic administration of lipopolysaccharide induces cyclooxygenase-2 immunoreactivity in endothelium and increases microglia in the mouse hippocampus. *Cell Mol Neurobiol, 30*(4), 531-541. doi:10.1007/s10571-009-9477-0

Cintron-Colon, R., Sanchez-Alavez, M., Nguyen, W., Mori, S., Gonzalez-Rivera, R., Lien, T., & Conti, B. (2017). Insulin-like growth factor 1 receptor regulates hypothermia during calorie restriction. *Proc Natl Acad Sci U S A, 114*(36), 9731-9736. doi:10.1073/pnas.1617876114

Citron, M., Oltersdorf, T., Haass, C., McConlogue, L., Hung, A. Y., Seubert, P., .& Selkoe, D. J. (1992). Mutation of the beta-amyloid precursor protein in familial Alzheimer's disease increases beta-protein production. *Nature, 360*(6405), 672-674. doi:10.1038/360672a0

Clarke, J. R., Lyra E Silva, N. M., Figueiredo, C. P., Frozza, R. L., Ledo, J. H., Beckman, D., & De Felice, F. G. (2015). Alzheimer-associated Aβ oligomers impact the central nervous system to induce peripheral metabolic deregulation. *EMBO molecular medicine, 7*(2), 190-210. doi:10.15252/emmm.201404183

Cohen, E., Paulsson, J. F., Blinder, P., Burstyn-Cohen, T., Du, D., Estepa, G., & Dillin, A. (2009). Reduced IGF-1 Signaling Delays Age-associated Proteotoxicity in Mice. *Cell, 139*(6), 1157-1169. doi:10.1016/j.cell.2009.11.014

Cole, S. L., & Vassar, R. (2007). The Alzheimer's disease beta-secretase enzyme, BACE1. *Mol Neurodegener, 2*, 22. doi:10.1186/1750-1326-2-22

Collins, S. M., Surette, M., & Bercik, P. (2012). The interplay between the intestinal microbiota and the brain. *Nat Rev Microbiol, 10*(11), 735-742. doi:10.1038/nrmicro2876

Cook-Mills, J. M., Marchese, M. E., & Abdala-Valencia, H. (2011). Vascular cell adhesion molecule-1 expression and signaling during disease: regulation by reactive oxygen species and antioxidants. *Antioxid Redox Signal, 15*(6), 1607-1638. doi:10.1089/ars.2010.3522

Cooks, T., Pateras, I. S., Tarcic, O., Solomon, H., Schetter, A. J., Wilder, S., & Oren, M. (2013). Mutant p53 prolongs NF-κB activation and promotes chronic inflammation and inflammation-associated colorectal cancer. *Cancer Cell, 23*(5), 634-646. doi:10.1016/j.ccr.2013.03.022

Cooper, H. S., Murthy, S. N., Shah, R. S., & Sedergran, D. J. (1993). Clinicopathologic study of dextran sulfate sodium experimental murine colitis. *Lab Invest, 69*(2), 238-249.

Corder, E. H., Saunders, A. M., Strittmatter, W. J., Schmechel, D. E., Gaskell, P. C., Small, G. W., & Pericak-Vance, M. A. (1993). Gene dose of apolipoprotein E type 4 allele and the risk of Alzheimer's disease in late onset families. *Science, 261*(5123), 921-923. doi:10.1126/science.8346443

Cosnes, J., Gower-Rousseau, C., Seksik, P., & Cortot, A. (2011). Epidemiology and natural history of inflammatory bowel diseases. *Gastroenterology, 140*(6), 1785-1794. doi:10.1053/j.gastro.2011.01.055

Crawley, J. N. (1985). Exploratory behavior models of anxiety in mice. *Neurosci Biobehav Rev, 9*(1), 37-44. doi:10.1016/0149-7634(85)90030-2

Crnčec, I., Modak, M., Gordziel, C., Svinka, J., Scharf, I., Moritsch, S., & Eferl, R. (2018). STAT1 is a sex-specific tumor suppressor in colitis-associated colorectal cancer. *Molecular oncology, 12*(4), 514-528. doi:10.1002/1878-0261.12178

Cryan, J. F., Mombereau, C., & Vassout, A. (2005). The tail suspension test as a model for assessing antidepressant activity: review of pharmacological and genetic studies in mice. *Neurosci Biobehav Rev, 29*(4-5), 571-625. doi:10.1016/j.neubiorev.2005.03.009

Dancey, C. P., Attree, E. A., Stuart, G., Wilson, C., & Sonnet, A. (2009). Words fail me: the verbal IQ deficit in inflammatory bowel disease and irritable bowel syndrome. *Inflamm Bowel Dis, 15*(6), 852-857. doi:10.1002/ibd.20837

de Bruijn, R. F., Janssen, J. A., Brugts, M. P., van Duijn, C. M., Hofman, A., Koudstaal, P. J., & Ikram, M. A. (2014). Insulin-like growth factor-I receptor stimulating activity is associated with dementia. *J Alzheimers Dis, 42*(1), 137-142. doi:10.3233/jad-140186

de la Monte, S. M., Tong, M., Schiano, I., & Didsbury, J. (2017). Improved Brain Insulin/IGF Signaling and Reduced Neuroinflammation with T3D-959 in an Experimental Model of Sporadic Alzheimer's Disease. *J Alzheimers Dis, 55*(2), 849-864. doi:10.3233/jad-160656

De Robertis, M., Massi, E., Poeta, M. L., Carotti, S., Morini, S., Cecchetelli, L., & Fazio, V. M. (2011). The AOM/DSS murine model for the study of colon carcinogenesis: From pathways to diagnosis and therapy studies. *J Carcinog, 10*, 9. doi:10.4103/1477-3163.78279

De Strooper, B. (2003). Aph-1, Pen-2, and Nicastrin with Presenilin generate an active gamma-Secretase complex. *Neuron, 38*(1), 9-12. doi:10.1016/s0896-6273(03)00205-8

Deane, R., Bell, R. D., Sagare, A., & Zlokovic, B. V. (2009). Clearance of amyloid-beta peptide across the blood-brain barrier: implication for therapies in Alzheimer's disease. *CNS Neurol Disord Drug Targets, 8*(1), 16-30. doi:10.2174/187152709787601867

Dhawan, G., Floden, A. M., & Combs, C. K. (2012). Amyloid-β oligomers stimulate microglia through a tyrosine kinase dependent mechanism. *Neurobiol Aging, 33*(10), 2247-2261. doi:10.1016/j.neurobiolaging.2011.10.027

Di Martino, L., Dave, M., Menghini, P., Xin, W., Arseneau, K. O., Pizarro, T. T., & Cominelli, F. (2016). Protective Role for TWEAK/Fn14 in Regulating Acute Intestinal Inflammation and Colitis-Associated Tumorigenesis. *Cancer Res, 76*(22), 6533-6542. doi:10.1158/0008-5472.Can-16-0400

Dinan, T. G., & Cryan, J. F. (2017). Gut instincts: microbiota as a key regulator of brain development, ageing and neurodegeneration. *J Physiol, 595*(2), 489-503. doi:10.1113/jp273106

Douaiher, J., Ravipati, A., Grams, B., Chowdhury, S., Alatise, O., & Are, C. (2017). Colorectal cancer-global burden, trends, and geographical variations. *J Surg Oncol, 115*(5), 619-630. doi:10.1002/jso.24578

Du, Y., Dodel, R. C., Eastwood, B. J., Bales, K. R., Gao, F., Lohmuller, F., & Farlow, M. R. (2000). Association of an interleukin 1 alpha polymorphism with Alzheimer's disease. *Neurology, 55*(4), 480-483. doi:10.1212/wnl.55.4.480

Economou, M. A., Andersson, S., Vasilcanu, D., All-Ericsson, C., Menu, E., Girnita, A., & Larsson, O. (2008). Oral picropodophyllin (PPP) is well tolerated in vivo and inhibits IGF-1R expression and growth of uveal melanoma. *Investigative Ophthalmology & Visual Science, 49*(6), 2337-2342. doi:10.1167/iovs.07-0819

Eggert, S., Paliga, K., Soba, P., Evin, G., Masters, C. L., Weidemann, A., & Beyreuther, K. (2004). The proteolytic processing of the amyloid precursor protein gene family members APLP-1 and APLP-2 involves alpha-, beta-, gamma-, and epsilon-like cleavages: modulation of APLP-1 processing by n-glycosylation. *J Biol Chem, 279*(18), 18146-18156. doi:10.1074/jbc.M311601200

Eichele, D. D., & Kharbanda, K. K. (2017). Dextran sodium sulfate colitis murine model: An indispensable tool for advancing our understanding of inflammatory bowel diseases pathogenesis. *World J Gastroenterol, 23*(33), 6016-6029. doi:10.3748/wjg.v23.i33.6016

El-Ami, T., Moll, L., Carvalhal Marques, F., Volovik, Y., Reuveni, H., & Cohen, E. (2014). A novel inhibitor of the insulin/IGF signaling pathway protects from age-onset, neurodegeneration-linked proteotoxicity. *Aging Cell, 13*(1), 165-174. doi:10.1111/acel.12171

Emge, J. R., Huynh, K., Miller, E. N., Kaur, M., Reardon, C., Barrett, K. E., & Gareau, M. G. (2016). Modulation of the microbiota-gut-brain axis by probiotics in a murine model of inflammatory bowel disease. *Am J Physiol Gastrointest Liver Physiol, 310*(11), G989-998. doi:10.1152/ajpgi.00086.2016

Endres, K., Postina, R., Schroeder, A., Mueller, U., & Fahrenholz, F. (2005). Shedding of the amyloid precursor protein-like protein APLP2 by disintegrin-metalloproteinases. *Febs j, 272*(22), 5808-5820. doi:10.1111/j.1742-4658.2005.04976.x

Erben, U., Loddenkemper, C., Doerfel, K., Spieckermann, S., Haller, D., Heimesaat, M. M., & Kühl, A. A. (2014). A guide to histomorphological evaluation of intestinal inflammation in mouse models. *Int J Clin Exp Pathol, 7*(8), 4557-4576.

Erny, D., Hrabě de Angelis, A. L., Jaitin, D., Wieghofer, P., Staszewski, O., David, E., & Prinz, M. (2015). Host microbiota constantly control maturation and function of microglia in the CNS. *Nat Neurosci, 18*(7), 965-977. doi:10.1038/nn.4030

Etminan, M., Gill, S., & Samii, A. (2003). Effect of non-steroidal anti-inflammatory drugs on risk of Alzheimer's disease: systematic review and meta-analysis of observational studies. *Bmj, 327*(7407), 128. doi:10.1136/bmj.327.7407.128

Euser, S. M., van Heemst, D., van Vliet, P., Breteler, M. M. B., & Westendorp, R. G. J. (2008). Insulin/Insulin-like growth factor-1 signaling and cognitive function in humans. *The Journals of Gerontology. Series A, Biological Sciences and Medical Sciences, 63*(9), 907-910. Retrieved from http://www.ncbi.nlm.nih.gov/pubmed/18840794

Farzi, A., Fröhlich, E. E., & Holzer, P. (2018). Gut Microbiota and the Neuroendocrine System. *Neurotherapeutics, 15*(1), 5-22. doi:10.1007/s13311-017-0600-5

Fathi, P., & Wu, S. (2016). Isolation, Detection, and Characterization of Enterotoxigenic Bacteroides fragilis in Clinical Samples. *Open Microbiol J, 10*, 57-63. doi:10.2174/1874285801610010057

Favelyukis, S., Till, J. H., Hubbard, S. R., & Miller, W. T. (2001). Structure and autoregulation of the insulin-like growth factor 1 receptor kinase. *Nature Structural and Molecular Biology, 8*(12), 1058. doi:10.1038/nsb721

Ferrara, N. (2011). From the discovery of vascular endothelial growth factor to the introduction of avastin in clinical trials - an interview with Napoleone Ferrara by Domenico Ribatti. *Int J Dev Biol, 55*(4-5), 383-388. doi:10.1387/ijdb.103216dr

Ferreira, S. T., Lourenco, M. V., Oliveira, M. M., & De Felice, F. G. (2015). Soluble amyloid-β oligomers as synaptotoxins leading to cognitive impairment in Alzheimer's disease. *Frontiers in Cellular Neuroscience, 9*. doi:10.3389/fncel.2015.00191

Fetler, L., & Amigorena, S. (2005). Neuroscience. Brain under surveillance: the microglia patrol. *Science, 309*(5733), 392-393. doi:10.1126/science.1114852

Floden, A. M., and Colin K. Combs. . (2006). "β-Amyloid stimulates murine postnatal and adult microglia cultures in a unique manner.". *Journal of Neuroscience, 26*(17), 4644-4648. doi:doi.org/10.1523/JNEUROSCI.4822-05.2006

Flurkey, K., Papaconstantinou, J., Miller, R. A., & Harrison, D. E. (2001). Lifespan extension and delayed immune and collagen aging in mutant mice with defects in growth hormone production. *Proc Natl Acad Sci U S A, 98*(12), 6736-6741. doi:10.1073/pnas.111158898

Franco-Bocanegra, D. K., McAuley, C., Nicoll, J. A. R., & Boche, D. (2019). Molecular Mechanisms of Microglial Motility: Changes in Ageing and Alzheimer's Disease. *Cells, 8*(6). doi:10.3390/cells8060639

Frank, D. N., St Amand, A. L., Feldman, R. A., Boedeker, E. C., Harpaz, N., & Pace, N. R. (2007). Molecular-phylogenetic characterization of microbial community imbalances in human inflammatory bowel diseases. *Proc Natl Acad Sci U S A, 104*(34), 13780-13785. doi:10.1073/pnas.0706625104

Freude, S., Hettich, M. M., Schumann, C., Stöhr, O., Koch, L., Köhler, C., & Schubert, M. (2009). Neuronal IGF-1 resistance reduces Abeta accumulation and protects against premature death in a model of Alzheimer's disease. *FASEB journal: official publication of the Federation of American Societies for Experimental Biology, 23*(10), 3315-3324. doi:10.1096/fj.09-132043

Furness, J. B. (2006). *The enteric nervous system*: Wiley Online Library.

Furness, J. B., Callaghan, B. P., Rivera, L. R., & Cho, H. J. (2014). The enteric nervous system and gastrointestinal innervation: integrated local and central control. *Adv Exp Med Biol, 817*, 39-71. doi:10.1007/978-1-4939-0897-4_3

Gallagher, E. J., & LeRoith, D. (2010). The Proliferating Role of Insulin and Insulin-Like Growth Factors in Cancer. *Trends in endocrinology and metabolism: TEM, 21*(10), 610-618. doi:10.1016/j.tem.2010.06.007

Gandy, S., Caporaso, G., Buxbaum, J., Frangione, B., & Greengard, P. (1994). APP processing, A beta-amyloidogenesis, and the pathogenesis of Alzheimer's disease. *Neurobiol Aging, 15*(2), 253-256. doi:10.1016/0197-4580(94)90125-2

George, C., Gontier, G., Lacube, P., François, J.-C., Holzenberger, M., & Aïd, S. (2017). The Alzheimer's disease transcriptome mimics the neuroprotective signature of IGF-1 receptor-deficient neurons. *Brain, 140*(7), 2012-2027. doi:10.1093/brain/awx132

Gershon, M. D. (1999). The enteric nervous system: a second brain. *Hosp Pract (1995), 34*(7), 31-32, 35-38, 41-32 passim. doi:10.3810/hp.1999.07.153

Gershon, M. D., Chalazonitis, A., & Rothman, T. P. (1993). From neural crest to bowel: development of the enteric nervous system. *J Neurobiol, 24*(2), 199-214. doi:10.1002/neu.480240207

Ghia, J. E., Blennerhassett, P., Kumar-Ondiveeran, H., Verdu, E. F., & Collins, S. M. (2006). The vagus nerve: a tonic inhibitory influence associated with inflammatory bowel disease in a murine model. *Gastroenterology, 131*(4), 1122-1130. doi:10.1053/j.gastro.2006.08.016

Girnita, A., Girnita, L., del Prete, F., Bartolazzi, A., Larsson, O., & Axelson, M. (2004). Cyclolignans as inhibitors of the insulin-like growth factor-1 receptor and malignant cell growth. *Cancer Research, 64*(1), 236-242. Retrieved from http://www.ncbi.nlm.nih.gov/pubmed/14729630

Giuffrida, M. L., Tomasello, M. F., Pandini, G., Caraci, F., Battaglia, G., Busceti, C., & Copani, A. (2015). Monomeric ß-amyloid interacts with type-1 insulin-like growth factor receptors to provide energy supply to neurons. *Front Cell Neurosci, 9*, 297. doi:10.3389/fncel.2015.00297

Glenner, G. G., & Wong, C. W. (1984a). Alzheimer's disease and Down's syndrome: sharing of a unique cerebrovascular amyloid fibril protein. *Biochem Biophys Res Commun, 122*(3), 1131-1135. doi:10.1016/0006-291x(84)91209-9

Glenner, G. G., & Wong, C. W. (1984b). Alzheimer's disease: initial report of the purification and characterization of a novel cerebrovascular amyloid protein. *Biochem Biophys Res Commun, 120*(3), 885-890. doi:10.1016/s0006-291x(84)80190-4

Goate, A., Chartier-Harlin, M. C., Mullan, M., Brown, J., Crawford, F., Fidani, L., & et al. (1991). Segregation of a missense mutation in the amyloid precursor protein gene with familial Alzheimer's disease. *Nature, 349*(6311), 704-706. doi:10.1038/349704a0

Golde, T. E., Estus, S., Usiak, M., Younkin, L. H., & Younkin, S. G. (1990). Expression of beta amyloid protein precursor mRNAs: recognition of a novel alternatively spliced form and quantitation in Alzheimer's disease using PCR. *Neuron, 4*(2), 253-267. doi:10.1016/0896-6273(90)90100-t

Golde, T. E., Estus, S., Younkin, L. H., Selkoe, D. J., & Younkin, S. G. (1992). Processing of the amyloid protein precursor to potentially amyloidogenic derivatives. *Science, 255*(5045), 728-730. doi:10.1126/science.1738847

Goldstein, A. M., Hofstra, R. M., & Burns, A. J. (2013). Building a brain in the gut: development of the enteric nervous system. *Clin Genet, 83*(4), 307-316. doi:10.1111/cge.12054

Gontier, G., George, C., Chaker, Z., Holzenberger, M., & Aïd, S. (2015). Blocking IGF Signaling in Adult Neurons Alleviates Alzheimer's Disease Pathology through Amyloid-β Clearance. *Journal of Neuroscience, 35*(33), 11500-11513. doi:10.1523/JNEUROSCI.0343-15.2015

Graham, W. V., Bonito-Oliva, A., & Sakmar, T. P. (2017). Update on Alzheimer's Disease Therapy and Prevention Strategies. *Annu Rev Med, 68*, 413-430. doi:10.1146/annurev-med-042915-103753

Greenfield, J. P., Tsai, J., Gouras, G. K., Hai, B., Thinakaran, G., Checler, F., & Xu, H. (1999). Endoplasmic reticulum and trans-Golgi network generate distinct populations of Alzheimer beta-amyloid peptides. *Proc Natl Acad Sci U S A, 96*(2), 742-747. doi:10.1073/pnas.96.2.742

Greten, F. R., Eckmann, L., Greten, T. F., Park, J. M., Li, Z. W., Egan, L. J., & Karin, M. (2004). IKKbeta links inflammation and tumorigenesis in a mouse model of colitis-associated cancer. *Cell, 118*(3), 285-296. doi:10.1016/j.cell.2004.07.013

Grivennikov, S., Karin, E., Terzic, J., Mucida, D., Yu, G. Y., Vallabhapurapu, S., & Karin, M. (2009). IL-6 and Stat3 are required for survival of intestinal epithelial cells and development of colitis-associated cancer. *Cancer Cell, 15*(2), 103-113. doi:10.1016/j.ccr.2009.01.001

Groden, J., Thliveris, A., Samowitz, W., Carlson, M., Gelbert, L., Albertsen, H., & et al. (1991). Identification and characterization of the familial adenomatous polyposis coli gene. *Cell, 66*(3), 589-600. doi:10.1016/0092-8674(81)90021-0

Guerreiro, R., & Bras, J. (2015). The age factor in Alzheimer's disease. *Genome Medicine, 7*. doi:10.1186/s13073-015-0232-5

Guevara-Aguirre, J., Balasubramanian, P., Guevara-Aguirre, M., Wei, M., Madia, F., Cheng, C.-W., & Longo, V. D. (2011). Growth hormone receptor deficiency is associated with a major reduction in pro-aging signaling, cancer, and diabetes in humans. *Science Translational Medicine, 3*(70), 70ra13. doi:10.1126/scitranslmed.3001845

Haass, C., Kaether, C., Thinakaran, G., & Sisodia, S. (2012). Trafficking and proteolytic processing of APP. *Cold Spring Harb Perspect Med, 2*(5), a006270. doi:10.1101/cshperspect.a006270

Haass, C., Lemere, C. A., Capell, A., Citron, M., Seubert, P., Schenk, D., & Selkoe, D. J. (1995). The Swedish mutation causes early-onset Alzheimer's disease by beta-secretase cleavage within the secretory pathway. *Nat Med, 1*(12), 1291-1296. doi:10.1038/nm1295-1291

Haass, C., & Selkoe, D. J. (1993). Cellular processing of beta-amyloid precursor protein and the genesis of amyloid beta-peptide. *Cell, 75*(6), 1039-1042. doi:10.1016/0092-8674(93)90312-e

Håkansson, Å., Tormo-Badia, N., Baridi, A., Xu, J., Molin, G., Hagslätt, M. L., & Ahrné, S. (2015). Immunological alteration and changes of gut microbiota after dextran sulfate sodium (DSS) administration in mice. *Clin Exp Med, 15*(1), 107-120. doi:10.1007/s10238-013-0270-5

Halfvarson, J., Brislawn, C. J., Lamendella, R., Vazquez-Baeza, Y., Walters, W. A., Bramer, L. M., & Jansson, J. K. (2017). Dynamics of the human gut microbiome in inflammatory bowel disease. *Nat Microbiol, 2*, 17004. doi:10.1038/nmicrobiol.2017.4

Ham, S., Kim, T. K., Ryu, J., Kim, Y. S., Tang, Y. P., & Im, H. I. (2018). Comprehensive MicroRNAome Analysis of the Relationship Between Alzheimer Disease and Cancer in PSEN Double-Knockout Mice. *Int Neurourol J, 22*(4), 237-245. doi:10.5213/inj.1836274.137

Hampel, H., Mesulam, M. M., Cuello, A. C., Khachaturian, A. S., Vergallo, A., Farlow, M. R., & Khachaturian, Z. S. (2019). Revisiting the Cholinergic Hypothesis in Alzheimer's Disease: Emerging Evidence from Translational and Clinical Research. *J Prev Alzheimers Dis, 6*(1), 2-15. doi:10.14283/jpad.2018.43

Han, Y., Zhao, T., Cheng, X., Zhao, M., Gong, S. H., Zhao, Y. Q., & Zhu, L. L. (2018). Cortical Inflammation is Increased in a DSS-Induced Colitis Mouse Model. *Neurosci Bull, 34*(6), 1058-1066. doi:10.1007/s12264-018-0288-5

Hansel, D. E., Rahman, A., Wehner, S., Herzog, V., Yeo, C. J., & Maitra, A. (2003). Increased expression and processing of the Alzheimer amyloid precursor protein in pancreatic cancer may influence cellular proliferation. *Cancer Res, 63*(21), 7032-7037.

Hansen, D. V., Hanson, J. E., & Sheng, M. (2018). Microglia in Alzheimer's disease. *J Cell Biol, 217*(2), 459-472. doi:10.1083/jcb.201709069

Hansen, M. B. (2003). The enteric nervous system I: organisation and classification. *Pharmacol Toxicol, 92*(3), 105-113. doi:10.1034/j.1600-0773.2003.t01-1-920301.x

Harach, T., Marungruang, N., Duthilleul, N., Cheatham, V., Mc Coy, K. D., Frisoni, G., & Bolmont, T. (2017). Reduction of Abeta amyloid pathology in APPPS1 transgenic mice in the absence of gut microbiota. *Sci Rep, 7*, 41802. doi:10.1038/srep41802

Hardy, J. A., & Higgins, G. A. (1992). Alzheimer's disease: the amyloid cascade hypothesis. *Science, 256*(5054), 184-185. doi:10.1126/science.1566067

Hassan, A. M., Jain, P., Reichmann, F., Mayerhofer, R., Farzi, A., Schuligoi, R., & Holzer, P. (2014). Repeated predictable stress causes resilience against colitis-induced behavioral changes in mice. *Front Behav Neurosci, 8*, 386. doi:10.3389/fnbeh.2014.00386

Health, N. I. o. (2018). National Institute on Aging. What Happens to the Brain in Alzheimer’s Disease. In.

Heber, S., Herms, J., Gajic, V., Hainfellner, J., Aguzzi, A., Rülicke, T., & Müller, U. (2000). Mice with combined gene knock-outs reveal essential and partially redundant functions of amyloid precursor protein family members. *J Neurosci, 20*(21), 7951-7963. doi:10.1523/jneurosci.20-21-07951.2000

Hefti, F., Hartikka, J., & Knusel, B. (1989). Function of neurotrophic factors in the adult and aging brain and their possible use in the treatment of neurodegenerative diseases. *Neurobiol Aging, 10*(5), 515-533. doi:10.1016/0197-4580(89)90118-8

Hendriks, L., van Duijn, C. M., Cras, P., Cruts, M., Van Hul, W., van Harskamp, F., & et al. (1992). Presenile dementia and cerebral haemorrhage linked to a mutation at codon 692 of the beta-amyloid precursor protein gene. *Nat Genet, 1*(3), 218-221. doi:10.1038/ng0692-218

Hill, J. M., Clement, C., Pogue, A. I., Bhattacharjee, S., Zhao, Y., & Lukiw, W. J. (2014). Pathogenic microbes, the microbiome, and Alzheimer's disease (AD). *Front Aging Neurosci, 6*, 127. doi:10.3389/fnagi.2014.00127

Hippius, H., & Neundörfer, G. (2003). The discovery of Alzheimer's disease. *Dialogues Clin Neurosci, 5*(1), 101-108.

Holmes, C., Cunningham, C., Zotova, E., Woolford, J., Dean, C., Kerr, S., & Perry, V. H. (2009). Systemic inflammation and disease progression in Alzheimer disease. *Neurology, 73*(10), 768-774. doi:10.1212/WNL.0b013e3181b6bb95

Holt, P. R. (2001). Diarrhea and malabsorption in the elderly. *Gastroenterol Clin North Am, 30*(2), 427-444. doi:10.1016/s0889-8553(05)70189-8

Holzenberger, M., Dupont, J., Ducos, B., Leneuve, P., Géloën, A., Even, P. C., &. Le Bouc, Y. (2003). IGF-1 receptor regulates lifespan and resistance to oxidative stress in mice. *Nature, 421*(6919), 182-187. doi:10.1038/nature01298

Huang, E. J., & Reichardt, L. F. (2003). Trk receptors: roles in neuronal signal transduction. *Annu Rev Biochem, 72*, 609-642. doi:10.1146/annurev.biochem.72.121801.161629

Hussain, I., Powell, D., Howlett, D. R., Tew, D. G., Meek, T. D., Chapman, C., & Christie, G. (1999). Identification of a novel aspartic protease (Asp 2) as beta-secretase. *Mol Cell Neurosci, 14*(6), 419-427. doi:10.1006/mcne.1999.0811

Ibáñez, K., Boullosa, C., Tabarés-Seisdedos, R., Baudot, A., & Valencia, A. (2014). Molecular evidence for the inverse comorbidity between central nervous system disorders and cancers detected by transcriptomic meta-analyses. *PLoS Genet, 10*(2), e1004173. doi:10.1371/journal.pgen.1004173

Ill-Raga, G., Palomer, E., Wozniak, M. A., Ramos-Fernandez, E., Bosch-Morato, M., Tajes, M., & Munoz, F. J. (2011). Activation of PKR causes amyloid ss-peptide accumulation via de-repression of BACE1 expression. *PLoS One, 6*(6), e21456. doi:10.1371/journal.pone.0021456

i

n t' Veld, B. A., Ruitenberg, A., Hofman, A., Launer, L. J., van Duijn, C. M., Stijnen, T., & Stricker, B. H. (2001). Nonsteroidal antiinflammatory drugs and the risk of Alzheimer's disease. *N Engl J Med, 345*(21), 1515-1521. doi:10.1056/NEJMoa010178

Itagaki, S., McGeer, P. L., Akiyama, H., Zhu, S., & Selkoe, D. (1989a). Relationship of microglia and astrocytes to amyloid deposits of Alzheimer disease. *J Neuroimmunol, 24*(3), 173-182. Retrieved from http://www.ncbi.nlm.nih.gov/pubmed/2808689

Itagaki, S., McGeer, P. L., Akiyama, H., Zhu, S., & Selkoe, D. (1989b). Relationship of microglia and astrocytes to amyloid deposits of Alzheimer disease. *J Neuroimmunol, 24*(3), 173-182. doi:10.1016/0165-5728(89)90115-x

Ito, S., Ménard, M., Atkinson, T., Gaudet, C., Brown, L., Whitfield, J., & Chakravarthy, B. (2012). Involvement of insulin-like growth factor 1 receptor signaling in the amyloid-β peptide oligomers-induced p75 neurotrophin receptor protein expression in mouse hippocampus. *Journal of Alzheimer's disease: JAD, 31*(3), 493-506. doi:10.3233/JAD-2012-120046

Itzhaki, R. F. (2018). Corroboration of a Major Role for Herpes Simplex Virus Type 1 in Alzheimer's Disease. *Front Aging Neurosci, 10*, 324. doi:10.3389/fnagi.2018.00324

Jabbur, S. J., el-Kak, F. H., & Nassar, C. F. (1988). The enteric nervous system--an overview. *Med Res Rev, 8*(3), 459-469. doi:10.1002/med.2610080306

Jang, S. E., Lim, S. M., Jeong, J. J., Jang, H. M., Lee, H. J., Han, M. J., & Kim, D. H. (2018). Gastrointestinal inflammation by gut microbiota disturbance induces memory impairment in mice. *Mucosal Immunol, 11*(2), 369-379. doi:10.1038/mi.2017.49

Jess, T., Frisch, M., & Simonsen, J. (2013). Trends in overall and cause-specific mortality among patients with inflammatory bowel disease from 1982 to 2010. *Clin Gastroenterol Hepatol, 11*(1), 43-48. doi:10.1016/j.cgh.2012.09.026

Jess, T., Rungoe, C., & Peyrin-Biroulet, L. (2012). Risk of colorectal cancer in patients with ulcerative colitis: a meta-analysis of population-based cohort studies. *Clin Gastroenterol Hepatol, 10*(6), 639-645. doi:10.1016/j.cgh.2012.01.010

Jiang, S., Li, Y., Zhang, X., Bu, G., Xu, H., & Zhang, Y. W. (2014). Trafficking regulation of proteins in Alzheimer's disease. *Mol Neurodegener, 9*, 6. doi:10.1186/1750-1326-9-6

Jin, K., Zhu, Y., Sun, Y., Mao, X. O., Xie, L., & Greenberg, D. A. (2002). Vascular endothelial growth factor (VEGF) stimulates neurogenesis in vitro and in vivo. *Proc Natl Acad Sci U S A, 99*(18), 11946-11950. doi:10.1073/pnas.182296499

Jirkof, P., Leucht, K., Cesarovic, N., Caj, M., Nicholls, F., Rogler, G., & Hausmann, M. (2013). Burrowing is a sensitive behavioural assay for monitoring general wellbeing during dextran sulfate sodium colitis in laboratory mice. *Lab Anim, 47*(4), 274-283. doi:10.1177/0023677213493409

Joachim, C. L., Mori, H., & Selkoe, D. J. (1989). Amyloid beta-protein deposition in tissues other than brain in Alzheimer's disease. *Nature, 341*(6239), 226-230. doi:10.1038/341226a0

Johansson, P., Åberg, D., Johansson, J.-O., Mattsson, N., Hansson, O., Ahrén, B., & Svensson, J. (2013). Serum but not cerebrospinal fluid levels of insulin-like growth factor-I (IGF-I) and IGF-binding protein-3 (IGFBP-3) are increased in Alzheimer's disease. *Psychoneuroendocrinology, 38*(9), 1729-1737. doi:10.1016/j.psyneuen.2013.02.006

Kameyama, H., Nagahashi, M., Shimada, Y., Tajima, Y., Ichikawa, H., Nakano, M., & Wakai, T. (2018). Genomic characterization of colitis-associated colorectal cancer. *World J Surg Oncol, 16*(1), 121. doi:10.1186/s12957-018-1428-0

Kang, J., Lemaire, H. G., Unterbeck, A., Salbaum, J. M., Masters, C. L., Grzeschik, K. H., & Muller-Hill, B. (1987). The precursor of Alzheimer's disease amyloid A4 protein resembles a cell-surface receptor. *Nature, 325*(6106), 733-736. doi:10.1038/325733a0

Kappeler, L., De Magalhaes Filho, C., Dupont, J., Leneuve, P., Cervera, P., Perin, L., & Holzenberger, M. (2008). Brain IGF-1 receptors control mammalian growth and lifespan through a neuroendocrine mechanism. *PLoS Biol, 6*(10), e254. doi:10.1371/journal.pbio.0060254

Kappeler, L., De Magalhaes Filho, C., Dupont, J., Leneuve, P., Cervera, P., Périn, L., &. Holzenberger, M. (2008). Brain IGF-1 receptors control mammalian growth and lifespan through a neuroendocrine mechanism. *PLoS biology, 6*(10), e254. doi:10.1371/journal.pbio.0060254

Kenyon, C. J. (2010). The genetics of ageing. *Nature, 464*(7288), 504-512. doi:10.1038/nature08980

Khanna, S., & Tosh, P. K. (2014). A clinician's primer on the role of the microbiome in human health and disease. *Mayo Clin Proc, 89*(1), 107-114. doi:10.1016/j.mayocp.2013.10.011

Kigerl, K. A., de Rivero Vaccari, J. P., Dietrich, W. D., Popovich, P. G., & Keane, R. W. (2014). Pattern recognition receptors and central nervous system repair. *Exp Neurol, 258*, 5-16. doi:10.1016/j.expneurol.2014.01.001

Kim, H. R., Lee, P., Seo, S. W., Roh, J. H., Oh, M., Oh, J. S., & Jeong, Y. (2019). Comparison of Amyloid beta and Tau Spread Models in Alzheimer's Disease. *Cereb Cortex, 29*(10), 4291-4302. doi:10.1093/cercor/bhy311

Kim, S. E., Paik, H. Y., Yoon, H., Lee, J. E., Kim, N., & Sung, M. K. (2015). Sex- and gender-specific disparities in colorectal cancer risk. *World J Gastroenterol, 21*(17), 5167-5175. doi:10.3748/wjg.v21.i17.5167

King, G. D., & Scott Turner, R. (2004). Adaptor protein interactions: modulators of amyloid precursor protein metabolism and Alzheimer's disease risk? *Exp Neurol, 185*(2), 208-219. doi:10.1016/j.expneurol.2003.10.011

Kinney, J. W., Bemiller, S. M., Murtishaw, A. S., Leisgang, A. M., Salazar, A. M., & Lamb, B. T. (2018). Inflammation as a central mechanism in Alzheimer's disease. *Alzheimers Dement (N Y), 4*, 575-590. doi:10.1016/j.trci.2018.06.014

Kjeldsen, L., Cowland, J. B., & Borregaard, N. (2000). Human neutrophil gelatinase-associated lipocalin and homologous proteins in rat and mouse. *Biochim Biophys Acta, 1482*(1-2), 272-283. doi:10.1016/s0167-4838(00)00152-7

Klingelhoefer, L., & Reichmann, H. (2015). Pathogenesis of Parkinson disease--the gut-brain axis and environmental factors. *Nat Rev Neurol, 11*(11), 625-636. doi:10.1038/nrneurol.2015.197

Ko, S. Y., Lin, S. C., Chang, K. W., Wong, Y. K., Liu, C. J., Chi, C. W., & Liu, T. Y. (2004). Increased expression of amyloid precursor protein in oral squamous cell carcinoma. *Int J Cancer, 111*(5), 727-732. doi:10.1002/ijc.20328

Kohler, C. A., Maes, M., Slyepchenko, A., Berk, M., Solmi, M., Lanctot, K. L., & Carvalho, A. F. (2016). The Gut-Brain Axis, Including the Microbiome, Leaky Gut and Bacterial Translocation: Mechanisms and Pathophysiological Role in Alzheimer's Disease. *Curr Pharm Des, 22*(40), 6152-6166. doi:10.2174/1381612822666160907093807

Konietzko, U. (2012). AICD nuclear signaling and its possible contribution to Alzheimer's disease. *Curr Alzheimer Res, 9*(2), 200-216. doi:10.2174/156720512799361673

Krause, K., Karger, S., Sheu, S. Y., Aigner, T., Kursawe, R., Gimm, O., & Fuhrer, D. (2008). Evidence for a role of the amyloid precursor protein in thyroid carcinogenesis. *J Endocrinol, 198*(2), 291-299. doi:10.1677/joe-08-0005

Kreutzberg, G. W. (1996). Microglia: a sensor for pathological events in the CNS. *Trends Neurosci, 19*(8), 312-318. doi:10.1016/0166-2236(96)10049-7

Kujawska, M., & Jodynis-Liebert, J. (2018). What is the Evidence That Parkinson's Disease is a Prion Disorder, Which Originates in the Gut? *Int J Mol Sci, 19*(11). doi:10.3390/ijms19113573

Kumar, D. K., Choi, S. H., Washicosky, K. J., Eimer, W. A., Tucker, S., Ghofrani, J., & Moir, R. D. (2016). Amyloid-β peptide protects against microbial infection in mouse and worm models of Alzheimer's disease. *Sci Transl Med, 8*(340), 340ra372. doi:10.1126/scitranslmed.aaf1059

Kumar, M., Kissoon-Singh, V., Coria, A. L., Moreau, F., & Chadee, K. (2017). Probiotic mixture VSL#3 reduces colonic inflammation and improves intestinal barrier function in Muc2 mucin-deficient mice. *Am J Physiol Gastrointest Liver Physiol, 312*(1), G34-g45. doi:10.1152/ajpgi.00298.2016

Kurina, L. M., Goldacre, M. J., Yeates, D., & Gill, L. E. (2001). Depression and anxiety in people with inflammatory bowel disease. *J Epidemiol Community Health, 55*(10), 716-720. doi:10.1136/jech.55.10.716

Lanz, T. A., Salatto, C. T., Semproni, A. R., Marconi, M., Brown, T. M., Richter, K. E. G., & Schachter, J. B. (2008). Peripheral elevation of IGF-1 fails to alter Abeta clearance in multiple in vivo models. *Biochemical Pharmacology, 75*(5), 1093-1103. doi:10.1016/j.bcp.2007.11.001

Larsson, O., Girnita, A., & Girnita, L. (2005). Role of insulin-like growth factor 1 receptor signalling in cancer. *British Journal of Cancer, 92*(12), 2097-2101. doi:10.1038/sj.bjc.6602627

Latina, V., Caioli, S., Zona, C., Ciotti, M. T., Amadoro, G., & Calissano, P. (2017). Impaired NGF/TrkA Signaling Causes Early AD-Linked Presynaptic Dysfunction in Cholinergic Primary Neurons. *Front Cell Neurosci, 11*, 68. doi:10.3389/fncel.2017.00068

Lee, J. E., Kim, D., & Lee, J. H. (2018). Association between Alzheimer's Disease and Cancer Risk in South Korea: an 11-year Nationwide Population-Based Study. *Dement Neurocogn Disord, 17*(4), 137-147. doi:10.12779/dnd.2018.17.4.137

Lee, J. W., Lee, Y. K., Yuk, D. Y., Choi, D. Y., Ban, S. B., Oh, K. W., & Hong, J. T. (2008). Neuro-inflammation induced by lipopolysaccharide causes cognitive impairment through enhancement of beta-amyloid generation. *J Neuroinflammation, 5*, 37. doi:10.1186/1742-2094-5-37

Lee, S. M., Kim, N., Son, H. J., Park, J. H., Nam, R. H., Ham, M. H., & Lee, H. N. (2016). The Effect of Sex on the Azoxymethane/Dextran Sulfate Sodium-treated Mice Model of Colon Cancer. *J Cancer Prev, 21*(4), 271-278. doi:10.15430/jcp.2016.21.4.271

LeRoith, D., Werner, H., Beitner-Johnson, D., & Roberts, C. T. (1995). Molecular and cellular aspects of the insulin-like growth factor I receptor. *Endocrine Reviews, 16*(2), 143-163. doi:10.1210/edrv-16-2-143

Lesné, S. E., Sherman, M. A., Grant, M., Kuskowski, M., Schneider, J. A., Bennett, D. A., & Ashe, K. H. (2013). Brain amyloid-β oligomers in ageing and Alzheimer's disease. *Brain: A Journal of Neurology, 136*(Pt 5), 1383-1398. doi:10.1093/brain/awt062

Leung, F. W., & Rao, S. S. (2009). Fecal incontinence in the elderly. *Gastroenterol Clin North Am, 38*(3), 503-511. doi:10.1016/j.gtc.2009.06.007

Levi-Montalcini, R. (1987). The nerve growth factor: thirty-five years later. *Embo j, 6*(5), 1145-1154.

Li, D., Ke, Y., Zhan, R., Liu, C., Zhao, M., Zeng, A., & Hong, H. (2018). Trimethylamine-N-oxide promotes brain aging and cognitive impairment in mice. *Aging Cell, 17*(4), e12768. doi:10.1111/acel.12768

Li, Y., Zhou, W., Tong, Y., He, G., & Song, W. (2006). Control of APP processing and Abeta generation level by BACE1 enzymatic activity and transcription. *Faseb j, 20*(2), 285-292. doi:10.1096/fj.05-4986com

Licht, T., Goshen, I., Avital, A., Kreisel, T., Zubedat, S., Eavri, R., & Keshet, E. (2011). Reversible modulations of neuronal plasticity by VEGF. *Proc Natl Acad Sci U S A, 108*(12), 5081-5086. doi:10.1073/pnas.1007640108

Lim, S., Yoo, B. K., Kim, H. S., Gilmore, H. L., Lee, Y., Lee, H. P., & Lee, H. G. (2014). Amyloid-β precursor protein promotes cell proliferation and motility of advanced breast cancer. *BMC Cancer, 14*, 928. doi:10.1186/1471-2407-14-928

Lim, V. S. (2010). A powerful new agonist: flooding the system with growth hormone. *Kidney Int, 77*(5), 385-387. doi:10.1038/ki.2009.487

Lin, X., Koelsch, G., Wu, S., Downs, D., Dashti, A., & Tang, J. (2000). Human aspartic protease memapsin 2 cleaves the beta-secretase site of beta-amyloid precursor protein. *Proc Natl Acad Sci U S A, 97*(4), 1456-1460. doi:10.1073/pnas.97.4.1456

Little, C. S., Hammond, C. J., MacIntyre, A., Balin, B. J., & Appelt, D. M. (2004). Chlamydia pneumoniae induces Alzheimer-like amyloid plaques in brains of BALB/c mice. *Neurobiol Aging, 25*(4), 419-429. doi:10.1016/s0197-4580(03)00127-1

Liu, F., Liang, Z., Shi, J., Yin, D., El-Akkad, E., Grundke-Iqbal, I., & Gong, C. X. (2006). PKA modulates GSK-3beta- and cdk5-catalyzed phosphorylation of tau in site- and kinase-specific manners. *FEBS Lett, 580*(26), 6269-6274. doi:10.1016/j.febslet.2006.10.033

Logan, S., Pharaoh, G. A., Marlin, M. C., Masser, D. R., Matsuzaki, S., Wronowski, B., & Sonntag, W. E. (2018). Insulin-like growth factor receptor signaling regulates working memory, mitochondrial metabolism, and amyloid-β uptake in astrocytes. *Mol Metab, 9*, 141-155. doi:10.1016/j.molmet.2018.01.013

Longo, V. D., Antebi, A., Bartke, A., Barzilai, N., Brown-Borg, H. M., Caruso, C., & Fontana, L. (2015). Interventions to Slow Aging in Humans: Are We Ready? *Aging Cell, 14*(4), 497-510. doi:10.1111/acel.12338

Loren, V., Manye, J., Fuentes, M. C., Cabre, E., Ojanguren, I., & Espadaler, J. (2017). Comparative Effect of the I3.1 Probiotic Formula in Two Animal Models of Colitis. *Probiotics Antimicrob Proteins, 9*(1), 71-80. doi:10.1007/s12602-016-9239-5

Lu, B., Nagappan, G., Guan, X., Nathan, P. J., & Wren, P. (2013). BDNF-based synaptic repair as a disease-modifying strategy for neurodegenerative diseases. *Nat Rev Neurosci, 14*(6), 401-416. doi:10.1038/nrn3505

Lu, F., Fernandes, S. M., & Davis, A. E., 3rd. (2010). The role of the complement and contact systems in the dextran sulfate sodium-induced colitis model: the effect of C1 inhibitor in inflammatory bowel disease. *Am J Physiol Gastrointest Liver Physiol, 298*(6), G878-883. doi:10.1152/ajpgi.00400.2009

Lukiw, W. J. (2016). Bacteroides fragilis Lipopolysaccharide and Inflammatory Signaling in Alzheimer's Disease. *Front Microbiol, 7*, 1544. doi:10.3389/fmicb.2016.01544

Majumder, S., Caccamo, A., Medina, D. X., Benavides, A. D., Javors, M. A., Kraig, E., & Oddo, S. (2012). Lifelong rapamycin administration ameliorates age-dependent cognitive deficits by reducing IL-1β and enhancing NMDA signaling. *Aging Cell, 11*(2), 326-335. doi:10.1111/j.1474-9726.2011.00791.x

Manocha, G., Ghatak, A., Puig, K., & Combs, C. (2018). Anti-alpha4beta1 Integrin Antibodies Attenuated Brain Inflammatory Changes in a Mouse Model of Alzheimer's Disease. *Curr Alzheimer Res, 15*(12), 1123-1135. doi:10.2174/1567205015666180801111033

Manocha, G. D., Floden, A. M., Miller, N. M., Smith, A. J., Nagamoto-Combs, K., Saito, T., & Combs, C. K. (2019). Temporal progression of Alzheimer's disease in brains and intestines of transgenic mice. *Neurobiol Aging, 81*, 166-176. doi:10.1016/j.neurobiolaging.2019.05.025

Mar, J. S., Nagalingam, N. A., Song, Y., Onizawa, M., Lee, J. W., & Lynch, S. V. (2014). Amelioration of DSS-induced murine colitis by VSL#3 supplementation is primarily associated with changes in ileal microbiota composition. *Gut Microbes, 5*(4), 494-503. doi:10.4161/gmic.32147

Mármol, I., Sánchez-de-Diego, C., Pradilla Dieste, A., Cerrada, E., & Rodriguez Yoldi, M. J. (2017). Colorectal Carcinoma: A General Overview and Future Perspectives in Colorectal Cancer. *Int J Mol Sci, 18*(1). doi:10.3390/ijms18010197

Martin, C. R., Osadchiy, V., Kalani, A., & Mayer, E. A. (2018). The Brain-Gut-Microbiome Axis. *Cell Mol Gastroenterol Hepatol, 6*(2), 133-148. doi:10.1016/j.jcmgh.2018.04.003

Masters, C. L., Bateman, R., Blennow, K., Rowe, C. C., Sperling, R. A., & Cummings, J. L. (2015). Alzheimer's disease. *Nat Rev Dis Primers, 1*, 15056. doi:10.1038/nrdp.2015.56

Masters, C. L., Simms, G., Weinman, N. A., Multhaup, G., McDonald, B. L., & Beyreuther, K. (1985). Amyloid plaque core protein in Alzheimer disease and Down syndrome. *Proc Natl Acad Sci U S A, 82*(12), 4245-4249. doi:10.1073/pnas.82.12.4245

Mateo, I., Llorca, J., Infante, J., Rodriguez-Rodriguez, E., Fernandez-Viadero, C., Pena, N., & Combarros, O. (2007). Low serum VEGF levels are associated with Alzheimer's disease. *Acta Neurol Scand, 116*(1), 56-58. doi:10.1111/j.1600-0404.2006.00775.x

Mauras, N. (1997). Growth hormone, IGF-I and growth. New views of old concepts. Modern endocrinology and diabetes series, volume 4: By Thomas J. Merimee and Zvi Laron. London, Freund, 1996, $130 (266 pages), ISBN 965-294-092-5. *Trends in Endocrinology & Metabolism, 8*(6), 256-257. doi:10.1016/S1043-2760(97)00054-4

Mawdsley, J. E., & Rampton, D. S. (2005). Psychological stress in IBD: new insights into pathogenic and therapeutic implications. *Gut, 54*(10), 1481-1491. doi:10.1136/gut.2005.064261

McElhanon, B. O., McCracken, C., Karpen, S., & Sharp, W. G. (2014). Gastrointestinal symptoms in autism spectrum disorder: a meta-analysis. *Pediatrics, 133*(5), 872-883. doi:10.1542/peds.2013-3995

McQuade, A., & Blurton-Jones, M. (2019). Microglia in Alzheimer's Disease: Exploring How Genetics and Phenotype Influence Risk. *J Mol Biol, 431*(9), 1805-1817. doi:10.1016/j.jmb.2019.01.045

Meng, J. Y., Kataoka, H., Itoh, H., & Koono, M. (2001). Amyloid beta protein precursor is involved in the growth of human colon carcinoma cell in vitro and in vivo. *Int J Cancer, 92*(1), 31-39.

Menu, E., Jernberg-Wiklund, H., Stromberg, T., De Raeve, H., Girnita, L., Larsson, O., & Vanderkerken, K. (2006). Inhibiting the IGF-1 receptor tyrosine kinase with the cyclolignan PPP: an in vitro and in vivo study in the 5T33MM mouse model. *Blood, 107*(2), 655-660. doi:10.1182/blood-2005-01-0293

Mielke, M. M. (2018). Sex and Gender Differences in Alzheimer's Disease Dementia. *Psychiatr Times, 35*(11), 14-17.

Millauer, B., Wizigmann-Voos, S., Schnurch, H., Martinez, R., Moller, N. P., Risau, W., & Ullrich, A. (1993). High affinity VEGF binding and developmental expression suggest Flk-1 as a major regulator of vasculogenesis and angiogenesis. *Cell, 72*(6), 835-846. doi:10.1016/0092-8674(93)90573-9

Milman, S., Atzmon, G., Huffman, D. M., Wan, J., Crandall, J. P., Cohen, P., & Barzilai, N. (2014). Low insulin-like growth factor-1 level predicts survival in humans with exceptional longevity. *Aging Cell, 13*(4), 769-771. doi:10.1111/acel.12213

Minter, M. R., Zhang, C., Leone, V., Ringus, D. L., Zhang, X., Oyler-Castrillo, P., & Sisodia, S. S. (2016). Antibiotic-induced perturbations in gut microbial diversity influences neuro-inflammation and amyloidosis in a murine model of Alzheimer's disease. *Sci Rep, 6*, 30028. doi:10.1038/srep30028

Mitra, S., Behbahani, H., & Eriksdotter, M. (2019). Innovative Therapy for Alzheimer's Disease-With Focus on Biodelivery of NGF. *Front Neurosci, 13*, 38. doi:10.3389/fnins.2019.00038

Mitrovic, M., Shahbazian, A., Bock, E., Pabst, M. A., & Holzer, P. (2010). Chemo-nociceptive signalling from the colon is enhanced by mild colitis and blocked by inhibition of transient receptor potential ankyrin 1 channels. *Br J Pharmacol, 160*(6), 1430-1442. doi:10.1111/j.1476-5381.2010.00794.x

Moir, R. D., Lathe, R., & Tanzi, R. E. (2018). The antimicrobial protection hypothesis of Alzheimer's disease. *Alzheimers Dement, 14*(12), 1602-1614. doi:10.1016/j.jalz.2018.06.3040

Moller, S., & Becker, U. (1992). Insulin-like growth factor 1 and growth hormone in chronic liver disease. *Dig Dis, 10*(4), 239-248. doi:10.1159/000171362

Moolenbeek, C., & Ruitenberg, E. J. (1981). The "Swiss roll": a simple technique for histological studies of the rodent intestine. *Lab Anim, 15*(1), 57-59.

Mosher, K. I., & Wyss-Coray, T. (2014). Microglial dysfunction in brain aging and Alzheimer's disease. *Biochem Pharmacol, 88*(4), 594-604. doi:10.1016/j.bcp.2014.01.008

Mullan, M., Crawford, F., Axelman, K., Houlden, H., Lilius, L., Winblad, B., & Lannfelt, L. (1992). A pathogenic mutation for probable Alzheimer's disease in the APP gene at the N-terminus of beta-amyloid. *Nat Genet, 1*(5), 345-347. doi:10.1038/ng0892-345

Musicco, M., Adorni, F., Di Santo, S., Prinelli, F., Pettenati, C., Caltagirone, C., & Russo, A. (2013). Inverse occurrence of cancer and Alzheimer disease: a population-based incidence study. *Neurology, 81*(4), 322-328. doi:10.1212/WNL.0b013e31829c5ec1

Mustafa, A., Lannfelt, L., Lilius, L., Islam, A., Winblad, B., & Adem, A. (1999). Decreased plasma insulin-like growth factor-I level in familial Alzheimer's disease patients carrying the Swedish APP 670/671 mutation. *Dementia and Geriatric Cognitive Disorders, 10*(6), 446-451. doi:10.1159/000017188

Nagamoto-Combs, K., Manocha, G. D., Puig, K., & Combs, C. K. (2016). An improved approach to align and embed multiple brain samples in a gelatin-based matrix for simultaneous histological processing. *J Neurosci Methods, 261*, 155-160. doi:10.1016/j.jneumeth.2015.12.008

Nagamoto-Combs, K., Manocha, G. D., Puig, K., & Combs, C. K. (2016). An improved approach to align and embed multiple brain samples in a gelatin-based matrix for simultaneous histological processing. *J Neurosci Methods, 261*, 155-160. doi:10.1016/j.jneumeth.2015.12.008

Nalivaeva, N. N., & Turner, A. J. (2013). The amyloid precursor protein: a biochemical enigma in brain development, function and disease. *FEBS Lett, 587*(13), 2046-2054. doi:10.1016/j.febslet.2013.05.010

Nava, P., Koch, S., Laukoetter, M. G., Lee, W. Y., Kolegraff, K., Capaldo, C. T., &. Nusrat, A. (2010). Interferon-gamma regulates intestinal epithelial homeostasis through converging beta-catenin signaling pathways. *Immunity, 32*(3), 392-402. doi:10.1016/j.immuni.2010.03.001

Navabi, S., Gorrepati, V. S., Yadav, S., Chintanaboina, J., Maher, S., Demuth, P., & Coates, M. D. (2018). Influences and Impact of Anxiety and Depression in the Setting of Inflammatory Bowel Disease. *Inflamm Bowel Dis, 24*(11), 2303-2308. doi:10.1093/ibd/izy143

Neufert, C., Becker, C., & Neurath, M. F. (2007). An inducible mouse model of colon carcinogenesis for the analysis of sporadic and inflammation-driven tumor progression. *Nat Protoc, 2*(8), 1998-2004. doi:10.1038/nprot.2007.279

Neurath, M. F. (2014). Cytokines in inflammatory bowel disease. *Nat Rev Immunol, 14*(5), 329-342. doi:10.1038/nri3661

Ng, S. C., Benjamin, J. L., McCarthy, N. E., Hedin, C. R., Koutsoumpas, A., Plamondon, S., & Stagg, A. J. (2011). Relationship between human intestinal dendritic cells, gut microbiota, and disease activity in Crohn's disease. *Inflamm Bowel Dis, 17*(10), 2027-2037. doi:10.1002/ibd.21590

Ng, T. K. S., Ho, C. S. H., Tam, W. W. S., Kua, E. H., & Ho, R. C. (2019). Decreased Serum Brain-Derived Neurotrophic Factor (BDNF) Levels in Patients with Alzheimer's Disease (AD): A Systematic Review and Meta-Analysis. *Int J Mol Sci, 20*(2). doi:10.3390/ijms20020257

Nichols, M. R., St-Pierre, M. K., Wendeln, A. C., Makoni, N. J., Gouwens, L. K., Garrad, E. C., & Combs, C. K. (2019). Inflammatory mechanisms in neurodegeneration. *J Neurochem, 149*(5), 562-581. doi:10.1111/jnc.14674

Nimmerjahn, A., Kirchhoff, F., & Helmchen, F. (2005). Resting microglial cells are highly dynamic surveillants of brain parenchyma in vivo. *Science, 308*(5726), 1314-1318. doi:10.1126/science.1110647

Nordstedt, C., Caporaso, G. L., Thyberg, J., Gandy, S. E., & Greengard, P. (1993). Identification of the Alzheimer beta/A4 amyloid precursor protein in clathrin-coated vesicles purified from PC12 cells. *J Biol Chem, 268*(1), 608-612.

Nunan, J., & Small, D. H. (2000). Regulation of APP cleavage by alpha-, beta- and gamma-secretases. *FEBS Lett, 483*(1), 6-10. doi:10.1016/s0014-5793(00)02076-7

Oddo, S. (2012). The role of mTOR signaling in Alzheimer disease. *Frontiers in bioscience (Scholar edition), 4*, 941-952. Retrieved from https://www.ncbi.nlm.nih.gov/pmc/articles/PMC4111148/

Okayasu, I., Hatakeyama, S., Yamada, M., Ohkusa, T., Inagaki, Y., & Nakaya, R. (1990). A novel method in the induction of reliable experimental acute and chronic ulcerative colitis in mice. *Gastroenterology, 98*(3), 694-702. doi:10.1016/0016-5085(90)90290-h

Okereke, O., Kang, J. H., Ma, J., Hankinson, S. E., Pollak, M. N., & Grodstein, F. (2007). Plasma IGF-I levels and cognitive performance in older women. *Neurobiology of Aging, 28*(1), 135-142. doi:10.1016/j.neurobiolaging.2005.10.012

Onos, K. D., Sukoff Rizzo, S. J., Howell, G. R., & Sasner, M. (2016). Toward more predictive genetic mouse models of Alzheimer's disease. *Brain Res Bull, 122*, 1-11. doi:10.1016/j.brainresbull.2015.12.003

Ortega-Martínez, S. (2015). A new perspective on the role of the CREB family of transcription factors in memory consolidation via adult hippocampal neurogenesis. *Front Mol Neurosci, 8*, 46. doi:10.3389/fnmol.2015.00046

Paramsothy, S., Rosenstein, A. K., Mehandru, S., & Colombel, J. F. (2018). The current state of the art for biological therapies and new small molecules in inflammatory bowel disease. *Mucosal Immunol, 11*(6), 1558-1570. doi:10.1038/s41385-018-0050-3

Parang, B., Barrett, C. W., & Williams, C. S. (2016). AOM/DSS Model of Colitis-Associated Cancer. *Methods Mol Biol, 1422*, 297-307. doi:10.1007/978-1-4939-3603-8_26

Paranjape, G. S., Gouwens, L. K., Osborn, D. C., & Nichols, M. R. (2012). Isolated amyloid-β(1-42) protofibrils, but not isolated fibrils, are robust stimulators of microglia. *ACS Chem Neurosci, 3*(4), 302-311. doi:10.1021/cn2001238

Parrella, E., Maxim, T., Maialetti, F., Zhang, L., Wan, J., Wei, M., & Longo, V. D. (2013). Protein restriction cycles reduce IGF-1 and phosphorylated Tau, and improve behavioral performance in an Alzheimer's disease mouse model. *Aging cell, 12*(2), 257-268. doi:10.1111/acel.12049

Pastorino, L., Ikin, A. F., Lamprianou, S., Vacaresse, N., Revelli, J. P., Platt, K., & Buxbaum, J. D. (2004). BACE (beta-secretase) modulates the processing of APLP2 in vivo. *Mol Cell Neurosci, 25*(4), 642-649. doi:10.1016/j.mcn.2003.12.013

Pei, J.-J., & Hugon, J. (2008). mTOR-dependent signalling in Alzheimer's disease. *Journal of Cellular and Molecular Medicine, 12*(6b), 2525-2532. doi:10.1111/j.1582-4934.2008.00509.x

Perše, M., & Cerar, A. (2012). Dextran sodium sulphate colitis mouse model: traps and tricks. *J Biomed Biotechnol, 2012*, 718617. doi:10.1155/2012/718617

Petit-Demouliere, B., Chenu, F., & Bourin, M. (2005). Forced swimming test in mice: a review of antidepressant activity. *Psychopharmacology (Berl), 177*(3), 245-255. doi:10.1007/s00213-004-2048-7

Petruo, V. A., Zeißig, S., Schmelz, R., Hampe, J., & Beste, C. (2017). Specific neurophysiological mechanisms underlie cognitive inflexibility in inflammatory bowel disease. *Sci Rep, 7*(1), 13943. doi:10.1038/s41598-017-14345-5

Pickert, G., Neufert, C., Leppkes, M., Zheng, Y., Wittkopf, N., Warntjen, M., & Becker, C. (2009). STAT3 links IL-22 signaling in intestinal epithelial cells to mucosal wound healing. *J Exp Med, 206*(7), 1465-1472. doi:10.1084/jem.20082683

Pietrzik, C. U., Hoffmann, J., Stöber, K., Chen, C. Y., Bauer, C., Otero, D. A., & Herzog, V. (1998). From differentiation to proliferation: the secretory amyloid precursor protein as a local mediator of growth in thyroid epithelial cells. *Proc Natl Acad Sci U S A, 95*(4), 1770-1775. doi:10.1073/pnas.95.4.1770

Pietrzik, C. U., Yoon, I. S., Jaeger, S., Busse, T., Weggen, S., & Koo, E. H. (2004). FE65 constitutes the functional link between the low-density lipoprotein receptor-related protein and the amyloid precursor protein. *J Neurosci, 24*(17), 4259-4265. doi:10.1523/jneurosci.5451-03.2004

Prasad, S., Mingrino, R., Kaukinen, K., Hayes, K. L., Powell, R. M., MacDonald, T. T., & Collins, J. E. (2005). Inflammatory processes have differential effects on claudins 2, 3 and 4 in colonic epithelial cells. *Lab Invest, 85*(9), 1139-1162. doi:10.1038/labinvest.3700316

Prinz, M., Priller, J., Sisodia, S. S., & Ransohoff, R. M. (2011). Heterogeneity of CNS myeloid cells and their roles in neurodegeneration. *Nat Neurosci, 14*(10), 1227-1235. doi:10.1038/nn.2923

Prinz, M., Priller, J., Sisodia, S. S., & Ransohoff, R. M. (2011). Heterogeneity of CNS myeloid cells and their roles in neurodegeneration. *Nature Neuroscience, 14*(10), 1227-1235. doi:10.1038/nn.2923

Provias, J., & Jeynes, B. (2014). Reduction in vascular endothelial growth factor expression in the superior temporal, hippocampal, and brainstem regions in Alzheimer's disease. *Curr Neurovasc Res, 11*(3), 202-209. doi:10.2174/1567202611666140520122316

Puig, K. L., & Combs, C. K. (2013). Expression and function of APP and its metabolites outside the central nervous system. *Exp Gerontol, 48*(7), 608-611. doi:10.1016/j.exger.2012.07.009

Puig, K. L., Kulas, J. A., Franklin, W., Rakoczy, S. G., Taglialatela, G., Brown-Borg, H. M., & Combs, C. K. (2016). The Ames dwarf mutation attenuates Alzheimer's disease phenotype of APP/PS1 mice. *Neurobiology of Aging, 40*, 22-40. doi:10.1016/j.neurobiolaging.2015.12.021

Puig, K. L., Lutz, B. M., Urquhart, S. A., Rebel, A. A., Zhou, X., Manocha, G. D., & Combs, C. K. (2015). Overexpression of mutant amyloid-β protein precursor and presenilin 1 modulates enteric nervous system. *J Alzheimers Dis, 44*(4), 1263-1278. doi:10.3233/jad-142259

Putignani, L., Del Chierico, F., Vernocchi, P., Cicala, M., Cucchiara, S., & Dallapiccola, B. (2016). Gut Microbiota Dysbiosis as Risk and Premorbid Factors of IBD and IBS Along the Childhood-Adulthood Transition. *Inflamm Bowel Dis, 22*(2), 487-504. doi:10.1097/mib.0000000000000602

Qin, J., Li, R., Raes, J., Arumugam, M., Burgdorf, K. S., Manichanh, C., & Wang, J. (2010). A human gut microbial gene catalogue established by metagenomic sequencing. *Nature, 464*(7285), 59-65. doi:10.1038/nature08821

Querfurth, H. W., & LaFerla, F. M. (2010). Alzheimer's disease. *N Engl J Med, 362*(4), 329-344. doi:10.1056/NEJMra0909142

Rajendran, L., Honsho, M., Zahn, T. R., Keller, P., Geiger, K. D., Verkade, P., & Simons, K. (2006). Alzheimer's disease beta-amyloid peptides are released in association with exosomes. *Proc Natl Acad Sci U S A, 103*(30), 11172-11177. doi:10.1073/pnas.0603838103

Rakic, S., Hung, Y. M. A., Smith, M., So, D., Tayler, H. M., Varney, W., & Boche, D. (2018). Systemic infection modifies the neuroinflammatory response in late stage Alzheimer's disease. *Acta Neuropathol Commun, 6*(1), 88. doi:10.1186/s40478-018-0592-3

Ransohoff, R. M., & Perry, V. H. (2009). Microglial physiology: unique stimuli, specialized responses. *Annu Rev Immunol, 27*, 119-145. doi:10.1146/annurev.immunol.021908.132528

Reichmann, F., Hassan, A. M., Farzi, A., Jain, P., Schuligoi, R., & Holzer, P. (2015). Dextran sulfate sodium-induced colitis alters stress-associated behaviour and neuropeptide gene expression in the amygdala-hippocampus network of mice. *Sci Rep, 5*, 9970. doi:10.1038/srep09970

Reichmann, F., Painsipp, E., & Holzer, P. (2013). Environmental enrichment and gut inflammation modify stress-induced c-Fos expression in the mouse corticolimbic system. *PLoS One, 8*(1), e54811. doi:10.1371/journal.pone.0054811

Rhee, K. J., Wu, S., Wu, X., Huso, D. L., Karim, B., Franco, A. A., & Sears, C. L. (2009). Induction of persistent colitis by a human commensal, enterotoxigenic Bacteroides fragilis, in wild-type C57BL/6 mice. *Infect Immun, 77*(4), 1708-1718. doi:10.1128/iai.00814-08

Rhee, S. H., Pothoulakis, C., & Mayer, E. A. (2009). Principles and clinical implications of the brain-gut-enteric microbiota axis. *Nat Rev Gastroenterol Hepatol, 6*(5), 306-314. doi:10.1038/nrgastro.2009.35

Riazi, K., Galic, M. A., Kuzmiski, J. B., Ho, W., Sharkey, K. A., & Pittman, Q. J. (2008). Microglial activation and TNFalpha production mediate altered CNS excitability following peripheral inflammation. *Proc Natl Acad Sci U S A, 105*(44), 17151-17156. doi:10.1073/pnas.0806682105

Ries, M., & Sastre, M. (2016). Mechanisms of Aβ Clearance and Degradation by Glial Cells. *Front Aging Neurosci, 8*, 160. doi:10.3389/fnagi.2016.00160

Roach, M., & Christie, J. A. (2008). Fecal incontinence in the elderly. *Geriatrics, 63*(2), 13-22.

Roe, C. M., Fitzpatrick, A. L., Xiong, C., Sieh, W., Kuller, L., Miller, J. P., & Morris, J. C. (2010). Cancer linked to Alzheimer disease but not vascular dementia. *Neurology, 74*(2), 106-112. doi:10.1212/WNL.0b013e3181c91873

Rosenberg, D. W., Giardina, C., & Tanaka, T. (2009). Mouse models for the study of colon carcinogenesis. *Carcinogenesis, 30*(2), 183-196. doi:10.1093/carcin/bgn267

Rossjohn, J., Cappai, R., Feil, S. C., Henry, A., McKinstry, W. J., Galatis, D., & Parker, M. W. (1999). Crystal structure of the N-terminal, growth factor-like domain of Alzheimer amyloid precursor protein. *Nat Struct Biol, 6*(4), 327-331. doi:10.1038/7562

Rothenberg, P., White, M. F., & Kahn, C. R. (1990). The Insulin Receptor Tyrosine Kinase. In *Insulin* (pp. 209-236): Springer, Berlin, Heidelberg.

Rowan, A. J., Lamlum, H., Ilyas, M., Wheeler, J., Straub, J., Papadopoulou, A., & Tomlinson, I. P. (2000). APC mutations in sporadic colorectal tumors: A mutational "hotspot" and interdependence of the "two hits". *Proc Natl Acad Sci U S A, 97*(7), 3352-3357. doi:10.1073/pnas.97.7.3352

Rugtveit, J., Brandtzaeg, P., Halstensen, T. S., Fausa, O., & Scott, H. (1994). Increased macrophage subset in inflammatory bowel disease: apparent recruitment from peripheral blood monocytes. *Gut, 35*(5), 669-674. doi:10.1136/gut.35.5.669

Saito, T., Matsuba, Y., Mihira, N., Takano, J., Nilsson, P., Itohara, S., & Saido, T. C. (2014). Single App knock-in mouse models of Alzheimer's disease. *Nat Neurosci, 17*(5), 661-663. doi:10.1038/nn.3697

Salmon, W. D., Jr., & Daughaday, W. H. (1957). A hormonally controlled serum factor which stimulates sulfate incorporation by cartilage in vitro. *J Lab Clin Med, 49*(6), 825-836.

Samani, A. A., Yakar, S., LeRoith, D., & Brodt, P. (2007). The role of the IGF system in cancer growth and metastasis: overview and recent insights. *Endocr Rev, 28*(1), 20-47. doi:10.1210/er.2006-0001

Sarlus, H., & Heneka, M. T. (2017). Microglia in Alzheimer's disease. *J Clin Invest, 127*(9), 3240-3249. doi:10.1172/jci90606

Scheinfeld, M. H., Ghersi, E., Laky, K., Fowlkes, B. J., & D'Adamio, L. (2002). Processing of beta-amyloid precursor-like protein-1 and -2 by gamma-secretase regulates transcription. *J Biol Chem, 277*(46), 44195-44201. doi:10.1074/jbc.M208110200

Schlossmacher, M. G., Ostaszewski, B. L., Hecker, L. I., Celi, A., Haass, C., Chin, D., & Selkoe, D. J. (1992). Detection of distinct isoform patterns of the beta-amyloid precursor protein in human platelets and lymphocytes. *Neurobiol Aging, 13*(3), 421-434. doi:10.1016/0197-4580(92)90117-g

Schneider, S., Wright, C. M., & Heuckeroth, R. O. (2019). Unexpected Roles for the Second Brain: Enteric Nervous System as Master Regulator of Bowel Function. *Annu Rev Physiol, 81*, 235-259. doi:10.1146/annurev-physiol-021317-121515

Schuster, B. G., Kosar, L., & Kamrul, R. (2015). Constipation in older adults: stepwise approach to keep things moving. *Can Fam Physician, 61*(2), 152-158.

Seguchi, K., Kataoka, H., Uchino, H., Nabeshima, K., & Koono, M. (1999). Secretion of protease nexin-II/amyloid beta protein precursor by human colorectal carcinoma cells and its modulation by cytokines/growth factors and proteinase inhibitors. *Biol Chem, 380*(4), 473-483. doi:10.1515/bc.1999.061

Semar, S., Klotz, M., Letiembre, M., Van Ginneken, C., Braun, A., Jost, V., & Schafer, K. H. (2013). Changes of the enteric nervous system in amyloid-beta protein precursor transgenic mice correlate with disease progression. *J Alzheimers Dis, 36*(1), 7-20. doi:10.3233/jad-120511

Serrano-Pozo, A., Frosch, M. P., Masliah, E., & Hyman, B. T. (2011). Neuropathological alterations in Alzheimer disease. *Cold Spring Harb Perspect Med, 1*(1), a006189. doi:10.1101/cshperspect.a006189

Sevigny, J. J., Ryan, J. M., van Dyck, C. H., Peng, Y., Lines, C. R., Nessly, M. L., & Group, M. K. P. S. (2008). Growth hormone secretagogue MK-677: no clinical effect on AD progression in a randomized trial. *Neurology, 71*(21), 1702-1708. doi:10.1212/01.wnl.0000335163.88054.e7

Sgambato, D., Miranda, A., Ranaldo, R., Federico, A., & Romano, M. (2017). The Role of Stress in Inflammatory Bowel Diseases. *Curr Pharm Des, 23*(27), 3997-4002. doi:10.2174/1381612823666170228123357

Shen, L., Liu, L., & Ji, H. F. (2017). Alzheimer's Disease Histological and Behavioral Manifestations in Transgenic Mice Correlate with Specific Gut Microbiome State. *J Alzheimers Dis, 56*(1), 385-390. doi:10.3233/jad-160884

Sherzai, A. Z., Parasram, M., Haider, J. M., & Sherzai, D. (2020). Alzheimer Disease and Cancer: A National Inpatient Sample Analysis. *Alzheimer Dis Assoc Disord*. doi:10.1097/wad.0000000000000369

Simons, M., Gordon, E., & Claesson-Welsh, L. (2016). Mechanisms and regulation of endothelial VEGF receptor signalling. *Nat Rev Mol Cell Biol, 17*(10), 611-625. doi:10.1038/nrm.2016.87

Sinha, S., Anderson, J. P., Barbour, R., Basi, G. S., Caccavello, R., Davis, D., & John, V. (1999). Purification and cloning of amyloid precursor protein beta-secretase from human brain. *Nature, 402*(6761), 537-540. doi:10.1038/990114

Sisodia, S. S. (1992). Beta-amyloid precursor protein cleavage by a membrane-bound protease. *Proc Natl Acad Sci U S A, 89*(13), 6075-6079. doi:10.1073/pnas.89.13.6075

Sisodia, S. S., & St George-Hyslop, P. H. (2002). gamma-Secretase, Notch, Abeta and Alzheimer's disease: where do the presenilins fit in? *Nat Rev Neurosci, 3*(4), 281-290. doi:10.1038/nrn785

Ślebioda, T. J., & Kmieć, Z. (2014). Tumour necrosis factor superfamily members in the pathogenesis of inflammatory bowel disease. *Mediators Inflamm, 2014*, 325129. doi:10.1155/2014/325129

Snider, A. J., Bialkowska, A. B., Ghaleb, A. M., Yang, V. W., Obeid, L. M., & Hannun, Y. A. (2016). Murine Model for Colitis-Associated Cancer of the Colon. *Methods Mol Biol, 1438*, 245-254. doi:10.1007/978-1-4939-3661-8_14

Sobol, A., Galluzzo, P., Liang, S., Rambo, B., Skucha, S., Weber, M. J., & Bocchetta, M. (2015). Amyloid precursor protein (APP) affects global protein synthesis in dividing human cells. *J Cell Physiol, 230*(5), 1064-1074. doi:10.1002/jcp.24835

Sohrabi, M., & Combs, C. K. (2019). A protocol for making and sectioning multiple embedded Swiss-rolls in a gelatin matrix. *MethodsX, 6*, 2028-2036. doi:10.1016/j.mex.2019.08.021

Son, H. J., Sohn, S. H., Kim, N., Lee, H. N., Lee, S. M., Nam, R. H., & Surh, Y. J. (2019). Effect of Estradiol in an Azoxymethane/Dextran Sulfate Sodium-Treated Mouse Model of Colorectal Cancer: Implication for Sex Difference in Colorectal Cancer Development. *Cancer Res Treat, 51*(2), 632-648. doi:10.4143/crt.2018.060

Song, C. H., Kim, N., Lee, S. M., Nam, R. H., Choi, S. I., Kang, S. R., & Surh, Y. J. (2019). Effects of 17β-estradiol on colorectal cancer development after azoxymethane/dextran sulfate sodium treatment of ovariectomized mice. *Biochem Pharmacol, 164*, 139-151. doi:10.1016/j.bcp.2019.04.011

Soscia, S. J., Kirby, J. E., Washicosky, K. J., Tucker, S. M., Ingelsson, M., Hyman, B., & Moir, R. D. (2010). The Alzheimer's disease-associated amyloid beta-protein is an antimicrobial peptide. *PLoS One, 5*(3), e9505. doi:10.1371/journal.pone.0009505

Sprecher, C. A., Grant, F. J., Grimm, G., O'Hara, P. J., Norris, F., Norris, K., & Foster, D. C. (1993). Molecular cloning of the cDNA for a human amyloid precursor protein homolog: evidence for a multigene family. *Biochemistry, 32*(17), 4481-4486. doi:10.1021/bi00068a002

Storkebaum, E., Lambrechts, D., & Carmeliet, P. (2004). VEGF: once regarded as a specific angiogenic factor, now implicated in neuroprotection. *Bioessays, 26*(9), 943-954. doi:10.1002/bies.20092

Streit, W. J., Miller, K. R., Lopes, K. O., & Njie, E. (2008). Microglial degeneration in the aging brain--bad news for neurons? *Front Biosci, 13*, 3423-3438. doi:10.2741/2937

Strittmatter, W. J., Saunders, A. M., Schmechel, D., Pericak-Vance, M., Enghild, J., Salvesen, G. S., & Roses, A. D. (1993). Apolipoprotein E: high-avidity binding to beta-amyloid and increased frequency of type 4 allele in late-onset familial Alzheimer disease. *Proc Natl Acad Sci U S A, 90*(5), 1977-1981. doi:10.1073/pnas.90.5.1977

Su, L., Nalle, S. C., Shen, L., Turner, E. S., Singh, G., Breskin, L. A., & Turner, J. R. (2013). TNFR2 activates MLCK-dependent tight junction dysregulation to cause apoptosis-mediated barrier loss and experimental colitis. *Gastroenterology, 145*(2), 407-415. doi:10.1053/j.gastro.2013.04.011

Suh, Y., Atzmon, G., Cho, M.-O., Hwang, D., Liu, B., Leahy, D. J., & Cohen, P. (2008). Functionally significant insulin-like growth factor I receptor mutations in centenarians. *Proceedings of the National Academy of Sciences of the United States of America, 105*(9), 3438-3442. doi:10.1073/pnas.0705467105

Sun, L. Y., Spong, A., Swindell, W. R., Fang, Y., Hill, C., Huber, J. A., & Bartke, A. (2013). Growth hormone-releasing hormone disruption extends lifespan and regulates response to caloric restriction in mice. *Elife, 2*, e01098. doi:10.7554/eLife.01098

Suzuki, N., Cheung, T. T., Cai, X. D., Odaka, A., Otvos, L., Jr., Eckman, C., & Younkin, S. G. (1994). An increased percentage of long amyloid beta protein secreted by familial amyloid beta protein precursor (beta APP717) mutants. *Science, 264*(5163), 1336-1340. doi:10.1126/science.8191290

Swardfager, W., Lanctot, K., Rothenburg, L., Wong, A., Cappell, J., & Herrmann, N. (2010). A meta-analysis of cytokines in Alzheimer's disease. *Biol Psychiatry, 68*(10), 930-941. doi:10.1016/j.biopsych.2010.06.012

Taguchi, A., Wartschow, L. M., & White, M. F. (2007). Brain IRS2 signaling coordinates life span and nutrient homeostasis. *Science (New York, N.Y.), 317*(5836), 369-372. doi:10.1126/science.1142179

Takagi, K., Ito, S., Miyazaki, T., Miki, Y., Shibahara, Y., Ishida, T., & Suzuki, T. (2013). Amyloid precursor protein in human breast cancer: an androgen-induced gene associated with cell proliferation. *Cancer Sci, 104*(11), 1532-1538. doi:10.1111/cas.12239

Takayama, K., Tsutsumi, S., Suzuki, T., Horie-Inoue, K., Ikeda, K., Kaneshiro, K., & Inoue, S. (2009). Amyloid precursor protein is a primary androgen target gene that promotes prostate cancer growth. *Cancer Res, 69*(1), 137-142. doi:10.1158/0008-5472.Can-08-3633

Talbot, K., Wang, H.-Y., Kazi, H., Han, L.-Y., Bakshi, K. P., Stucky, A., & Arnold, S. E. (2012). Demonstrated brain insulin resistance in Alzheimer's disease patients is associated with IGF-1 resistance, IRS-1 dysregulation, and cognitive decline. *The Journal of Clinical Investigation, 122*(4), 1316-1338. doi:10.1172/JCI59903

Taleban, S., Colombel, J. F., Mohler, M. J., & Fain, M. J. (2015). Inflammatory bowel disease and the elderly: a review. *J Crohns Colitis, 9*(6), 507-515. doi:10.1093/ecco-jcc/jjv059

Tanaka, T., Oyama, T., Sugie, S., & Shimizu, M. (2016). Different Susceptibilities between Apoe- and Ldlr-Deficient Mice to Inflammation-Associated Colorectal Carcinogenesis. *Int J Mol Sci, 17*(11). doi:10.3390/ijms17111806

Tang, K., Wang, C., Shen, C., Sheng, S., Ravid, R., & Jing, N. (2003). Identification of a novel alternative splicing isoform of human amyloid precursor protein gene, APP639. *Eur J Neurosci, 18*(1), 102-108. doi:10.1046/j.1460-9568.2003.02731.x

Tanila, H. (2017). The role of BDNF in Alzheimer's disease. *Neurobiol Dis, 97*(Pt B), 114-118. doi:10.1016/j.nbd.2016.05.008

Tarkowski, E., Liljeroth, A. M., Minthon, L., Tarkowski, A., Wallin, A., & Blennow, K. (2003). Cerebral pattern of pro- and anti-inflammatory cytokines in dementias. *Brain Res Bull, 61*(3), 255-260. doi:10.1016/s0361-9230(03)00088-1

Tatar, M., Bartke, A., & Antebi, A. (2003). The endocrine regulation of aging by insulin-like signals. *Science (New York, N.Y.), 299*(5611), 1346-1351. doi:10.1126/science.1081447

Tejera, D., Mercan, D., Sanchez-Caro, J. M., Hanan, M., Greenberg, D., Soreq, H., & Heneka, M. T. (2019). Systemic inflammation impairs microglial Aβ clearance through NLRP3 inflammasome. *Embo j, 38*(17), e101064. doi:10.15252/embj.2018101064

Terry, R. D. (1963). THE FINE STRUCTURE OF NEUROFIBRILLARY TANGLES IN ALZHEIMER'S DISEASE. *J Neuropathol Exp Neurol, 22*, 629-642. doi:10.1097/00005072-196310000-00005

Thal, D. R., Rub, U., Orantes, M., & Braak, H. (2002). Phases of A beta-deposition in the human brain and its relevance for the development of AD. *Neurology, 58*(12), 1791-1800. doi:10.1212/wnl.58.12.1791

Thinakaran, G., & Koo, E. H. (2008). Amyloid precursor protein trafficking, processing, and function. *J Biol Chem, 283*(44), 29615-29619. doi:10.1074/jbc.R800019200

Tilstra, J. S., Robinson, A. R., Wang, J., Gregg, S. Q., Clauson, C. L., Reay, D. P., & Robbins, P. D. (2012). NF-κB inhibition delays DNA damage-induced senescence and aging in mice. *J Clin Invest, 122*(7), 2601-2612. doi:10.1172/jci45785

Tramutola, A., Triplett, J. C., Di Domenico, F., Niedowicz, D. M., Murphy, M. P., Coccia, R., & Butterfield, D. A. (2015). Alteration of mTOR signaling occurs early in the progression of Alzheimer disease (AD): analysis of brain from subjects with pre-clinical AD, amnestic mild cognitive impairment and late-stage AD. *Journal of Neurochemistry, 133*(5), 739-749. doi:10.1111/jnc.13037

Trommsdorff, M., Borg, J. P., Margolis, B., & Herz, J. (1998). Interaction of cytosolic adaptor proteins with neuronal apolipoprotein E receptors and the amyloid precursor protein. *J Biol Chem, 273*(50), 33556-33560. doi:10.1074/jbc.273.50.33556

Tsang, J. Y. S., Lee, M. A., Chan, T. H., Li, J., Ni, Y. B., Shao, Y., & Tse, G. M. K. (2018). Proteolytic cleavage of amyloid precursor protein by ADAM10 mediates proliferation and migration in breast cancer. *EBioMedicine, 38*, 89-99. doi:10.1016/j.ebiom.2018.11.012

Tubbs, R. S., Rizk, E., Shoja, M. M., Loukas, M., Barbaro, N., & Spinner, R. J. (2015). *Nerves and Nerve Injuries: Vol 1: History, Embryology, Anatomy, Imaging, and Diagnostics*: Academic Press.

Tumati, S., Burger, H., Martens, S., van der Schouw, Y. T., & Aleman, A. (2016). Association between Cognition and Serum Insulin-Like Growth Factor-1 in Middle-Aged & Older Men: An 8 Year Follow-Up Study. *PLoS ONE, 11*(4). doi:10.1371/journal.pone.0154450

Turner, J. R. (2009). Intestinal mucosal barrier function in health and disease. *Nat Rev Immunol, 9*(11), 799-809. doi:10.1038/nri2653

van der Kant, R., & Goldstein, L. S. (2015). Cellular functions of the amyloid precursor protein from development to dementia. *Dev Cell, 32*(4), 502-515. doi:10.1016/j.devcel.2015.01.022

van der Spoel, E., Rozing, M. P., Houwing-Duistermaat, J. J., Slagboom, P. E., Beekman, M., de Craen, A. J. M., & van Heemst, D. (2015). Association analysis of insulin-like growth factor-1 axis parameters with survival and functional status in nonagenarians of the Leiden Longevity Study. *Aging, 7*(11), 956-963. doi:10.18632/aging.100841

van Exel, E., Eikelenboom, P., Comijs, H., Deeg, D. J. H., Stek, M. L., & Westendorp, R. G. J. (2014). Insulin-like growth factor-1 and risk of late-onset Alzheimer's disease: findings from a family study. *Neurobiology of Aging, 35*(3), 725.e727-710. doi:10.1016/j.neurobiolaging.2013.08.014

Van Gool, B., Storck, S. E., Reekmans, S. M., Lechat, B., Gordts, P., Pradier, L., & Roebroek, A. J. M. (2019). LRP1 Has a Predominant Role in Production over Clearance of Aβ in a Mouse Model of Alzheimer's Disease. *Mol Neurobiol, 56*(10), 7234-7245. doi:10.1007/s12035-019-1594-2

van Hemert, S., Skonieczna-Żydecka, K., Loniewski, I., Szredzki, P., & Marlicz, W. (2018). Microscopic colitis-microbiome, barrier function and associated diseases. *Ann Transl Med, 6*(3), 39. doi:10.21037/atm.2017.03.83

van Langenberg, D. R., Yelland, G. W., Robinson, S. R., & Gibson, P. R. (2017). Cognitive impairment in Crohn's disease is associated with systemic inflammation, symptom burden and sleep disturbance. *United European Gastroenterol J, 5*(4), 579-587. doi:10.1177/2050640616663397

Vardy, E. R. L. C., Rice, P. J., Bowie, P. C. W., Holmes, J. D., Grant, P. J., & Hooper, N. M. (2007). Increased circulating insulin-like growth factor-1 in late-onset Alzheimer's disease. *Journal of Alzheimer's disease: JAD, 12*(4), 285-290. Retrieved from http://www.ncbi.nlm.nih.gov/pubmed/18198415

Vasilcanu, D., Girnita, A., Girnita, L., Vasilcanu, R., Axelson, M., & Larsson, O. (2004). The cyclolignan PPP induces activation loop-specific inhibition of tyrosine phosphorylation of the insulin-like growth factor-1 receptor. Link to the phosphatidyl inositol-3 kinase/Akt apoptotic pathway. *Oncogene, 23*(47), 7854-7862. doi:10.1038/sj.onc.1208065

Vasilcanu, R., Vasilcanu, D., Rosengren, L., Natalishvili, N., Sehat, B., Yin, S., & Larsson, O. (2008). Picropodophyllin induces downregulation of the insulin-like growth factor 1 receptor: potential mechanistic involvement of Mdm2 and beta-arrestin1. *Oncogene, 27*(11), 1629-1638. doi:10.1038/sj.onc.1210797

Vassar, R., Bennett, B. D., Babu-Khan, S., Kahn, S., Mendiaz, E. A., Denis, P., & Citron, M. (1999). Beta-secretase cleavage of Alzheimer's amyloid precursor protein by the transmembrane aspartic protease BACE. *Science, 286*(5440), 735-741. doi:10.1126/science.286.5440.735

Venkataramani, V., Rossner, C., Iffland, L., Schweyer, S., Tamboli, I. Y., Walter, J., & Bayer, T. A. (2010). Histone deacetylase inhibitor valproic acid inhibits cancer cell proliferation via down-regulation of the alzheimer amyloid precursor protein. *J Biol Chem, 285*(14), 10678-10689. doi:10.1074/jbc.M109.057836

Villaran, R. F., Espinosa-Oliva, A. M., Sarmiento, M., De Pablos, R. M., Arguelles, S., Delgado-Cortes, M. J., & Machado, A. (2010). Ulcerative colitis exacerbates lipopolysaccharide-induced damage to the nigral dopaminergic system: potential risk factor in Parkinson`s disease. *J Neurochem, 114*(6), 1687-1700. doi:10.1111/j.1471-4159.2010.06879.x

Vina, J., & Lloret, A. (2010). Why women have more Alzheimer's disease than men: gender and mitochondrial toxicity of amyloid-beta peptide. *J Alzheimers Dis, 20 Suppl 2*, S527-533. doi:10.3233/jad-2010-100501

Vogt, N. M., Kerby, R. L., Dill-McFarland, K. A., Harding, S. J., Merluzzi, A. P., Johnson, S. C., & Rey, F. E. (2017). Gut microbiome alterations in Alzheimer's disease. *Sci Rep, 7*(1), 13537. doi:10.1038/s41598-017-13601-y

Vogt, N. M., Romano, K. A., Darst, B. F., Engelman, C. D., Johnson, S. C., Carlsson, C. M., & Rey, F. E. (2018). The gut microbiota-derived metabolite trimethylamine N-oxide is elevated in Alzheimer's disease. *Alzheimers Res Ther, 10*(1), 124. doi:10.1186/s13195-018-0451-2

von Koch, C. S., Zheng, H., Chen, H., Trumbauer, M., Thinakaran, G., van der Ploeg, L. H., & Sisodia, S. S. (1997). Generation of APLP2 KO mice and early postnatal lethality in APLP2/APP double KO mice. *Neurobiol Aging, 18*(6), 661-669. doi:10.1016/s0197-4580(97)00151-6

Walker, K. A., Ficek, B. N., & Westbrook, R. (2019). Understanding the Role of Systemic Inflammation in Alzheimer's Disease. *ACS Chem Neurosci, 10*(8), 3340-3342. doi:10.1021/acschemneuro.9b00333

Walker, K. A., Gottesman, R. F., Wu, A., Knopman, D. S., Gross, A. L., Mosley, T. H., Jr., & Windham, B. G. (2019). Systemic inflammation during midlife and cognitive change over 20 years: The ARIC Study. *Neurology, 92*(11), e1256-e1267. doi:10.1212/wnl.0000000000007094

Walsh, D. M., Fadeeva, J. V., LaVoie, M. J., Paliga, K., Eggert, S., Kimberly, W. T., & Selkoe, D. J. (2003). gamma-Secretase cleavage and binding to FE65 regulate the nuclear translocation of the intracellular C-terminal domain (ICD) of the APP family of proteins. *Biochemistry, 42*(22), 6664-6673. doi:10.1021/bi027375c

Walter, J., & Haass, C. (2000). Posttranslational modifications of amyloid precursor protein : ectodomain phosphorylation and sulfation. *Methods Mol Med, 32*, 149-168. doi:10.1385/1-59259-195-7:149

Wang, B., Liu, Y., Huang, L., Chen, J., Li, J. J., Wang, R., & Liao, F. F. (2017). A CNS-permeable Hsp90 inhibitor rescues synaptic dysfunction and memory loss in APP-overexpressing Alzheimer's mouse model via an HSF1-mediated mechanism. *Mol Psychiatry, 22*(7), 990-1001. doi:10.1038/mp.2016.104

Wang, C., Zhang, X., Teng, Z., Zhang, T., & Li, Y. (2014). Downregulation of PI3K/Akt/mTOR signaling pathway in curcumin-induced autophagy in APP/PS1 double transgenic mice. *Eur J Pharmacol, 740*, 312-320. doi:10.1016/j.ejphar.2014.06.051

Wang, J., Tan, L., Wang, H. F., Tan, C. C., Meng, X. F., Wang, C., & Yu, J. T. (2015). Anti-inflammatory drugs and risk of Alzheimer's disease: an updated systematic review and meta-analysis. *J Alzheimers Dis, 44*(2), 385-396. doi:10.3233/jad-141506

Wang, S. L., Shao, B. Z., Zhao, S. B., Chang, X., Wang, P., Miao, C. Y., & Bai, Y. (2019). Intestinal autophagy links psychosocial stress with gut microbiota to promote inflammatory bowel disease. *Cell Death Dis, 10*(6), 391. doi:10.1038/s41419-019-1634-x

Wang, W.-Y., Tan, M.-S., Yu, J.-T., & Tan, L. (2015). Role of pro-inflammatory cytokines released from microglia in Alzheimer's disease. *Annals of Translational Medicine, 3*(10). doi:10.3978/j.issn.2305-5839.2015.03.49

Wang, W. Y., Tan, M. S., Yu, J. T., & Tan, L. (2015). Role of pro-inflammatory cytokines released from microglia in Alzheimer's disease. *Ann Transl Med, 3*(10), 136. doi:10.3978/j.issn.2305-5839.2015.03.49

Wang, Y., Telesford, K. M., Ochoa-Repáraz, J., Haque-Begum, S., Christy, M., Kasper, E. J., & Kasper, L. H. (2014). An intestinal commensal symbiosis factor controls neuroinflammation via TLR2-mediated CD39 signalling. *Nat Commun, 5*, 4432. doi:10.1038/ncomms5432

Wasco, W., Gurubhagavatula, S., Paradis, M. D., Romano, D. M., Sisodia, S. S., Hyman, B. T., & Tanzi, R. E. (1993). Isolation and characterization of APLP2 encoding a homologue of the Alzheimer's associated amyloid beta protein precursor. *Nat Genet, 5*(1), 95-100. doi:10.1038/ng0993-95

Waxenbaum, J. A., & Varacallo, M. (2019). Anatomy, autonomic nervous system. In *StatPearls [Internet]*: StatPearls Publishing.

Westfall, S., Lomis, N., Kahouli, I., Dia, S. Y., Singh, S. P., & Prakash, S. (2017). Microbiome, probiotics and neurodegenerative diseases: deciphering the gut brain axis. *Cell Mol Life Sci, 74*(20), 3769-3787. doi:10.1007/s00018-017-2550-9

Westwood, A. J., Beiser, A., DeCarli, C., Harris, T. B., Chen, T. C., He, X.-m., & Seshadri, S. (2014). Insulin-like growth factor-1 and risk of Alzheimer dementia and brain atrophy. *Neurology, 82*(18), 1613-1619. doi:10.1212/WNL.0000000000000382

White, A., Ironmonger, L., Steele, R. J. C., Ormiston-Smith, N., Crawford, C., & Seims, A. (2018). A review of sex-related differences in colorectal cancer incidence, screening uptake, routes to diagnosis, cancer stage and survival in the UK. *BMC Cancer, 18*(1), 906. doi:10.1186/s12885-018-4786-7

Whittem, C. G., Williams, A. D., & Williams, C. S. (2010). Murine Colitis modeling using Dextran Sulfate Sodium (DSS). *J Vis Exp*(35). doi:10.3791/1652

Wirtz, S., Popp, V., Kindermann, M., Gerlach, K., Weigmann, B., Fichtner-Feigl, S., & Neurath, M. F. (2017). Chemically induced mouse models of acute and chronic intestinal inflammation. *Nat Protoc, 12*(7), 1295-1309. doi:10.1038/nprot.2017.044

Wisniewski, T., Ghiso, J., & Frangione, B. (1991). Peptides homologous to the amyloid protein of Alzheimer's disease containing a glutamine for glutamic acid substitution have accelerated amyloid fibril formation. *Biochem Biophys Res Commun, 179*(3), 1247-1254. doi:10.1016/0006-291x(91)91706-i

Wolfe, C. M., Fitz, N. F., Nam, K. N., Lefterov, I., & Koldamova, R. (2018). The Role of APOE and TREM2 in Alzheimer's Disease-Current Understanding and Perspectives. *Int J Mol Sci, 20*(1). doi:10.3390/ijms20010081

Woods, N. K., & Padmanabhan, J. (2013). Inhibition of amyloid precursor protein processing enhances gemcitabine-mediated cytotoxicity in pancreatic cancer cells. *J Biol Chem, 288*(42), 30114-30124. doi:10.1074/jbc.M113.459255

Wozniak, M. A., Mee, A. P., & Itzhaki, R. F. (2009). Herpes simplex virus type 1 DNA is located within Alzheimer's disease amyloid plaques. *J Pathol, 217*(1), 131-138. doi:10.1002/path.2449

Wu, F., & Yao, P. J. (2009). Clathrin-mediated endocytosis and Alzheimer's disease: an update. *Ageing Res Rev, 8*(3), 147-149. doi:10.1016/j.arr.2009.03.002

Wu, W., Song, W., Li, S., Ouyang, S., Fok, K. L., Diao, R., & Wang, L. (2012). Regulation of apoptosis by Bat3-enhanced YWK-II/APLP2 protein stability. *J Cell Sci, 125*(Pt 18), 4219-4229. doi:10.1242/jcs.086553

Xu, J., Gontier, G., Chaker, Z., Lacube, P., Dupont, J., & Holzenberger, M. (2014). Longevity effect of IGF-1R(+/-) mutation depends on genetic background-specific receptor activation. *Aging Cell, 13*(1), 19-28. doi:10.1111/acel.12145

Yamamoto, H., & Murphy, L. J. (1995). Enzymatic conversion of IGF-I to des(1-3)IGF-I in rat serum and tissues: a further potential site of growth hormone regulation of IGF-I action. *The Journal of Endocrinology, 146*(1), 141-148. Retrieved from http://www.ncbi.nlm.nih.gov/pubmed/7561610

Yamazaki, Y., Painter, M. M., Bu, G., & Kanekiyo, T. (2016). Apolipoprotein E as a Therapeutic Target in Alzheimer's Disease: A Review of Basic Research and Clinical Evidence. *CNS Drugs, 30*(9), 773-789. doi:10.1007/s40263-016-0361-4

Yan, R., Bienkowski, M. J., Shuck, M. E., Miao, H., Tory, M. C., Pauley, A. M., & Gurney, M. E. (1999). Membrane-anchored aspartyl protease with Alzheimer's disease beta-secretase activity. *Nature, 402*(6761), 533-537. doi:10.1038/990107

Yin, S., Girnita, A., Strömberg, T., Khan, Z., Andersson, S., Zheng, H., & Girnita, L. (2010). Targeting the insulin-like growth factor-1 receptor by picropodophyllin as a treatment option for glioblastoma. *Neuro-Oncology, 12*(1), 19-27. doi:10.1093/neuonc/nop008

Zhang, C., Wang, Y., Wang, D., Zhang, J., & Zhang, F. (2018). NSAID Exposure and Risk of Alzheimer's Disease: An Updated Meta-Analysis From Cohort Studies. *Front Aging Neurosci, 10*, 83. doi:10.3389/fnagi.2018.00083

Zhang, J. B., Li, M. F., Zhang, H. X., Li, Z. G., Sun, H. R., Zhang, J. S., & Wang, P. F. (2016). Association of serum vascular endothelial growth factor levels and cerebral microbleeds in patients with Alzheimer's disease. *Eur J Neurol, 23*(8), 1337-1342. doi:10.1111/ene.13030

Zhang, L., Wang, Y., Xiayu, X., Shi, C., Chen, W., Song, N., & Qin, C. (2017). Altered Gut Microbiota in a Mouse Model of Alzheimer's Disease. *J Alzheimers Dis, 60*(4), 1241-1257. doi:10.3233/jad-170020

Zhang, T., Han, Y., Wang, J., Hou, D., Deng, H., Deng, Y. L., & Song, Z. (2018). Comparative Epidemiological Investigation of Alzheimer's Disease and Colorectal Cancer: The Possible Role of Gastrointestinal Conditions in the Pathogenesis of AD. *Front Aging Neurosci, 10*, 176. doi:10.3389/fnagi.2018.00176

Zhao, J., Bi, W., Xiao, S., Lan, X., Cheng, X., Zhang, J., & Zhu, L. (2019). Neuroinflammation induced by lipopolysaccharide causes cognitive impairment in mice. *Sci Rep, 9*(1), 5790. doi:10.1038/s41598-019-42286-8

Zheng, H., Jiang, M., Trumbauer, M. E., Sirinathsinghji, D. J., Hopkins, R., Smith, D. W., & Van der Ploeg, L. H. (1995). beta-Amyloid precursor protein-deficient mice show reactive gliosis and decreased locomotor activity. *Cell, 81*(4), 525-531. doi:10.1016/0092-8674(95)90073-x

Zheng, H., & Koo, E. H. (2006). The amyloid precursor protein: beyond amyloid. *Mol Neurodegener, 1*, 5. doi:10.1186/1750-1326-1-5

Zimbone, S., Monaco, I., Gianì, F., Pandini, G., Copani, A. G., Giuffrida, M. L., & Rizzarelli, E. (2018). Amyloid Beta monomers regulate cyclic adenosine monophosphate response element binding protein functions by activating type-1 insulin-like growth factor receptors in neuronal cells. *Aging Cell, 17*(1). doi:10.1111/acel.12684

Zonis, S., Pechnick, R. N., Ljubimov, V. A., Mahgerefteh, M., Wawrowsky, K., Michelsen, K. S., & Chesnokova, V. (2015). Chronic intestinal inflammation alters hippocampal neurogenesis. *J Neuroinflammation, 12*, 65. doi:10.1186/s12974-015-0281-0

Zuo, T., & Ng, S. C. (2018). The Gut Microbiota in the Pathogenesis and Therapeutics of Inflammatory Bowel Disease. *Front Microbiol, 9*, 2247. doi:10.3389/fmicb.2018.02247